

Aus dem Adolf Butenandt Institut der Ludwig-Maximilians-Universität München

Vorstand: Prof. Dr. rer. nat. Dr. h.c. Christian Haass

Lehrstuhl: Stoffwechselbiochemie

**Transmembrane protein 106B, a risk factor in frontotemporal  
lobar degeneration, is a lysosomal type II transmembrane  
protein and affects autophagy**

Dissertation

zum Erwerb des Doktorgrades der Naturwissenschaften

an der Medizinischen Fakultät

der Ludwig-Maximilians-Universität München



vorgelegt von

**Christina Maria Lang**

aus Landsberg am Lech

2015

Gedruckt mit Genehmigung der Medizinischen Fakultät der Ludwigs-Maximilians-Universität  
München

Betreuer: Prof. Dr. Christian Haass

Zweitgutachter: Prof. Dr. Dierk Niessing

Dekan: Prof. Dr. med. dent. Reinhard Hickel

Tag der mündlichen Prüfung: 11.02.2016

*Meiner Familie*



*Nach Wissen suchen, heißt Tag für Tag dazugewinnen.*

(Laotse)



# Contents

<b>Abstract</b> . . . . .	<b>1</b>
<b>Zusammenfassung</b> . . . . .	<b>3</b>
<b>1 Introduction</b> . . . . .	<b>7</b>
1.1 Frontotemporal lobar degeneration (FTLD) . . . . .	7
1.1.1 Epidemiology and clinical phenotypes of FTLD . . . . .	7
1.1.2 Molecular Pathology . . . . .	8
1.1.3 Molecular Genetics . . . . .	9
1.1.3.1 Autosomal dominant genes . . . . .	9
1.1.3.1.1 Microtubule-associated protein tau . . . . .	9
1.1.3.1.2 Progranulin (GRN) . . . . .	12
1.1.3.1.3 C9orf72 . . . . .	14
1.1.3.1.4 Charged multivesicular body protein 2B (CHMP2B) . .	16
1.1.3.1.5 Valosin containing protein (VCP) . . . . .	17
1.1.3.1.6 TAR-DNA binding protein 43 (TDP-43) and Fused in Sarcoma (FUS) . . . . .	18
1.1.3.2 Risk factors . . . . .	20
1.1.3.2.1 Triggering receptor expressed on myeloid cells 2 (TREM2)	20
1.1.3.2.2 Transmembrane protein 106B (TMEM106B) . . . . .	20
1.2 Transmembrane protein 106B . . . . .	21
1.2.1 Biochemical characteristics of TMEM106B . . . . .	22
1.2.2 The relationship between TMEM106B and GRN . . . . .	22
1.2.3 Interaction partners of TMEM106B . . . . .	23
1.2.4 Impact of TMEM106B on cognition . . . . .	23
1.2.5 TMEM106B in other neurodegenerative diseases . . . . .	23
1.3 Lysosomal function in protein degradation . . . . .	24
1.3.1 General information about lysosomes . . . . .	25
1.3.2 Lysosomal degradation through endolysosomal sorting . . . . .	26
1.3.3 Lysosomal degradation through autophagy . . . . .	29
1.3.4 Regulation of lysosomal degradation . . . . .	33

1.4	Lysosomal dysfunction in neurodegenerative diseases? . . . . .	35
1.4.1	Alzheimer’s disease (AD) . . . . .	36
1.4.2	Parkinson’s disease (PD) . . . . .	38
1.4.3	Huntington’s disease (HD) . . . . .	40
1.4.4	Frontotemporal lobar degeneration (FTLD) . . . . .	41
<b>2</b>	<b>Aims of this study . . . . .</b>	<b>43</b>
<b>3</b>	<b>Results . . . . .</b>	<b>45</b>
3.1	Establishment of a method for analysing TMEM106B on immunoblot . . . . .	45
3.2	TMEM106B is a highly glycosylated type II transmembrane protein . . . . .	49
3.2.1	TMEM106B is a glycosylated integral membrane protein . . . . .	49
3.2.2	TMEM106B is a type II transmembrane protein . . . . .	51
3.3	TMEM106B is localized to the late endosomal/lysosomal compartment . . . . .	53
3.4	Complex glycosylation of TMEM106B is required for its cellular transport . . . . .	57
3.5	TMEM106B and GRN do not influence each other directly . . . . .	59
3.6	Impaired acidification increases TMEM106B protein levels . . . . .	62
3.7	Lysosomal positioning changes upon TMEM106B knockdown . . . . .	65
3.7.1	Upon TMEM106B knockdown, lysosomes cluster in the perinuclear region of the cell . . . . .	65
3.7.2	Lysosomal clustering upon TMEM106B knockdown can be rescued by overexpressing wt TMEM106B . . . . .	69
3.7.3	Lysosomes cluster at the microtubule-organizing center . . . . .	71
3.7.4	Quantification of lysosomal positioning after TMEM106B knockdown . . . . .	71
3.8	Influence of TMEM106B knockdown on other cellular organelles and structures . . . . .	72
3.9	Clustering is dependent on functional retrograde transport along microtubules . . . . .	77
3.10	Lysosomes are still acidic and functional upon TMEM106B knockdown . . . . .	80
3.11	Autophagosomal markers are altered upon TMEM106B knockdown . . . . .	84
3.12	Starvation reveals an increase in autophagosomal proteins upon TMEM106B knockdown . . . . .	88
<b>4</b>	<b>Discussion . . . . .</b>	<b>91</b>
4.1	The molecular weight of TMEM106B . . . . .	91
4.2	TMEM106B is a lysosomal type II transmembrane protein . . . . .	92
4.3	TMEM106B is degraded in the lysosome but not in the proteasome . . . . .	94
4.4	The relationship between TMEM106B and GRN . . . . .	95
4.5	TMEM106B influences lysosomal positioning . . . . .	98
4.6	TMEM106B and microtubule-dependent transport . . . . .	101
4.7	The autophagic pathway is influenced by TMEM106B knockdown . . . . .	104
4.8	Hypotheses of how TMEM106B might influence the pathogenesis of FTLD-TDP . . . . .	106

---

4.9	Is an increase in TMEM106B levels detrimental or beneficial for FTLD-TDP? . . .	110
4.10	Impaired trafficking and autophagy as common disease mechanisms in FTLD? . .	111
4.11	Concluding remarks . . . . .	112
<b>5</b>	<b>Material and Methods . . . . .</b>	<b>115</b>
5.1	Material . . . . .	115
5.1.1	Laboratory equipment and chemicals . . . . .	115
5.1.2	Primers . . . . .	115
5.1.3	Constructs . . . . .	116
5.1.4	Small interfering RNAs . . . . .	118
5.1.5	Drugs and fluorescent dyes . . . . .	119
5.1.6	Cell lines . . . . .	120
5.1.7	The T-REx <sup>TM</sup> system . . . . .	121
5.1.8	Antibodies . . . . .	123
5.1.9	Validation of the anti-TMEM106B antibody 6F2 . . . . .	125
5.2	Methods . . . . .	126
5.2.1	Molecular biology and nucleic acid techniques . . . . .	126
5.2.1.1	Polymerase chain reaction (PCR) . . . . .	126
5.2.1.2	Site-directed mutagenesis . . . . .	126
5.2.1.3	Restriction digest . . . . .	127
5.2.1.4	Agarose gel electrophoresis and gel extraction of DNA . . . . .	128
5.2.1.5	Ligation . . . . .	128
5.2.1.6	Preparation of competent bacteria . . . . .	128
5.2.1.7	Transformation of bacteria . . . . .	129
5.2.1.8	Plasmid DNA preparation . . . . .	129
5.2.1.8.1	Small scale, analytical plasmid preparation ("Miniprep")	129
5.2.1.8.2	Large scale, preparative plasmid preparation ("Midiprep" or "Maxiprep") . . . . .	130
5.2.1.9	Sequencing of DNA . . . . .	130
5.2.1.10	Isolation of cellular RNA . . . . .	130
5.2.1.11	Reverse transcription of RNA . . . . .	131
5.2.1.12	Real-time PCR . . . . .	131
5.2.2	Cell culture methods . . . . .	131
5.2.2.1	Cultivation of continuous cell lines . . . . .	131
5.2.2.2	Preparation of stable cell lines . . . . .	132
5.2.2.3	Cryopreservation of cell lines . . . . .	132
5.2.2.4	Transfection of cells via lipofection . . . . .	132
5.2.2.5	Drug treatment . . . . .	133
5.2.3	Protein biochemistry . . . . .	133

5.2.3.1	Collection of media and cell harvest . . . . .	133
5.2.3.2	Preparation of total cell lysates . . . . .	134
5.2.3.3	Measurement of the protein concentration . . . . .	134
5.2.3.4	Membrane preparation . . . . .	134
5.2.3.5	Direct deglycosylation with N-glycosidase F . . . . .	135
5.2.3.6	Immunoprecipitation and Deglycosylation . . . . .	135
5.2.3.7	Sodium dodecyl sulfate polyacrylamid gel electrophoresis (SDS- PAGE) . . . . .	136
5.2.3.8	Western blotting and immunodetection . . . . .	137
5.2.3.9	Cathepsin D activity assay . . . . .	137
5.2.3.10	Enzyme-linked immunosorbent assay (ELISA) for human GRN .	137
5.2.4	Microscopy . . . . .	138
5.2.4.1	Immunofluorescence . . . . .	138
5.2.4.2	DQ-BSA and lysotracker staining . . . . .	138
5.2.5	Quantification of lysosomal clustering . . . . .	139
5.2.6	Statistics . . . . .	139
<b>List of abbreviations . . . . .</b>		<b>141</b>
<b>Bibliography . . . . .</b>		<b>145</b>
<b>Acknowledgements . . . . .</b>		<b>147</b>

# Abstract

Frontotemporal lobar degeneration (FTLD) is a fatal neurodegenerative disease with presenile onset. Clinically, it mainly presents with language disorders or personality and behavioural changes whereas pathologically patients show atrophy of the frontal and temporal lobes of the brain. Like in other neurodegenerative disorders, abnormal protein deposition can be detected in the affected areas of the brain nervous system. However, several different proteins have been identified to be the main component of these inclusions accordingly leading to the differentiation of so far five distinct types of FTLD, namely FTLD-tau, FTLD-TDP (TAR DNA-binding protein 43), FTLD-FUS (Fused in Sarcoma), FTLD-DPR (dipeptide repeat protein) and FTLD-UPS (ubiquitin-proteasome system). FTLD-TDP comprises 45 % of all FTLD cases and thus represents one of the two main pathological subtypes of FTLD.

In the last few years, tremendous progress has been made in the identification of the genetic causes for FTLD-subtypes; among them, the identification of mutations in the progranulin (*GRN*) gene in FTLD-TDP. Interestingly, even though haploinsufficiency of progranulin was demonstrated to be causative for FTLD-TDP, the same *GRN* mutation could present with different ages of disease onset in different patients. This argued for additional factors that might modulate disease onset. In order to identify such genetic factors, a genome-wide association study was performed in genetically or pathologically confirmed FTLD-TDP cases. Thereby, twelve single-nucleotide polymorphisms mapped to a 68 kb interval located on chromosome 7p21.3 implicating that this might be a common genetic susceptibility locus for FTLD-TDP. This region only comprised one gene encoding for the transmembrane protein 106B (*TMEM106B*). Interestingly, the risk allele of *TMEM106B* was especially associated with FTLD risk in patients carrying a *GRN* mutation which suggested a functional relationship between those two proteins. However, *TMEM106B* was an uncharacterized protein of unknown function. Thus, the motivation of my study was to investigate the biochemical features of *TMEM106B*, followed by examining the relationship between *TMEM106B* and *GRN* and finally, by investigating *TMEM106B* function.

In the first part of this study, membrane orientation, cellular localization and the glycosylation status of *TMEM106B* were determined and tools developed. By sequential inactivation of the five predicted N-glycosylation motifs, *TMEM106B* was demonstrated to be a type II transmembrane protein that is N-glycosylated at the amino acid positions 146 (N1), 152 (N2), 165 (N3), 184 (N4) and 257 (N5). Moreover, only N4 and N5 proved to be complex glycosylated whereas N1, N2 and N3 did not. By immunofluorescence, *TMEM106B* was determined to be a lysosomal protein.

Interestingly, mutants where one of the two complex glycosylation motifs was deleted showed a different intracellular localization whereas deleting the non-complex glycosylation motifs did not change TMEM106B localization. This indicated that complex glycosylation was essential for correct TMEM106B positioning in the cell.

In the second part of this study, the influence of TMEM106B expression on GRN levels was analysed in various cell lines. However, neither overexpression nor knockdown of TMEM106B changed intracellular or secreted GRN levels indicating that both proteins probably do not influence each other directly. However, interestingly, bafilomycin A1 (BafA1) treatment which inhibits lysosomal acidification and thus lysosomal function increased both GRN and TMEM106B protein levels suggesting that both proteins might act in a common pathway or might be located in the same compartment. Since treatment with proteasomal inhibitors did not increase TMEM106B levels, this observation further indicated that TMEM106B is mainly degraded by the lysosome.

In the third part of this study, the endogenous function of TMEM106B was investigated using siRNA-mediated TMEM106B knockdown in a cell culture model. Thereby, TMEM106B knockdown was shown to change lysosomal positioning as lysosomes clustered tightly at the microtubule-organizing center instead of being distributed throughout the cell. A rescue experiment, where endogenous TMEM106B was knocked down first and then, additionally, either a control vector or exogenous TMEM106B was transfected, proved that lysosomal clustering was the result of TMEM106B loss and not a side effect of siRNA transfection.

Furthermore, lysosomal clustering upon TMEM106B knockdown was shown to be dependent on functional retrograde transport and an intact microtubule network. In addition, lysosomes were demonstrated to be still acidic and, in principle, functional upon TMEM106B knockdown. Interestingly, however, lysosomal and autophagosomal protein levels increased significantly upon TMEM106B knockdown, suggesting that the autophagic pathway might be affected by TMEM106B levels. Since GRN had been implicated in playing an important role for lysosomal function and thus in the autophagic pathway, the finding that TMEM106B also has an impact on this pathway might explain why *TMEM106B* polymorphisms are especially associated with *GRN* mutation carriers but also why TMEM106B is a general risk factor for FTLD. Changes in the autophagic pathway seem to be common in neurodegenerative disorders as for example in Alzheimer's, Parkinson's and Huntington's disease, the autophagic pathway has been reported to be impaired in the course of disease. My findings would support the notion that also in FTLD, autophagy plays an essential part in disease progression.

# Zusammenfassung

Frontotemporale lobäre Degeneration (FTLD) ist die zweithäufigste Ursache präseniler Demenz. Klinische Symptome beinhalten vor allem eine Veränderung der Persönlichkeit und des sozialen Verhaltens sowie Sprachstörungen. Auf pathologischer Ebene ist die Krankheit durch eine Atrophie der Frontal- und Temporallappen des Gehirns gekennzeichnet. Außerdem können, ähnlich wie bei anderen neurodegenerativen Erkrankungen, in den betroffenen Bereichen des Nervensystems unnatürliche Proteinablagerungen festgestellt werden. Interessanterweise wurden allerdings mehrere unterschiedliche Proteine als Hauptkomponente dieser Einschlusskörper identifiziert. Dies führte zur Unterscheidung von fünf verschiedenen FTLD-Untergruppen: FTLD-Tau, FTLD-TDP (TAR DNA-bindendes Protein 43), FTLD-FUS (“Fused in Sarcoma”), FTLD-DPR (“dipeptide repeat” Protein) und FTLD-UPS (Ubiquitin-Proteasom System). Mit 45 % stellt FTLD-TDP neben FTLD-Tau die größte pathologische FTLD-Untergruppe dar.

In den letzten Jahren wurden große Fortschritte bei der Identifizierung der genetischen Ursachen dieser FTLD-Untergruppen gemacht. So wurden auch Mutationen im Progranulin-Gen (*GRN*) als Ursache für FTLD-TDP entdeckt, die zu einer Haploinsuffizienz führen. Jedoch ist immer noch unklar, weshalb Patienten mit der gleichen *GRN*-Mutation in unterschiedlichem Alter erkranken. Es ist allerdings sehr wahrscheinlich, dass dies auf weitere Faktoren, die sich auf das Erkrankungsalter auswirken, zurückzuführen ist. Deshalb wurde eine Genom-weite Assoziationsstudie mit pathologisch verifizierten FTLD-TDP-Fällen durchgeführt, um zusätzliche genetische Faktoren zu ermitteln. Dabei wurde ein 68 kb-großer Bereich auf Chromosom 7p21.3 als gemeinsamer genetischer Suszeptibilitätsloкус identifiziert. Diese Region beinhaltet nur ein Gen, welches das bisher nicht charakterisierte Transmembranprotein 106B (TMEM106B) kodiert. Des Weiteren zeigte das Risikoallel von *TMEM106B* (T/T) eine besonders starke Assoziation zum Erkrankungsrisiko bei FTLD-Patienten, die zusätzlich eine *GRN*-Mutation aufwiesen, was auf einen funktionalen Zusammenhang zwischen diesen beiden Proteinen schließen lässt.

Allerdings war zu diesem Zeitpunkt noch nichts über die Eigenschaften des Proteins TMEM106B bekannt. Das Ziel dieser Studie bestand deshalb darin, die Rolle von TMEM106B in FTLD-TDP zu untersuchen. Dafür wurden zunächst dessen biochemische Charakteristika untersucht, gefolgt von dem Einfluss von TMEM106B auf GRN und schließlich seine Funktion.

Im ersten Teil dieser Arbeit wurden deshalb die Membranorientierung, die zelluläre Lokalisierung und der Glykosylierungsstatus von TMEM106B bestimmt sowie Methoden und Antikörper etabliert. Durch sequenzielle Inhibierung der durch Computeranalysen prognostizierten N-Glykosylierungsmotive konnte gezeigt werden, dass es sich bei TMEM106B um ein Typ-II-

Transmembranprotein handelt, das an den Aminosäurepositionen 146 (N1), 152 (N2), 165 (N3), 184 (N4) und 257 (N5) N-glykosyliert ist. Dabei sind N4 und N5 komplex glykosyliert, während bei N1, N2 und N3 keine komplexen Glykosylierungen nachgewiesen werden konnten. Durch Immunfluoreszenzversuche wurde ersichtlich, dass es sich bei TMEM106B um ein lysosomales Protein handelt. Interessanterweise änderte sich die zelluläre Lokalisierung von TMEM106B-Mutanten, bei denen eines oder beide der komplex glykosylierten Arginine deletiert wurden, wohingegen die Mutation der nicht-komplex glykosylierten Motive keinen Einfluss auf die Lokalisation von TMEM106B ausübte. Dies deutet darauf hin, dass die komplexe Glykosylierung von TMEM106B die Positionierung von TMEM106B in der Zelle maßgeblich beeinflusst.

Im zweiten Teil der Studie wurde unter Verwendung verschiedener Zelllinien der Einfluss von TMEM106B auf GRN ermittelt. Allerdings veränderten sich nach Überexpression oder Herabregulation von TMEM106B durch RNA-Interferenz weder die intra- noch die extrazellulären GRN-Proteinmengen, was darauf hindeutet, dass sich TMEM106B und GRN auf Expressionsebene wahrscheinlich nicht gegenseitig beeinflussen. Interessanterweise aber führte die Behandlung mit Bafilomycin A1 (BafA1), einer Chemikalie, die die lysosomale Ansäuerung und damit die lysosomale Funktion inhibiert, sowohl zu einem Anstieg der GRN- als auch der TMEM106B-Proteinmenge. Dies könnte darauf hinweisen, dass beide Proteine in einem gemeinsamen Signalweg agieren oder sich im gleichen zellulären Kompartiment befinden. Da eine Behandlung mit proteasomalen Inhibitoren die TMEM106B-Mengen nicht erhöhte, deutet diese Beobachtung außerdem darauf hin, dass überschüssiges TMEM106B vor allem über den lysosomalen Abbauweg degradiert wird.

Im dritten Teil dieser Arbeit wurde mit Hilfe eines Zellkulturmodells, bei welchem TMEM106B durch RNA-Interferenz herunterreguliert wurde, die endogene Funktion von TMEM106B untersucht. Interessanterweise führte dabei die Herabregulation von TMEM106B zu einer Veränderung der Lokalisierung von Lysosomen in der Zelle: Statt sich über das gesamte Zellvolumen zu verteilen, sammelten sich die Lysosomen hauptsächlich in Form eines engen "Clusters" am Zentrosom. Dieses Phänomen wurde durch ein "Rescue"-Experiment bestätigt. Hierbei konnte gezeigt werden, dass Zellen, in welchen endogenes TMEM106B durch RNA-Interferenz herabreguliert und in welche zusätzlich exogenes TMEM106B transfiziert worden war, eine normale Verteilung der Lysosomen aufwiesen.

Außerdem wurde gezeigt, dass das Clustern der Lysosomen nach der Herabregulation von TMEM106B sowohl von einem intakten Mikrotubuli-Netzwerk also auch von einer funktionalen retrograden Transportmaschinerie abhängig ist. Darüber hinaus wurde nachgewiesen, dass nach TMEM106B-Herabregulation Lysosomen nach wie vor einen sauren pH-Wert aufweisen und prinzipiell funktionell sind. Allerdings waren nach TMEM106B-Herabregulation sowohl lysosomale als auch autophagosomale Proteinmengen signifikant erhöht, was darauf hindeutet, dass der lysosomale Abbauweg durch TMEM106B beeinflusst wird.

Es wird vermutet, dass GRN eine wichtige Rolle für die Funktion von Lysosomen und damit für Autophagie spielt. Dass TMEM106B wahrscheinlich ebenfalls diesen Abbauweg beeinflusst,

könnte erklären, warum *TMEM106B*-Polymorphismen in besonderer Weise mit *GRN*-Mutationsträgern assoziiert sind und warum *TMEM106B* einen allgemeinen Risikofaktor für FTLD darstellt.

Veränderungen im lysosomalen Abbauweg sind ein häufiges Erscheinungsbild in neurodegenerativen Erkrankungen. So konnte beispielsweise ab einem bestimmten Zeitpunkt des Krankheitsverlaufs sowohl bei Alzheimer- als auch bei Parkinson- oder Huntington-Erkrankten eine Hemmung des Autophagie-Signalwegs festgestellt werden. Die Ergebnisse dieser Arbeit deuten darauf hin, dass auch bei der FTLD-TDP Autophagie eine wesentliche Rolle für das Fortschreiten der Krankheit spielen könnte.



# 1 Introduction

## 1.1 Frontotemporal lobar degeneration (FTLD)

### 1.1.1 Epidemiology and clinical phenotypes of FTLD

In 1892, Arnold Pick was the first to describe lobar atrophy in a patient with presenile dementia and aphasia [217]. Accordingly, the disease has been called Pick's Disease, a term which had become to represent a class of clinical syndromes with symptoms attributed to frontal and temporal lobe dysfunction. More than a century later, it has been renamed frontotemporal lobar degeneration. Nowadays, the term Pick's Disease is only used for a subtype of FTLD with specific histopathological features like round inclusions of tau filaments, also called Pick bodies [239, 227, 217].

FTLD is a comprehensive term for a clinically, genetically and pathologically heterogeneous group of dementias characterized by a relatively selective and progressive atrophy of the frontal and temporal lobes of the brain [315, 270, 239] (figure 1.1 a). It is the second most common form of presenile dementia after Alzheimer's disease (AD) and accounts for about 20 % of cases with an onset before the age of 65 years [192, 233]. FTLD has an incidence of about 3.5 cases per 100,000 person-years compared to 4.2 cases for AD in a group with the age range of 45 to 64 years in the United Kingdom (UK) [182]. The exact prevalence of FTLD is uncertain as only few studies were conducted with estimates between 3.6 (in the Netherlands) and 15 per 100,000 persons (in the UK), depending on the age range [264, 246, 233]. According to the Office of Rare Diseases (ORD) of the National Institutes of Health (NIH) and the Ophanet, FTLD is listed to be a so called "rare disease" which means that only 1 in 2,000 persons is affected. However, still more than an estimated 50,000 to 60,000 Americans suffer from this disease. Moreover, the symptoms of FTLD are often misinterpreted as symptoms of a midlife crises or a psychiatric disorder. Therefore, the true number of individuals suffering from FTLD could be even higher [143, 106, 290, 54, 30]. FTLD can start as early as in the third decade of life but also late onsets in the eighth decade have been reported. The mean age-at-onset is about 58 years [126] and the median survival is estimated at six to eleven years from symptom onset and three to four years from diagnosis [225]. This means that often people are affected before they are retired which places an additional heavy burden not only on the family of the patients but also on economics [290].

Two clinical syndromes of FTLD, namely language disorders (primary progressive aphasia, PPA) or personality and behavioural changes (behavioural variant frontotemporal dementia, bvFTD),

are described [225]. People suffering from bvFTD, the most common FTLN syndrome [126, 130, 270], show loss of empathy, apathy, neglect of personal hygiene and impaired regulation of personal conduct that could present, among others, with increased aggressiveness, inactivity to overactivity and pacing [130, 232, 274, 270, 13, 264, 193]. The language syndrome of FTLN is subdivided into the semantic variant PPA (svPPA), the nonfluent variant PPA (nfvPPA) and the logopenic variant PPA (lvPPA) [23]. The characteristics of the semantic variant PPA are a gradual loss of the semantic memory, i.e. a loss of word meaning, whereas speech remains fluent [315, 239, 193]. In contrast, nonfluent variant PPA presents with a dominant agrammatism and effortful non-fluent speech [23]. The third language variant, lvPPA, is characterized by an impairment of speech comprehension and difficulty with repetition probably due to a disorder in the phonological loop function [23]. However, as this classification is a very recent development, the terminology and criteria for the three subtypes is still inconsistent across institutions what makes the comparison of studies difficult [23].

### 1.1.2 Molecular Pathology

Not only the syndromes of FTLN are heterogeneous, but also the molecular pathology. Like in other neurodegenerative disorders, FTLN shows abnormal protein aggregation in the affected parts of the nervous system [307]. However, the nature of the aggregates is not as uniform as for example in AD where the pathology is dominated by amyloid- $\beta$  plaques and neurofibrillary tangles [93, 307]. In FTLN, different proteins have been identified to be the main component of the inclusions that were found in the nervous system. A major component to be identified was hyperphosphorylated tau, a microtubule-associated protein that accumulated in neurons and glia (figure 1.1 b) [239, 171]. In 1998, mutations in the *microtubule-associated protein tau (MAPT)* gene, were found to be causative for the disease which has been termed FTLN-tau accordingly [116, 276] (figure 1.3). Pick's disease, characterized by round inclusions of tau filaments (figure 1.1 c), belongs to this pathological subgroup [307]. The remaining group of FTLN pathology mainly comprised tau-negative, but ubiquitin-positive inclusions and firstly has been named FTLN-U for ubiquitin. In 2006, Neumann *et al.* were able to identify the TAR-DNA binding protein 43 (TDP-43) as the major component of ubiquitin-positive inclusions in the majority of FTLN-U cases (figure 1.1 d) [195] that were subsequently termed FTLN-TDP (figure 1.3). Only a total of 5 to 20 % of all FTLN-U cases were negative for TDP-43. Of these, about 9 % stained positive for a protein called Fused in Sarcoma (FUS) (FTLN-FUS) [196] (figure 1.1 e and 1.3). For the remaining FTLN cases, the major component of their inclusions has not been identified, yet [173, 225, 307]. However, as in these cases, inclusions are positive for ubiquitin, they are termed FTLN-UPS (ubiquitin-proteasome system) (figure 1.3) [173, 225, 307]. Interestingly, in 2013, Mori *et al.* described an FTLN-UPS patient with a *C9orf72* repeat expansion which showed inclusions that mainly contained the dipeptide species poly-GA [187] hinting that FTLN-DPR (for dipeptide-repeat proteins) might be another important pathological subtype of FTLN (see also section 1.1.3.1.3, page 14). In the same year, Mori's finding was confirmed by Ash *et al.*

who also examined *C9orf72*-repeat expansion-positive cases of FTLD and amyotrophic lateral sclerosis (ALS), a motor neuron disease closely related to FTLD, for their immunoreactivity with generated dipeptids [5] (figure 1.3).

Thus, until today, five or even six major pathological subtypes of FTLD can be distinguished: FTLD-tau (45 % of all FTLD cases), FTLD-TDP (45 % of all FTLD cases), FTLD-FUS (9 % of all FTLD cases), FTLD-UPS (about 1 % of all FTLD cases), FTLD without inclusions (number unknown) [199] and probably also FTLD-DPR (included in number of FTLD-TDP and FTLD-UPS cases) [171, 270, 162, 64] (figure 1.2).

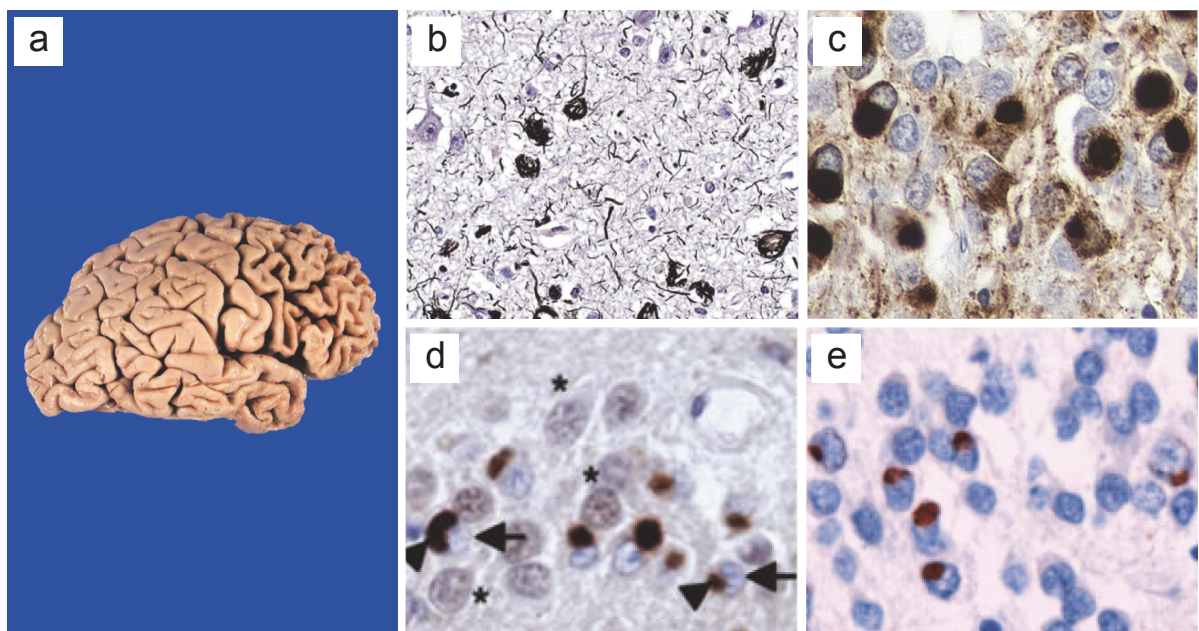


**Figure 1.1: Pathological features of FTLD**

(a) Severe atrophy of the frontal and temporal lobes of a patient with Pick's disease [197]. (b) Neuronal and glial tau pathology in the frontal cortex of an FTLD-tau patient [197]. (c) Pick bodies labelled with tau [20]. (d) Staining of TDP-43-positive inclusions (arrowheads) in hippocampal dentate granule neurons of an FTLD-TDP patient. Note that nuclei are cleared of TDP-43 (arrow) in neurons with inclusions compared to normal neurons (\*) [195]. (e) Neuronal cytoplasmic inclusions in the dentate granule cells of the hippocampus of an FTLD-FUS patient [196] (modified from [196, 195, 197, 20]).

### 1.1.3 Molecular Genetics

In FTLD, approximately 40 to 50 % of patients have a family history, of which 10 % to 30 % show an autosomal dominant inheritance pattern [239, 225] highlighting the important contribution of genetic factors in this disease [61]. In the last few years, tremendous progress has been made in the identification of the genes involved in FTLD. In the following sections, the role of causal genes and genetic risk factors for FTLD will be discussed.

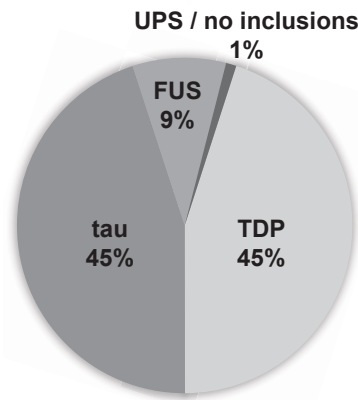


**Figure 1.2: Overview of the pathological subtypes of FTLD**

The percentages of the pathological subtypes of FTLD are shown according to the major protein accumulated [199, 171, 270, 162, 64](modified from [162]).

### 1.1.3.1 Autosomal dominant genes

#### 1.1.3.1.1 Microtubule-associated protein tau

The first gene discovered to be causative for FTLD was *MAPT*, encoding for tau. Already in 1994, frontotemporal dementia with parkinsonism had been linked to chromosome 17q21.1 (FTLD-17). Four years later, in 1998, tau was identified as the most probable candidate gene [116] of which today, more than 60 different mutations have been detected in FTLD patients [2, 270]. Tau is mainly expressed in neurons of the central and peripheral nervous system [293, 226], but can also be found in astrocytes and oligodendrocytes [163]. It is a microtubule-associated protein whose main function is to stabilize microtubules and promote microtubule assembly by binding to tubulin [110]. Moreover, tau has been shown to tune kinesin-mediated transport of vesicles and organelles along microtubules depending on its isoforms and relative amounts [258, 65, 63, 311]. In total, six major isoforms of tau are produced by alternative splicing of exons 2, 3 and 10 of the *MAPT* gene (reviewed in [226, 308]).

Mutations in *MAPT* perturb the subtle equilibrium between cytoskeletal assembly and disassembly by destabilizing microtubules leading to impaired axonal transport and neuronal plasticity and promoting pathological tau filament aggregation [239, 270]. Furthermore, the ratio of tau isoforms is usually altered in disease, favouring tau aggregation [308, 245]. Deposition of hyperphosphorylated tau is a hallmark for several neuropathological diseases also termed tauopathies [275]. These include corticobasal degeneration (CBD), AD and FTLD [226]. Of all familial cases, FTLD-tau accounts for about 45 % and is mainly associated with bvFTD [239, 270].

disease	FTLD				FTLD/ALS
	FTLD-tau	FTLD-TDP	FTLD-UPS	FTLD-FUS	ALS/ FTLD-DPR
subtype					
associated genes	<i>MAPT</i>	<i>GRN</i> <i>VCP</i> ( <i>TARDBP</i> )	<i>CHMP2B</i>	( <i>FUS</i> )	<i>C9orf72</i>
disease modifiers	?	<i>TMEM106B</i>	?	?	<i>TMEM106B</i>

**Figure 1.3: Classification of FTLD**

Pathologically, FTLD and FTLD/ALS are considered as different diseases of probably one FTLD-ALS spectrum and can be divided into different clinical subtypes in regard to the deposited protein found in the nervous system of the patient. The disease-causing genes are indicated in italic letters of which the very rare genes are shown in parenthesis. Only one disease modifying or risk gene is known for FTLD and has been associated with FTLD-TDP patients carrying a *GRN* mutation or are *C9orf72* expansion carriers (modified from [64]).

#### 1.1.3.1.2 Progranulin (*GRN*)

Concerning all families with autosomal dominant FTLD linked to chromosome 17q21, there were still some that did not harbour a mutation in the *MAPT* gene [76] pointing to another gene to be responsible for the disease. Therefore, systematic mutation analysis of all remaining genes within the candidate region was performed leading to the identification of mutations in the progranulin (*GRN*) gene [9, 52]

Progranulin, with a molecular weight of 68.5 kDa, is a 593-amino-acid-long-secreted glycoprotein composed of seven and a half tandem repeats of 12-cysteiny motifs, separated by linker regions [9, 312] (figure 1.4).



**Figure 1.4: Schematic protein structure of GRN**

GRN consists of seven and a half cystein-rich tandem repeats, also called granulin (grn) domains, which are represented by the lettered boxes (grnP (P), grnG (G), grnF (F), grnB (B), grnA (A), grnC (C), grnD (D) and grnE (E)). N and C represent the N- and C-terminus of the protein (modified from [138]).

It is ubiquitously expressed, but can mainly be found in hematopoietic and epithelial cells as well as in neurons and especially in activated microglia (reviewed in [138]). Full-length progranulin can be proteolytically cleaved into 6 kDa granulin peptides by neutrophil elastase and proteinase-3, a process that can be inhibited by secretory leukocyte protease inhibitor (SLPI) [105, 135, 329]. GRN and its granulin peptides (figure 1.4) are involved in the regulation of inflammatory reactions whereas the full-length protein exerts an anti-inflammatory function and granulin peptides are probably pro-inflammatory [329, 138]. Furthermore, progranulin

also plays an essential part in other cellular processes including proliferation, development, cell motility and wound repair (reviewed in [138]). Interestingly, whereas decreased GRN levels lead to neurodegeneration, increased levels are associated with accelerated tumor growth and tumorigenesis [104].

Mutations in *GRN* account for 5 to 10 % of all FTLD cases and up to 20 % of all familial cases [171, 9, 52]. Neuropathologically, *GRN* mutation carriers consistently show TDP-43- and ubiquitin-positive, lentiform neuronal intranuclear inclusions (NII) in the neocortex and striatum [170, 3, 195]. Furthermore, hippocampal sclerosis and irregular dystrophic neurites as well as extensive astrogliosis and loss of myelin in the underlying white matter can be observed [308] (reviewed in [138]). Biochemically, TDP-43 C-terminal fragments accumulate in affected brain regions [195].

Until now, more than 60 pathogenic mutations that are evenly distributed throughout the gene were described [21]. As most of the *GRN* mutations are loss-of-function mutations, which reduce functional protein levels, or mutations that lead to reduced GRN secretion [80, 9, 52, 268], haploinsufficiency seems to be the most probable pathomechanism [272, 228]. Thus, increasing GRN levels in *GRN* mutation carriers by increasing the production from the still intact wild-type (wt) allele of *GRN* was suggested to be beneficial for preventing the disease [138]. In 2011, Capell *et al.* demonstrated that alkalizing agents and v-ATPase inhibitors such as bafilomycin A1 (BafA1) and chloroquine (CQ) could restore GRN levels in patient lymphoblasts with loss-of-function mutations in *GRN* [37]. For treating FTLD-TDP patients carrying a *GRN* mutation, CQ seems to be the most promising drug, as it is already used in treating malaria and has been reported to be able to cross the blood-brain-barrier, at least to some extent [37]. However, as increased GRN levels are also implicated in tumorigenesis, it is absolutely crucial to further study and monitor possible side effects of GRN elevation and titrate GRN levels very carefully.

GRN is ubiquitously expressed and even though overall expression levels in the brain are very low compared to other tissues like skin and gut, *GRN* is highly expressed in specific subsets of adult neuronal cells, notably cortical neurons, Purkinje cells of the cerebellum and granule cells of the hippocampus [56]. Importantly, GRN levels in microglia seem to be higher than in neurons and increase rapidly and excessively (approximately 500-fold) upon microglial activation implicating that GRN plays a crucial role in neuroinflammatory processes [216]. Moreover, it was suggested that GRN is neuroprotective [78], involved in the function or maintenance of mature neurons [216] and that it promotes neurite outgrowth [300, 78].

Very recently, another aspect of progranulin came into focus, namely its role in lysosomes. In 2012, Smith *et al.* described two siblings that suffered from adult-onset neuronal ceroid lipofuscinosis (NCL), a lysosomal storage disorder, which resulted from a homozygous mutation in *GRN* [273]. The patients were in their twenties and showed mild cerebellar ataxia, early cognitive deterioration and retinal dystrophy [273]. The reported frameshift mutation resulted in the premature termination of GRN translation and had already been described in patients

suffering from FTLD-TDP, however, they had only been heterozygous for this mutation [320]. Therefore, apparently, *GRN* mutations can present with two different phenotypes depending on whether they are homozygous (NCL) or heterozygous (FTLD-TDP) which suggests a role for GRN in lysosomal function [273]. Already in 2011, *GRN* was included in the top ranked genes of a transcriptional gene network inference study to identify human disease genes that may have a role in lysosomal function and organization [15]. The authors validated their hit and found that, indeed, GRN responded to sucrose treatment, a known inducer of lysosomal biogenesis, by a two-fold increase in *GRN* mRNA levels. Moreover, upon overexpression of GRN, levels of lysosome-associated membrane protein 1 (LAMP1) and lysosome-associated membrane protein 2 (LAMP2), two lysosomal marker proteins, increased concomitantly supporting a lysosomal involvement of GRN [15]. In 2013, Tanaka *et al.* observed co-localization of GRN and LAMP1 in activated microglia after experimental induction of traumatic brain injury (TBI) [286]. Furthermore, lysosomal marker protein CD68 and microglial marker Iba1 were more dramatically increased in activated microglia of *Grn* knockout than of control mice [286]. Concomitantly, the authors found the activity of mammalian target of rapamycin complex 1 (mTORC1) to be decreased which would explain the increased expression of lysosomal genes [286]. mTORC1 is a protein complex located on the lysosomal membrane that is responsible for transcription factor EB (TFEB) phosphorylation [243]. The phosphorylation of TFEB prevents it from nuclear translocation and thus from inducing lysosomal biogenesis [254] (see also figure 1.13 and for detailed description of this pathway section 1.3.4, page 33).

In addition, exacerbated neuronal damage was observed supporting the authors hypothesis that due to GRN deficiency, lysosomal biogenesis increases which subsequently leads to exacerbated neuronal damage after TBI [286]. In accordance with these findings, Götzl *et al.* also found lysosomal proteins like LAMP1, LAMP2 and cathepsin D to be increased in a homozygous *Grn* knockout mouse model as well as in brain lysates of GRN-associated FTLD patients [87]. As in the mouse model, the changes in lysosomal protein levels occurred long before pathological signatures of FTLD-TDP, like microgliosis or phosphorylation of TDP-43, were detected, Götzl *et al.* concluded that lysosomal dysfunction seems to be a primary and early cause for neurodegeneration [87]. However, also proteins that were reported to play a role in NCL like saposin D were elevated [87]. Interestingly, in *CTSD* (gene encoding cathepsin D) knockout mice, a model for NCL, not only lysosomal proteins but also phospho-TDP-43, a hallmark for FTLD-TDP, was found to be increased along with GRN levels [87]. These findings suggest that lysosomal storage disorders, like NCL, and GRN-associated FTLD-TDP share common features and that lysosomal dysfunction might be a general process in neurodegeneration [286, 87].

#### 1.1.3.1.3 *C9orf72*

The most common genetic abnormality causing FTLD and ALS has only been discovered recently, in 2011, by DeJesus-Hernandez *et al.* and Renton *et al.* [61, 238]. They found an uncommon hexanucleotide repeat expansion located in the non-coding promoter region of the *C9orf72*

gene causative for chromosome 9p21-linked ALS-FTD as well as familial FTLD (11 to 21 %) and familial ALS (23 to 37 %) [238, 61, 227]. Patients that harbour the hexanucleotide expansion have at least 60 units, but the number of repeats can also increase to up to 1600 compared to less than 26 in healthy individuals [61, 238, 84, 303]. So far, the pathomechanism has not been elucidated even though several different ones have been proposed. Firstly, a loss of C9orf72 protein function due to incorrect splicing because of the length of the repeat expansion might cause the disease. This hypothesis is supported by the findings of DeJesus-Hernandes *et al.*, Gijssels *et al.* and van der Zee *et al.* who reported decreased *C9orf72* mRNA expression levels and decreased transcriptional activity of the *C9orf72* promoter [61, 84, 303]. Moreover, essential RNA-binding proteins like hnRNP A3 seem to be trapped by the formation of RNA foci causing RNA toxicity [61, 186]. However, by so far the most unusual disease mechanism has been proposed by Mori *et al.* [187] and Ash *et al.* [5]. They hypothesized that the repeat region might be translated into dipeptides via a mechanism called non-ATG-initiated translation. This would result in five (poly-GA, -GP, -GR, -AP and -PR) different dipeptide-repeat proteins (DPRs) due to the translation of the sense as well as the antisense strand of the expanded GGGGCC repeats [185, 187, 5] (figure 1.5).

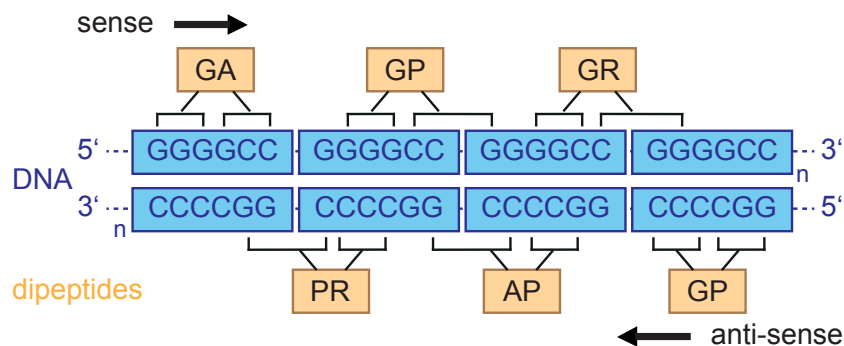


**Figure 1.5: Scheme of *C9orf72* repeat expansions and resulting dipeptides**

The repeat region  $(GGGGCC)_n$  can be translated into five different DPRs due to repeat-associated non-ATG (RAN) translation of the sense and antisense strand [5, 185, 187].

Mori *et al.* and Ash *et al.* [5] were able to show that indeed these DPRs are formed and found in the inclusions of FTLD and ALS patients carrying a *C9orf72* hexanucleotide expansion [185, 187]. Especially poly-GA and poly-GP proteins that are extremely hydrophobic are the main component of these aggregates [187]. Currently, there is evidence for all of these three scenarios and it is quite conceivable that they may all occur in parallel.

Functionally, C9orf72 was identified to be a potential DENN-type guanine nucleotide exchange factor (GEF) [324] and was shown to co-localize with the Ras-related proteins (Rabs) Rab1, Rab5, Rab7 and Rab11 [70]. Accordingly, C9orf72 was found to play an important role in regulating endosomal trafficking [70] and seems to facilitate both autophagy and endosomal

transport [70]. This suggests that disease pathology might also result from haploinsufficiency of C9orf72 leading to impaired intracellular membrane traffic. Interestingly, in motor neurons from C9orf72 ALS patients, increased co-localization between C9orf72 and Rab7 and Rab11 was observed compared to controls [70].

#### 1.1.3.1.4 Charged multivesicular body protein 2B (CHMP2B)

In 2005, linkage analyses in a Danish FTLD family identified a mutation on chromosome 3 in the acceptor splice site of exon 6 in a gene called *CHMP2B* [271]. This mutation was predicted to disrupt the processing of *CHMP2B* mRNA [271] leading to a C-terminally truncated protein [271] that results from the two aberrant transcripts. Three years later, van der Zee *et al.* reported a Belgian familial FTLD patient with a nonsense mutation in exon 5 of the *CHMP2B* gene. Interestingly, this mutation also resulted in a C-terminally truncated protein that, upon overexpression in a cellular system, caused an enlarged endosomal phenotype similar to the one that was observed when the splice site mutants of the Danish FTLD family were overexpressed [304, 271]. CHMP2B is part of the endosomal sorting complex required for transport (ESCRT) III complex (figure 1.6, left panel). Usually, its acidic C-terminus auto-inhibits CHMP2B protein function via intramolecular interaction with the basic N-terminus [304] (figure 1.6, left panel). However, mutant CHMP2B that lacks its C-terminus is permanently activated and remains bound in ESCRT-III complexes that accumulate on the endosomal membrane arguing for a toxic gain-of-function mechanism [201, 83] (figure 1.6, right panel). In addition, the truncated protein does not contain the coiled-coil domain located at the C-terminus of CHMP2B. This domain is important for the binding of the VPS4 AAA-ATPase that mediates active dissociation of the ESCRT complex (figure 1.6, right panel).

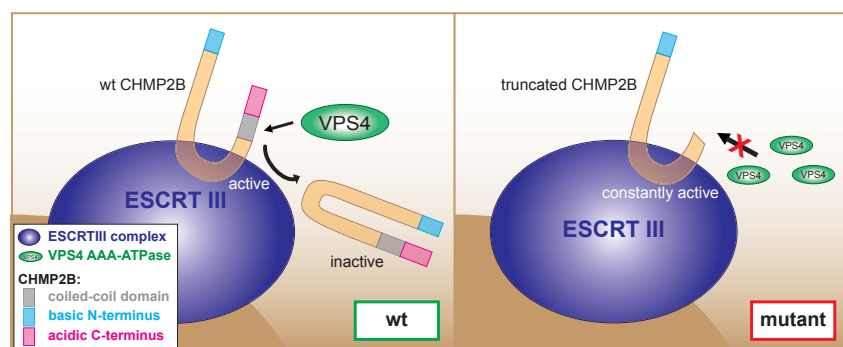


**Figure 1.6: Scheme of wt and mutant CHMP2B**

On the left, wt CHMP2B is depicted which still contains the coiled-coil domain (grey) which allows for VPS4-ATPase binding. After dissociation from the ESCRT III complex (purple), the acidic C-terminus (pink) binds to the basic N-terminus (blue) of wt CHMP2B and thus auto-inhibits the protein. On the right, mutant CHMP2B lacking the coiled-coil domain as well as the C-terminus is depicted. As the VPS4 AAA-ATPase (green) cannot bind to CHMP2B any more, CHMP2B remains bound to the ESCRT III complex. Moreover, due to the missing C-terminus, mutant CHMP2B remains constantly active [304, 201, 83].

Together, this blocks the invagination process and intraluminal vesicle formation that is essential for multivesicular body formation (see also section 1.3.2, page 26) subsequently resulting in endosomal dysfunction [304, 296]. Moreover, the constitutive binding of mutant CHMP2B prevents the recruitment of proteins necessary for endosome-lysosome fusion, like Rab7, a key member of the fusion machinery [120, 294]. Hence, autophagy is likewise impaired leading to the accumulation of p62- and ubiquitin-positive aggregates [71]. However, Rab7 is also implicated in long-range retrograde axonal trafficking [60] and thus, not only endosomal function and autophagy but also axonal transport could be perturbed by the FTLN-linked *CHMP2B* mutations [83]. Indeed, axonal swellings containing mitochondria and vesicles from the endo-lysosomal and autophagy pathways are observed in transgenic *CHMP2B* mutant mice, along with inclusion formation and gliosis [83]. Moreover, Belly *et al.* found that dendritic spine development was heavily impaired in cultured hippocampal neurons of *CHMP2B* mutants [17], further supporting the role of CHMP2B in causing neurodegeneration.

### 1.1.3.1.5 Valosin containing protein (VCP)

Mutations in *VCP* are relatively rare with a mutation frequency of less than 1 % of all familial FTLN cases [239, 270] and are associated with FTLN-TDP. They cause a rare autosomal dominant disorder with disabling muscle weakness called inclusion body myopathy (IBM) associated with Paget's disease of the bone (PDB) and FTLN, in short IBMPFD [316, 307]. However, also familial ALS can result from *VCP* mutations [125]. *VCP* is a highly conserved AAA<sup>+</sup>-ATPase that is implicated in multiple cellular processes especially the ubiquitin-regulated ones i.e. the degradation pathways [292, 317, 313]. Thereby, *VCP* facilitates the extraction of endoplasmic reticulum (ER)-associated degradation (ERAD) substrates, like misfolded proteins, from the ER (figure 1.7). Moreover, it is also involved in their subsequent ubiquitination, and in the delivery of ubiquitinated proteins (ERAD substrates but also cytosolic proteins) to the proteasome for degradation [317] (figure 1.7). Furthermore, *VCP* promotes perinuclear aggresome formation [131, 32] and seems to play an important role in endosomal trafficking [32, 241] (figure 1.7). Also, *VCP* has been implicated to be required for correct dendrite pruning through influencing mRNA metabolism thereby highlighting its importance during neuronal development [249] (figure 1.7). In 2009, Ju *et al.* reported that *VCP* was essential for autophagy and that loss of *VCP* activity leads to autophagosome accumulation due to impaired autophagosome maturation as well as impaired autophagic flux. Interestingly, they also found that subsequently, TDP-43 accumulated in the cytoplasm [131]. Tresse *et al.* additionally showed that *VCP* is essential for autophagosome-lysosome fusion [292] (figure 1.7). Although it is still controversially discussed, impairment of lysosomal degradation in the autophagic pathway rather than proteasomal impairment seems to be the most relevant disease pathomechanism, as no evidence was found that mutations of *VCP* also impaired the ubiquitin-dependent degradation by the proteasome [292].

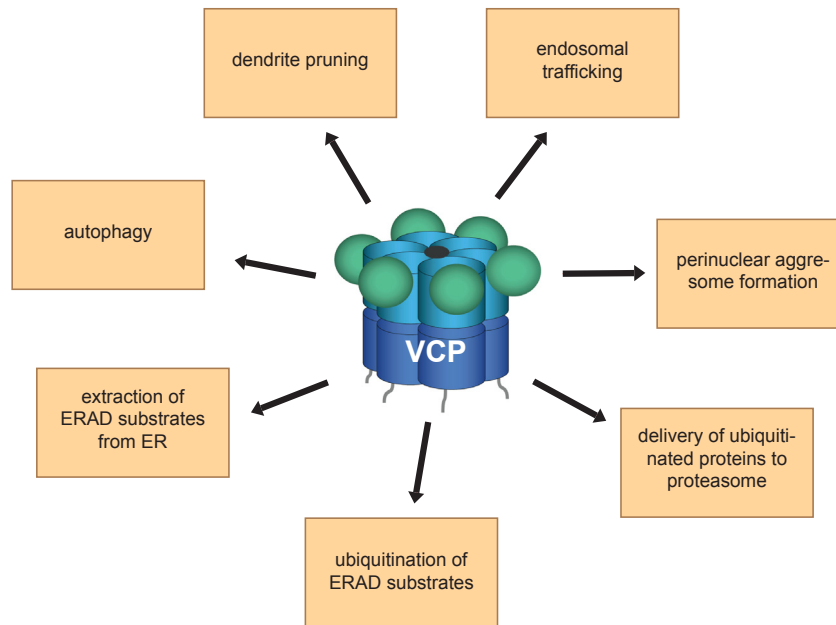


**Figure 1.7: Scheme of VCP functions**

The AAA<sup>+</sup>-ATPase VCP is implicated in many cellular processes [292, 317, 313, 131, 32, 241, 249] (modified from [183]).

#### 1.1.3.1.6 TAR-DNA binding protein 43 (TDP-43) and Fused in Sarcoma (FUS)

Only very few *TARDBP* (three) and *FUS* (one) mutations have been found in FTLD patients indicating that even though they are a major cause for ALS, they only play a limited role in the genetic etiology of FTLD [307, 172]. TDP-43, encoded by the *TARDBP* gene, is a highly conserved RNA-binding protein (figure 1.8) with apparently several thousand targets in the brain (reviewed in [19]). It can continuously shuttle between the nucleus and the cytosol, however, its predominant localization is in the nucleus (reviewed in [19, 172]). Moreover, TDP-43 seems to be involved in further RNA regulation processes namely control of RNA splicing, microRNA processing, local translation in dendritic spines and RNA stability (reviewed in [227, 19]).

FUS belongs to the FUS, Ewing sarcoma breakpoint region 1 (EWS) and TATA-binding protein-associated factor 2N (TAF15) (FET) protein family and is a multifunctional DNA/RNA-binding protein (reviewed in [227, 172]; figure 1.8). Like TDP-43, it shuttles between the cytosol and the nucleus and can bind a large number of RNA targets (reviewed in [227, 172]). Among others, it is involved in mRNA transport, cell proliferation, DNA repair, RNA and microRNA processing and neuronal plasticity (reviewed in [227, 19, 172]).

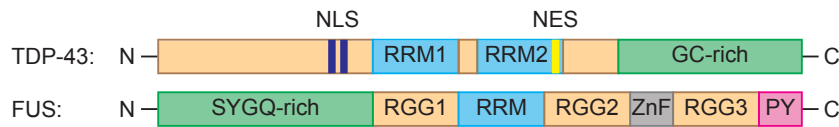


**Figure 1.8: Schematic domain structure of TDP-43 and FUS**

The N-terminal domain of TDP-43 contains the nuclear localization signal (NLS). Then, two RNA recognition motif (RRM) domains follow of which the second one contains the nuclear export signal (NES). The C-terminal part of TDP-43 consists of a glycine (GC)-rich domain. The N-terminus of FUS is a serine-tyrosine-glycine-glutamine-rich (SYGQ)-rich domain which is followed by three arginine-glycine-glycine (RGG) domains, an RRM domain and a zinc-finger (ZnF) domain. The proline-tyrosine (PY)-motif at the C-terminal end of FUS serves as NLS [19] (modified from [19]).

In summary, in the last few years, major progress has been made in the identification of the genes that are causative for familial FTLD. In addition to the *MAPT* gene encoding for tau, *GRN*, *VCP*, *CHMP2B* and, to a minor extent, *TARDBP* and *FUS* mutations as well as *C9orf72* hexanucleotide repeat expansions were found to be crucially involved in the development of FTLD. However, still 23 % of familial FTLD-TDP cases are not caused by any of the known disease genes indicating the presence of other genetic factors that still remain to be elucidated [84].

### 1.1.3.2 Risk factors

#### 1.1.3.2.1 Triggering receptor expressed on myeloid cells 2 (*TREM2*)

One of these risk factors might be *TREM2*, an innate immune receptor [46]. Homozygous loss-of-function mutations of *TREM2* are causative for the so-called Nasu-Hakola disease [211] characterized by multiple bone cyst-like lesions and progressive neurodegeneration predominantly affecting the frontal and temporal lobes [210]. Moreover, recently, *TREM2* mutations were identified in patients with Alzheimer’s disease [128, 91], Parkinson’s disease [237], and ALS [35] suggesting a broader role for *TREM2* in neurodegeneration. Interestingly, homozygous *TREM2* mutations have also been described in patients with early-onset dementia without bone cysts [42] and with bvFTD [91, 85] as well as in patients with clinically diagnosed FTLD [237, 24, 55] implying that *TREM2* mutations might confer a risk for developing FTLD.

*TREM2*, a type I transmembrane glycoprotein [46], is expressed on osteoclasts, immature dendritic cells, activated macrophages and microglia [46], but not on neurons [113]. It has been reported to play a role in various signalling events including differentiation of dendritic cells and osteoclasts, immune response and phagocytosis [208, 113, 285]. In the brain, *TREM2* promotes phagocytosis of apoptotic neurons without eliciting inflammation [113, 285]. Mutations in *TREM2* causing FTD-like disease result in decreased surface localization of the protein due to severe transport deficits and thus impaired *TREM2*-mediated phagocytosis [139]. Interestingly, the p.R47H mutation, that represents as a risk factor for AD, only showed a mild effect on *TREM2* maturation compared to the severe phenotype of the p.Y38C and p.T66M mutations

that are considered causative for FTLD when in a homozygous state [139, 91]. This might be in line with the p.R47H mutation being a risk factor.

#### 1.1.3.2.2 Transmembrane protein 106B (*TMEM106B*)

Another factor is *TMEM106B*, which was discovered in a genome-wide association study (GWAS) in 2010 designed to identify susceptibility loci for FTLD-TDP [301]. Until then, *TMEM106B* was an uncharacterized protein of unknown function. However, while I was working on this *TMEM106B* study, results about *TMEM106B* function in health and disease were achieved which are presented in the following section.

## 1.2 Transmembrane protein 106B

*GRN* mutations have a reduced penetrance and patients show variable ages of disease onset [301] which indicates that there are additional factors that modulate FTLD disease progression. Therefore, a GWAS was performed in a homogeneous population of either pathologically or genetically confirmed FTLD-TDP cases in order to identify new genetic modulators [301, 307]. Thereby, twelve single-nucleotide polymorphisms (SNPs) of which three reached genome-wide significance mapped to a 68 kb interval located on chromosome 7p21.3 implicating that this might be a common genetic susceptibility locus for FTLD-TDP [301]. Within this region, only one gene was located namely the gene encoding for the previously uncharacterized transmembrane protein 106B (*TMEM106B*). The most significantly associated SNPs lay within intron 3 or 5 (rs1020004, rs6966915) or 6.9 kb downstream (rs1990622) of this gene (see also figure 3.1 a). Thereby, in FTLD-TDP patients, the frequency of the protective minor allele of the associated SNPs was significantly decreased. In three subsequent studies, *TMEM106B* could be confirmed as risk factor for FTLD-TDP [51, 72, 306]. Moreover, another SNP, rs3173615 (C/G), that was in perfect linkage disequilibrium to the top SNP rs1990622 (T/C) was identified as a coding variant in *TMEM106B* dictating an amino acid change from threonine (disease-associated) to serine (protective) at position 185 within the *TMEM106B* gene (p.T185S) (see also figure 3.1 a) [72, 200].

Apart from these genetic studies, nothing was known about *TMEM106B* at the beginning of my studies. However, while working on *TMEM106B*, results about *TMEM106B* function in health and disease were achieved. These are summarized below.

*TMEM106B* is a highly conserved protein with two paralogues, *TMEM106A* and *TMEM106C*, with a sequence homology of 49 % and 47 %, respectively [257]. Even though more data is needed to verify their localization, both paralogues probably reside in the lysosomal membrane [26, 277]. Of note, *TMEM106A* is associated with breast cancer [81] whereas *TMEM106C* represents a positional and functional candidate for *arthrogryposis multiplex congenita* (AMC) [82], a disease where multiple contractures of the joints and muscle weakness occurs [95].

TMEM106B comprises seven coding exons [66]. Its transcript length is approximately 12.5 kb and eight different splice variants are annotated [66]. The translation length of TMEM106B is 274 amino acids with a predicted molecular weight of 31.12 kDa [66].

### 1.2.1 Biochemical characteristics of TMEM106B

I found that TMEM106B is a type II transmembrane protein with five N-glycosylation sites of which the two most C-terminal ones are complex glycosylated [155] (see also sections 3.2, page 49; 3.2.2, page 51 and 3.4, page 57). In the brain, TMEM106B is highly expressed, especially in neurons [263, 34, 39] and microglia, but also in cells surrounding blood vessels [34]. Moreover, it shows a polarized, perikaryal distribution in neurons [34], where TMEM106B localizes to late endosomes and lysosomes [263, 39], which is also observed in cultured cells [155, 25, 39] (see also section 3.3, page 53). Interestingly, in FTL-D-TDP patients, TMEM106B appeared more widely distributed throughout the cell body, which was especially prominent in *GRN* mutation carriers [39, 34].

Furthermore, TMEM106B seems to be cleaved by lysosomal hydrolases to create a stable N-terminal fragment (NTF) before it undergoes regulated intramembrane proteolysis (RIP) mediated by SPPL2a and, to a minor extent, by SPPL2b [26]. Thereby, a highly unstable intracellular domain (ICD) is produced which is located in the lysosome implying that RIP processing probably serves as a quality control system that allows for the removal of excess TMEM106B thereby controlling TMEM106B levels [26]. Interestingly, the lysosomal degradation rate of the protective S185 TMEM106B isoform seems to be faster than of the risk variant (T185) [200]. Moreover, TMEM106B has been implicated in lysosomal trafficking [263, 277] and might play a role in lysosomal stress response [277], data which still have to be confirmed. Hence, the endogenous function of TMEM106B as well as its role in FTL-D-TDP disease progression are still unknown and remain to be elucidated.

### 1.2.2 The relationship between TMEM106B and GRN

Accumulating evidence suggests a relationship between TMEM106B and GRN [72, 301] as an increase in TMEM106B mRNA and protein levels was found to be especially associated with *GRN* mutation carriers [301, 87]. Moreover, homozygosity of the risk allele of rs1990622 seems to be associated with decreased levels of GRN in the plasma of patients as well as of healthy controls arguing for a generally increasing risk for FTL-D-TDP in the population and modifying the age-at-onset in *GRN* mutation carriers [72, 51]. However, these data have not been confirmed, yet [51]. Additionally, some overexpression studies suggested that increased TMEM106B levels would subsequently increase GRN levels [39, 200, 25] whereas others could not detect any correlation between TMEM106B and GRN expression levels [155, 257, 77]. Thus, it is still under debate whether TMEM106B and GRN influence each other directly or through acting in a common pathway.

### 1.2.3 Interaction partners of TMEM106B

It was suggested that two microRNAs (miRs) of the miR-132 cluster, miR-132 and miR-212, can bind to the 3' UTR of *TMEM106B* thereby repressing its expression [39]. Interestingly, this miR-cluster seems to be downregulated in FTLD-TDP patients [39].

Moreover, in a yeast-two-hybrid study, the N-terminus of TMEM106B was reported to interact with a subunit of AP-2 and clathrin [277] as well as with VPS11 [277], a class C protein of the homotypic fusion and protein sorting (HOPS) complex and the class C core vacuole/endosome tethering factor (COVERT) [140], and VPS13D [277], which is implicated in the delivery of proteins to the vacuole [212]. Additionally, the microtubule-associated protein 6 (MAP6), also known as stable tubule-only polypeptide (STOP), was claimed to be an interaction partner of TMEM106B [263]. Interestingly, even though these interaction partners of TMEM106B have not yet been confirmed by others, they indicate that TMEM106B might play a role in endocytic vesicle maturation, their delivery to lysosomes [277] and late endosomal/lysosomal trafficking [263].

### 1.2.4 Impact of TMEM106B on cognition

In 2010, it was observed that ALS patients with the protective alleles of *TMEM106B* were significantly associated with preserved cognition compared to matched controls implying that TMEM106B might affect cognitive impairment in ALS [309]. Moreover, *in vitro* studies suggest that TMEM106B might influence dendritic branching [263, 277]. Interestingly, a recent study with asymptomatic carriers of the *GRN Thr272fs* mutation revealed that *TMEM106B* polymorphism modulates brain connectivity as homozygosity for the risk allele (T/T) was associated with decreased connectivity within the ventral salience and the left frontoparietal network [224]. In addition, the *TMEM106B* risk allele of rs1990622 might decrease the volume of temporal brain regions, especially the left hemisphere, and the interconnectivity of the temporal lobes not only in FTLD patients but also in healthy elderly affecting structures important for language [1]. Therefore, the risk allele of rs1990622 is probably associated with cognitive decline which seems not to be restricted to FTLD-TDP.

### 1.2.5 TMEM106B in other neurodegenerative diseases

In 2014, TMEM106B has also been found to be a modifier of FTLD with *C9orf72* hexanucleotide repeat expansions [77, 299]. Van Blitterswijk *et al.* reported that homozygosity for the minor allele of the rs3173615 variant of *TMEM106B*, a SNP that is in perfect linkage disequilibrium with the top SNP rs1990622, protects carriers of *C9orf72* repeat expansions from developing the disease [299]. Moreover, patients that were homozygous for the protective minor allele showed a decreased TDP-43 burden compared to those with the risk allele implying that TMEM106B might also influence TDP-43 [299]. Gallagher *et al.* confirmed that TMEM106B affects risk for FTLD in the *C9orf72* expansion carriers to about the same extent than in *GRN*

mutation carriers [77]. However, in contrast, Lattente *et al.* recently reported that the *C9orf72* expansion did not correlate with *TMEM106B* genotypes [156]. Therefore, it is still under debate whether *TMEM106B* indeed is also a genetic modifier in FTLD-DPR caused by a hexanucleotide expansion in *C9orf72*.

Interestingly, not only FTLD but also ALS and AD seem to be influenced by *TMEM106B*. As already mentioned (see section 1.2.4), *TMEM106B* might affect cognitive decline in ALS as protective alleles of *TMEM106B* were significantly associated with preserved cognition [309]. In AD, patients with TDP-43 pathology revealed a highly significant decrease in the frequency of the minor (protective) allele of *TMEM106B* compared to cases without TDP-43 pathology [250]. Moreover, the risk allele (T) for rs1990622 was found to be strongly associated with late-onset AD (LOAD) in *apolipoprotein E (APOE) $\epsilon$ 4* allele carriers [165]. *APOE $\epsilon$ 4* is a risk factor for LOAD [259, 282] and has been reported to decrease the age-at-onset in homozygous carriers of AD as well as FTLD patients [50, 184]. Interestingly, recently, mRNA levels of *TMEM106B* have been found to be reduced, and concomitantly, *GRN* mRNA levels to be increased in AD patients [257].

### 1.3 Lysosomal function in protein degradation

Neurodegenerative diseases such as Alzheimer's, Parkinson's and Huntington's disease as well as FTLD are proteinopathies characterized by progressive neuronal dysfunction accompanied by a selective loss of neurons [326] and the presence of aggregates (inclusions) in cells of the target tissues [235, 79]. In many cases, the accumulation of aggregate-prone mutant protein correlates with the severity of the disease [235]. Thus, clearance of these proteins and aggregates is particularly important in post-mitotic cells, which cannot dilute their toxic burden by cell division [235, 319, 158]. Accordingly, neurons are especially vulnerable to an alteration in protein degradation which can cause protein accumulation and cytotoxicity ultimately leading to neurodegeneration [158].

One of the intracellular clearance pathways is the ubiquitin-proteasome system which operates through the proteasome, a barrel-shaped, multi-protein complex that predominantly degrades short-lived cytosolic and nuclear proteins as well as retro-translocated, misfolded ER proteins which usually have been covalently modified with polyubiquitin [149]. The second one is the autophagy-lysosome pathway where bulky substrates or substrates with a long half-life are sequestered by double-layered membranes before being directed to the lysosome where they are degraded [149].

While examining the biochemical characteristics of *TMEM106B*, I found that *TMEM106B* is a lysosomal transmembrane protein which might be involved in autophagy. Therefore, in the following sections, the characteristics of lysosomes and their most important components, the two different routes of lysosomal degradation, endolysosomal sorting (heterophagy) and autophagy, as well as the regulation of lysosomal degradation are described in more detail.

### 1.3.1 General information about lysosomes

Lysosomes that have been discovered by Christian de Duve in 1949 (reviewed in [57]) are ubiquitous, membrane-delimited organelles which are primarily involved in recycling and degradation [148, 251, 252]. However, they are not only the “waste bin” of the endocytic pathway, but are involved in many different physiological processes including metal ion homeostasis [188], intracellular calcium homeostasis [10], bone and tissue remodelling, plasma-membrane wound repair [179], pathogen defense, cholesterol homeostasis, membrane repair, cell death [252] and immune response [262]. Aside from their acid pH ( $\leq 5$ ) and the absence of the mannose-6-phosphate receptor which distinguishes them from endosomes, lysosomes are characterized by more than 50 soluble acid hydrolases (with a pH optimum below 6 [251]) and over 120 highly glycosylated lysosomal membrane proteins [27, 252].

Lysosomal hydrolases are activated in the acidic environment of the lysosome by proteolytic cleavage and are responsible for the degradation of the material that has been targeted to the lysosome, i.e. proteins, lipids, carbohydrates and nucleic acids [251]. Two examples for typical lysosomal hydrolases are cathepsin D and B. Cathepsin D is an aspartic endopeptidase with numerous physiological functions including metabolic degradation of intracellular proteins, activation and degradation of polypeptide hormones and growth factors, activation of enzymatic precursors, processing of enzyme activators and inhibitors, brain antigen processing and regulation of programmed cell death [18, 47]. Cathepsin B is a cysteine protease with exo- and endopeptidase function [48]. Like cathepsin D, it plays a role in the apoptosis of immune cells as reactive-oxygen-species-dependent release of the enzyme into the cytosol results in the activation of a pro-apoptotic factor [48] leading to T-lymphocyte death. Furthermore, cathepsin B is required for toll-like-receptor signalling and tumor necrosis factor  $\alpha$  (TNF $\alpha$ ) production [48].

However, the most abundant lysosomal components are the lysosome-associated membrane proteins LAMP1 and LAMP2. [262]. As both proteins form a continuous carbohydrate lining on the inner leaflet of lysosomes, they were suggested to be important for the maintenance of the structural integrity of the lysosomal membrane [117]. Furthermore, as LAMP1 and LAMP2 contribute to about 50 % of all lysosomal membrane proteins [67], they are used as lysosomal markers. Loss-of-LAMP2-protein-mutations in humans can cause a fatal cardiomyopathy and myopathy associated with mental retardation, called Danon disease, which is characterized by the accumulation of late autophagic vacuoles in the heart and skeletal muscle which might impair the turnover of mitochondria [202, 67]. Yet, the most severe phenotype was reported in mice where both *LAMP1* and *LAMP2* had been knocked out. They presented with embryonic lethality along with abnormally high amounts of autophagic vacuoles and accumulated non-esterified cholesterol [68] as well as defects in phagosome maturation due to impaired organellar motility [117]. Moreover, lysosomes were more dispersed and phagosome and lysosome migration towards the microtubule-organizing center (MTOC) was delayed [248]. These results clearly highlighted

that both LAMPs are essential for many cellular mechanisms far beyond their initially suggested role in maintaining the structural integrity of the lysosomal membrane [67].

### 1.3.2 Lysosomal degradation through endolysosomal sorting

Extracellular macromolecules destined for lysosomal degradation can be ingested by the cell by several different mechanisms. The best studied route is receptor-mediated endocytosis via clathrin-coated pits. However, there are also non-clathrin-mediated pathways like phagocytosis, caveolae-mediated uptake, macropinocytosis and a constitutive cholesterol-sensitive uptake pathway carrying lipid rafts to the Golgi complex [167].

Transmembrane proteins targeted for the lysosome are ubiquitinated and reach the lysosome via multivesicular bodies (MVBs), a morphologically distinctive late endosome that accumulates internally small membrane vesicles containing the cargo protein (figure 1.9) [69]. To form these internal vesicles, the ESCRT machinery binds to the ubiquitin subunits attached to the targeted molecule and mediates the invagination and constriction of small luminal vesicles (figure 1.9) [69].

For cargo transport to the lysosome, four models have been proposed (figure 1.10). The first one is the maturation model suggesting that endocytic vesicles mature into early endosomes, late endosomes and subsequently into lysosomes where the cargo molecule is degraded, by the gradual addition of lysosomal in exchange for late endosomal components (figure 1.10) [280]. Another possibility is the formation of an endocytic carrier vesicle that buds from the late endosome and delivers its content to the lysosome (figure 1.10) [89, 168]. In the *kiss and run* model, late endosomes and lysosomes transiently fuse which allows an exchange of contents between these organelles before they depart again (figure 1.10) [28, 281]. The fourth model, so-called direct fusion or hybrid model, suggests that endosomes and lysosomes permanently fuse to form a hybrid organelle that contains late endosomal and lysosomal components. By selective retrieval of late endosomal components, lysosomes are subsequently re-formed (figure 1.10) [168, 28, 75, 166]. Even though all four models might not be mutually exclusive, the two most probable means of delivery are *kiss and run* events and direct fusion [167, 188].

The fusion events between late endosomes and lysosomes occur mainly in the juxtannuclear region of the cell, also called MTOC where late endosomes and lysosomes are concentrated [168]. Late endosomal and lysosomal positioning at the MTOC thereby reflects the balance of long-range bidirectional movement of late endosomes and lysosomes on microtubules and short-range movement on actin filaments. In both cases, the movement is mediated by motor proteins and proteins that are required for the optimal attachment of these motors to late endosomes and lysosomes [168, 177]. Two of these proteins are the small GTPase Rab7, which associates with late endosomes [322], and the Rab7 effector RAB7-interaction lysosomal protein (RILP). Both are responsible for the attachment of the dynein-dynactin motor complex that mediates the retrograde transport of lysosomes [129].

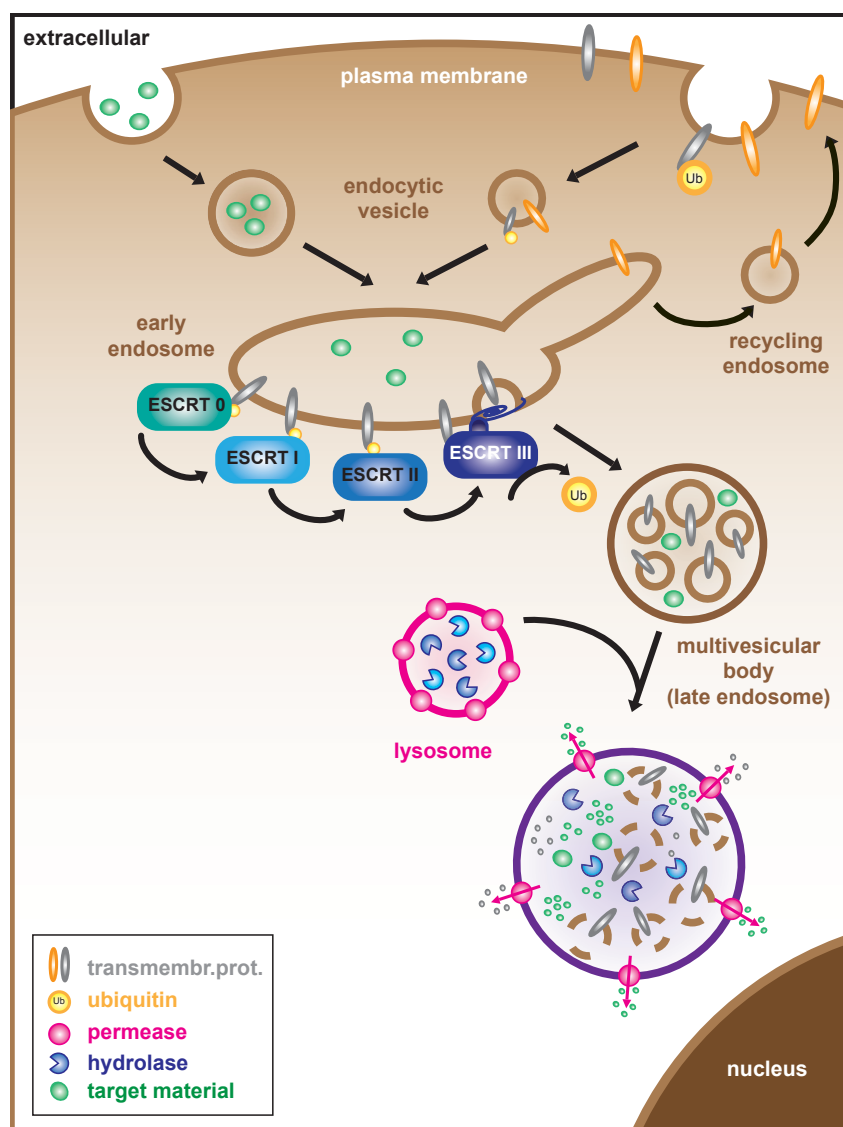


**Figure 1.9: The endocytosis pathway**

Surface transmembrane proteins that are destined for degradation are ubiquitinated before being internalized [69] whereas extracellular molecules are directly endocytosed [167]. To facilitate the degradation of the transmembrane proteins, the ESCRT machinery assembles (ESCRT0-III) at the endosomal membrane and mediates their sorting into small luminal vesicles. The resulting multivesicular body can subsequently fuse with the lysosome followed by the degradation of the vesicles and their cargo proteins by its enzymes [69] (modified from [71]).

### 1.3.3 Lysosomal degradation through autophagy

In eukaryotic cells, intracellular proteins can either be degraded by the ubiquitin-proteasome system or by the autophagic pathway that involves degradation through lysosomes [288]. Whereas the first is limited primarily to targeting individual proteins for destruction, larger structures including aggregated, misfolded or long-lived proteins, dysfunctional organelles or even pathogens can be degraded via autophagy (Greek words for “self” and “eating”) [142]. Constitutive, basal

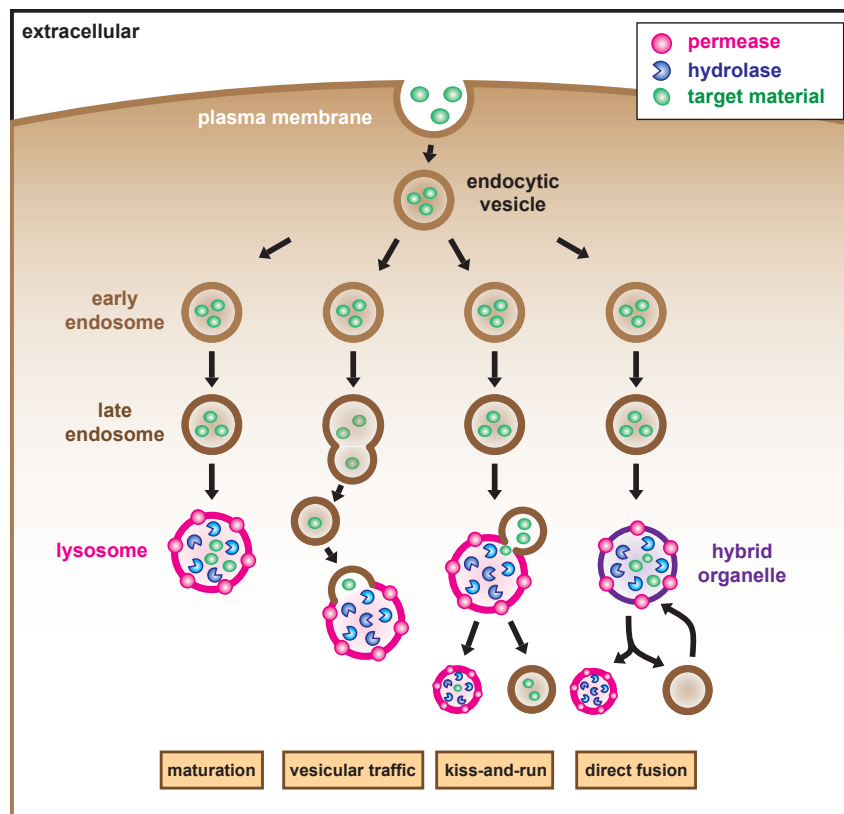


**Figure 1.10: Models for cargo transport to the lysosome**

Cargo is internalized via endocytosis and subsequently transported to the lysosome, where four different trafficking models have been suggested. The maturation model proposes that the endocytic vesicle matures from an endosome to a late endosome and finally to the lysosome by changing its protein composition. The second model postulates that a vesicle buds from the late endosome which delivers the proteins destined for degradation to the lysosome. In the third model, late endosomes and lysosomes transiently fuse (kiss) to exchange proteins and subsequently depart again (run). Finally, the fourth model presumes that the late endosome directly fuses with the lysosome to form a hybrid organelle from which lysosomes can be re-formed by selective retrieval of late endosomal components [168] (modified from [168]).

autophagy that occurs under nutrient-rich conditions serves as a quality control mechanism and maintains cellular homeostasis as it protects cells from the consequences of dysfunctional organelles and proteins [98, 69]. Furthermore, autophagy can be induced by extra- and intracellular signals like glucose-, amino acid- and serum-starvation, oxidative stress (hypoxia), growth factors, ceramide and lysosomal or ER stress [288] leading to a massive increase in the autophagic flux, i.e. the rate at which autophagic vacuoles are processed by lysosomes [221]. Abnormalities in autophagy not only contribute to pathologies like tumorigenesis and certain muscle diseases, but also to various neurodegenerative diseases because postmitotic cells are particularly susceptible to the accumulation of defective proteins or organelles as they cannot dilute their amount by cell division [174, 99, 247, 319].

There are three different types of the autophagic pathway, namely microautophagy, chaperone-mediated autophagy (CMA) and macroautophagy, the latter of which people are usually referring to when they talk about autophagy (figure 1.11) [288].

Microautophagy involves the direct sequestering of cytosolic vesicles by lysosomes without the formation of nascent vacuoles (figure 1.11) [288, 221]. CMA is a selective form of autophagy. It targets cytosolic proteins with a specific pentapeptide signal sequence called the KFERQ motif which is recognized by the heat shock cognate protein of 70 kDa (Hsc70), a molecular chaperone [221, 288]. The substrate-bound Hsc70 subsequently docks on lysosomes via binding to LAMP2a. This transmembrane protein of the lysosome acts as a receptor for CMA and participates in the translocation of unfolded proteins into the lysosome (figure 1.11) [221, 288]. Interestingly, CMA, which plays an important role in quality control but also in stress response, has only been described in mammals and shows some distinct features [160]. Firstly, it selectively targets non-essential proteins for degradation to obtain amino acids required for the synthesis of essential proteins [160]. Secondly, it removes specific proteins that were damaged under stress conditions without interfering with the still functional forms of the same protein as the KFERQ motif is only accessible when the protein is not folded correctly [160]. Notably, as levels of LAMP2a are limited, the process of translocation can become saturated which makes a tight regulation of CMA crucial [160].

Macroautophagy, hereafter referred to as autophagy, evolved as both, an adaptation of the eukaryotic cell to starvation and a quality control mechanism to protect against damage caused by dysfunctional proteins and organelles [123, 244]. It involves the bulk sequestration of cytosolic content including large protein complexes and organelles into autophagic vesicles, so-called autophagosomes (figures 1.11 and 1.12) [221, 142]. In order to meet this challenge, a high degree of flexibility and different vesicles sizes (0.5  $\mu\text{m}$  to 1.5  $\mu\text{m}$ ) are needed [142, 244]. As a first step, a pre-autophagosome or phagophore is formed in the cytosol as a cup-shaped structure (figure 1.12) [97, 284]. However, the origin of the phagophore still remains elusive [142] as reports state that the membranes could be either derived from mitochondria, the ER, the plasma membrane or even from several distinct locations [247]. The nucleation of the phagophore is controlled by the lipid kinase hVPS34, which forms a complex with ATG14L, beclin-1 and hVPS15 and produces phosphatidylinositol 3-phosphate (PI3P) that subsequently recruits factors promoting phagophore nucleation [244]. After autophagy initiation, the phagophore double membrane elongates sequentially, probably via homotypic fusion events, thereby actively engulfing its cargo [142, 247]. This step is regulated by two ubiquitination-like reactions of which the second involves the conjugation of microtubule-associated protein 1 light chain 3 (LC3), GABARAP and GATE-16 to the phospholipid phosphatidylethanolamine (PE) [247]. LC3 or more precisely its autophagosome membrane-bound, PE-conjugated form LC3II is a well-known autophagosomal marker protein as it can be nicely distinguished from its soluble, cytosolic form LC3I [247, 288, 98]. Subsequently, the double membrane structure closes to form the autophagosome (figure 1.12) [288, 69]. Normally, autophagosomal vesicles that appear randomly throughout the

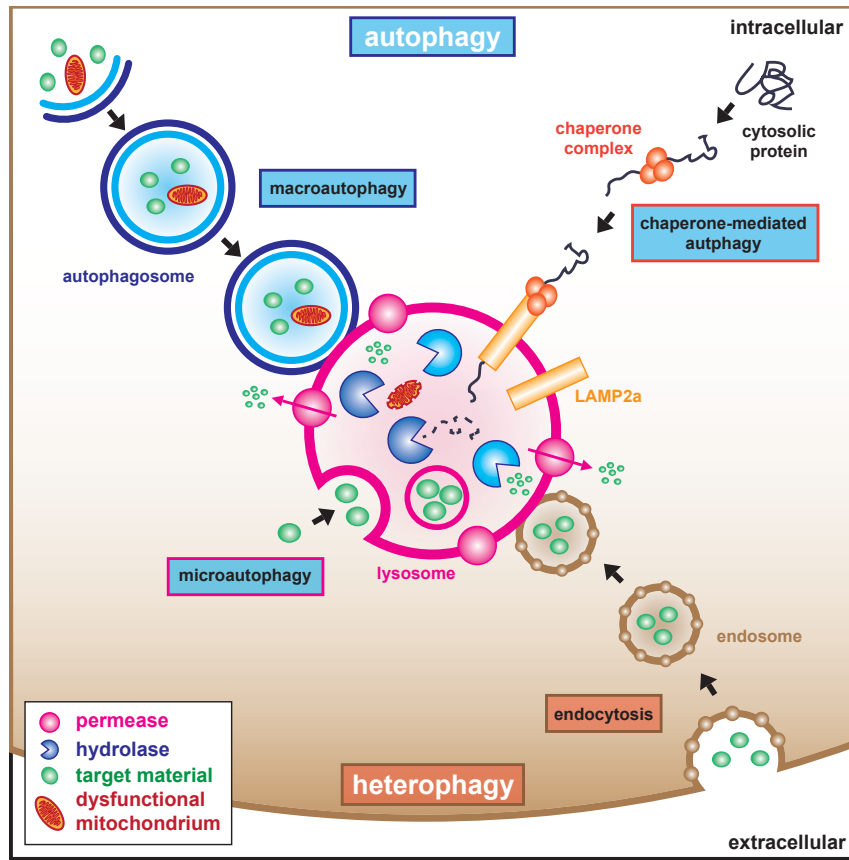


**Figure 1.11: Lysosomal degradation within the mammalian cell**

Proteins destined for degradation are either delivered to the lysosome from the extracellular media (heterophagy) or from the intracellular compartment (autophagy). For the latter, three different types have been proposed: macroautophagy, chaperone-mediated autophagy and microautophagy. Whereas lysosomes directly internalize cargo during microautophagy, in macroautophagy, intracellular components are sequestered in autophagosomes that subsequently fuse with lysosomes. In chaperone-mediated autophagy, substrate proteins are selectively recognized and transported to the lysosome where they are translocated into the lysosomal lumen by LAMP2a [176] (modified from [176]).

cytoplasm, traffic, while they are maturing, along microtubules towards the MTOC, where lysosomes are concentrated [247, 174].

Along the way, autophagosomes may fuse with endosomes to form amphisomes (figure 1.12) that are enriched in proteins of early endosomes, like early endosome antigen 1 (EEA1), and of late endosomes, like mannose 6-phosphate receptors (MPRs) [69]. Finally, either the outer membrane of the autophagosome or of the amphisome, which is already more acidic than the autophagosome and represents a pre-lysosomal compartment, fuses with the lysosome (figure 1.12). Following this autolysosome formation, the inner vesicle containing the sequestered cargo as well as the cargo itself are degraded by lysosomal hydrolases and the degradation products are released through membrane permeases (figure 1.12) [69, 247, 142].

Even though (macro-) autophagy has been considered to be a very unselective process for bulk sequestration of long-lived proteins and organelles during starvation to restore the energy bal-

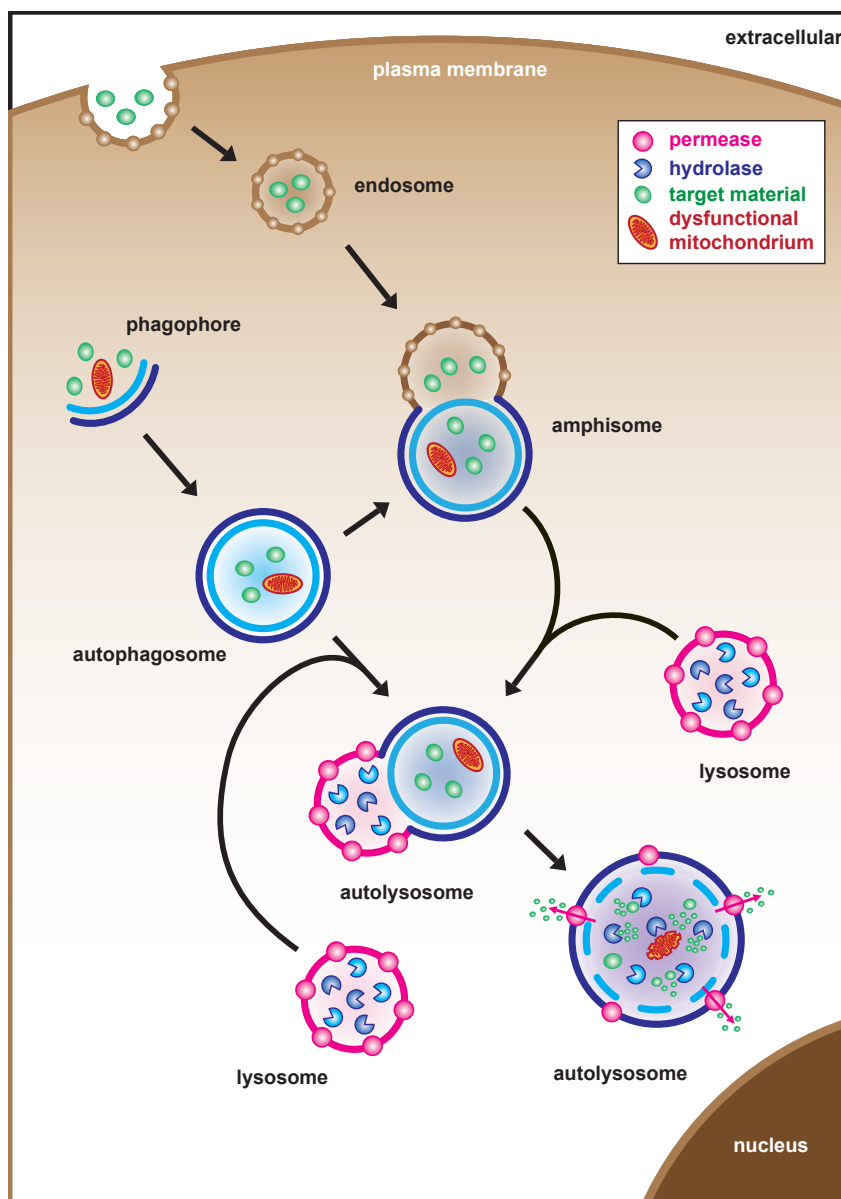


**Figure 1.12: The process of macroautophagy**

Autophagy is initiated by the formation of a phagophore that expands into an autophagosome while engulfing a portion of the cytosol. During the movement towards the MTOC, autophagosomes can fuse with endosomes forming amphisomes. Finally, the autophagosome or amphisome fuses with the lysosome which supplies the acid hydrolases required for the degradation of the inner membrane of the autophagosome or amphisome and subsequently their content. The resulting macromolecules are released through permeases into the cytosol [141] (modified from [141]).

ance of the cell, recently, evidence mounted of selective autophagic degradation operating during nutrient-rich conditions [244, 123]. Selective autophagy is mediated by specific autophagic receptors such as sequestosome-1 (p62/SQSTM1) and neighbour of Brca1 gene (NBR1) which both show a strong oligomeric potential [244] and recognize their cargo by binding to unfolded

regions of a protein or to conjugated ubiquitin (Ub), a universal signal for degradation [137, 123].

P62, the first described mammalian selective autophagy receptor [22], interacts with ubiquitin, preferentially mono-ubiquitin (at Lys63), via its Ub-associated (UBA) domain [123]. However, ubiquitin binding can be inhibited by homo-polymerization of p62 via its Phox and Bem 1p (PB1) domain [123]. To mediate selective autophagy, the ubiquitinated substrate (protein aggregates, organelles or pathogens) recruits p62 which sequesters its target into larger units or aggregates, also called p62 bodies [123, 319]. Subsequently, non-covalent binding of the LC3-interaction region (LIR) of p62 [244] to LC3 mediates the recruitment of the phagophore. This process might be further supported by aggregation which itself is a signal for degradation. Following phagophore recruitment, the autophagosome forms around the aggregated substrate [123].

P62 is involved in many cellular processes like NF $\kappa$ B signalling pathways, bone remodelling, obesity, oxidative and proteotoxic stress response, cell spreading and cancer development [123]. Furthermore, it was also suggested to affect both pro-survival and pro-apoptotic signalling pathways and to play an important role in innate immunity [123].

Like p62, NBR1 is also involved in the recruitment of ubiquitin-positive cargo via cross-linking [137, 244]. Interestingly, both, p62 and NBR1, accumulate in inclusion bodies upon autophagy inhibition [137, 244]. Moreover, p62 is detected in most of the cytoplasmic and nuclear protein aggregates found in human diseases, like FTLN with *C9orf72* hexanucleotide expansions [187] or Huntington's disease [191]. However, recruitment of p62 is considered to be a secondary mechanism promoted by the ubiquitination of aggregates which had been induced by other proteins [123, 191]. Interestingly, accumulation of p62 due to impaired autophagy compromises the ubiquitin-proteasome system. This results in increased levels of proteasome substrates because p62 competes with other ubiquitinated proteins for delivery to the proteasome [149]. Thus, not only aggregation-prone proteins but also short-lived regulatory proteins like p53 or  $\beta$ -catenin accumulate leading to deleterious consequences [149].

### 1.3.4 Regulation of lysosomal degradation

In 2009, Sardiello *et al.* identified a gene network that regulates lysosomal biogenesis and function [254]. They found that the palindromic GTCACGTGAC motif, they called CLEAR element, was highly enriched in the promoter region of many lysosomal genes. The transcription factor TFEB is able to bind to the CLEAR motif thereby upregulating lysosomal and autophagosomal gene expression, like the expression of cathepsin D or p62, and is thus considered as a master regulator for genes of the autophagy-lysosome pathway [209, 266].

In resting cells, TFEB is mainly located in the cytoplasm with focal concentrations associated with lysosomes [243]. Roczniak-Ferguson *et al.* were able to show that mTORC1, located at the surface of lysosomes under nutrient-rich conditions, recruits TFEB to lysosomes and mediates TFEB phosphorylation (figure 1.13) [243]. In turn, phosphorylated TFEB binds to 14-3-3 proteins in the cytosol whose binding masks the nuclear localization signal (NLS) of TFEB thereby

preventing its translocation to the nucleus as well as subsequent transcriptional activation of autophagosomal and lysosomal genes (figure 1.13) [243, 267].

However, upon cellular stress signals like starvation or an increase of intracellular pH, mTORC1 translocates from the lysosomal surface [150] and hence, TFEB is not phosphorylated and thus inhibited any longer leading to enhanced accumulation of TFEB in the nucleus (figure 1.13) [243, 266, 254].

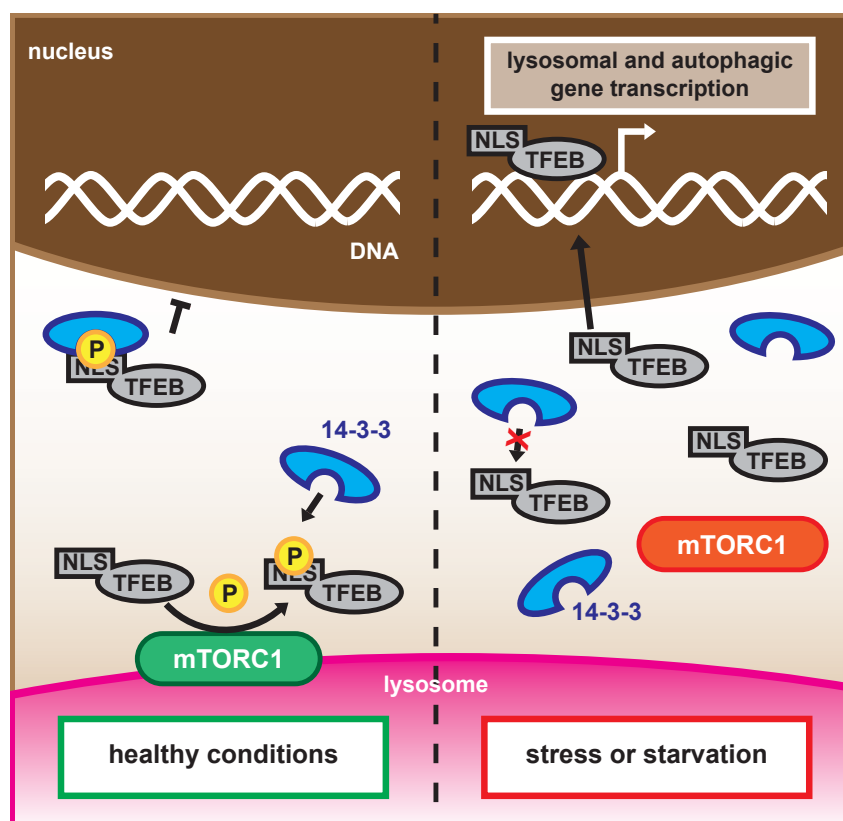


**Figure 1.13: Model of the TFEB signalling pathway**

Under healthy conditions, the mTORC1 complex is localized at the lysosomal membrane and mediates the phosphorylation (P) of the transcription factor EB (TFEB). Consequently, the 14-3-3 protein is able to bind to TFEB which masks the nuclear localisation signal (NLS) of TFEB thereby sequestering it in the cytosol [243]. However, under stress or starvation, mTORC1 detaches from the lysosome resulting in its inactivation. Thus, TFEB is no longer phosphorylated, 14-3-3 proteins cannot bind and TFEB translocates to the nucleus where it promotes the transcription of autophagic and lysosomal genes [267] (modified from [267, 243]).

Moreover, upon starvation and the associated increase in intracellular pH, lysosomes change their localization and mainly cluster at the MTOC (figure 1.14) probably due to a pH-dependent loss of proteins that regulate the anterograde transport of lysosomes [150]. This favours autophagosome-lysosome fusion which together with an increased synthesis of autophagosomal and lysosomal proteins enhances autophagy-mediated nutrient release and therefore enables subsequent cell survival under starvation conditions (figures 1.13 and 1.14) [150]. Interestingly, lysosomal positioning was also shown to modulate mTORC1 activity as the overexpression of kinesins KIF2A

and KIF1B- $\beta$ , that promote the anterograde transport of lysosomes, as well as of the ARF-like GTPase ARL8B, which is also involved in lysosomal trafficking [7], increased mTORC1 activity. Conversely, their knockdown decreased peripheral positioning and subsequently mTORC1 activity [150, 223].

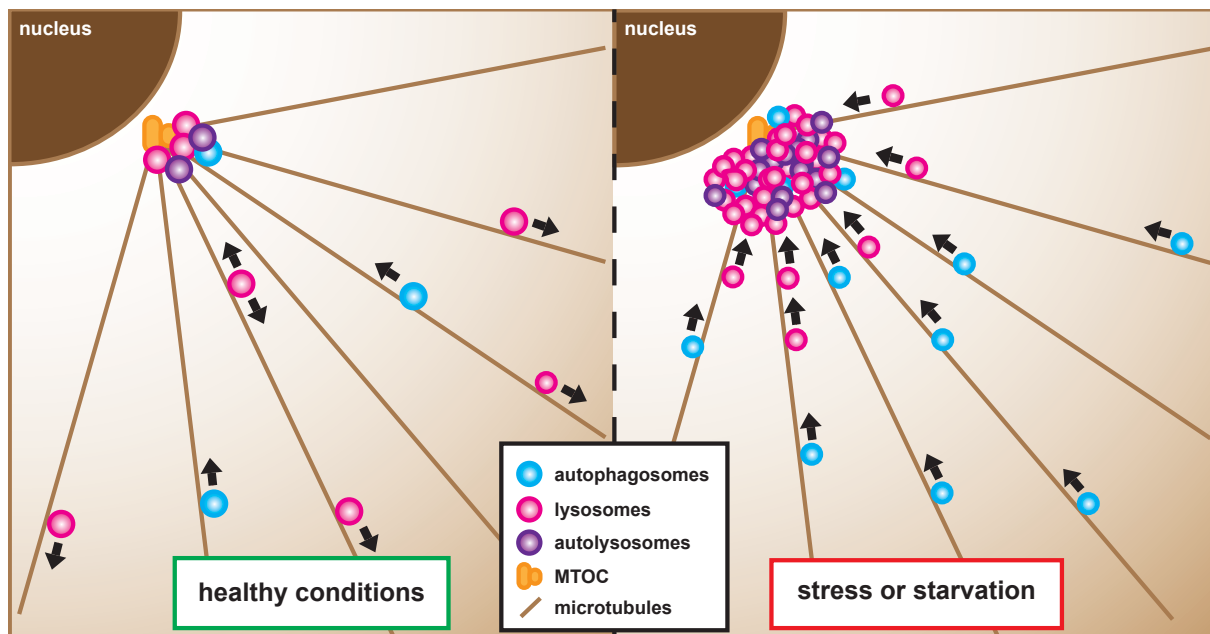


**Figure 1.14: Lysosomal positioning modulates autophagy**

Under healthy, nutrient-rich conditions, mTORC1 activity is high which blocks lysosome and autophagosome biogenesis. Moreover, autophagy is inhibited facilitated by the mainly peripheral localization of lysosomes [150]. However, upon lysosomal stress or starvation, mTORC1 activity decreases leading to the activation of lysosome and autophagosome synthesis. Also, lysosomes cluster at the MTOC which promotes autophagosome-lysosome fusion [150] (modified from [150]).

Another pathway in starvation response involves the regulation of membrane protein degradation [127]. Thereby, during stress conditions or after initiation of autophagy, a specific set of plasma membrane proteins that is not essential for survival is increasingly endocytosed [127]. Moreover, the efficiency of MVB sorting is enhanced through the downregulation of increased sodium tolerance protein 1 (Ist1) which in turn promotes efficient VPS4 recruitment to endosomes, a protein that is required for the release of the ESCRT machinery from the endosomal membrane allowing for further MVB formation [127]. These two mechanisms provide an immediate source of amino acids during the time of acute starvation and enable the synthesis of starvation-response proteins which are vital for the cell to adapt to stress conditions until the major starvation-response system, autophagy, is fully active [127]. Therefore, the MVB pathway is essential for the initial phase of starvation response (first one to two hours), but is subsequently replaced by the long-term starvation response pathway, autophagy [127, 6].

## 1.4 Lysosomal dysfunction in neurodegenerative diseases?

Neurons are postmitotic cells and therefore particularly susceptible to lysosomal dysfunction as they cannot dilute their toxic burden, i.e. aggregated proteins and dysfunctional organelles, by cell division [319]. Accordingly, the brain is often the most severely affected organ in primary lysosomal disorders [205] as lost neurons cannot be replaced and the progressive loss finally gives rise to the symptoms of neurodegenerative diseases [176]. Moreover, due to the very large expanses of dendritic and axonal cytosol, neurons need to transport their cellular waste over long distances towards the cell body, where the majority of lysosomes is located. An impairment of transport or a slowdown of proteolytic clearance of the autolysosomal substrates is therefore detrimental to neurons [205].

In 2006, Taichi Hara *et al.* were able to prove that suppression of basal autophagy in neuronal cells was already sufficient to induce neurodegeneration in mice, even without the presence of any disease-associated mutant protein [99]. This finding was confirmed by Komatsu *et al.* [146, 145]. The generated mice in which two different autophagic genes, namely *Atg5* or *Atg7*, were exclusively deleted in neurons showed progressive neurodegeneration and symptoms of neurological pathology along with a high number of ubiquitin-positive inclusion bodies in neurons [99, 146, 145]. Interestingly, inclusion bodies only appeared in later phases of autophagy deficiency suggesting that the primary role of autophagy in neurons is the turnover of diffuse ubiquitinated, cytosolic proteins rather than the elimination of inclusion bodies and that these mutant cytosolic proteins could present the main source of toxicity [99]. However, as impaired autophagy seemed to affect specific neuronal cell-types stronger than others, it was speculated that neurons exposed to high stress levels probably also need higher levels of basal autophagy and are therefore more vulnerable to defective autophagy than cells that only require low levels of basal autophagy and are therefore more resistant to impaired autophagy [229]. These studies not only stress the importance of autophagy for the progression of neurodegenerative diseases, but also show that under basal, nutrient-rich conditions, autophagy seems to be constantly active in the brain and is required for neuronal survival [99].

In neurodegenerative diseases, the autophagic pathway has been found to be impaired at all stages - the initiation of autophagy (even though very rarely), the selection of the autophagic substrates, the sequestration of the cargo, the transport along microtubules towards the lysosomes, the fusion between autophagosomes/amphisomes and lysosomes and finally the degradation within the autolysosomal lumen [205]. Clinical manifestations of neurodegeneration include progressive cognitive decline and changes in behaviour. These phenotypes are also observed in lysosomal storage disorders (LSDs), diseases that result from mutations in lysosomal genes [221, 74, 16]. This suggests that lysosomal disturbances play a role in both neurodegeneration and lysosomal storage disorders [8] and further stresses the importance of lysosomes to proper nervous system function [203].

In the following, lysosomal dysfunction in the four different neurodegenerative diseases AD, Parkinson's and Huntington's disease as well as in FTLD will be set out in more detail.

### 1.4.1 Alzheimer's disease (AD)

AD is a progressive neurodegenerative disease which is pathologically characterized by the occurrence of intraneuronal fibrillary tangles (NFTs) consisting of aggregated, abnormally phosphorylated tau (see also section 1.1.3.1.1, page 9) [90, 151, 207, 93] and senile plaques composed of amyloid- $\beta$  peptide ( $A\beta$ ) [86]. Amyloid- $\beta$  is produced by the processing of its precursor, the  $\beta$ -amyloid precursor protein (APP). Thereby, APP is shedded by  $\beta$ -secretase followed by  $\gamma$ -secretase cleavage which releases an  $A\beta$  peptide ( $A\beta$  38, 40 or 42) [93, 327]. This pathway is called the amyloidogenic pathway. The major toxic species in AD is considered to be  $A\beta$ 42 and has a strong potential to oligomerize [327, 93].

One of the earliest manifestations that can be detected in AD, however, is not the deposition of  $A\beta$ , but an upregulation of the endocytic-lysosomal system [203, 176]. Therefore, it is discussed whether the endocytic-lysosomal system, including autophagy, is disturbed. Evidence for this hypothesis are the giant neuritic swellings found in AD brains that mainly contain autolysosomes [206] suggesting that autophagic substrate elimination is defective [205]. However, these swellings might also result from microtubule destabilization caused by tau hyperphosphorylation subsequently leading to impaired neuronal trafficking [204].

Moreover, intracellular transport, which is essential for proper neuronal functioning, might also be disrupted due to the accumulation of autophagic vacuoles (AVs) as a consequence of impaired autophagosome-lysosome fusion, another theory which is discussed [206, 176, 321]. Furthermore, Yu *et al.* argue that persistent AVs might present as major internal source for  $A\beta$  because AVs contain full-length APP,  $\beta$ -cleaved APP C-terminal fragments as well as its cleaving enzyme  $\gamma$ -secretase (which is highly enriched in these AVs), proteins that are crucial for the generation of  $A\beta$  [321].

In addition, the toxic and aggregative  $A\beta$ 42 which is taken up by neurons via endocytosis and subsequently trafficked to lysosomes was shown to be degraded slowly and thus to accumulate within the lysosome [203]. Lysosomal as well as autophagosomal accumulation of  $A\beta$ 42 might then result in a leakage of lysosomal enzymes and of toxic undigested substrates into the cytosol adding to cellular toxicity and leading to apoptosis [203, 124, 326, 176].

*APOE* $\epsilon$ 4 is the strongest risk factor for LOAD and encodes a neuronal cholesterol transport protein [205]. The primary pathway by which it increases the LOAD risk is probably by binding with high affinity to  $A\beta$  which might enhance plaque formation [101]. However, interestingly, it is discussed whether it might also destabilize lysosomal membranes thereby contributing to accelerated cell death via apoptosis [205]. Moreover, it has been reported that apoE isoforms differentially influence the neuronal uptake of  $A\beta$ , its subsequent trafficking to the lysosome and thus its degradation [159]. Thereby, apoE3 seems to be more efficient to accelerate lysosomal

degradation than apoE4, another explanation for why A $\beta$  aggregation is promoted in *APOE* $\epsilon$ 4 carriers [159].

Mature APP can be re-internalized from the cell surface and targeted to endosomes and lysosomes where it is processed [92]. Moreover, as  $\beta$ -secretase (BACE) seems to be more active at mild acidic pH, making endosomes the most likely location for BACE cleavage of APP [136], internalization of cell surface APP therefore leads to elevated A $\beta$  generation [147, 136]. Thus, increased endocytosis and impaired lysosomal degradation might result in A $\beta$  accumulation thereby enhancing the AD phenotype. Accordingly, the risk factor APOE $\epsilon$ 4 as well as mutant forms of APP, APP duplications and elevated amounts of dietary cholesterol interfere with lysosomal proteolysis via promoting Ras-related protein 5 (Rab5)-upregulation and thereby accelerated endocytosis [203].

Furthermore, Lee *et al.* claim that mutations in presenilin-1, which is part of the  $\gamma$ -secretase complex, result in impaired targeting of the a1 subunit of V0-ATPase from the ER to the lysosome [102, 157]. As the V0-ATPase is essential for lysosomal acidification, presenilin-1 mutations might be responsible for the defective proteolysis of autophagic substrates leading to the accumulation of AVs and, accordingly, of A $\beta$  [102, 157, 194]. However, this mechanism is controversially discussed as neither Coen *et al.* nor Zhang *et al.* could reproduce the findings of Lee *et al.* [328, 45]. Coen *et al.* argue that endo-lysosomal dysfunction of presenilin-deficient cells rather results from impaired lysosomal calcium storage and/or release which in turn might hamper lysosomal-autophagosomal fusion [45]. Zhang *et al.* report a significant increase in CLEAR network genes in samples of presenilin-1 and -2 knockout mouse brains hinting that presenilin might influence lysosomal biogenesis [328]. In 2013, Wolfe *et al.* reconfirmed their original findings that lysosomal acidification is impaired in AD [157]. Thus, it still remains to be determined if one of the proposed mechanisms leads to the lysosomal phenotype observed in AD.

Another evidence for disrupted autophagy in AD are the reduced expression levels of beclin-1 in AD patients [218]. As beclin-1 is a protein that is required for autophagy initiation [244], its reduction might result in impaired neuronal autophagic activity [218] thereby increasing A $\beta$ -accumulation and neurodegeneration [102].

To summarize, there is some evidence that, in AD, autophagy might be disrupted at both the initiation as well as the clearance stage which subsequently might lead to the accumulation of autophagic vesicles in dystrophic neurites, increased A $\beta$  levels, altered trafficking, impaired degradation of toxic proteins and increased apoptosis adding to neurodegeneration.

#### 1.4.2 Parkinson's disease (PD)

In Parkinson's disease, the dopaminergic neurons of the *substantia nigra pars compacta* and of the *striatum* degenerate. One of the main reasons for this degeneration is an  $\alpha$ -synuclein accumulation within inclusions called Lewy bodies [79, 176].  $\alpha$ -synuclein is located in the presynaptic terminals of neurons and has been implicated in synaptic function [176]. Post-

translational modifications of  $\alpha$ -synuclein promote the formation of oligomeric protofibril intermediates that subsequently progress to insoluble fibrils [176]. However, when  $\alpha$ -synuclein interacts with dopamine, fibrillation is inhibited and  $\alpha$ -synuclein accumulates in its soluble toxic form which makes dopaminergic neurons most susceptible to neurodegeneration [176]. Soluble  $\alpha$ -synuclein is degraded by the proteasome, however, fibrillar  $\alpha$ -synuclein gets jammed inside the proteasome thereby blocking its activity [176, 278]. Moreover, soluble forms can also be degraded by chaperone-mediated autophagy [53].

However, pathogenic mutants of  $\alpha$ -synuclein bind to the CMA receptor LAMP2a with high affinity thereby inhibiting their translocation into the lysosomal lumen [176, 53]. Even more, they also compromise the uptake of other CMA substrates resulting in a complete blockage of CMA [176, 53]. As a consequence of both proteasome and CMA inhibition, macroautophagy is upregulated rendering the cells very susceptible to stressors and stress conditions [176, 53]. Over time, the autophagic system probably becomes overloaded which results in its failure subsequently leading to neurodegeneration [176, 53].

Along with  *$\alpha$ -synuclein (SNCA)* mutations, *leucine-rich repeat kinase 2 (LRRK2)* mutations that have been linked to defects in endosomal-lysosomal trafficking, lysosomal pH and calcium regulation as well as CMA, have also been reported to cause autosomal-dominant PD by an as yet unidentified mechanism [220, 176, 175].

Furthermore, autosomal-recessive PD is associated with two genes that play an important role in mitophagy, the removal of damaged mitochondria by autophagy, namely *PINK* and *PARK2*, encoding Parkin [102]. During mitophagy, Parkin is selectively recruited to damaged mitochondria due to the accumulation of PINK at the outer mitochondrial membrane [220]. Subsequently, Parkin mediates the ubiquitination of the mitochondrial surface which allows for the recruitment of the autophagic machinery [220]. Thus, mutant PINK or Parkin contribute to mitochondrial dysfunction and thereby increase oxidative stress which further damages the cell and promotes neurodegeneration [176].

Another gene that causes autosomal-recessive PD is *ATP13A2*, encoding a lysosomal transmembrane protein [230]. Loss-of-function mutations of *ATP13A2* result in impaired lysosomal acidification, subsequent decreased proteolytic processing of lysosomal enzymes and reduced degradation of lysosomal substrates leading to an accumulation of autophagosomes and enlarged lysosomes as well as neuronal toxicity [297, 59].

Interestingly, mutations in the glucocerebrosidase (*GBA*) gene which cause Gaucher disease, a lysosomal storage disorder, increase the risk for developing PD when only one allele is affected [169, 256]. Probably, glucosylceramide accumulation leads to decreased lysosomal degradation resulting in an accumulation of  $\alpha$ -synuclein which promotes oligomer formation and neurotoxicity [178]. In addition,  $\alpha$ -synuclein accumulation impairs the trafficking of GBA thereby further decreasing lysosomal GBA activity resulting in a positive feedback loop that may lead to a self-propagating disease [178, 58].

Together, in PD, the proteasome and CMA as well as autophagy in the clearance stage were reported to be disrupted. Thereby, it was claimed that either the degradation of mitochondria, lysosomal function or trafficking was compromised resulting in the accumulation of autophagosomes and toxic protein species like soluble  $\alpha$ -synuclein and increased oxidative stress due to dysfunctional mitochondria promoting the progression of neurodegeneration.

### 1.4.3 Huntington's disease (HD)

Huntington's disease is an autosomal-dominant polyglutamine-repeat disorder [8] caused by an abnormally long CAG repeat expansion in the N-terminal region of the huntingtin protein [176, 291]. Huntingtin plays a multifunctional role in various cellular processes like gene transcription, signalling and intracellular trafficking and interacts with other proteins through its N-terminus [176]. Therefore, huntingtin-interacting proteins are usually co-sequestered into the huntingtin inclusion bodies that are formed upon mutant huntingtin expression, amplifying the loss of function [176]. However, inclusion bodies seem to be cytoprotective [4, 289]. Whereas the amount of diffuse intracellular huntingtin together with the polyglutamine expansion length predicts neuronal death [4], inclusion body formation correlates with improved survival as the levels of diffuse huntingtin are reduced [4]. During formation of the inclusion bodies, huntingtin filaments are formed that inhibit the ubiquitin-proteasome system [62] which makes autophagy the essential mechanism for mutant huntingtin degradation [229]. Indeed, autophagy was found to be upregulated in response to huntingtin aggregate formation and contributes to the removal of huntingtin aggregates [255, 133].

Interestingly, one of the proteins sequestered by mutant huntingtin inclusion bodies is the mammalian target of rapamycin (mTOR) [236]. As a consequence of sequestration, mTOR kinase activity is inhibited which in turn induces autophagy [236]. Moreover, inhibition of the UPS might also cause autophagy induction [176]. Of note, increased cathepsin D activity has been detected in affected areas of HD brains. This might enhance the degradation of mutant huntingtin that is more resistant to cathepsin D degradation than the wild-type protein [326].

Mutant huntingtin also recruits beclin-1, which is an important factor for phagosome nucleation, and thereby impairs the turnover of long-lived proteins [269]. Moreover, beclin-1 sequestration reduces autophagic degradation of mutant huntingtin thereby promoting its further accumulation and mediating disease progression [269]. An age-dependent decline in *beclin-1* expression may add to the reduction of autophagic activity thereby accelerating disease progression with age [269]. In part, this might explain the failure of autophagy in advanced stages of the disease [176].

Treatment of a fly model of HD with rapamycin, an mTOR inhibitor and autophagy stimulator, protected against neurodegeneration and provided evidence for the importance of autophagy for clearing cells from mutant huntingtin [236].

Moreover, huntingtin was reported to link cargo to actin and to coordinate the switching between actin- to microtubule-based movement [88]. Disruption of huntingtin thus was demonstrated to

cause peripheral accumulation of all endocytic compartments consistent with impaired dynein-dependent trafficking [38].

In summary, in HD, autophagy was found to be upregulated due to UPS inhibition. However, during disease progression, co-sequestering of an important nucleation factor for phagophore formation inhibits autophagy at the initiation stage resulting in reduced autophagic activity which accelerates neurodegeneration. Moreover, sequestration of huntingtin might inhibit retrograde trafficking of cargo destined for lysosomal/autophagic degradation.

### 1.4.4 Frontotemporal lobar degeneration (FTLD)

Only recently, evidence accumulated that also in FTLD, dysfunction in the endosomal-lysosomal-autophagic pathway plays an important role in disease development and progression.

For instance, VCP was found to influence the autophagic pathway. Upon VCP loss or expression of mutant VCP, different stages of autophagy like autophagosome maturation and autophagosome-lysosome fusion were shown to be impaired [292, 131] (for more details see also section 1.1.3.1.5, page 17). Moreover, CHMP2B mutations, which cause a block in MVB formation, impair Rab7 recruitment to endosomes [295] which is essential for autophagosome maturation and endosome-lysosome fusion [118]. Thus, CHMP2B mutations also influence lysosomal function by inhibiting lysosomal degradation (for more details see also section 1.1.3.1.4, page 16).

In 2011, *GRN* appeared among the best hits of a transcriptional gene network inference study which investigated human disease genes connected to lysosomal function and organization [15]. Furthermore, alkalizing agents as well as v-ATPase inhibitors were shown to restore GRN levels in patient lymphoblasts with *GRN* mutations [37]. Strikingly, one year later, homozygous *GRN* mutations were described to be causative for NCL [273], a lysosomal storage disorder, a finding which strongly supported a linkage between GRN and lysosomal function. As heterozygous *GRN* mutations cause FTLD, a gene dosage effect was suggested [273]. In addition, lysosomal proteins were demonstrated to be increased in *Grn* knockout mice [87, 286] along with a decreased mTORC1 activity [286] at early stages of disease progression, i.e. before neuroinflammation became apparent [87]. Together, this suggested that loss-of-function mutations in *GRN* might result in lysosomal dysfunction leading to neurodegeneration (for more details see also section 1.1.3.1.2, page 12).

To summarize, in FTLD, autophagy was found to be impaired in *VCP* and *CHMP2B* mutation carriers resulting in autophagosome accumulation and subsequent neurodegeneration. Moreover, *GRN* mutations were implicated in causing lysosomal dysfunction, however, the exact disease mechanism has not been elucidated, yet.

## 2 Aims of this study

The motivation of my study was to investigate how TMEM106B could confer a risk for developing FTLD-TDP and/or how it might influence disease progression.

Since very little was known about this protein at the time when I started my studies, the first aim was to characterize TMEM106B in regard to its location, its orientation in the membrane and its glycosylation status.

The second aim was to find out whether TMEM106B levels could directly influence GRN expression. *GRN* mutation carriers were found to be especially associated with increased TMEM106B mRNA and protein levels [301, 87] suggesting a direct functional relationship between GRN and TMEM106B [72, 301]. To know whether TMEM106B might have a direct impact on GRN levels is crucial as a reduction in GRN levels causes FTLD-TDP [9, 52]. Moreover, the knowledge of whether and how TMEM106B might influence GRN expression levels could provide an approach to overcome GRN haploinsufficiency in *GRN* mutation carriers, namely by manipulating TMEM106B expression.

The third aim of my study concentrated on elucidating the endogenous function of TMEM106B in order to understand how malfunctioning of TMEM106B might increase the risk for developing FTLD. Thus, I analysed whether TMEM106B knockdown had any influence on cellular structures or organelles in order to elucidate whether TMEM106B might affect one or several cellular structures as well as to get some information about its possible endogenous function. Moreover, as TMEM106B proved to be a lysosomal protein, I examined whether lysosomal function was influenced by TMEM106B. Since it is known that lysosomal dysfunction might result in neurodegeneration, an impact of TMEM106B on lysosomal function would explain how it contributes to FTLD-TDP disease progression. Finally, I investigated whether TMEM106B plays a role in the autophagic pathway which is affected in many neurodegenerative disorders and is known to accelerate disease progression (see also section 1.4, page 35).

Together, an understanding of TMEM106B's characteristics, the knowledge of its interaction partners as well as in which molecular pathway it is involved will aid the development of a therapeutical approach against FTLD-TDP, a disease where still no cure exists.



## 3 Results<sup>1</sup>

### 3.1 Establishment of a method for analysing TMEM106B on immunoblot

At the time when I started this study, little was known about the biochemical features of TMEM106B. Only predictions based on its DNA (figure 3.1 a and b) and protein sequence (figure 3.1 c) were made. The *TMEM106B* gene comprises eight or nine exons of which seven are protein-coding (figure 3.1 a). In the longest variant, the transcript length is 12.5 kb whereas the *TMEM106B* complementary DNA (cDNA) comprises 825 nucleotides (figure 3.1 b). The *TMEM106B* gene is translated into a protein of 274 amino acids (figure 3.1 c) with a predicted molecular weight of 31.12 kDa. Moreover, by the bioinformatic prediction programmes for transmembrane helices TMHMM 2.0 and TMpred, TMEM106B was predicted to be a transmembrane protein with one or two transmembrane domains (figure 3.1 c).

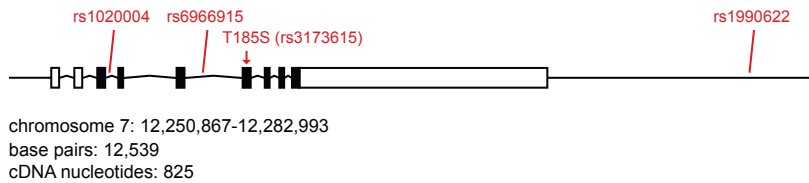
To analyse TMEM106B, human TMEM106B cDNA was amplified from the IMAGE full length clone IRAT p970G1031D. An N-terminal human influenza haemagglutinin (HA)-tag was added by PCR (see section 5.1.2, page 115) in order to be able to detect TMEM106B with an anti-HA antibody as, at the time, no anti-TMEM106B antibody was available. Subsequently, the construct was cloned into both a pcDNA6/V5-HisA and a pcDNA4/TO/myc vector backbone (see section 5.1.3, page 116). The latter construct was used for generating a stable N-terminally HA-tagged TMEM106B expressing T-REx<sup>TM</sup>293 cell line. It was produced because transient overexpression of TMEM106B resulted in variable TMEM106B expression levels which also influenced the intracellular localization of TMEM106B, i.e. heavily overexpressed TMEM106B resulted in its surface localization or its localization within the lumen of lysosomes. Occasionally, HA-tagged TMEM106B was also found to be retained in the ER (data not shown).

The use of single, TMEM106B-expressing cell clones enables a homogeneous expression pattern of TMEM106B. Moreover, especially for immunofluorescence, cell lines with low expression levels of HA-tagged TMEM106B were chosen to avoid overexpression artefacts and to better mimic endogenous TMEM106B expression. In the following study, clone number 18 was used as it presented with the lowest expression of HA-tagged TMEM106B (figure 3.2). All results were confirmed with other cell clones (data not shown).

---

<sup>1</sup>Parts of the results presented in this study have already been published in Lang *et al.* [155], Schwenk *et al.* [263] and Götzl *et al.* [87].

a)



b)

```

ATG GGA AAG TCT CTT TCT CAT TTG CCT TTG CAT TCA AGC AAA GAA GAT GCT TAT GAT GGA GTC
ACA TCT GAA AAC ATG AGG AAT GGA CTG GTT AAT AGT GAA GTC CAT AAT GAA GAT GGA AGA AAT
GGA GAT GTC TCT CAG TTT CCA TAT GTG GAA TTT ACA GGA AGA GAT AGT GTC ACC TGC CCT ACT
TGT CAG GGA ACA GGA AGA ATT CCT AGG GGG CAA GAA AAC CAA CTG GTG GCA TTG ATT CCA TAT
AGT GAT CAG AGA TTA AGG CCA AGA AGA ACA AAG CTG TAT GTG ATG GCT TCT GTG TTT GTC TGT
CTA CTC CTT TCT GGA TTG GCT GTG TTT TTC CTT TTC CCT CGC TCT ATC GAC GTG AAA TAC ATT
GGT GTA AAA TCA GCC TAT GTC AGT TAT GAT GTT CAG AAG CGT ACA ATT TAT TTA AAT ATC ACA
AAC ACA CTA AAT ATA ACA AAC AAT AAC TAT TAC TCT GTC GAA GTT GAA AAC ATC ACT GCC CAA
GTT CAA TTT TCA AAA ACA GTT ATT GGA AAG GCA CGC TTA AAC AAC ATA ACC ATT ATT GGT CCA
CTT GAT ATG AAA CAA ATT GAT TAC ACA GTA CCT ACC GTT ATA GCA GAG GAA ATG AGT TAT ATG
TAT GAT TTC TGT ACT CTG ATA TCC ATC AAA GTG CAT AAC ATA GTA CTC ATG ATG CAA GTT ACT
GTG ACA ACA ACA TAC TTT GGC CAC TCT GAA CAG ATA TCC CAG GAG AGG TAT CAG TAT GTC GAC
TGT GGA AGA AAC ACA ACT TAT CAG TTG GGG CAG TCT GAA TAT TTA AAT GTA CTT CAG CCA CAA
CAG TAA
    
```

c)

```

1      11      21      31      41
MGKSLSHLPL HSSKEDAYDG VTSENMRNGL VNSEVHNEDG RRGDVSQFPY
51     61     71     81     91
VEFTGRDSVT CPTCQGTGRI PRGQENQLVA LIPYSDQRLR PRRTKLYVMA
101    111    121    131    141
SVFVCLLLSG LAVFFLFPRS IDVKYIGVKS AYVSYDVQKR TIYLNITNTL
151    161    171    181    191
NITNNNYYSV EVENITAQVQ FSKTVIGKAR LNNIT IIGPL DMKQIDYTPV
201    211    221    231    241
TVIAEEMSYM YDFCTLISIK VHNIVLMMQV TVTTTTYFGHS EQISQERYQY
251    261    271
VDCGRNTTYQ LGQSEYLNVL QPQQ
    
```

1st predicted transmembrane domain
2nd predicted transmembrane domain
predicted N-glycosylation motifs
disease-associated mutation

**Figure 3.1: cDNA and protein sequences of TMEM106B**

a) The gene structure of the longest *TMEM106B* variant is depicted. Empty boxes represent non-protein-coding exons or the 3' UTR, black boxes represent protein-coding exons. In red, the location of the SNPs found in the GWAS in 2010 [301] is depicted (modified from [305]). b) The cDNA sequence of the longest *TMEM106B* variant is depicted. In the cDNA sequence, start and stop codons are underlined. c) The protein sequence of *TMEM106B* is shown. Predicted transmembrane domains and glycosylation sites are highlighted in different colours (figure legend). The disease-associated mutation site is underlined (T185S).

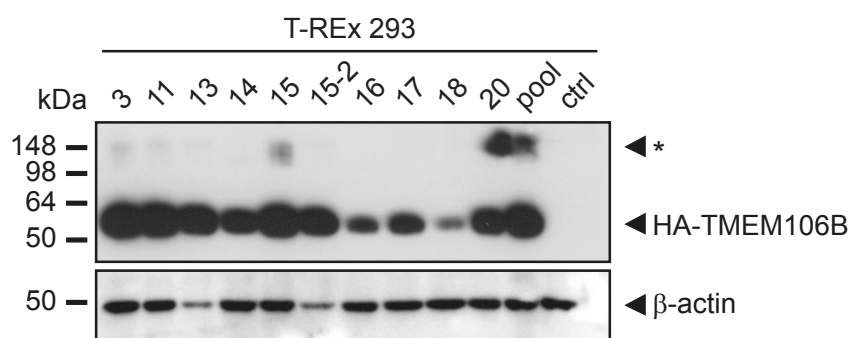


**Figure 3.2: Stable expression of HA-tagged TMEM106B in different cell clones of HA-tagged wild-type (wt) TMEM106B-transfected T-REx<sup>TM</sup>293 cells**

T-REx<sup>TM</sup>293 cells stably expressing N-terminally HA-tagged wt TMEM106B were generated and a pool as well as single cell clones were isolated (number of cell clones see figure). HA-TMEM106B expression was induced with 0.2  $\mu$ g/ml tetracycline and cell lysates were analysed for HA-tagged TMEM106B by SDS-PAGE and subsequent immunoblotting with the anti-HA antibody 3F10. Untransfected T-REx<sup>TM</sup>293 cells served as negative control (ctrl) and  $\beta$ -actin as loading control. The asterisk (\*) marks putative HA-TMEM106B aggregates.

At the beginning of my studies, I established conditions for SDS-PAGE and immunoblotting of TMEM106B. Since HA-tagged TMEM106B showed a high tendency to aggregate upon SDS-PAGE separation (data not shown), I chose to use urea-SDS gels instead to reduce TMEM106B aggregation. Moreover, better results were gained when non-reducing urea Laemmli buffer (without  $\beta$ -mercaptoethanol) was used (data not shown; also compare to results see figure 3.3).

For endogenous TMEM106B detection, Anja Capell<sup>2</sup>, Elizabeth Kremmer<sup>3</sup> and I started to raise and test monoclonal antibodies against TMEM106B peptide. After selecting a hybridoma cell clone producing an antibody suitable for immunoblotting (anti-TMEM106B antibody 6F2; see also section 5.1.8, page 123 and section 5.1.9, page 125), I investigated whether urea-SDS-PAGE followed by immunoblotting was also an applicable method for endogenous TMEM106B protein detection. Furthermore, I tested whether indeed non-reducing conditions lead to better results than reducing ones. In addition, I varied the incubation temperature of the protein samples in their appropriate Laemmli buffer (figure 3.3).

The specificity of the antibody was shown by knocking down endogenous TMEM106B with small interfering RNAs (siRNAs) (figure 3.3; see lanes marked with KD). As upon TMEM106B knockdown, both the band at about 75 kDa, a potential dimer, as well as the band at about 40 kDa disappeared, both bands are considered to be specific for TMEM106B.

<sup>2</sup>Dr. Anja Capell, Ludwig-Maximilians-University Munich, Adolf Butenandt Institute, Munich, Germany

<sup>3</sup>Dr. Elisabeth Kremmer, Institute of Molecular Immunology, Helmholtz Center, Munich, Germany

Interestingly, TMEM106B showed a molecular weight band profile which was dependent on the conditions used for the denaturation of the proteins, namely temperature and reducing conditions (figure 3.3). Furthermore, the addition of urea to the SDS gel as well as to the Laemmli buffer reduced TMEM106B aggregation.

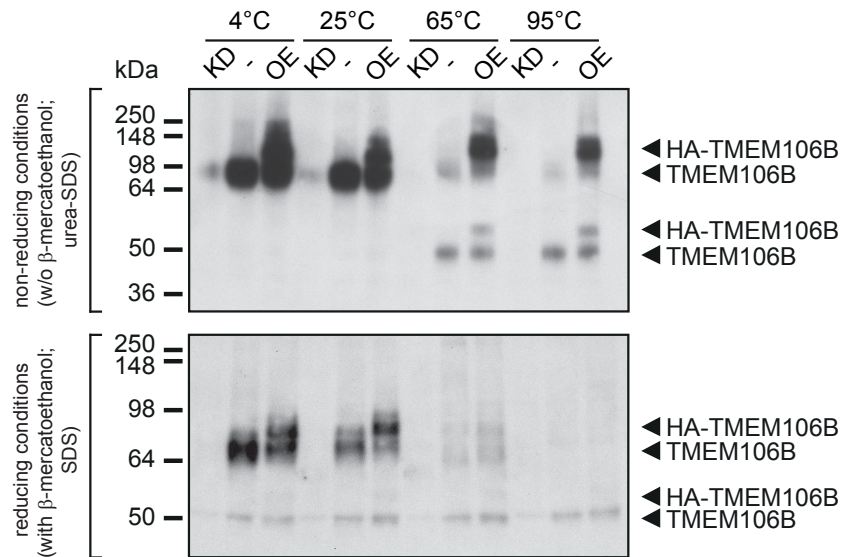


**Figure 3.3: Running behaviour of TMEM106B on immunoblot, depending on temperature and reducing conditions**

SH-SY5Y cells were transfected with an siRNA pool against TMEM106B (KD), with an N-terminally HA-tagged wt TMEM106B construct (OE) or with non-targeting siRNA as control (-). Before loading on the urea-SDS gel, samples were incubated in urea Laemmli buffer without  $\beta$ -mercaptoethanol for 30 min at 4 °C or at 25 °C, for 15 min at 65 °C or for 5 min at 95 °C. Equal amounts of the same samples were incubated for the same time ranges and temperatures in “normal” Laemmli buffer with  $\beta$ -mercaptoethanol and loaded on an SDS gel. Subsequently, TMEM106B variants were separated by SDS-PAGE and detected by immunoblotting with the anti-TMEM106B antibody 6F2.

Under non-reducing conditions (no  $\beta$ -mercaptoethanol), at 4 °C and 25 °C, only one band appeared at about 75 kDa. However, at 65 °C and 95 °C, the band at about 75 kDa increasingly decreased whereas a band at about 40 kDa was detected. Furthermore, a large amount of protein does not seem to be detectable any longer. HA-tagged TMEM106B ran at a higher molecular weight than expected possibly because the HA-tag interferes with the running behaviour of the TMEM106B protein. Thus, on immunoblot, HA-tagged TMEM106B was detected at about 100 kDa and 55 kDa.

Notably, the TMEM106B band with the higher molecular weight was more prominent in case of HA-tagged than of endogenous TMEM106B. This might indicate that HA-tagged TMEM106B is more prone to aggregation than endogenous TMEM106B. However, the fact that at lower temperatures, only the 75 kDa band of endogenous TMEM106B is visible might also imply that TMEM106B dimerizes.

Strikingly, under reducing conditions, the band at about 40 kDa was not changed in regard to different temperatures. However, the band at about 75 kDa increasingly disappeared with

increasing temperatures and, at 95 °C, was almost undetectable. Moreover, comparing both reducing conditions (using Laemmli buffer with  $\beta$ -mercaptoethanol) and non-reducing conditions (using urea Laemmli buffer without  $\beta$ -mercaptoethanol), it became apparent that even though equal amounts of protein were loaded, less protein was detected in case of the reducing conditions. Since it was not clear whether the band at about 75 kDa represented a natively-existing TMEM106B dimer or whether it was just an artefact due to protein aggregation, and as under non-reducing conditions, I could detect higher levels of TMEM106B protein, I decided to use urea-SDS gels with pre-heating of the protein lysates at 65 °C in Laemmli buffer without  $\beta$ -mercaptoethanol for detecting TMEM106B.

## 3.2 TMEM106B is a highly glycosylated type II transmembrane protein

### 3.2.1 TMEM106B is a glycosylated integral membrane protein

To determine whether TMEM106B was a transmembrane protein as predicted or just membrane-attached, a membrane preparation followed by carbonate extraction was performed with T-REx<sup>TM</sup>293 cells stably expressing N-terminally HA-tagged wild-type TMEM106B (figure 3.4 a). As TMEM106B was recovered in the membrane/membrane-associated protein fraction and, upon further fractionation, in the pellet of the carbonate extraction, TMEM106B was confirmed to be an integral membrane protein (figure 3.4 a). However, the molecular weight of the protein detected on western blot was about 55 kDa and not the predicted 31.12 kDa, which could not only be explained by the added HA-tag of the overexpressed protein.

Interestingly, the consensus sequence for N-glycosylation, N-X-T/S, was found to appear five-times in the amino acid sequence of TMEM106B (figure 3.1 c, yellow highlights). Bioinformatic tools (NetNGlyc 1.0 and NetOGlyc 4.0, figure 3.1) confirmed the presence of five possible N-glycosylation sites at amino acid positions 146 (N1), 152 (N2), 165 (N3), 184 (N4) and 257 (N5). Thus, it was investigated whether the different molecular weight of TMEM106B could be explained by glycosylation. Indeed, upon treatment with either N-glycosidase F, to remove N-linked glycans, or endoglycosidase H, to only remove non-complex sugars, the molecular weight of TMEM106B shifted towards a smaller size suggesting that TMEM106B is both non-complex and complex glycosylated (figure 3.4 b).

Of note, on immunoblot, TMEM106B appeared as a double band which was especially prominent after deglycosylation. However, this phenomenon cannot be attributed to phosphorylation as after treatment with okadaic acid, a drug that inhibits protein serine/threonine phosphatases, the double band was still present (data not shown). Therefore, another post-translational modification of TMEM106B might be responsible for the doublet. Alternatively, it might be a methodological problem as without  $\beta$ -mercaptoethanol and without boiling, TMEM106B might not be fully reduced and/or denatured.

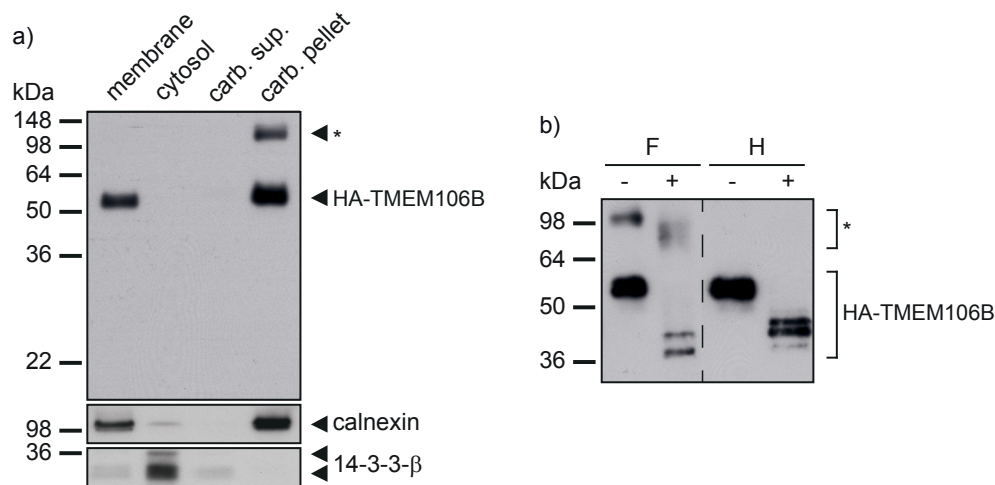


**Figure 3.4: TMEM106B is a glycosylated integral membrane protein**

a) Tetracycline-induced T-REx<sup>TM</sup>293 cells stably expressing N-terminally HA-tagged wt TMEM106B were subjected to cellular fractionation. Total membranes, cytosol and carbonate-extracted membranes (carb. supernatant (sup.) which is the membrane-associated protein fraction; carb. pellet which is the integral membrane fraction) were subsequently analysed for TMEM106B by SDS-PAGE and immunoblotting with the anti-HA antibody 3F10. Calnexin served as a control for an integral membrane protein, 14-3-3-β as control for a cytosolic soluble protein, respectively. The asterisk (\*) marks putative TMEM106B aggregates. b) Lysates of tetracycline-induced T-REx<sup>TM</sup>293 cells stably expressing N-terminally HA-tagged wt TMEM106B were treated for 16 h with either N-glycosidase F (F) to remove all N-linked glycans or with endoglycosidase H (H) to only remove non-complex glycans. Controls were incubated in the appropriate buffer, but without the enzyme. The asterisk (\*) marks putative TMEM106B aggregates [155].

### 3.2.2 TMEM106B is a type II transmembrane protein

The suggested existence of one or two transmembrane domains within TMEM106B together with a robust molecular weight shift due to N-glycosylation would result in two possible topologies of the protein (figure 3.5). If both transmembrane domains were utilized, TMEM106B would be inserted into the membrane as hairpin-like structure with its N- and C-termini located within the cytosol (see model on the left side of figure 3.5). However, if only the more N-terminal transmembrane domain (which was predicted with a higher probability) was inserted, TMEM106B would be type II-oriented, with its C-terminus in the lumen and the N-terminus in the cytosol (see model on the right side of figure 3.5).

The predicted fifth glycosylation site at position 257 (N5) is C-terminal of the second predicted transmembrane domain (figure 3.5). Accordingly, if TMEM106B is a type II transmembrane protein, N5 would be glycosylated, however, if it adopts a hairpin-like structure and thus its C-terminus is located in the cytosol, N5 would not be glycosylated.

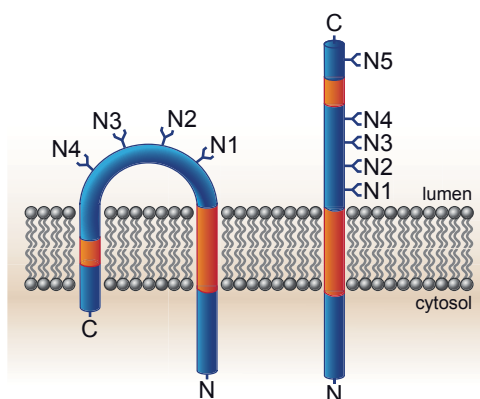


**Figure 3.5: The two possible topologies of TMEM106B**

On the left, the hairpin-like structure that TMEM106B would adopt if both predicted transmembrane domains were used is depicted. On the right, the model of TMEM106B as a type II transmembrane protein is shown. The N-glycosylation sites are marked as N1 to N5 (modified from [155]).

Therefore, in order to determine the membrane orientation of TMEM106B, the five predicted N-glycosylation sites were sequentially inactivated by mutating the asparagines (N) to serines (S) (figure 3.6 a). Indeed, sequential deletion of the predicted N-glycosylation sites resulted in a gradual reduction of the molecular weight of TMEM106B, and importantly, also after deleting the last (N5) glycosylation site, a further reduction of the molecular weight could be noticed (figure 3.6 a).

To verify the result, only the N5-glycosylation site was mutated and compared to wild-type TMEM106B (figure 3.6 b and c). As a control, also N4 and N3 were singly mutated. Again, deletion of N5 resulted in a decreased molecular weight which was comparable to the decreased weight in the N3 and N4 mutants (figure 3.6 b and c). As the HA-tag might interfere with the membrane orientation, the experiment was performed with both an N- (figure 3.6 b) and

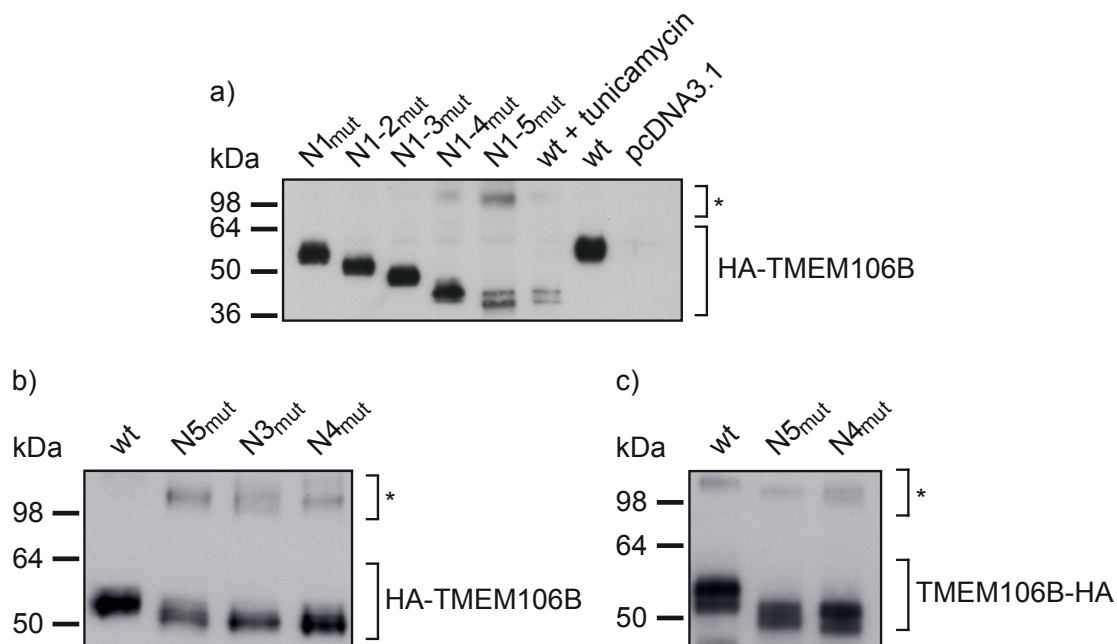


**Figure 3.6: TMEM106B is a type II transmembrane protein**

a) The asparagines of the five N-glycosylation motifs of TMEM106B were sequentially mutated to serines to abolish glycosylation. Each mutant contains an additionally deleted glycosylation site (N1<sub>mut</sub> to N1-5<sub>mut</sub>). The mutated cDNA constructs were transiently transfected into HEK293T cells. To control for migration of fully glycosylated and unglycosylated TMEM106B in SDS-PAGE, HEK293T cells were transfected with the HA-TMEM106B wt construct and treated with solvent or 10 µg/ml tunicamycin for 16 h. HA-TMEM106B variants were separated by SDS-PAGE and detected by immunoblotting with the anti-HA antibody 3F10. The asterisk (\*) marks putative TMEM106B aggregates. Note that both the treatment with tunicamycin and the deletion of all five glycosylation sites lead to the same molecular weight shift and that in both cases, reduced expression levels can be observed probably due to impaired folding and thus increased degradation [155]. b) & c) TMEM106B constructs either tagged N- (b) or C-terminally (c) were subjected to site-directed mutagenesis to only mutate the single glycosylation motifs at N3, N4 or N5. The resulting constructs N3<sub>mut</sub>, N4<sub>mut</sub> and N5<sub>mut</sub> and, as a control, the wt construct were transiently transfected into HEK293T cells. Lysates were analysed for TMEM106B expression by SDS-PAGE and subsequent immunoblotting with the anti-HA antibody 3F10. The asterisk (\*) marks putative TMEM106B aggregates. Importantly, the HA-tag does not interfere with glycosylation at N5 and thus with the membrane orientation of TMEM106B [155].

a C-terminally (figure 3.6 c) tagged construct. Both led to consistent results proving that TMEM106B is indeed a type II transmembrane protein (figure 3.7).

Moreover, deletion of all glycosylation sites (N1-5) resulted in a shift of the molecular weight equal to the one observed after treatment with tunicamycin, a drug that abolishes N-glycosylation (figure 3.6 a). Hence, the five examined N-glycosylation sites of TMEM106B are the only ones utilized.

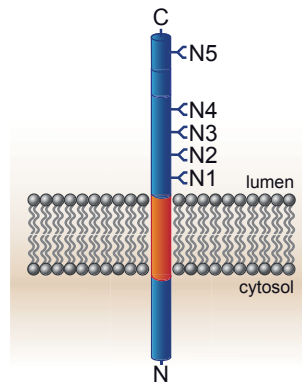


**Figure 3.7: Topology of TMEM106B**

The model of TMEM106B as a type II transmembrane protein is shown. The N-glycosylation sites are marked as N1 to N5 (modified from [155]).

### 3.3 TMEM106B is localized to the late endosomal/lysosomal compartment

To determine the localisation of TMEM106B within the cell, immunofluorescence experiments were performed with various marker antibodies against different cellular structures. As at the beginning of my studies no TMEM106B antibody was available, experiments were executed in tetracycline-induced T-REx<sup>TM</sup>293 cells stably expressing N-terminally HA-tagged wt TMEM106B at low levels to avoid overexpression artefacts. Thereby, TMEM106B predominantly co-localized with the lysosomal marker protein LAMP1, but did not or only to a minor amount co-localize with the ER marker binding immunoglobulin protein (BiP) and the Golgi marker giantin (figure 3.8 a). Treatment with BafA1, a drug that inhibits lysosomal acidification, further increased the lysosomal co-localization of TMEM106B (figure 3.8 a).

To further specify TMEM106B localization, either tetracycline-induced T-REx<sup>TM</sup>293 cells stably expressing N-terminally HA-tagged wt TMEM106B (figure 3.8 c) or HeLa cells transiently transfected with N-terminally HA-tagged wt TMEM106B (figure 3.8 d) were co-transfected with different Rab-green fluorescent protein (GFP) constructs and subjected to immunofluorescence. TMEM106B wt-positive cells thereby showed a clear co-localization with Rab7-GFP-positive vesicles, i.e. late endosomes or lysosomes [323]. However, TMEM106B did not or only to a minor extent co-localize with Rab4a-, Rab5- or Rab11-GFP-positive vesicles, i.e. early or recycling endosomes [323].

Thus, TMEM106B seems to be mainly localized to the late endosomal/lysosomal compartment, a finding, that was later also confirmed by staining endogenous TMEM106B using an anti-TMEM106B antibody whose specificity is shown by the absence of staining in the TMEM106B knockdown (figure 3.8 b).

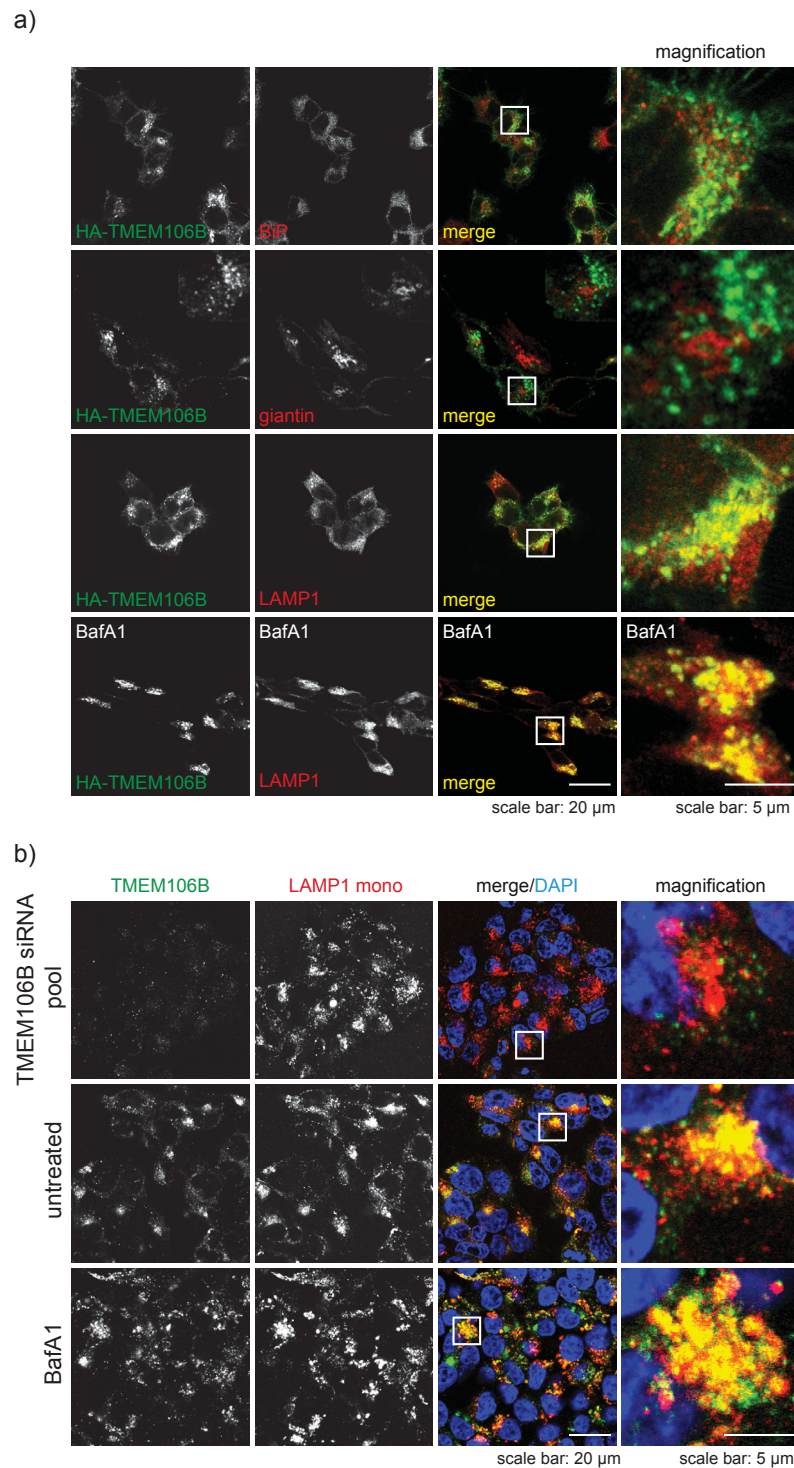


**Figure 3.8: TMEM106B is localized to the late endosomal/lysosomal compartment**

a) Tetracycline-induced T-REx<sup>TM</sup>293 cells stably expressing N-terminally HA-tagged wt TMEM106B at very low levels were grown on coated coverslips and TMEM106B expression was induced with 0.2  $\mu$ g/ml tetracycline for 16 h. One set of cells was additionally treated with 25 nM BafA1 for 16 h. Then, cells were fixed with PFA and stained for TMEM106B with an anti-HA antibody (green). The co-staining (red) was executed with the use of the indicated cell marker antibodies (anti-BiP for ER, anti-giantin for Golgi, anti-LAMP1 for lysosomes) [155].

3.3 TMEM106B is localized to the late endosomal/lysosomal compartment

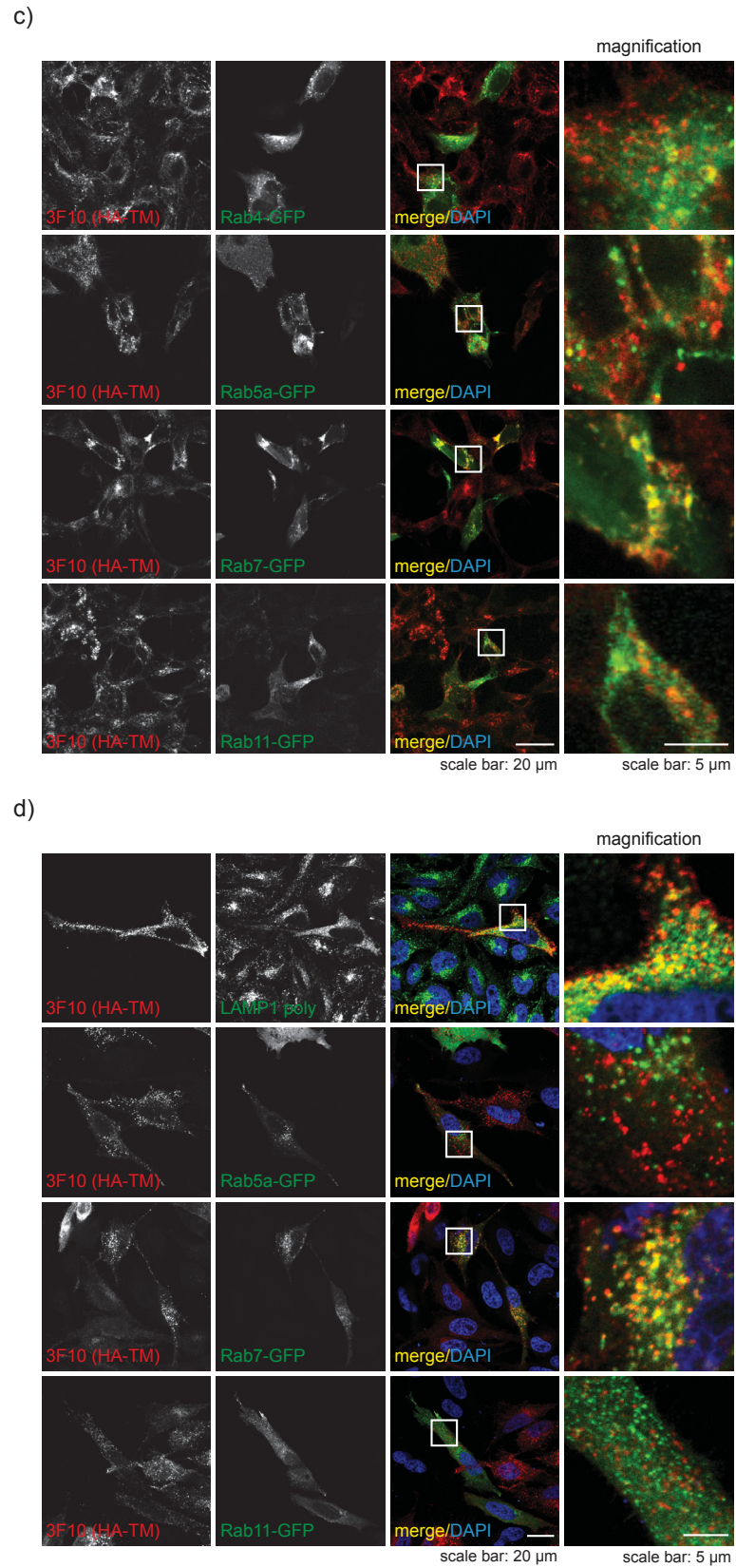


Figure 3.8 (continued): TMEM106B is localized to the late endosomal/lysosomal compartment

**Figure 3.8 (continued): TMEM106B is localized to the late endosomal/lysosomal compartment**

b) HEK293T cells were grown on coated coverslips and subsequently stained for TMEM106B with an anti-TMEM106B antibody (green) and co-stained with the monoclonal lysosomal marker antibody anti-LAMP1 (red). Additionally, one set of cells had been transfected with an siRNA pool against TMEM106B to knockdown the protein and one set had been treated for 16 h with 25 nM BafA1 before being stained. Note that the TMEM106B staining is abolished in the siRNA-transfected cells proving the specificity of the antibody [155]. c) Tetracycline-induced T-REx<sup>TM</sup>293 cells stably expressing N-terminally HA-tagged wt TMEM106B at very low levels were grown on coated coverslips and transiently transfected with carboxy-terminal GFP fusion cDNA constructs of Rab4, Rab5a, Rab7 or Rab11 as indicated. 8 h after transfection, TMEM106B expression was induced for 16 h. Subsequently, TMEM106B was stained with an anti-HA antibody (red). Note that TMEM106B co-localizes best with the late endosome marker Rab7, but hardly co-localizes with early endosome markers Rab4 and Rab5a or with the recycling endosome marker Rab11 [155]. d) HeLa cells were grown on coverslips and co-transfected with N-terminally HA-tagged wt TMEM106B cDNA and the indicated Rab-GFP constructs. Cells were fixed in PFA and stained for TMEM106B with an anti-HA antibody and for lysosomes with an anti-LAMP1 antibody. Note that like in the stable T-REx<sup>TM</sup>293 cells (c), TMEM106B mainly co-localizes with Rab7 and LAMP1, but not with Rab5a or Rab11.

### 3.4 Complex glycosylation of TMEM106B is required for its cellular transport

To analyse which of the five N-glycosylation motifs of TMEM106B is complex glycosylated, HEK293T cells were transfected with the already mentioned glycosylation site mutants (N1<sub>mut</sub> to N1-5<sub>mut</sub>, see section 3.2.2, page 51) as well as the single glycosylation site mutants N4<sub>mut</sub> and N5<sub>mut</sub> and the double-mutant N4+5<sub>mut</sub>. Subsequently, cells were lysed and treated with either N-glycosidase F or endoglycosidase H (figure 3.9 a). Interestingly, combined mutation of the first three glycosylation motifs (N1-3<sub>mut</sub>) resulted in an endoglycosidase H-resistant TMEM106B variant suggesting that the fourth and the fifth glycosylation site are complex glycosylated whereas the first to the third are non-complex glycosylated (figure 3.9 a and b).

As glycosylation might play a role in cellular transport, I investigated the localization of the TMEM106B glycosylation variants in immunofluorescence. Thereby, abolishing non-complex glycosylation did not present with any obvious impact on TMEM106B localization shown by co-localization of N1-3<sub>mut</sub> with the lysosomal marker LAMP2 (figure 3.9 c). However, additional deletion of one (N1-4<sub>mut</sub>) or both (N1-5<sub>mut</sub>) complex glycosylation sites resulted in an accumulation of TMEM106B in the ER and an impaired transport to late endosomes/lysosomes (figure 3.9 c and d). To further investigate whether and which complex glycosylation site is responsible for cellular trafficking of TMEM106B, HeLa cells were transfected with either N4<sub>mut</sub>, N5<sub>mut</sub> or N4+5<sub>mut</sub> (figure 3.9 c and d). As the deletion of both complex glycosylation sites (N4+5<sub>mut</sub>) led to a similar phenotype than N1-4<sub>mut</sub> or N1-5<sub>mut</sub>, complex glycosylation indeed seems to play a role in cellular trafficking of TMEM106B (figure 3.9 c and d). Interestingly, whereas mutation of the fifth glycosylation site (N5) resulted in a strong lamellipodia-like staining suggesting prominent cell surface localization, mutation of the fourth glycosylation site only (N4) led to ER retention of TMEM106B and thus impaired forward transport to late endosomes/lysosomes (figure 3.9 c and d). Accordingly, complex glycosylation seems to be important for correct TMEM106B localization within the cell.

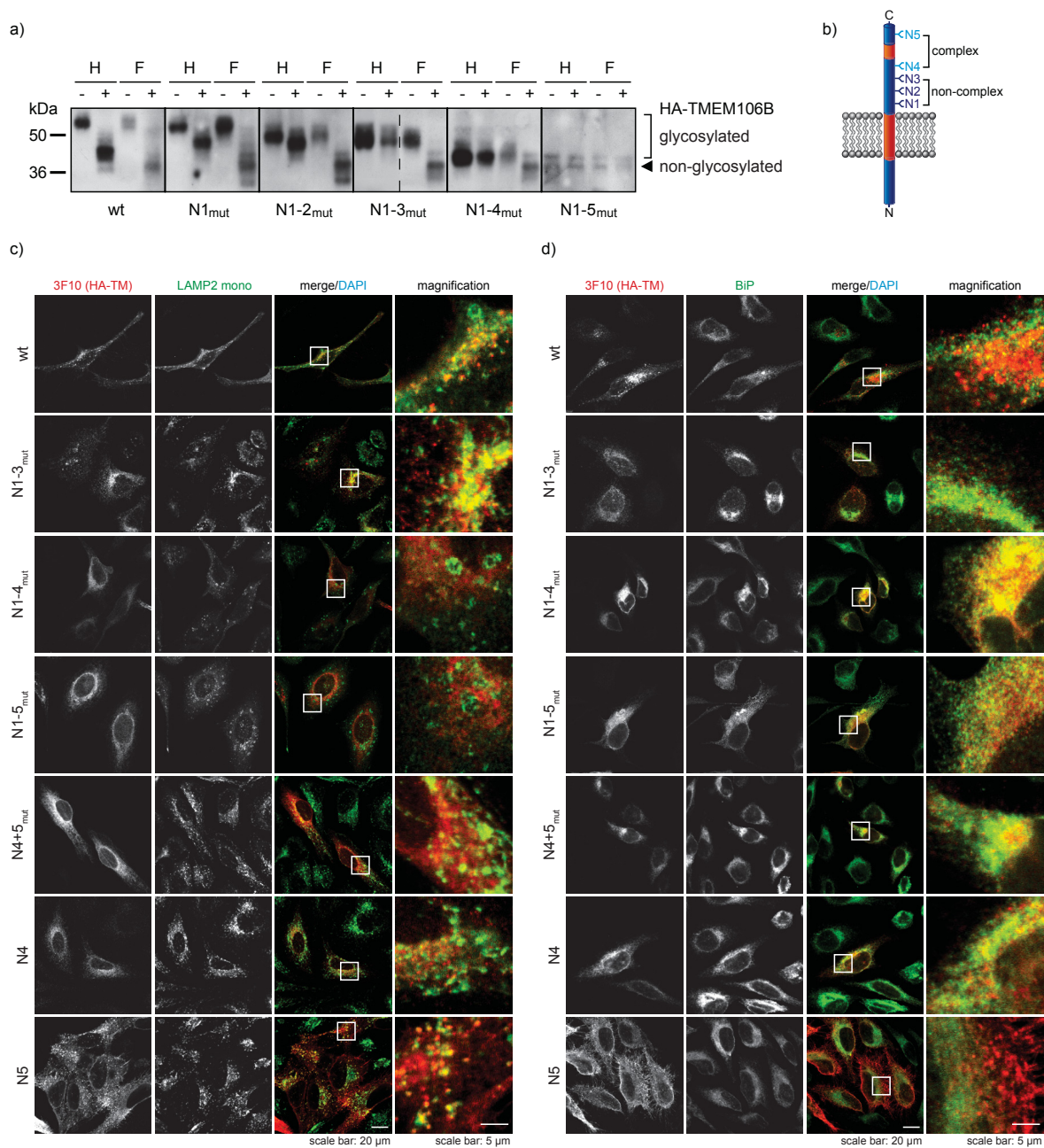


**Figure 3.9: Localization of TMEM106B is influenced by complex glycosylation**

a) Lysates of HEK293T cells transiently transfected with the indicated N-terminally HA-tagged TMEM106B glycosylation mutants were treated with either N-glycosidase F (F) or endoglycosidase H (H) for 16 h before separation by SDS-PAGE and immunoblotting with an anti-HA antibody. Controls were incubated in the appropriate buffer without the enzyme [155]. b) Model of TMEM106B depicting the non-complex glycosylation sites (in dark blue) and the complex ones (in light blue). c & d) HeLa cells were transiently transfected with the indicated N-terminally HA-tagged TMEM106B glycosylation mutants and subjected to immunofluorescence. Thereby, the cells were stained for TMEM106B with an anti-HA antibody (red) and either co-stained with the lysosomal marker anti-LAMP2 (c) or the ER marker anti-BiP (d) (green) [155].

### 3.5 *TMEM106B* and *GRN* do not influence each other directly

*TMEM106B* risk variants were found to be especially associated with *GRN* mutation carriers [301] (see also section 1.2.2, page 22). Moreover, van Deerlin *et al.* claimed that risk carriers showed higher *TMEM106B* expression and that in FTLT-TDP cases, *TMEM106B* mRNA levels were 2.5-fold increased compared to controls [301]. Together, this suggested a direct relationship between *GRN* and *TMEM106B* expression levels. Therefore, I investigated the influence of *TMEM106B* overexpression and knockdown on *GRN* in a cell culture model. For *TMEM106B* overexpression, tetracycline-induced T-REx<sup>TM</sup>293 cells stably expressing N-terminally HA-tagged wt *TMEM106B* were used (figure 3.10 a and b). As control served non-induced stable cells as well as non-transfected T-REx<sup>TM</sup>293 cells. However, neither on mRNA nor on protein level (media and lysate), any changes of *GRN* could be observed (figure 3.10 a and b). The same applied to SH-SY5Y cells transiently transfected with N-terminally HA-tagged *TMEM106B* (figure 3.10 c). Next, the influence of *TMEM106B* knockdown on *GRN* was examined with the use of the anti-*TMEM106B* antibody 6F2 (validation of the antibody see Material and Methods 5.1.9), but even though the *TMEM106B* knockdown efficiency was more than 90 % (on mRNA level), no differences on either *GRN* mRNA or on protein levels were observed in both HEK293T and SH-SY5Y cells (figure 3.11). Thus, *TMEM106B* and *GRN* probably do not interact directly, but may influence each other indirectly through a common pathway.

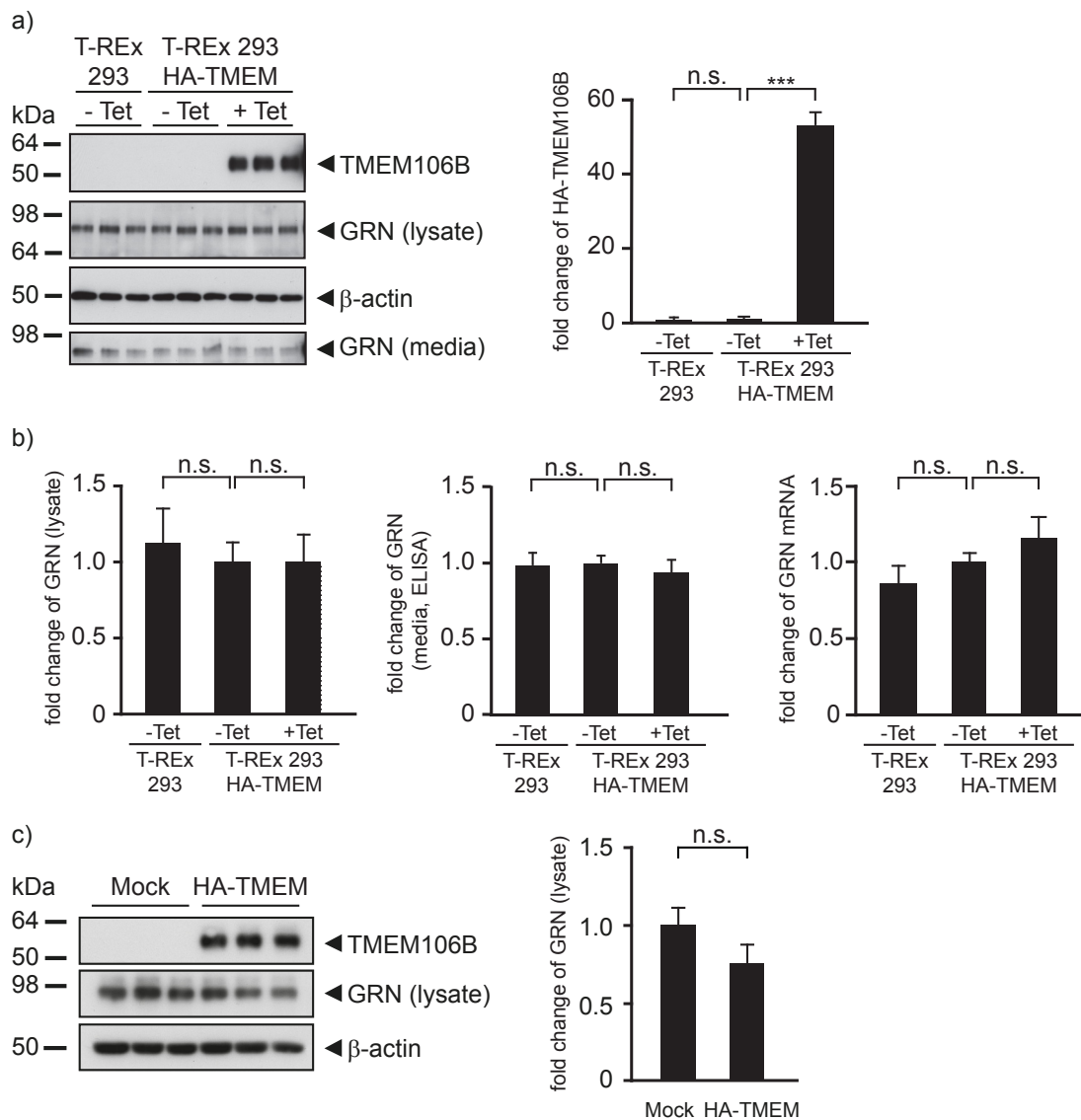


**Figure 3.10: TMEM106B overexpression does not influence GRN levels**

a) T-REx<sup>TM</sup>293 cells stably expressing N-terminally HA-tagged wt TMEM106B were (+Tet) and were not (-Tet) tetracycline-treated for 16 h. As a control served untransfected and non-induced T-REx<sup>TM</sup>293 cells. Conditioned media and lysates were analysed for GRN and TMEM106B expression by SDS-PAGE and subsequent immunoblotting where β-actin served as loading control. The bar graph represents the quantification of TMEM106B expression by measuring the chemiluminescence on the immunoblot. Data are shown as fold change normalized to non-induced cells, means ± S.D. (n=3) are depicted (\*\*\*:  $p < 0.001$  and not significant (n.s.) by one-way ANOVA *post hoc* Dunnett's test) [155]. b) Bar graphs represent the quantification of GRN protein levels from the immunoblot by chemiluminescence and from the media by ELISA. GRN mRNA levels were quantified by real-time PCR. Data are shown as fold change in GRN levels after TMEM106B induction, means ± S.D. (n= 3) are depicted (n.s. by one-way ANOVA *post hoc* Dunnett's test) [155]. c) SH-SY5Y cells were transiently transfected with N-terminally HA-tagged wt TMEM106B and TMEM106B and GRN levels were detected by SDS-PAGE and subsequent immunoblotting. β-actin served as loading control. The bar graph represents the quantification of GRN levels by measuring the chemiluminescence of the immunoblot. Data are shown as fold change normalized to mock-treated control cells, means ± S.D. (n=3) are depicted (n.s. by unpaired student's t-test).

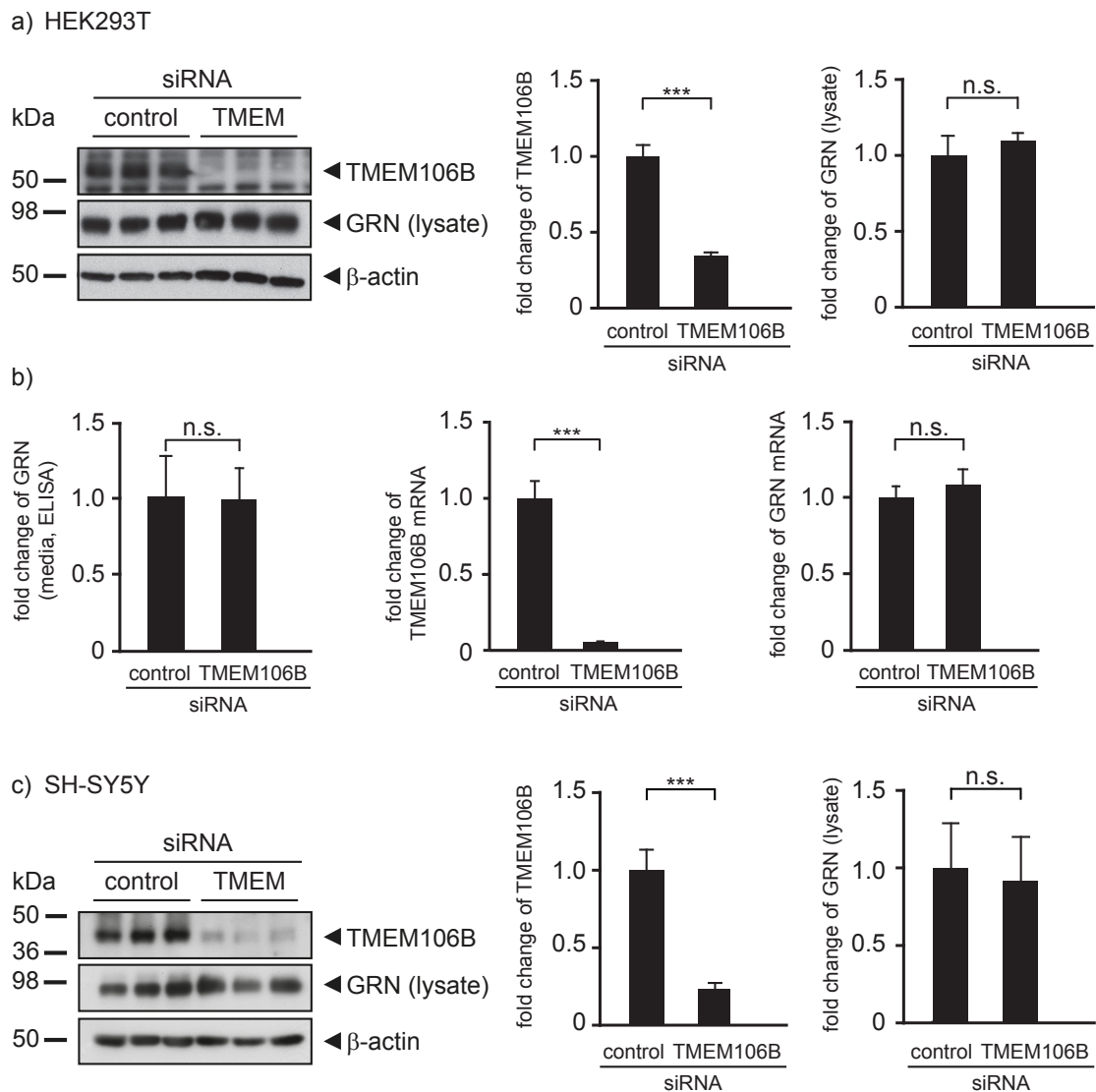


**Figure 3.11: TMEM106B knockdown does not influence GRN levels**

a) HEK293T cells were either transfected with an siRNA pool against TMEM106B or with non-targeting control siRNA. 72 h after transfection, conditioned media of the last 16 h of siRNA transfection was collected, and total RNA or cell lysates prepared. TMEM106B and GRN expression were analysed by SDS-PAGE and subsequent immunoblotting. The bar graphs represents the quantification of TMEM106B and GRN expression by measuring the chemiluminescence on the immunoblot. Data are shown as fold change normalized to non-targeting siRNA-treated cells, means  $\pm$  S.D. ( $n=3$ ) are depicted (\*\*\*:  $p < 0.001$  and n.s. by unpaired student's t-test) [155]. b) Bar graphs represent the quantification of GRN protein levels from the media by ELISA. GRN and TMEM106B mRNA levels were quantified by real-time PCR. Data are shown as fold change normalized to non-targeting siRNA-treated cells, means  $\pm$  S.D. ( $n=3$ ) are depicted (n.s. by unpaired student's t-test) [155]. c) SH-SY5Y cells were transfected with an siRNA pool against TMEM106B or with non-targeting control siRNA and cell lysates were analysed 72 h post transfection. The bar graph represents the quantification of TMEM106B and GRN levels by measuring the chemiluminescence of the immunoblot. Data are shown as fold change normalized to non-targeting control siRNA-treated cells, means  $\pm$  S.D. ( $n=3$ ) are depicted (\*\*\*:  $p < 0.001$  and n.s. by unpaired student's t-test) [155].

### 3.6 Impaired acidification increases TMEM106B protein levels

In 2011, Capell *et al.* showed that GRN deficiency, which is associated with FTLD-TDP, can be rescued by inhibiting the vacuolar H<sup>+</sup>-ATPase with BafA1, a drug that compromises lysosomal acidification [37]. Moreover, as Van Deerlin *et al.* suggested a relationship (even though probably indirect) between TMEM106B and GRN [301] and TMEM106B seems to be localized in BafA1-sensitive compartments, i.e. in lysosomes, I examined whether TMEM106B is required for the elevation of GRN levels after BafA1 treatment and whether inhibition of the H<sup>+</sup>-ATPase had an impact on TMEM106B levels.

Indeed, upon induction of TMEM106B expression in T-REx<sup>TM</sup>293 cells stably expressing N-terminally HA-tagged wt TMEM106B and subsequent BafA1 treatment, a significant increase in TMEM106B levels could be observed (figure 3.12 a). However, even though GRN levels increased upon BafA1 treatment, the increase was not influenced by TMEM106B overexpression (figure 3.12 a). Next, TMEM106B and GRN levels were analysed under TMEM106B knockdown conditions with and without BafA1 treatment. Again, the increase in GRN levels after BafA1 treatment was not influenced by TMEM106B (figure 3.12 b), but interestingly, endogenous TMEM106B levels were elevated dramatically upon H<sup>+</sup>-ATPase inhibition (figure 3.12 b). Thus, even though GRN and TMEM106B did not influence each other directly, BafA1 treatment had an impact on both proteins hinting that they may act in a common pathway.

Analysing TMEM106B mRNA levels revealed a slight increase (1.5-fold) upon BafA1 treatment, however, to a much lesser extent than on protein level (figure 3.12 c). Therefore, I tested whether either impaired transcription or translation could abolish the increase in TMEM106B protein levels after BafA1 treatment. Interestingly, whereas treatment with actinomycin, a drug that inhibits transcription, did not impair the increase in TMEM106B levels after BafA1 treatment, treatment with cycloheximide, which compromises translation, strongly reduced the BafA1 effect on TMEM106B levels (figure 3.13 a). Thus, protein stabilization alone probably cannot account for the elevated protein levels of TMEM106B after BafA1 treatment. Supporting this finding, cells treated with lysosomal protease inhibitors did not result in elevated TMEM106B levels comparable to BafA1 treatment (figure 3.13 b). Also, inhibition of proteasomal degradation by epoxomicin did not influence TMEM106B expression levels to the same extent than BafA1 (figure 3.13 b). In summary, these data therefore suggest a predominant post-transcriptional mechanism to be involved in the BafA1-mediated increase in TMEM106B protein levels.

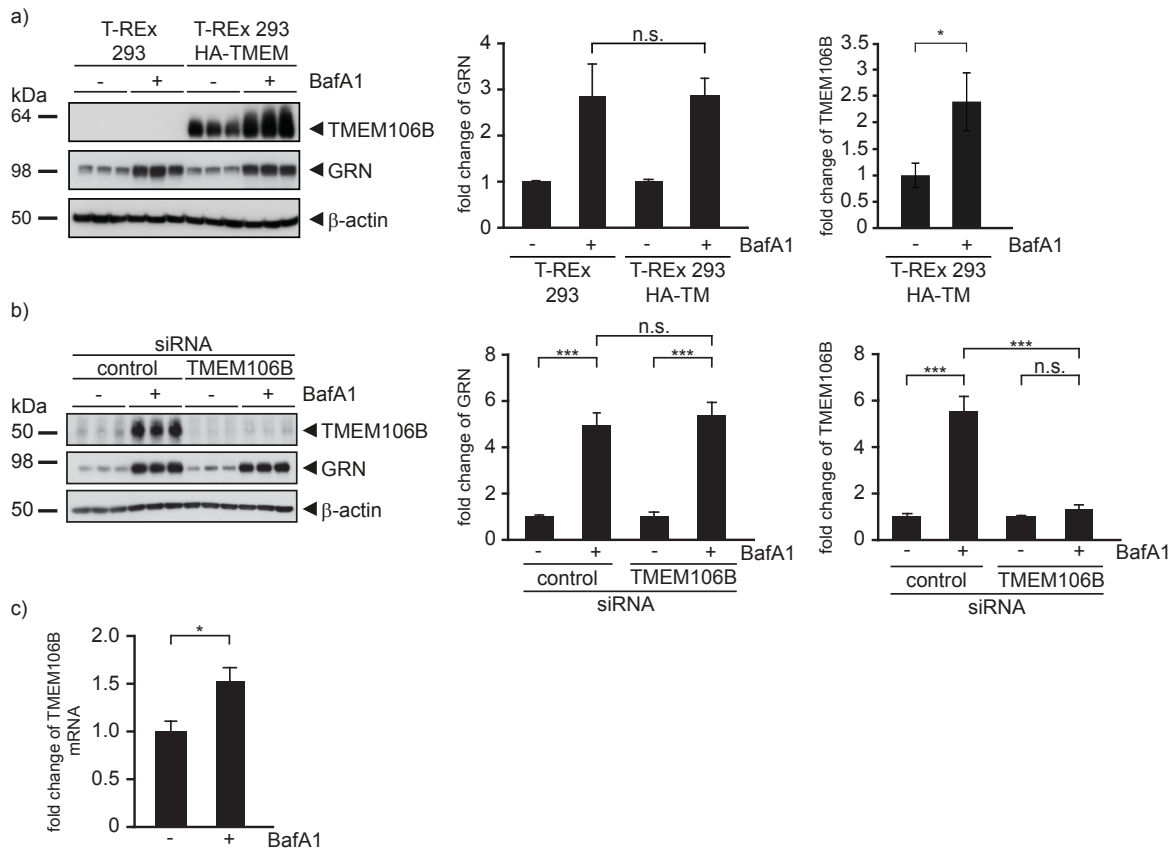


**Figure 3.12: TMEM106B accumulates in lysosomes upon BafA1 treatment**

a) TMEM106B expression was induced with 0.2  $\mu$ g/ml tetracycline in T-REx<sup>TM</sup>293 cells stably expressing N-terminally HA-tagged wt TMEM106B and cells were either treated or not treated with BafA1 for 16 h. As a control, T-REx<sup>TM</sup>293 cells were also treated or not treated with BafA1. Cells were lysed and TMEM106B and GRN expression were analysed by SDS-PAGE and subsequent immunoblotting and quantified via chemiluminescence.  $\beta$ -actin served as loading control. Data are shown as fold change normalized to the untreated controls, means  $\pm$  S.D. (n=3) are depicted (n.s. and \*:  $p < 0.05$  by one-way ANOVA *post hoc* Tukey's test and unpaired student's t-test) [155]. b) HEK293T cells were either transfected with an siRNA pool against TMEM106B or with non-targeting siRNA as a control and treated with or without BafA1 for 16 h. Cell lysates were subjected to SDS-PAGE and immunoblotting to analyse TMEM106B and GRN expression levels.  $\beta$ -actin served as loading control. Subsequently, TMEM106B and GRN levels were quantified by chemiluminescence. Data was normalized to untreated cells, and depicted as means  $\pm$  S.D. (n=3; \*\*\*:  $p < 0.001$  and n.s. by one-way ANOVA *post hoc* Tukey's test) [155]. c) TMEM106B mRNA levels of BafA1- and control-treated cells were analysed by real-time PCR. Data are normalized to control cells and depicted as means  $\pm$  S.D. (n=3; \*:  $p < 0.05$  by unpaired student's t-test) [155].

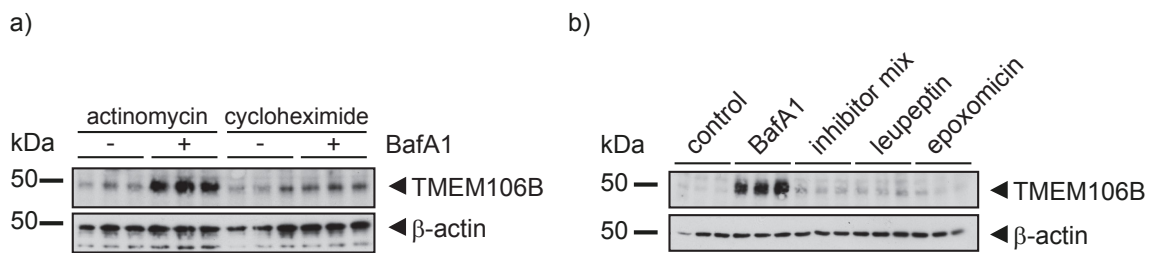


**Figure 3.13: Stabilization of TMEM106B alone cannot account for the increase in protein levels after BafA1 treatment**

a) HEK293T cells were either treated with actinomycin (to inhibit transcription) or cycloheximide (to inhibit translation) during treatment with/without BafA1. Cell lysates were analysed on immunoblot for TMEM106B expression with an anti-TMEM106B antibody. β-actin served as loading control [155]. b) HEK293T cells were treated with BafA1, a mixture of lysosomal protease inhibitors (leupeptin, E64, antipain), leupeptin or epoxomicin, a proteasomal inhibitor. Cell lysates were analysed on immunoblot for TMEM106B expression with an anti-TMEM106B antibody. β-actin served as loading control [155].

## 3.7 Lysosomal positioning changes upon TMEM106B knockdown

### 3.7.1 Upon TMEM106B knockdown, lysosomes cluster in the perinuclear region of the cell

For analysing TMEM106B function, I focused on knockdown experiments. Before I started to examine the effects of TMEM106B knockdown, however, I established the conditions for further experiments. Thus, to test the knockdown efficiency of the TMEM106B siRNAs used in this study (see also Material and Methods, section 5.1.4, page 118), mRNA levels of TMEM106B were analysed by real-time PCR after knocking down TMEM106B with TMEM106B siRNA (figure 3.14 a and b). Thereby, TMEM106B #17 (#17) siRNA showed a TMEM106B knockdown efficiency of only less than 25 % (in HEK293T cells), whereas the other siRNAs presented with a very good knockdown efficiency (siRNA pool: 96 %; TMEM106B #2 (#2): 95 %; TMEM106B #3 (#3): 94 %; TMEM106B #4 (#4): 87 % in HEK293T cells; TMEM106B #3 (#3): 90 % in HeLa cells). The knockdown efficiency was also analysed on protein level by immunoblotting, where the remaining TMEM106B levels were 33 % (siRNA pool), 17 % (#2), 27 % (#3), 27 % (#4) and 63 % (#17) of TMEM106B levels detected in the non-targeting siRNA treated-cells, respectively (figure 3.14 c). Of note, cells treated with TMEM106B #2 siRNA seemed to die to a much greater extent than cells that were treated with the other siRNAs (data not shown). Thus, for the following experiments, TMEM106B knockdown was performed with TMEM106B #3 siRNA as it presented with the best knockdown efficiency compared to the remaining TMEM106B siRNAs.

Strikingly, knocking down TMEM106B resulted in a change in lysosomal positioning, namely lysosomal clustering in the perinuclear region of the cell (figure 3.15 a). This phenotype was especially prominent in HeLa cells (figure 3.15 b, left panel) but could also be observed in SH-SY5Y cells where lysosomes did not predominantly cluster at one site near the nucleus, but were found to be arranged in a ring-like form around the nucleus (figure 3.15 b, right panel). Thus, for the following experiments, I chose HeLa cells to further investigate this clustering phenotype. To exclude that lysosomal clustering was due to side effects of the siRNAs used, I transfected not only the siRNA pool against TMEM106B, but also the single siRNAs of the pool, namely TMEM106B #2, TMEM106B #3, TMEM106B #4 and TMEM106B #17. Whereas the transfection of TMEM106B #2 siRNA was too toxic for the cells as evidenced by a large amount of cell death (data not shown), transfection of either TMEM106B #3 or TMEM106B #4 siRNA resulted in pronounced lysosomal clustering (figure 3.15 b). However, cells transfected with TMEM106B #17 only showed a very mild clustering phenotype, if at all (figure 3.15 b). These observations correlate well with the knockdown efficiencies of the respective siRNAs (see figure 3.14) thus hinting that lysosomal clustering might indeed be caused by TMEM106B knockdown and not be the result of siRNA side effects.

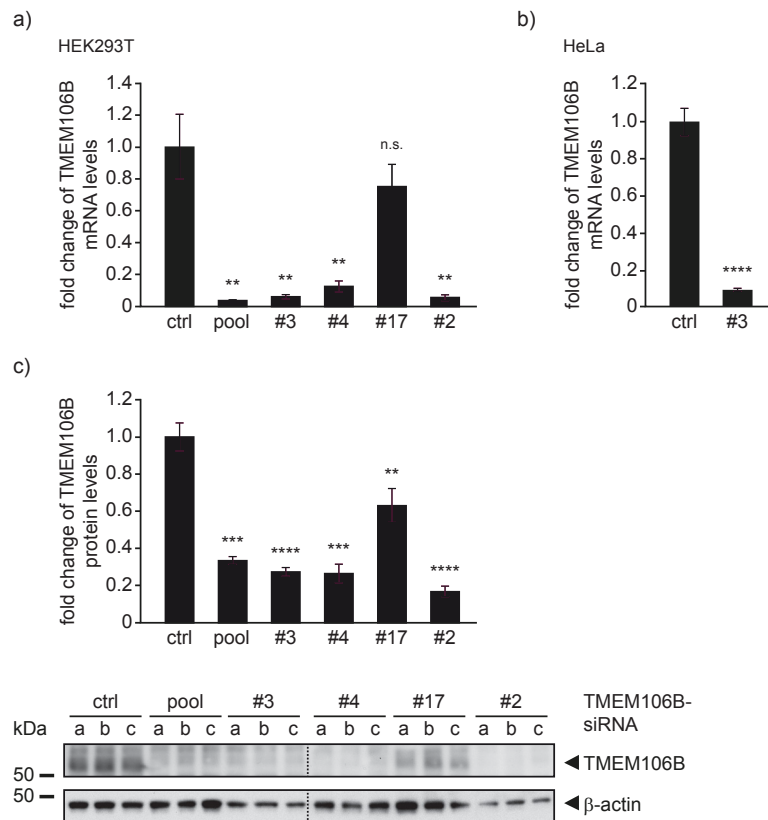


**Figure 3.14: TMEM106B knockdown efficiencies**

a) HEK293T cells were transfected with either non-targeting control (ctrl) siRNA, an siRNA pool against TMEM106B (pool) or with the single siRNAs against TMEM106B, TMEM106B #2 (#2), TMEM106B #3 (#3), TMEM106B #4 (#4) and TMEM106B #17 (#17). Subsequently, real-time PCR was performed to measure TMEM106B mRNA levels. Data are normalized to control-treated cells according to the  $\Delta\Delta C_t$  method and depicted as means  $\pm$  S.D. (n=3; \*\*:  $p < 0.01$  and n.s. by unpaired student's t-test). b) HeLa cells were transfected with either non-targeting control (ctrl) siRNA or with TMEM106B siRNA TMEM106B #3 (#3). TMEM106B mRNA levels were quantified by real-time PCR. Data are normalized to control-treated cells and depicted as means  $\pm$  S.D. (n=3; \*\*\*\*:  $p < 0.0001$  by unpaired student's t-test). c) HEK293T cells were transfected with either non-targeting control (ctrl) siRNA, an siRNA pool against TMEM106B (pool) or with the single siRNAs against TMEM106B, TMEM106B #2 (#2), TMEM106B #3 (#3), TMEM106B #4 (#4) and TMEM106B #17 (#17). Cell lysates were analysed on immunoblot for TMEM106B expression with an anti-TMEM106B antibody.  $\beta$ -actin served as loading control. The bar graph represents the quantification of the immunoblot by chemiluminescence. Data are normalized to control siRNA-treated cells and depicted as means  $\pm$  S.D. (n=3; \*\*\*\*:  $p < 0.0001$ , \*\*\*:  $p < 0.001$ , \*\*:  $p < 0.01$  by unpaired student's t-test).

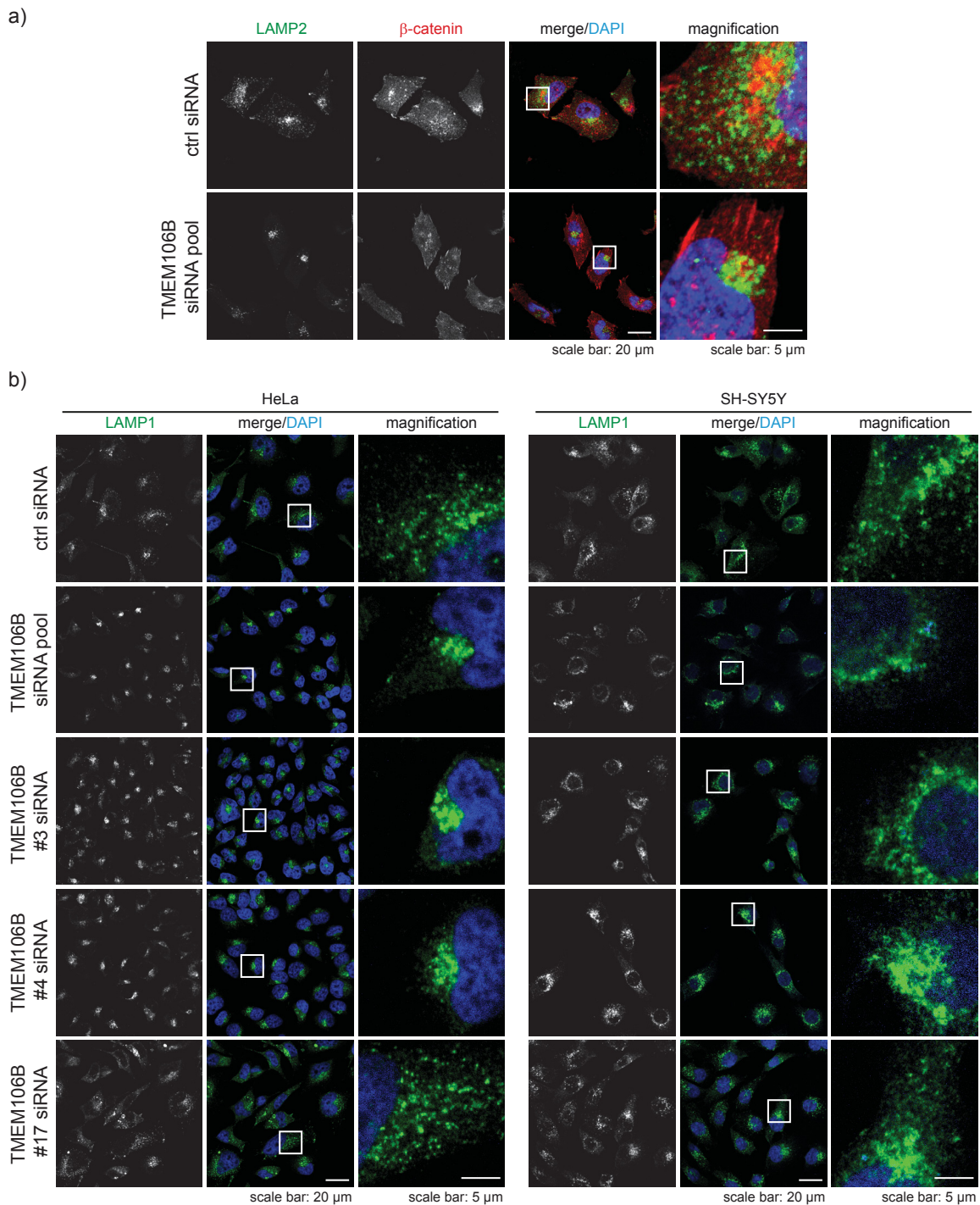


**Figure 3.15: Lysosomal clustering upon TMEM106B knockdown**

a) HeLa cells were transfected with either non-targeting control siRNA or an siRNA pool against TMEM106B and immunostained with antibodies against LAMP2 (green) and  $\beta$ -catenin (red) to visualize the cell size. Note the tight clustering of lysosomes in the perinuclear region of TMEM106B siRNA-treated cells [263].

b) HeLa (left panel) and SH-SY5Y (right panel) cells were transfected with control (ctrl), non-targeting siRNA, an siRNA pool against TMEM106B and with the single siRNAs against TMEM106B, TMEM106B #3, TMEM106B #4 and TMEM106B #17. Cells were immunostained with an antibody against LAMP1. Note that lysosomes clustered in the perinuclear region in cells transfected with either TMEM106B #3, TMEM106B #4 or the siRNA pool against TMEM106B, whereas the lysosomal phenotype in TMEM106B #17 siRNA-transfected cells resembled the one in control siRNA-treated cells.

### 3 Results

---

To establish the experimental set-up for TMEM106B knockdown experiments, HeLa cells were transfected with TMEM106B siRNA TMEM106B #3 on day 0 and fixed at day 1, day 2 and day 3 after transfection in order to find the optimal conditions for analysing the clustering phenotype (figure 3.16). On day 1, lysosomes were still distributed throughout the whole cell with only a mild clustering at the perinuclear region. However, the phenotype became more obvious the longer the knockdown period lasted and was best at day 3 (figure 3.16, right panel). Therefore, for the following experiments, cells were harvested or fixed on day 3, which was 72 h post transfection.

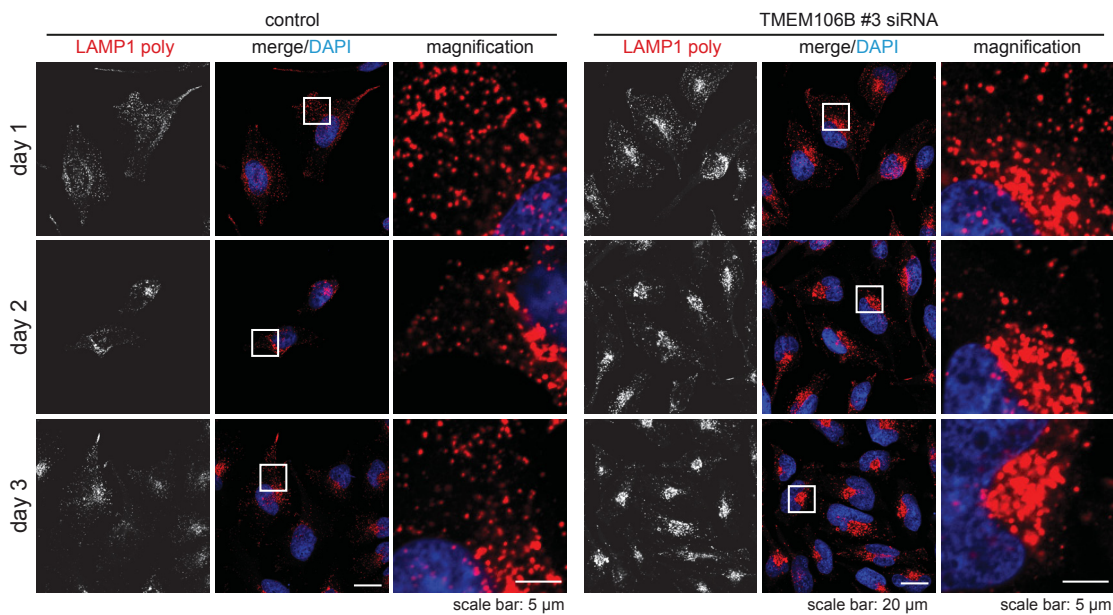


**Figure 3.16: Lysosomal clustering phenotype increases with TMEM106B knockdown duration**  
On day 0, HeLa cells were transfected with either non-targeting control siRNA (control) or with TMEM106B siRNA TMEM106B #3 and fixed on day 1, day 2 or day 3 post-transfection. Subsequently, cells were immunostained for lysosomes with an anti-LAMP1 antibody. Note that in control cells, lysosomes remain distributed throughout the whole cell whereas in TMEM106B siRNA-treated cells, lysosomes increasingly cluster in the perinuclear region.

### 3.7.2 Lysosomal clustering upon TMEM106B knockdown can be rescued by overexpressing wt TMEM106B

To verify that the lysosomal clustering phenotype resulted from the lack of TMEM106B protein and was not caused by side effects of the TMEM106B siRNAs, a rescue experiment was performed (figure 3.17). Thereby, HeLa cells were either transfected with non-targeting control siRNA or with TMEM106B #3 siRNA to knockdown TMEM106B. Two days after siRNA transfection, either an empty control vector or a vector carrying a TMEM106B #3 siRNA-resistant, N-terminally HA-tagged TMEM106B wt construct was transfected. Importantly, to avoid overexpression artefacts, TMEM106B levels were carefully titrated. The TMEM106B #3 siRNA-resistant N4 glycosylation TMEM106B variant served as an additional control as this protein variant has been shown to be retained in the ER (see section 3.4, page 57). Accordingly, the N4 variant would not reach the lysosome and thus not be able to rescue the clustering phenotype. On day 3 after siRNA transfection, cells were subjected to immunofluorescence.

In control siRNA-transfected cells expressing HA-tagged TMEM106B, lysosomes were distributed throughout the cell with a tendency to be more localized to the tips (figure 3.17). In TMEM106B #3 siRNA transfected cells, lysosomes clustered in the perinuclear region and transfection of the empty vector did not influence this phenotype (figure 3.17). However, in TMEM106B #3 siRNA transfected cells that expressed HA-tagged wt TMEM106B, lysosomes were almost normally distributed throughout the cell, suggesting a successful rescue of the clustering phenotype (figure 3.17). As there was no good antibody available for the staining of TMEM106B, I did not co-stain for endogenous TMEM106B expression to verify the TMEM106B knockdown. However, TMEM106B knockdown efficiency in general is very high and in TMEM106B #3 siRNA-transfected cells, almost every cell shows lysosomal clustering. Thus, TMEM106B knockdown had very likely been successful and, accordingly, the observed spreading of lysosomes in the rescue set-up was due to exogenous TMEM106B wt expression. This was further supported by the fact that overexpression of the siRNA-resistant N4 TMEM106B construct could not rescue the lysosomal clustering phenotype (figure 3.17).

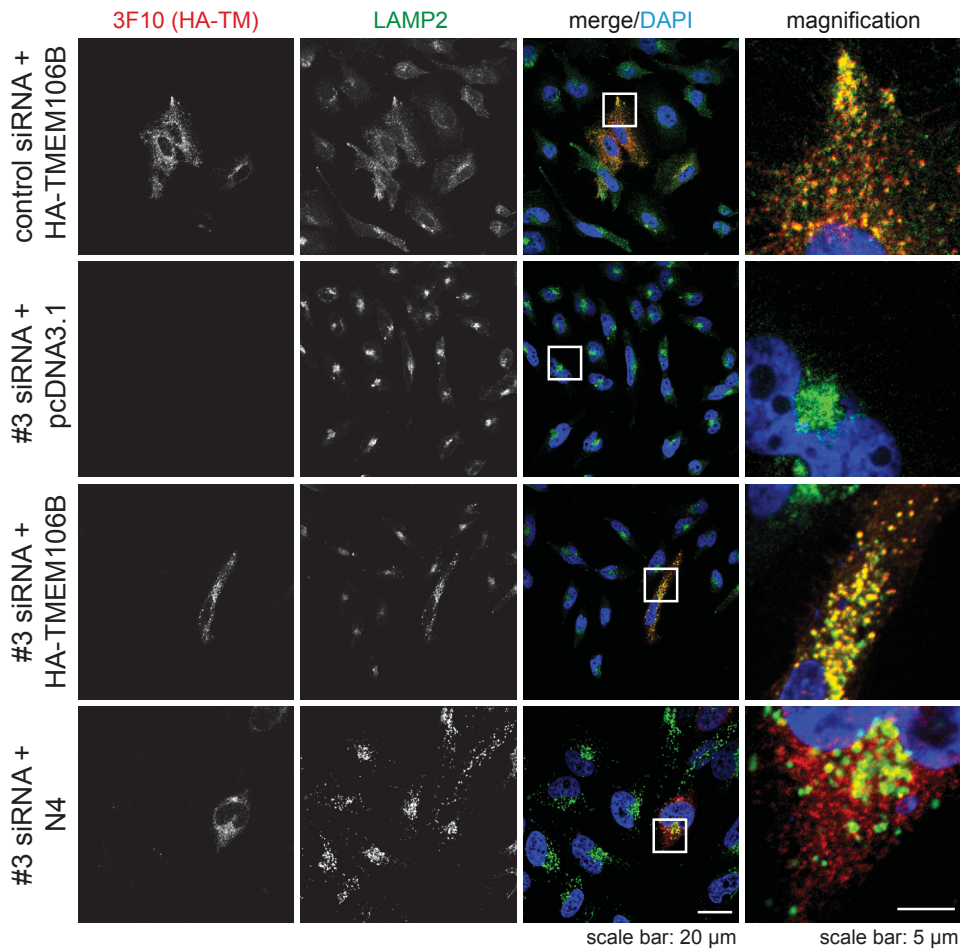


**Figure 3.17: Lysosomal clustering upon TMEM106B knockdown can be rescued by the overexpression of wt TMEM106B**

HeLa cells were reversly transfected with either non-targeting control siRNA (control) or with TMEM106B siRNA TMEM106B #3 (#3). After two days of siRNA transfection, TMEM106B #3 siRNA-resistant HA-TMEM106B (wt TMEM106B) and N4 (fourth glycosylation site of TMEM106B deleted) were transfected. The empty vector pcDNA3.1 served as a control. On day 3 after siRNA transfection, cells were subjected to immunofluorescence and stained with antibodies against LAMP2 (lysosomal marker, green) and HA (red) to mark exogeneous TMEM106B. Note that lysosomal clustering could be rescued by overexpressing the N-terminally HA-tagged wt TMEM106B construct [263], but not by overexpression of the glycosylation mutant N4.

### 3.7.3 Lysosomes cluster at the microtubule-organizing center

From the literature, it is known that lysosomes traffic along microtubules and tend to cluster at the microtubule-organizing center [31, 177]. Hence, I investigated whether upon TMEM106B knockdown, lysosomes were indeed concentrated at the MTOC. Therefore, I transfected HeLa cells with TMEM106B siRNA TMEM106B #3 and analysed lysosomal clustering by immunofluorescence. Lysosomes were co-stained with  $\gamma$ -tubulin, a marker for the MTOC (figure 3.18). In fact, lysosomes clustered at the MTOC suggesting a role for lysosomal transport along microtubules in lysosomal clustering mediated by TMEM106B knockdown.

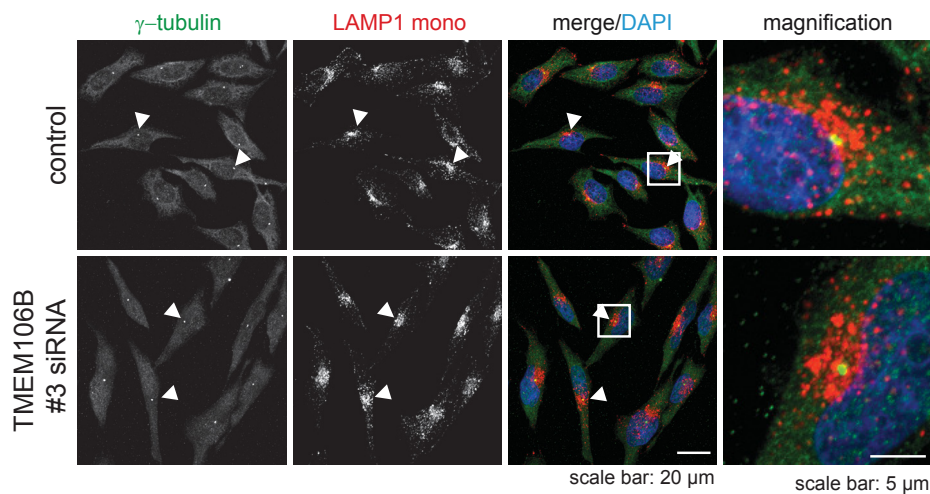


**Figure 3.18: Upon TMEM106B knockdown, lysosomes cluster at the microtubule-organizing center** HeLa cells were transfected with either non-targeting control siRNA (control) or with TMEM106B siRNA TMEM106B #3 and immunostained with antibodies against LAMP1 (red) and  $\gamma$ -tubulin (marker for the MTOC, green). The arrowheads point towards the MTOC [263].

### 3.7.4 Quantification of lysosomal positioning after TMEM106B knockdown

To quantify lysosomal clustering, automated quantitative image analysis was performed measuring the average distance of lysosomes to the nucleus and the lysosomal distribution using the Clark aggregation index (see Material and Methods, section 5.2.5, page 139) [44] (figure 3.19). Thereby, in TMEM106B siRNA-transfected cells, lysosomes were clearly more shifted towards the nucleus and showed a more compact subcellular distribution of lysosomes than the controls (figure 3.19).

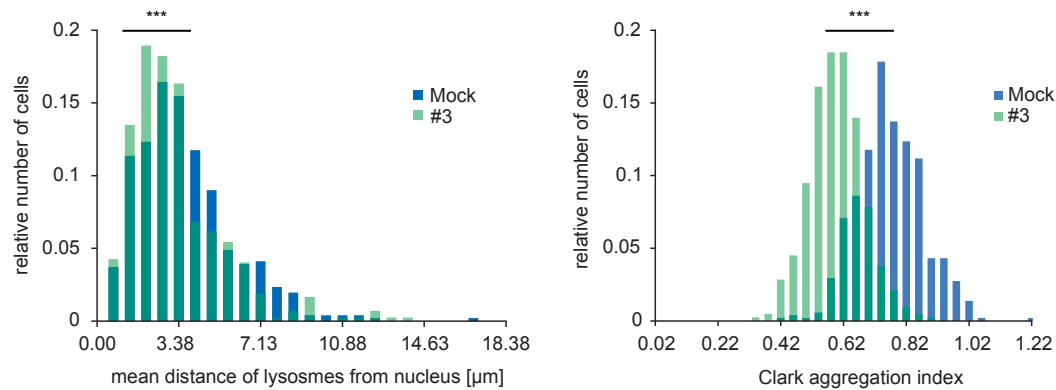


**Figure 3.19: Quantification of the lysosomal clustering phenotype mediated by TMEM106B knock-down**

Immunofluorescence pictures of HeLa cells transfected with TMEM106B siRNA TMEM106B #3 (#3) or transfection reagent only (Mock) were analysed according to lysosomal positioning by automated quantitative image analysis. Thereby, the mean distance of the lysosomes to the nucleus was measured and clustering was quantified by the Clark aggregation index [44]. In three independent experiments, a total of 510 control cells and 422 TMEM106B siRNA-treated cells were analysed. Data showed significant differences between control and knockdown of TMEM106B according to the Mann-Whitney-U-test (\*\*\*:  $p < 0.001$ ) [263].

In summary, these data suggest that TMEM106B is involved in lysosomal localization and trafficking.

### 3.8 Influence of TMEM106B knockdown on other cellular organelles and structures

One explanation for the altered lysosomal positioning observed after TMEM106B knockdown might be a general modification of cellular trafficking which would then not only affect lysosomes but other cellular organelles as well. Therefore, I investigated whether TMEM106B knockdown also influenced the localization of the ER, the Golgi, mitochondria or early endosomes. Yet, neither the morphology of the ER nor of the Golgi apparatus showed any obvious differences upon TMEM106B knockdown (figure 3.20 a, b and c). Also, mitochondria did not cluster even though they might be slightly elongated (figure 3.20 d). However, interestingly, EEA1-positive vesicles (early endosomes or amphisomes [69]) seemed to cluster in the same region as lysosomes (figure 3.21 a and b) suggesting that TMEM106B influences not only lysosomal positioning but might have a broader impact on endocytic vesicle trafficking.

Since for vesicle trafficking, an intact cytoskeleton is essential, I analysed whether the actin or microtubule network morphology was altered upon TMEM106B knockdown. Therefore, I knocked down TMEM106B in HeLa cells and stained for either the actin (phalloidin) or the microtubule ( $\alpha$ -tubulin) cytoskeleton (figure 3.22). Even though both seemed to be intact, it was conspicuous that upon TMEM106B knockdown, HeLa cells often presented with an elongated shape (figure 3.22).

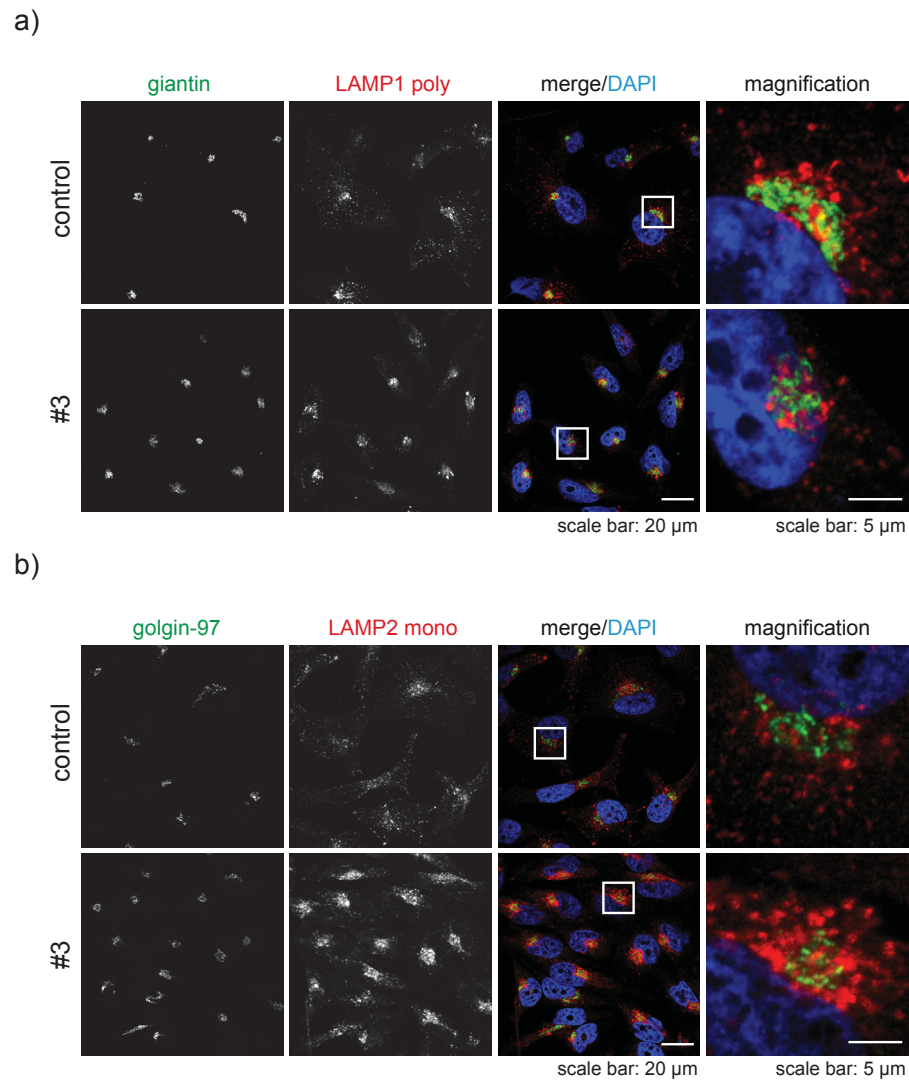


**Figure 3.20: ER, Golgi and mitochondria morphology was not altered upon TMEM106B knockdown**  
HeLa cells were transfected with either non-targeting control siRNA or TMEM106B #3 siRNA (#3) to knock-down TMEM106B and subsequently subjected to immunofluorescence. To visualize successful TMEM106B knockdown or more precisely, lysosomal clustering, lysosomes were stained with antibodies against LAMP1 or LAMP2 (red). a) The Golgi apparatus was stained with the cis-Golgi marker antibody anti-giantin (green) and b) with the trans-Golgi marker antibody anti-golgin-97 (green).

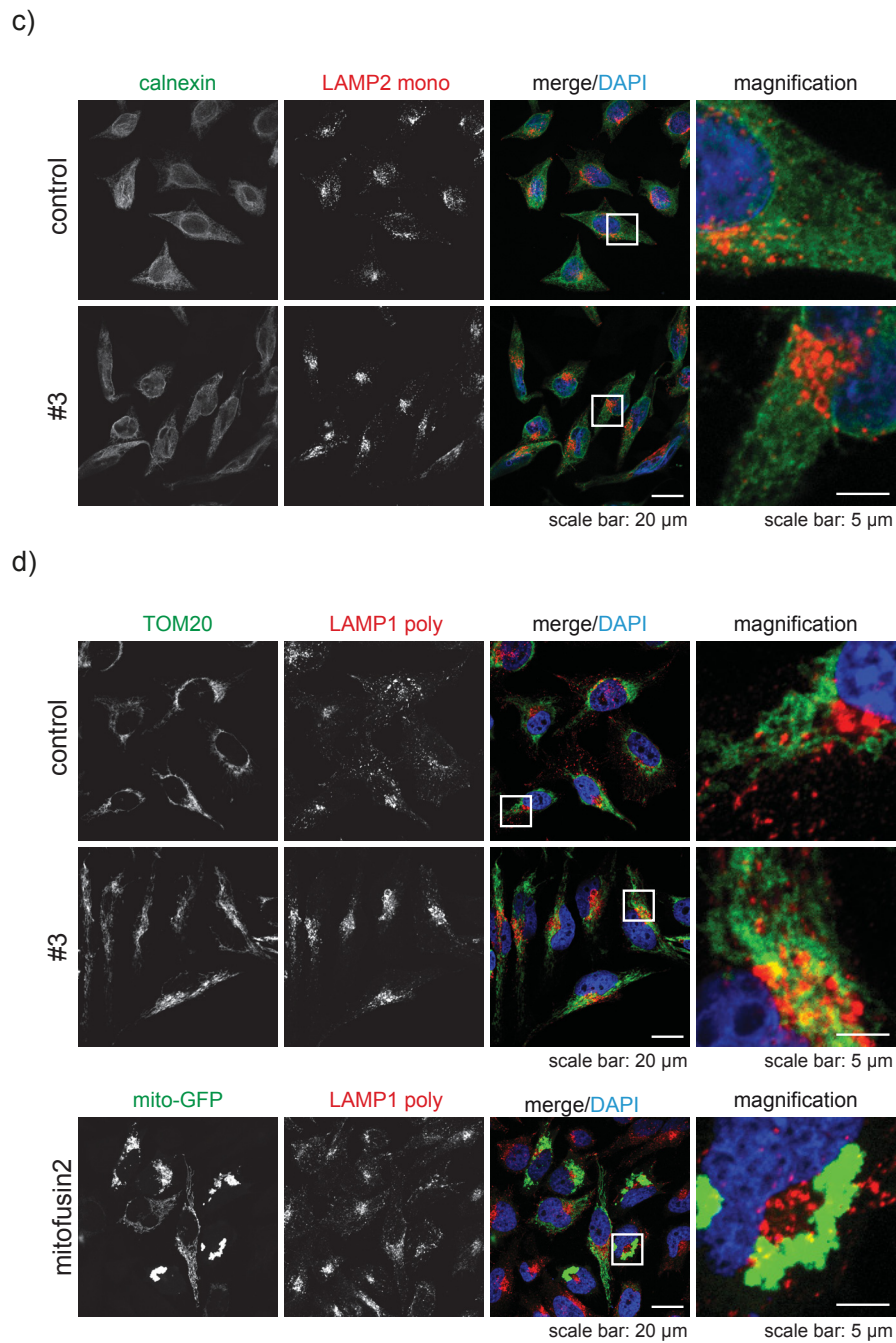


**Figure 3.20 (continued): ER, Golgi and mitochondria morphology was not altered upon TMEM106B knockdown**

c) The ER was stained with the marker antibody anti-calnexin (green) and d) mitochondria were stained with the marker antibody anti-TOM20 (green). To demonstrate how mitochondrial clustering would look like, HeLa cells were transfected with a mitofusin2-cDNA construct [214]. Mitochondria were stained with mito-GFP, respectively.

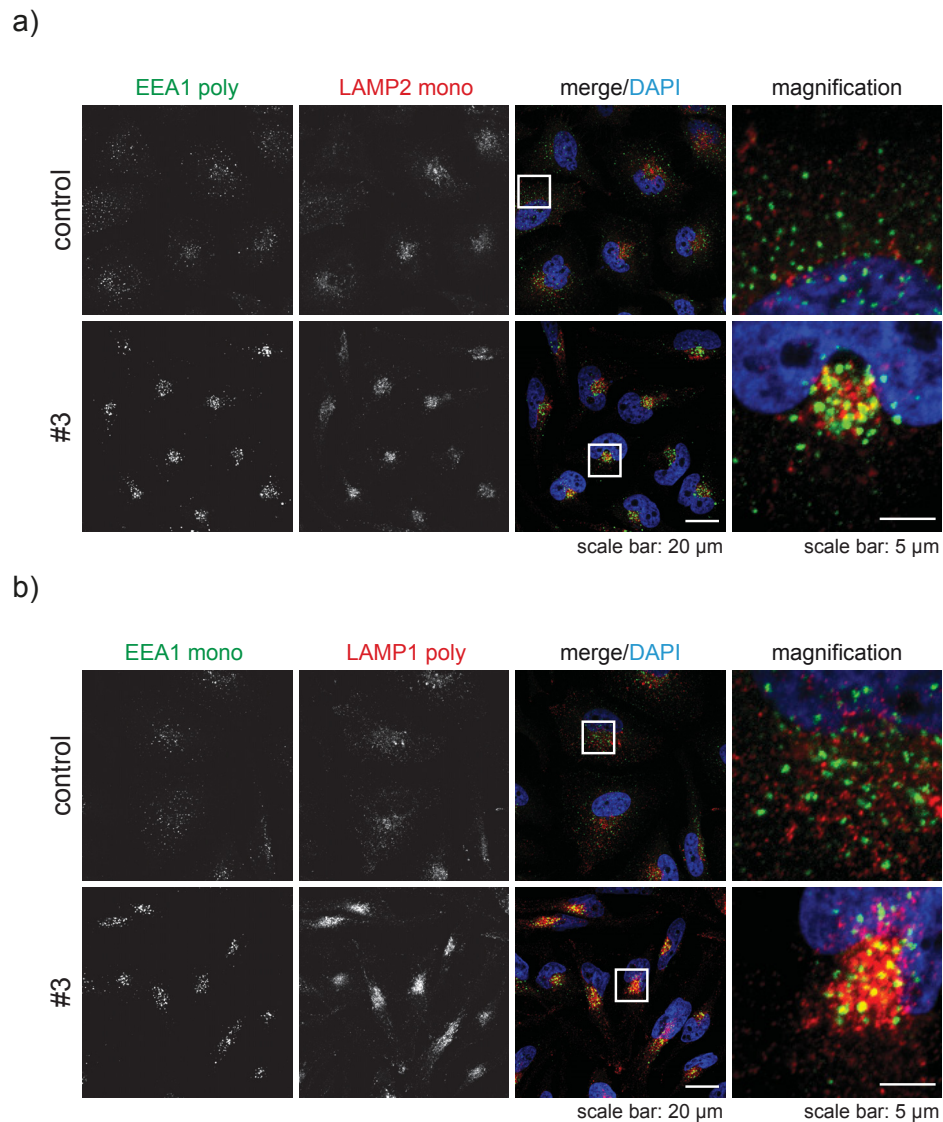


**Figure 3.21: EEA1-positive vesicles cluster in the perinuclear region upon TMEM106B knockdown**

HeLa cells were transfected with either non-targeting control siRNA or TMEM106B #3 siRNA (#3) to knockdown TMEM106B and subjected to immunofluorescence. a) Cells were co-stained with antibodies against EEA1 (green) and LAMP2 (red), respectively. b) To confirm the observed clustering of EEA1-positive vesicles upon TMEM106B knockdown, HeLa cells were stained with a different antibody against EEA1 (green) and co-stained with an anti-LAMP1 antibody (red).

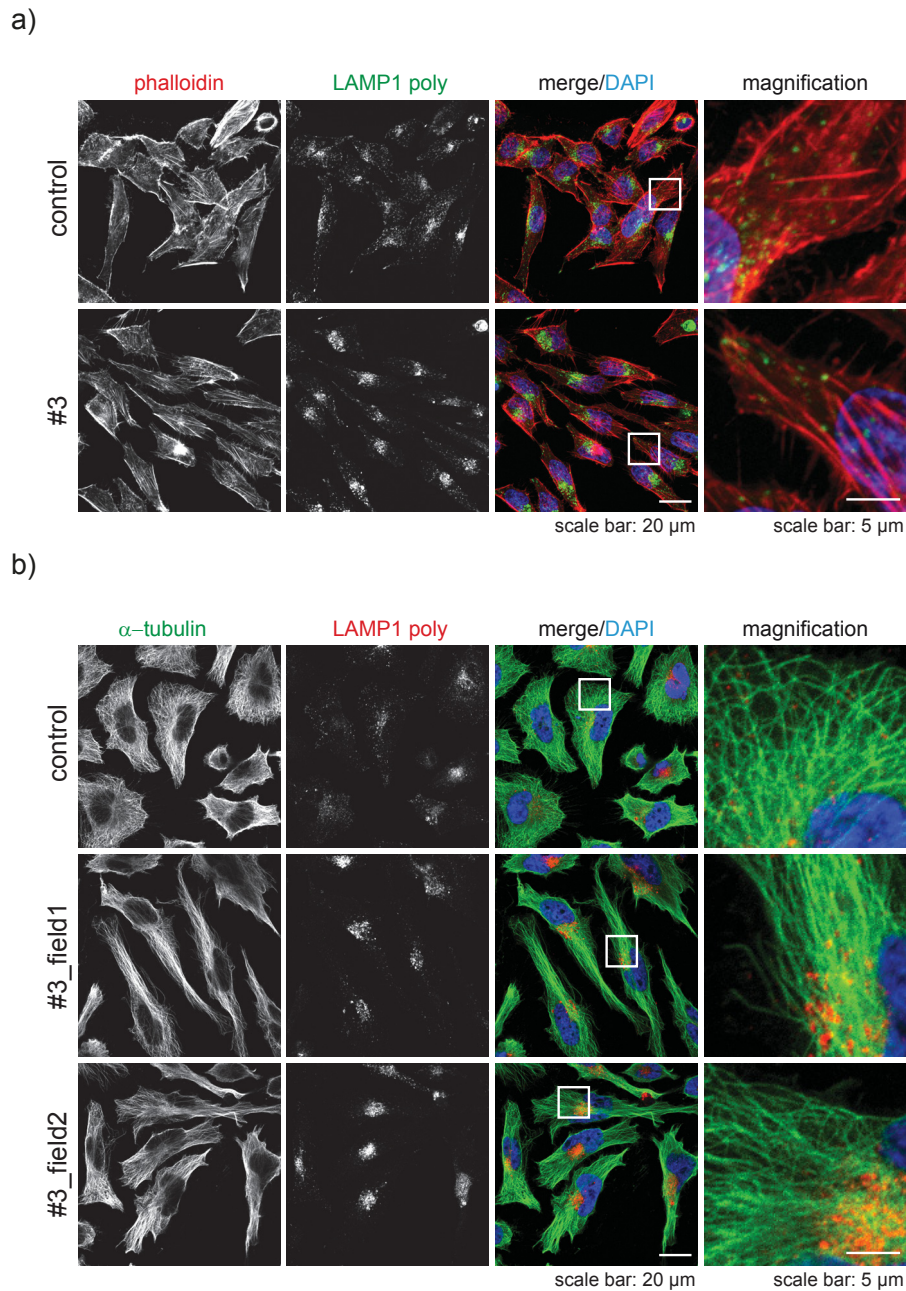


**Figure 3.22: Cytoskeleton morphology is not altered upon TMEM106B knockdown**

HeLa cells were transfected with either non-targeting control siRNA or TMEM106B #3 siRNA (#3) to knockdown TMEM106B and subjected to immunofluorescence. a) Cells were either co-stained with phalloidin (actin cytoskeleton marker, red), a drug that binds to F-actin, and an anti-LAMP1 antibody (green) b) or with antibodies against  $\alpha$ -tubulin (microtubule marker, green) and LAMP1 (red). Note that upon TMEM106B knockdown, HeLa cells show a more elongated shape compared to control-treated cells.

### 3.9 Clustering is dependent on functional retrograde transport along microtubules

As already mentioned, microtubules are essential for vesicular transport [177] (see section 1.3.2, page 26). Thus, it is conceivable that lysosomal clustering would be abolished if the microtubule network was defective. To test whether indeed, the clustering phenotype observed upon TMEM106B knockdown is dependent on microtubule network integrity, I treated non-targeting siRNA- or TMEM106B #3 siRNA-transfected HeLa cells with different concentrations of nocodazole, a drug that interferes with microtubule polymerization as it binds to  $\beta$ -tubulin and prevents the formation of one of the two interchain disulfide linkages [253] (figure 3.23 a). Thereby, the lower concentration (0.33  $\mu$ M) only partly destroyed the microtubule network and lysosomes were concentrated in the area where microtubules were still intact (figure 3.23 a). However, higher nocodazole concentrations (3.3  $\mu$ M) completely inhibited microtubule network formation (figure 3.23 a). Importantly, in TMEM106B #3 siRNA-treated HeLa cells, lysosomes did not cluster any longer but were distributed throughout the cell like in controls (figure 3.23 a) suggesting that an intact microtubule network is indeed essential for the clustering phenotype.

Moreover, motor proteins ensure successful vesicle trafficking along the cytoskeleton [260, 115] and thus play an important role for lysosomal positioning. Thereby, kinesins are the major motor protein species that mediate anterograde transport towards the plus-end of microtubules whereas dynein is responsible for the retrograde transport towards the MTOC [260, 111]. To test whether dyneins influence the lysosomal positioning in the perinuclear region of the cell in the TMEM106B knockdown, I inhibited the retrograde transport by dynamitin transfection. Dynamitin is part of the dynein-dynactin machinery and upon overexpression, it prevents dynein-dynactin assembly and thus inhibits retrograde transport [121, 33, 181]. Accordingly, I transfected control or TMEM106B #3 siRNA-treated HeLa cells with a GFP-tagged chicken dynamitin construct, which is more efficient than human dynamitin in inhibiting dynactin functions [121] (figure 3.23 b). Dynamitin constructs were either transfected on day 1 or day 2 after siRNA transfection (see also figure 3.16, page 68), namely when lysosomes were not yet clustered (day 1) and when they already were (day 2) (figure 3.23 b). Interestingly, both earlier and later transfection of dynamitin resulted in a reversed phenotype, with lysosomes positioned at the cellular tips (figure 3.23 b). Hence, lysosomal clustering upon TMEM106B knockdown indeed is dependent on retrograde transport mediated by the dynein-dynactin complex. Moreover, the balance between retrograde and anterograde transport might apparently be important for lysosomal positioning and be influenced by TMEM106B knockdown (an overview of lysosomal positioning within the cell with the mentioned treatments is presented in figure 3.23 c).

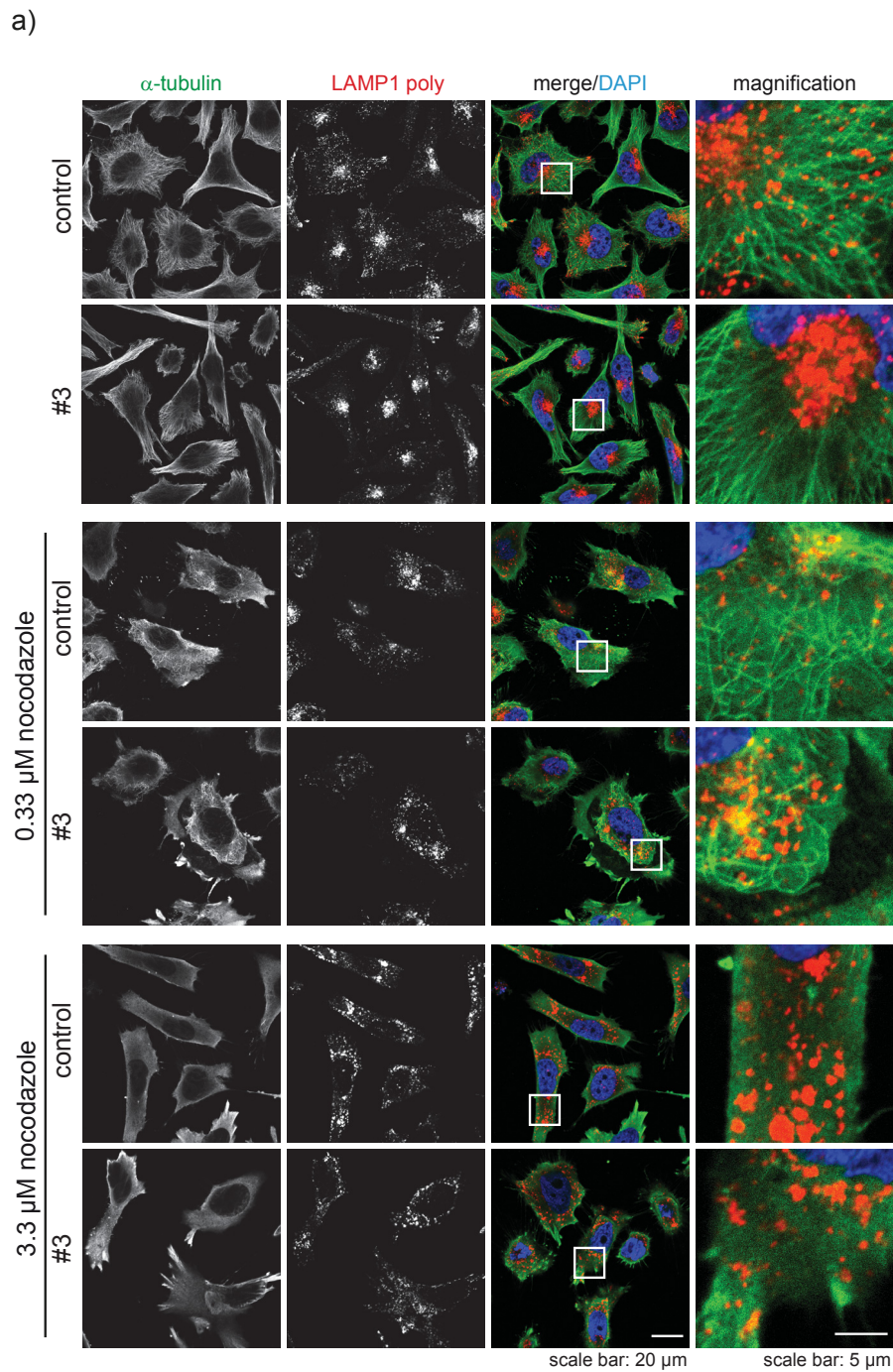


**Figure 3.23: A functional microtubule network and retrograde transport are required for lysosomal clustering upon TMEM106B knockdown**

a) HeLa cells were transfected with either non-targeting control siRNA or TMEM106B #3 siRNA (#3) to knockdown TMEM106B. Before fixation, cells were incubated in 0.33  $\mu$ M or 3.3  $\mu$ M nocodazole for 16 h. Untreated cells served as a control. Subsequently, HeLa cells were subjected to immunofluorescence and stained for lysosomes (anti-LAMP1 antibody, red) and microtubules (anti- $\alpha$ -tubulin antibody, green).

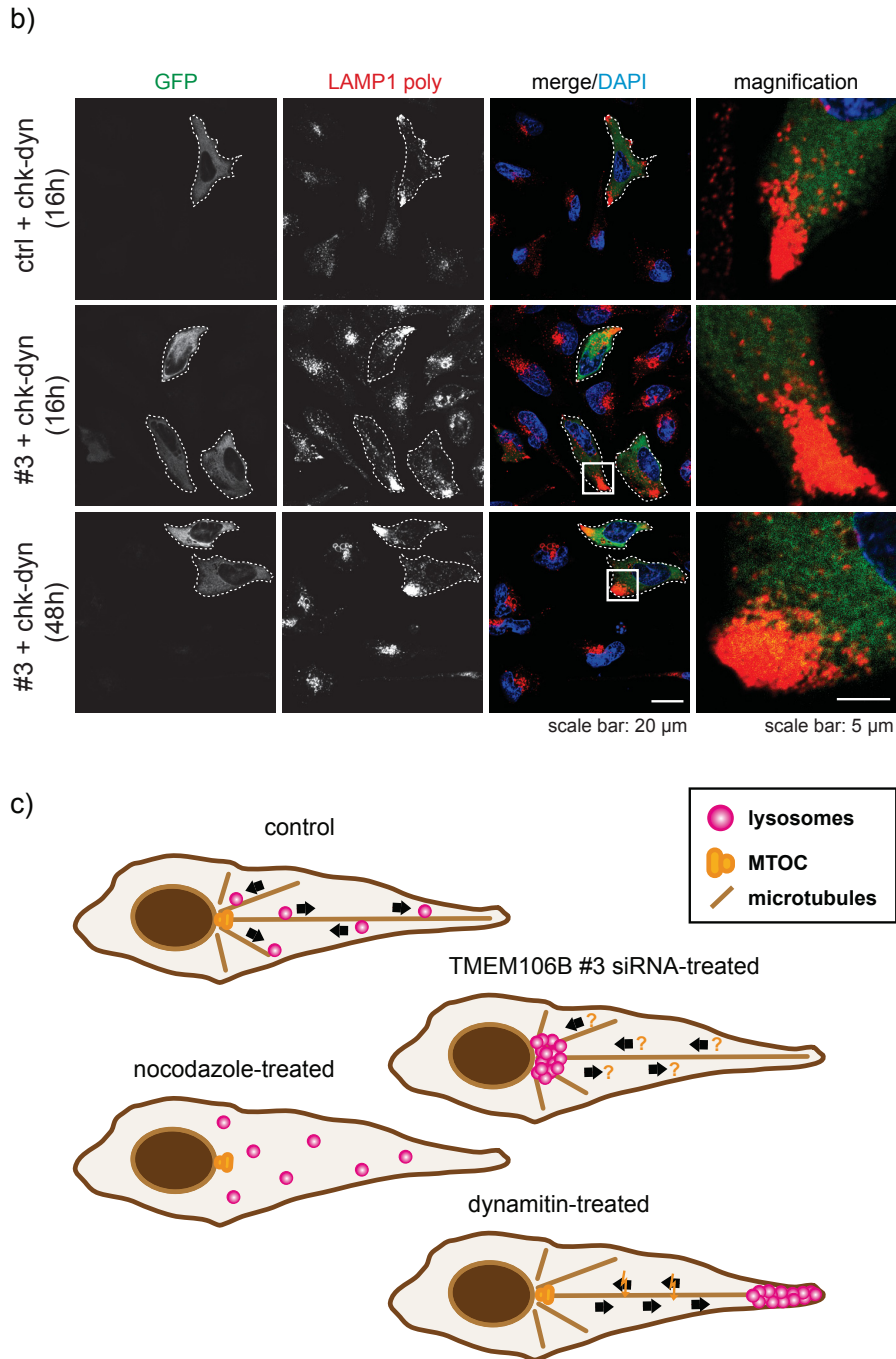


**Figure 3.23 (continued): A functional microtubule network and retrograde transport are required for lysosomal clustering upon TMEM106B knockdown**

b) On day 1 or day 2 after either control or TMEM106B #3 siRNA transfection, HeLa cells were co-transfected with a GFP-tagged chicken-dynamitin cDNA construct (chk-dyn) to abolish the assembly of the dynein-dynactin complex and thus retrograde transport. After the indicated periods of chk-dyn-transfection, cells were fixed and subjected to immunofluorescence. Lysosomes were stained with an anti-LAMP1 antibody (red), cells transfected with the GFP-chk-dyn construct fluoresced in green (transfected cells were surrounded by a dotted line). Note that chk-dyn-transfected cells present with a reversed phenotype with lysosomes clustered at the tips of the cell. c) Scheme of lysosomal transport along microtubules which shows the control case, TMEM106B #3 siRNA-treated cells and nocodazole- or dynamitin-treated cells. Impairment is depicted as lightning and unknown mechanisms as question marks.

### 3.10 Lysosomes are still acidic and functional upon TMEM106B knockdown

As from these data, it is still not conceivable whether TMEM106B has a direct impact on vesicular trafficking, I also investigated another possibility which might explain lysosomal clustering, namely whether clustering upon TMEM106B knockdown represents a cellular stress response to lysosomal dysfunction (figure 3.24).

It is known that lysosomes can cluster due to lysosomal stress like amino acid deprivation or treatment with bafilomycin A1 or chloroquine, drugs that impair lysosomal acidification (see section 1.3.4, page 33). Therefore, I investigated whether lysosomal function was altered in TMEM106B siRNA-treated cells. If TMEM106B knockdown resulted in impaired lysosomal function, the cell would respond with lysosomal clustering and enhance lysosomal biogenesis through activating the TFEB pathway (figure 3.24; see also section 1.3.4, page 33). Hence, to test lysosomal function, I investigated whether typical lysosomal enzymes like cathepsin B and D still matured after TMEM106B knockdown, a process that requires acidic conditions (see section 1.3.1, page 25). However, the knockdown of TMEM106B did not change the maturation of cathepsin B and D (figure 3.25 a). Moreover, the cathepsin D activity assay of the cell lysate of TMEM106B #3 siRNA-treated cells showed the same activity as control lysates (figure 3.25 b). These results already suggested that lysosomes were still acidic upon TMEM106B knockdown and thus, that processing and activity of lysosomal enzymes were not impaired. To verify this finding, HeLa cells transfected with TMEM106B #3 siRNA were either stained with lysotracker or DQ-BSA and compared to controls (figure 3.25 c and d). Lysotracker is a dye that is incorporated by the cell and accumulates in acidic organelles where its fluorescence is brightest [219]. In contrast, DQ-BSA is a quenched fluorogenic substrate for proteases which only fluoresce when it is hydrolysed, a process that requires functional lysosomal enzymes [310]. Upon TMEM106B knockdown, both the lysotracker- and the DQ-BSA-treated cells showed an intense fluorescent staining arguing for unimpaired lysosomal acidification and thus functional lysosomes (figure 3.25 c and d).

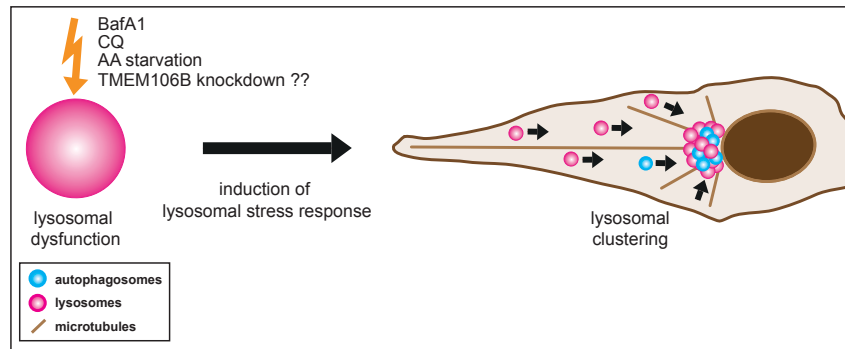


**Figure 3.24: Lysosomal dysfunction and the lysosomal stress response pathway**

BafA1 or CQ treatment as well as amino acid (AA) deprivation are known to result in lysosomal dysfunction which subsequently causes the induction of the lysosomal stress response pathway. As a consequence, lysosomes begin to cluster at the MTOC [150]. If TMEM106B knockdown also caused lysosomal dysfunction, this would explain the clustering phenotype seen upon TMEM106B knockdown.

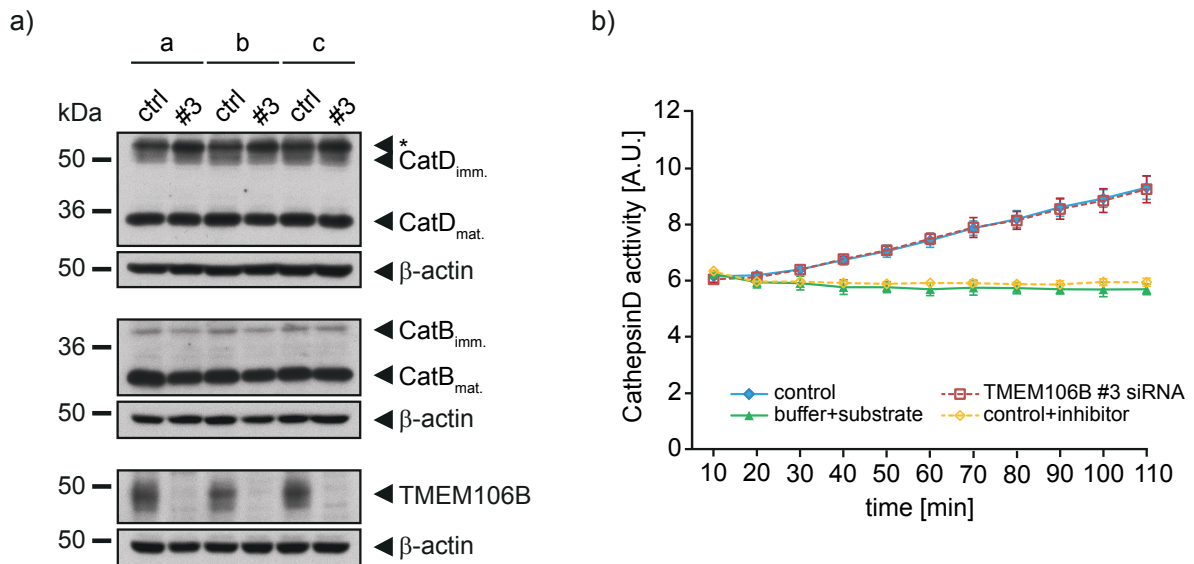


**Figure 3.25: Lysosomal enzyme activity and lysosomal acidification were not impaired upon TMEM106B knockdown**

a) HeLa cells were transfected with non-targeting control (ctrl) siRNA or with TMEM106B #3 siRNA (#3) and subjected to SDS-PAGE and immunoblotting. Lysosomal enzymes were detected with antibodies against cathepsin B (CatB) and cathepsin D (CatD). The immature (imm.) and mature (mat.) forms are labelled. The asterisk (\*) represents a probably unspecific band.  $\beta$ -actin served as loading control and TMEM106B as control for successful TMEM106B knockdown. b) The graph represents cathepsin D activity analysed by a cathepsin D activity assay. As assay controls served one sample that only contained the cathepsin D substrate in the appropriate buffer and one sample that had been treated with control siRNA and the cathepsin D inhibitor pepstatin. Note that there was no difference in cathepsin D activity between TMEM106B #3 and control siRNA-treated cells.

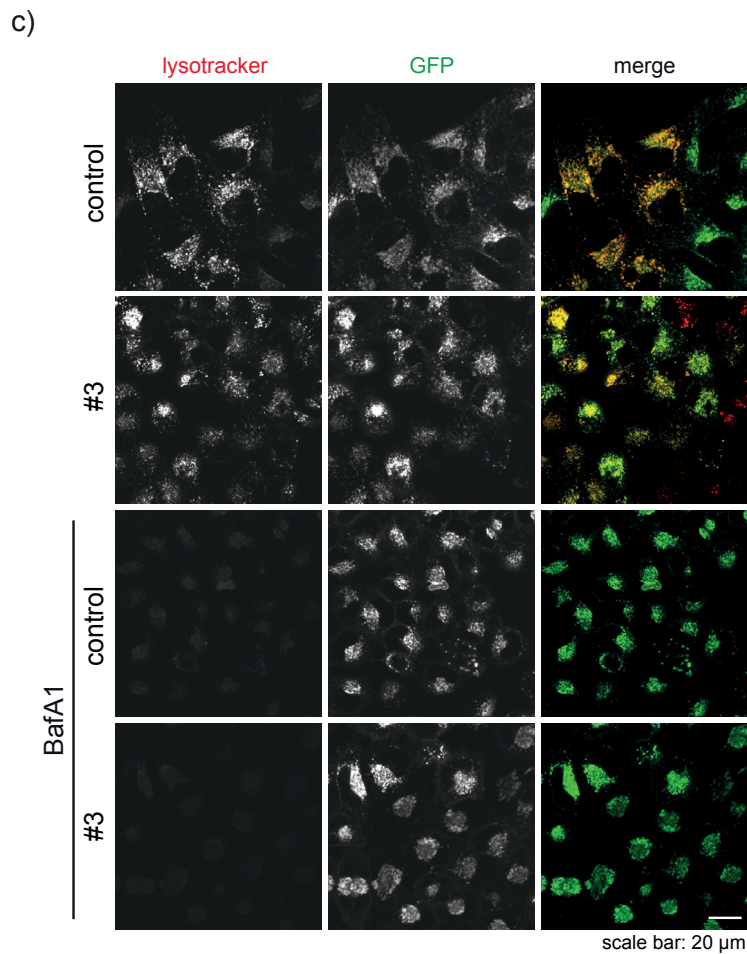


**Figure 3.25 (continued): Lysosomal enzyme activity and lysosomal acidification were not impaired upon TMEM106B knockdown**

c) HeLa Kyoto cells stably expressing LAMP1-GFP were transfected with either non-targeting control siRNA or with TMEM106B #3 siRNA (#3). On day 3 after transfection, cells were incubated with lysotracker and with or without BafA1 and subsequently, life cell imaging was performed. Note that also in TMEM106B #3 siRNA-treated cells, lysosomes were stained with lysotracker. In BafA1-treated controls, lysotracker staining was abolished as lysosomes were not acidic.

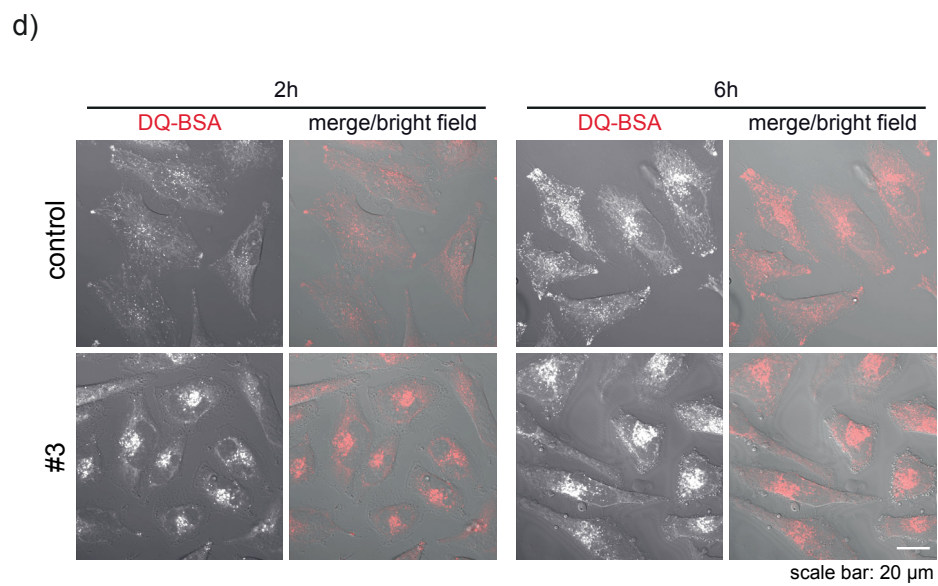


**Figure 3.25 (continued): Lysosomal enzyme activity and lysosomal acidification were not impaired upon TMEM106B knockdown**

d) Three days after control or TMEM106B #3 siRNA (#3) transfection, HeLa cells were incubated with DQ-BSA for the indicated periods and subjected to live cell imaging. Note that also in TMEM106B #3 siRNA-treated cells, the fluorescent signal of DQ-BSA was clearly visible indicating that DQ-BSA was hydrolysed by functional lysosomal enzymes.

### 3.11 Autophagosomal markers are altered upon TMEM106B knockdown

Lysosomal stress response does not only include lysosomal clustering but also influences lysosomal biogenesis and autophagy (see section 1.3.4, page 33). As lysosomal function appeared to be unaffected by TMEM106B knockdown, I investigated autophagosomal markers in order to find out whether clustering might be induced by a defect in the autophagic pathway. One of these markers was p62, a selective autophagy receptor that binds to ubiquitinated proteins and can mediate phagophore recruitment by binding to LC3 (see section 1.3.3, page 29). In immunofluorescence experiments, p62 particles seemed to be increased in TMEM106B #3 siRNA-treated HeLa cells compared to controls and moreover, in some cells, even huge p62 aggregates/particles were observed (figure 3.26 a). To verify this phenotype, another p62 antibody was used (figure 3.26 b) and particles counted and partitioned into size classes (figure 3.26 c and d). Thereby, p62 particle numbers were shown to be significantly increased in general (figure 3.26 d), but especially in the smaller size classes (figure 3.26 c). In the larger size groups, differences were not significant probably due to great variation between single cells, but still it became obvious that in TMEM106B #3 siRNA-treated cells, larger p62 particles were present in greater quantities than in controls (figure 3.26 c). Of note, the p62 particle numbers seemed to decrease again at day 4 after TMEM106B #3 siRNA transfection (data not shown), however, this is only preliminary data and still has to be confirmed in additional experiments.

Furthermore, p62 levels of TMEM106B #3 siRNA-treated cells were also found to be increased on immunoblot, however, the differences even though significant, were quite small (about 1.2- to 1.3-times increased compared to controls; figure 3.27 a and b). An explanation for the discrepancy between the immunofluorescence experiments and the immunoblot might be that p62 is not sufficiently extracted from cell lysates. To block p62 degradation, cells were additionally treated with BafA1 and analysed on immunoblot (figure 3.27 a). Accordingly, p62 levels were elevated but the ratio between control and TMEM106B #3 siRNA-treated cells remained the same (figure 3.27 b). A second examined autophagic marker was LC3, a protein that binds to autophagosomal membranes (see section 1.3.3, page 29). Like p62, LC3 levels were increased upon TMEM106B knockdown (figure 3.28 a). To discriminate whether p62 either mediated proteasomal or lysosomal degradation, I examined LC3 and p62 co-localization in an immunofluorescence experiment (figure 3.28 b). Indeed, a huge proportion of p62-positive particles co-stained with LC3. In addition, LC3 levels were increased on immunoblot (data not shown) confirming a link between TMEM106B and autophagy. Interestingly, there seemed not only a connection to the autophagic system but also to the proteasomal degradation system. A staining for polyubiquitin, a marker for proteasomal degradation, revealed co-localization with some very large and also mid-sized p62 particles (figure 3.28 c).

In summary, these data suggest an alteration in the degradation systems as both marker proteins for autophagic and proteasomal degradation were increased upon TMEM106B knockdown.

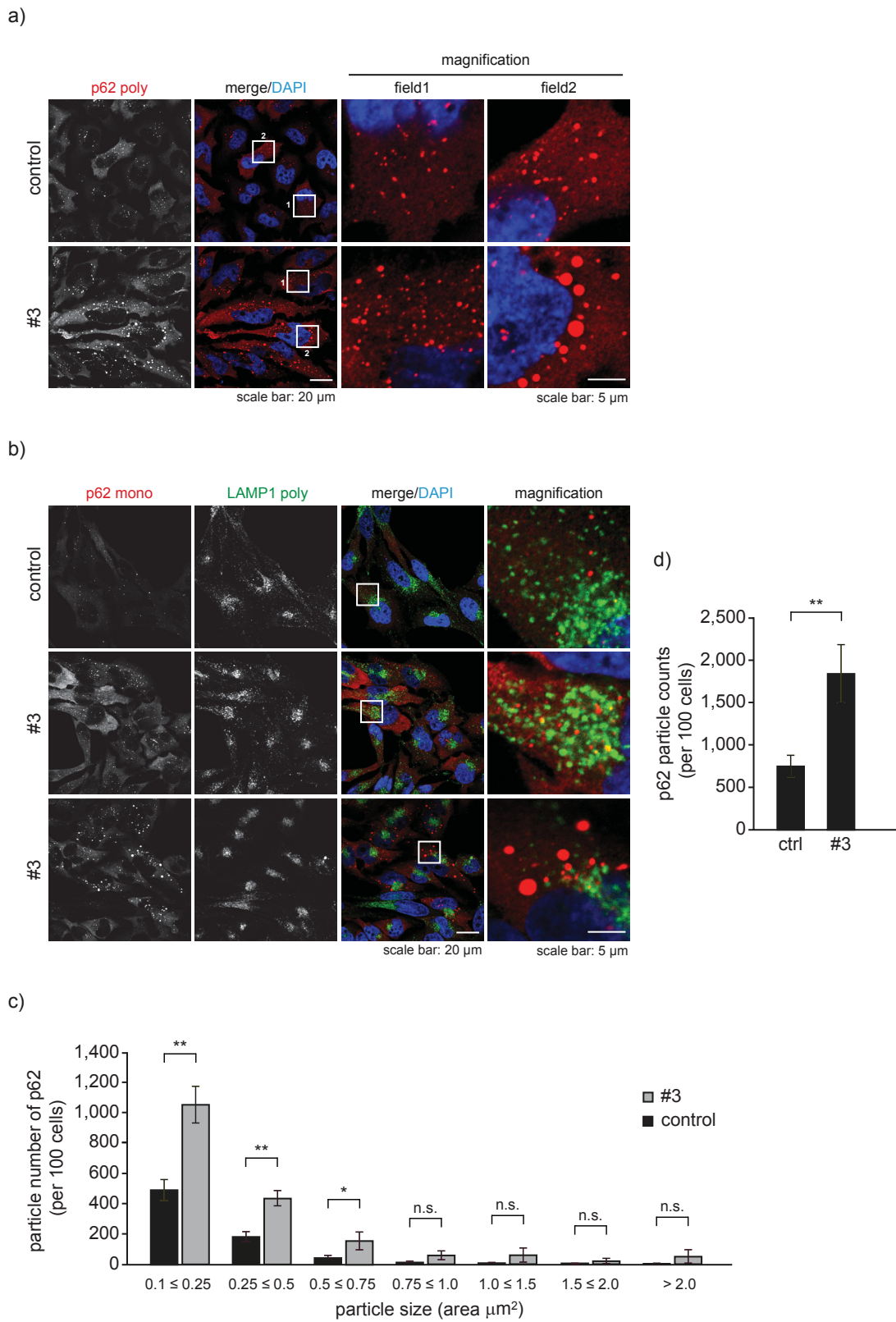
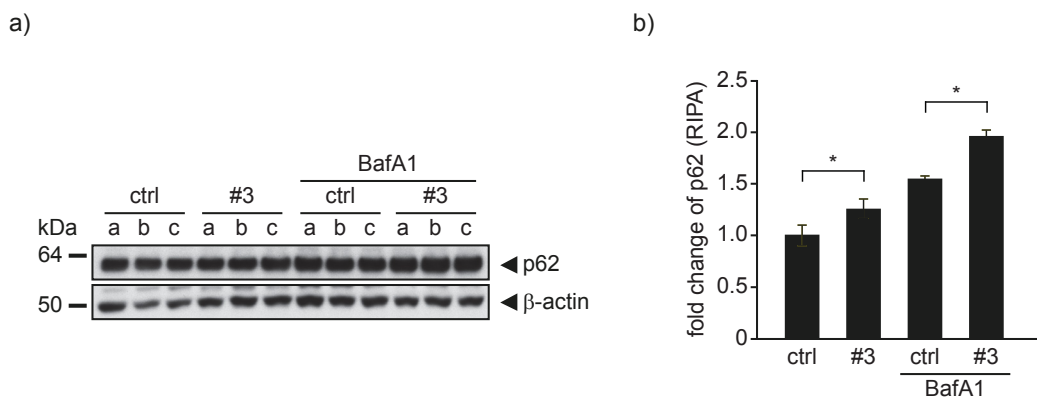


Figure 3.26: p62 levels are increased upon TMEM106B knockdown in immunofluorescence

### Figure 3.26 (continued): p62 levels are increased upon TMEM106B knockdown in immunofluorescence

a) HeLa cells were transfected with either non-targeting control siRNA or with TMEM106B #3 siRNA (#3) to knockdown TMEM106B. Subsequently, cells were subjected to immunofluorescence and stained with an antibody against p62. Note the increased p62 levels in TMEM106B #3 siRNA-treated cells. Field1 shows the increase of smaller p62 particles whereas field2 depicts also the increase in p62 particle size. b) To verify the results, another anti-p62 antibody was utilized and HeLa cells co-stained with an antibody against LAMP1 to verify successful TMEM106B knockdown by lysosomal clustering. Two different pictures of TMEM106B #3 siRNA-treated cells (#3) are depicted to demonstrate the increase in small p62 particles and the appearance of large aggregates. c) The bar graph represents the quantification of p62 particle numbers and sizes in immunofluorescence pictures. In a total of three independent experiments, 287 control and 237 TMEM106B #3 siRNA-treated (#3) HeLa cells were analysed. Data are presented in particle number per 100 cells, partitioned in particle size groups and depicted as means  $\pm$  S.D. (n=3; \*\*: p < 0.01, \*: p < 0.05 and n.s. by unpaired student's t-test). d) The bar graph represents the quantification of total p62 particle counts per 100 cells in immunofluorescence pictures of HeLa cells treated with non-targeting siRNA (ctrl) or TMEM106B #3 siRNA (#3). In a total of three independent experiments, 287 control and 237 TMEM106B #3 siRNA-treated HeLa cells were analysed. Data are depicted as means  $\pm$  S.D. (n=3; \*\*: p < 0.01 by unpaired student's t-test).



### Figure 3.27: p62 levels are increased upon TMEM106B knockdown in immunoblot

a) HeLa cells were transfected with either non-targeting control siRNA (ctrl) or with TMEM106B #3 siRNA (#3) to knockdown TMEM106B and treated with or without BafA1 for 3h before being harvested. Subsequently, cells were lysed in RIPA buffer and analysed on immunoblot for p62.  $\beta$ -actin served as loading control. b) The bar graph represents the quantification of the immunoblot by chemiluminescence. Data are normalized to control siRNA-treated cells without BafA1 treatment and depicted as means  $\pm$  S.D. (n=3; \*: p < 0.05 by unpaired student's test).

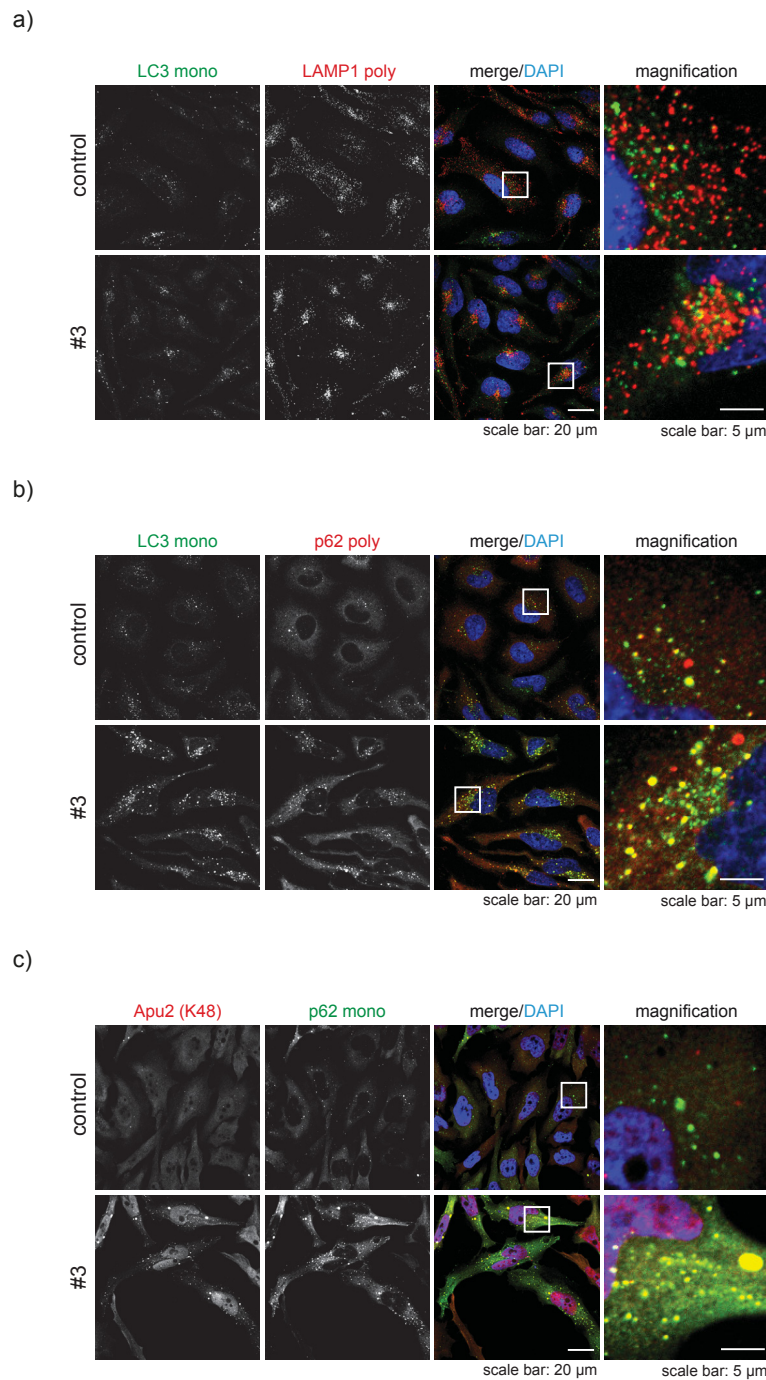


**Figure 3.28: LC3 and ubiquitin levels are increased upon *TMEM106B* knockdown in immunofluorescence**

a) HeLa cells were transfected with either non-targeting control siRNA or with *TMEM106B* #3 siRNA (#3) to knockdown *TMEM106B*. Subsequently, cells were subjected to immunofluorescence and stained with antibodies against LC3 and LAMP1. Note the increase in LC3 levels in *TMEM106B* #3 siRNA-treated cells. b) Control and *TMEM106B* #3 siRNA (#3)-treated HeLa cells were analysed by immunofluorescence for LC3 and p62. Note the increase in both LC3 and p62 levels in *TMEM106B* #3 siRNA-treated cells. c) HeLa cells transfected with non-targeting control siRNA and *TMEM106B* #3 siRNA (#3) were subjected to immunofluorescence and stained with antibodies against p62 and lysine 48-linked polyubiquitin (Apu2) which labels proteins targeted for proteasomal degradation. Note the co-localization of mainly the large p62-positive particles with ubiquitin in *TMEM106B* #3 siRNA-treated cells.

### 3.12 Starvation reveals an increase in autophagosomal and lysosomal proteins upon TMEM106B knockdown

Even though some alterations like the p62 increase in immunofluorescence experiments or a slight increase in LC3 levels on immunoblot were already apparent under normal growth conditions, so far, an influence of TMEM106B knockdown on lysosomal protein levels could not be observed (see section 3.10, page 80 and figure 3.25 a). However, a “second hit” like additional lysosomal stress might be needed to reveal differences between control siRNA- and TMEM106B #3 siRNA-treated cells.

Therefore, before harvesting, I starved non-targeting control siRNA- and TMEM106B #3 siRNA-treated HeLa cells in OptiMEM for 16 h and analysed the lysates by immunoblot (figure 3.29 a). Strikingly, in TMEM106B knockdown cells, mature cathepsin D levels were about 2.5-fold increased (figure 3.29 a and b), a finding that only became obvious upon starvation but could not be observed under normal growth conditions (compare with figure 3.25 a). Furthermore, immature cathepsin D levels also increased, however, to a lesser extent than the mature ones, which might be attributed to an increase in lysosomal biogenesis.

Moreover, LAMP2 and LC3I and II protein levels were significantly increased upon TMEM106B knockdown following OptiMEM treatment over night (figure 3.29 a and b). However, a trend towards elevated LC3 levels had already been observed under normal growth conditions (data not shown). As both LC3I and LC3II levels were elevated upon TMEM106B knockdown, autophagosomal biogenesis might be enhanced under these conditions.

Together, these data indicate that the knockdown of TMEM106B does not only mediate changes in lysosomal positioning but also in the expression levels of lysosomal and autophagic proteins. Moreover, to investigate TMEM106B function, additional stressors seem to be indeed needed, a finding which is in line with *TMEM106B* being a risk factor and not a disease-causing gene.

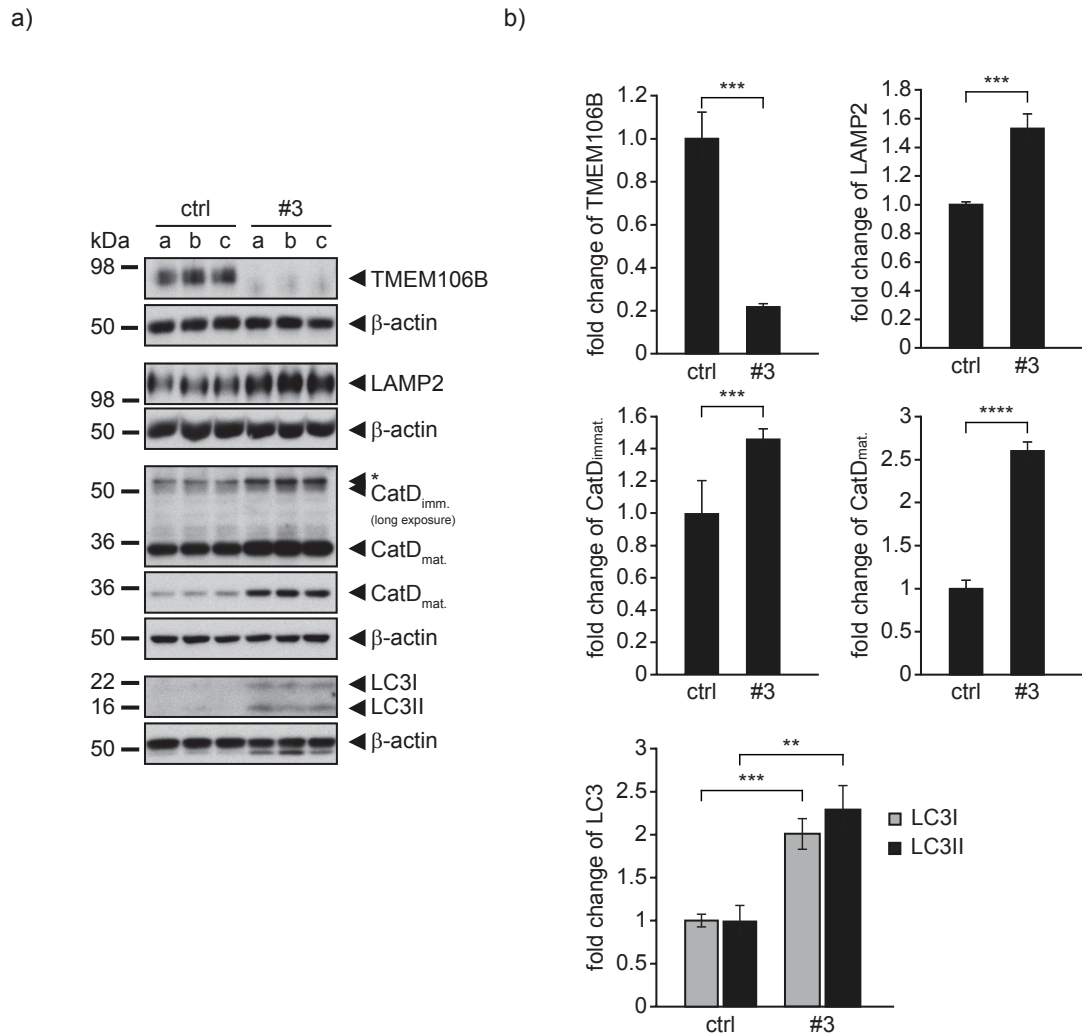


**Figure 3.29: Lysosomal and autophagosomal proteins are elevated upon TMEM106B knockdown in immunoblot**

a) HeLa cells were either transfected with non-targeting control (ctrl) siRNA or TMEM106B #3 siRNA (#3) to knockdown TMEM106B. 16 h before harvesting, the cells were incubated in OptiMEM overnight. Subsequently, cells were lysed and analysed for TMEM106B, LAMP2, LC3 and immature (immat.) and mature (mat.) cathepsin D (CatD) on immunoblot. The asterisk (\*) marks a probably unspecific band of the cathepsin D antibody.  $\beta$ -actin served as loading control. Of note, lysates for analysing TMEM106B were incubated in Laemmli buffer at room temperature. b) The bar graphs represent the quantification of the immunoblots by chemiluminescence. Data are normalized to control siRNA-treated cells and depicted as means  $\pm$  S.D. (n=3; \*\*\*\*:  $p < 0.0001$ , \*\*\*:  $p < 0.001$ , \*\*:  $p < 0.01$  by unpaired student's t-test).



## 4 Discussion

### 4.1 The molecular weight of TMEM106B

In 2010, *TMEM106B* was the first risk factor to be described for FTLT-DTP [301]. However, at that time, very little was known about the previously uncharacterised protein. Therefore, I started my studies with a characterization of its basic biochemical and cell biological features. When I analysed TMEM106B on immunoblot after SDS-PAGE, it became evident that TMEM106B detection in terms of amount and apparent molecular weight depended on the conditions of denaturation, i.e. sample buffer composition and temperature. It seems that upon strong denaturation due to high temperatures and the use of  $\beta$ -mercaptoethanol, low TMEM106B protein amounts were detected, mainly as monomers. However, upon milder denaturation, i.e. moderate temperatures and without the use of  $\beta$ -mercaptoethanol, higher levels of TMEM106B protein were detected in their monomeric as well as in their dimeric form.

More precisely, the very prominent band at about 75 kDa became weaker while increasing the temperature from 4 °C to 95 °C. This phenomenon was confirmed by Chen-Plotkin *et al.* who also found that the 75 kDa species which they recognized with two different anti-TMEM106B antibodies was very heat-sensitive [39]. Moreover, they observed that at 37 °C, more than 50 % of the protein they were able to detect at 4 °C was lost [39], a finding that I also made and which might be explained by a higher sensitivity of the generated anti-TMEM106B antibodies to native (maybe dimerized) TMEM106B. Furthermore, the second band at about 40 kDa increased with rising temperatures [39] confirming my findings at non-reducing conditions. Brady *et al.* were able to show that in immunoblots loaded with protein samples which were not boiled but incubated at 4 °C, TMEM106B appeared at a molecular weight of about 86 kDa [25]. From this, they concluded that at these temperatures, an SDS-resistant dimer seems to exist [25].

Interestingly, Chen-Plotkin *et al.* reported that frontal cortex samples of healthy individuals showed a similar heat-sensitive behaviour than cell lysates, however with the 40 kDa band being much less prominent [39]. Therefore, for further studies, they decided on incubating their samples at 4 °C [39]. Notably, the 40 kDa band, at least in the brain samples, seemed to be unaffected by temperature elevation, a finding that I also made concerning reducing conditions. In contrast, Nicolson *et al.* showed that at 22 °C and reducing conditions, in frontal cortex samples of healthy individuals, the 40 kDa band was more prominent than the higher molecular weight band at about 70 kDa to 90 kDa [200]. Moreover, they claim that this higher molecular weight band is not specific for TMEM106B as when they incubated their TMEM106B anti-

body with TMEM106B peptide, this band was still present whereas the lower molecular weight band disappeared [200]. Thus, they decided on focussing on the 40 kDa band when analysing TMEM106B.

In summary, until now, it is still not clear which method will represent TMEM106B expression best. In all biochemical studies about TMEM106B, specific bands at similar molecular weights were observed for TMEM106B when using similar denaturation temperatures [200, 263, 155, 39, 25]. However, there are conflicting results regarding the molecular weight of TMEM106B in brain samples.

Moreover, the used anti-TMEM106B antibodies seem to recognize the various TMEM106B species with a different sensitivity. For example, Chen-Plotkin *et al.* state that their generated antibody against TMEM106B, N2077, showed a greater affinity for the 75 kDa band than the commercially available antibody from Bethyl Laboratories [39]. Likewise, the 6F2 antibody I used in my studies probably is also more sensitive towards the 75 kDa band as detected protein levels at 4 °C were much higher than at 95 °C. Furthermore, the 6F2 antibody seems to recognize TMEM106B better in non-reducing conditions as detected TMEM106B amounts were a lot higher when  $\beta$ -mercaptoethanol was not added to the protein samples.

Therefore, as it remains uncertain if the 40 kDa or the 75 kDa band should be considered when analysing TMEM106B, for my studies, I chose to use a condition where both bands could be detected, namely 65 °C under non-reducing conditions.

### 4.2 TMEM106B is a lysosomal type II transmembrane protein

Having established a method for TMEM106B detection on immunoblot, I further investigated the biological characteristics of TMEM106B. By sequential membrane extraction, TMEM106B was shown to be an integral membrane protein (see figure 3.4 a, page 50) [155]. Furthermore, I was able to confirm all five predicted N-glycosylation sites of TMEM106B to be utilized. Thereby I also demonstrated that TMEM106B adopts a type II membrane orientation as the most C-terminal N-glycosylation site at position 256 (N5) proved to be glycosylated and thus to be located in the lumen (see figures 3.5 and 3.6, pages 51 and 52) [155]. Consistent with a transport into late secretory compartments, TMEM106B was partially endoglycosidase H-resistant (see figure 3.9 a, page 58) and co-localized mainly with lysosomal marker proteins (see figure 3.8, pages 54 and 55). This also indicated that TMEM106B is a lysosomal transmembrane protein [155].

Brady *et al.* confirmed these data in N2A cells, a mouse neuroblastoma cell line, as they also showed that TMEM106B was a type II transmembrane protein with a predominantly late endosomal/lysosomal localization [25], findings that were also verified in neurons [277, 263]. Lysosomal localization was furthermore demonstrated in HeLa cells by Nicholson *et al.* [200]. Moreover, Chen-Plotkin *et al.* confirmed TMEM106B N-glycosylation in HEK293 cells and, more impor-

tantly, in human brain homogenates [39]. Together, these data strongly suggest that TMEM106B indeed is an N-glycosylated type II-oriented lysosomal membrane protein [155].

Interestingly, abolishing complex glycosylation resulted in an altered localization of TMEM106B, namely in either a lamellipodia-like staining (N5 deletion) indicating surface localization of TMEM106B or in a retainment of TMEM106B in the ER (N4 deletion) suggesting that the forward transport to lysosomes was impaired (see figure 3.9 c and d, page 58) [155]. Thus, complex glycosylation seems to be essential for correct TMEM106B maturation and localization within the cell [155], a finding that has been confirmed, at least in part, by Nicholson *et al.* [200]. Intriguingly, the TMEM106B coding variant p.T185S, which is in perfect linkage disequilibrium with the top SNP rs1990622 (see section 1.2, page 21), is located within the N-X-T/S N-glycosylation consensus motif of the fourth N-glycosylation site of TMEM106B (N4 at position 183). In 2013, Nicholson *et al.* demonstrated that the disease-associated T185 TMEM106B variant was about two-fold higher expressed than the protective S185 variant which they attributed to a more rapid degradation of the S185 TMEM106B isoform [200]. They claim that even though complex glycosylation at N4 was not compromised by the serine mutation, a slight change in the glycan composition and/or complexity modifying the protein stability might still be a possible explanation for the decrease in S185 TMEM106B protein levels [200]. Supporting their hypothesis, Bause *et al.* reported that a replacement of threonine by serine within the N-glycosylation motif would result in less efficient N-glycosylation transfer rates [200, 14]. Interestingly, Nicholson *et al.* reported that the T185 TMEM106B isoform co-localized better with lysosomal marker proteins than the protective S185 variant [200], which indicates that protein localization indeed might be altered due to subtle changes in glycan composition. Like Nicholson *et al.*, I also observed less co-localization of S185 with lysosomal markers compared to the T185 isoform (data not shown).

In summary, the initial finding of mutant N4 being retained in the ER stressed the importance of complex glycosylation at position 183 for TMEM106B localization and maturation and therefore presented the basis for the findings of Nicholson *et al.*, namely that differences in protein stability probably due to changes in the glycosylation pattern of TMEM106B variants T185 and S185 might modify TMEM106B levels [200].

### 4.3 TMEM106B is degraded in the lysosome but not in the proteasome

As TMEM106B seemed to be localized to BafA1-sensitive compartments, I tested whether inhibition of lysosomal acidification or of lysosomal proteases would influence TMEM106B levels. In addition, I also investigated whether proteasomal inhibition would have an impact on TMEM106B levels. Interestingly, whereas neither inhibiting lysosomal proteases nor

proteasomal activity revealed any differences in TMEM106B protein levels, BafA1 treatment which inhibits lysosomal acidification, strongly increased overexpressed as well as endogenous TMEM106B protein levels (see figures 3.12 and 3.13, pages 63 and 64) [155]. Moreover, transcriptional inhibition had no influence on the BafA1-mediated increase in TMEM106B protein levels whereas translational inhibition abolished the effect suggesting a predominant post-transcriptional mechanism to be involved [155]. Brady *et al.* and Chen-Plotkin *et al.* confirmed that TMEM106B levels increase upon inhibition of lysosomal acidification [25, 39]. In addition, Brady *et al.* were able to show that autophagy inhibition by 3-methyladenine treatment increased TMEM106B levels [25]. As they also found no effects of proteasome inhibitors on TMEM106B levels, they concluded that TMEM106B levels are regulated by membrane-trafficking events, but not by the ubiquitin-proteasome pathway [25]. Also, Nicholson *et al.* could not detect any influence of proteasomal degradation on TMEM106B levels [200].

However, in contrast to my findings, Nicholson *et al.* observed an increase in TMEM106B levels upon leupeptin treatment, a drug that inhibits lysosomal serine- and cysteine proteases. Thus, they concluded that the lysosome is the main subcellular compartment to be involved in TMEM106B degradation [200]. Compared to Nicholson *et al.* who overexpressed TMEM106B and were able to detect a modest increase in TMEM106B levels upon leupeptin treatment [200], I investigated endogenous levels of TMEM106B. Moreover, compared to the increase in TMEM106B levels I observed after BafA1 treatment, the increase Nicholson *et al.* observed after leupeptin treatment was relatively weak. Thus, it might be possible that I was not able to detect the increase in endogenous TMEM106B levels upon leupeptin treatment.

Very recently, TMEM106B was shown to be lumenally cleaved by lysosomal proteases to generate an N-terminal fragment that subsequently undergoes regulated intermembrane proteolysis mediated by SPPL2a thereby generating a highly unstable intracellular domain [26]. RIP is a process in which a transmembrane protein is consecutively cleaved starting with the shedding of its ectodomain followed by cleavage within the remaining transmembrane stump of the protein [161]. Thereby, an ICD as well as a small peptide are released [161]. As the ICD of TMEM106B was found to be located in the lysosome, but not in the nucleus, the authors concluded that RIP processing probably served as a quality control system to remove excess TMEM106B protein rather than having any signalling capacities [26]. These data explain my observation of TMEM106B levels being increased after BafA1 treatment. As BafA1 inhibits lysosomal acidification, concomitantly, it also prohibits the maturation of all lysosomal hydrolases that need an acidic pH for maturation. Therefore, BafA1 treatment would also impair the cleavage and, consequently, the degradation of TMEM106B thus explaining the increase in TMEM106B protein levels.

Moreover, BafA1 can potently activate the lysosomal stress response pathway which results in an increase in lysosomal biogenesis (see section 1.3.4, page 33). The latter is regulated by TFEB, a transcription factor that recognizes CLEAR motifs in the promotor region of lysosomal and autophagic genes (see also figure 1.13, page 34). As TMEM106B is a lysosomal membrane protein

and has a putative CLEAR motif (GTCACGcGca) in its 5'UTR, it is tempting to speculate that *TMEM106B* thus might be a TFEB target. Supporting this assumption, *TMEM106B* mRNA levels showed a 1.5-fold increase after BafA1 treatment. This is in line with a reported 1.5- to 5.0-fold increase in mRNA levels of genes encoding the complex components of H<sup>+</sup>-ATPase, a known TFEB target, upon TFEB activation [265]. Hence, the increase of *TMEM106B* protein levels upon BafA1 treatment might be explained by an increase in *TMEM106B* expression possibly due to the TFEB stress response pathway coupled with decreased *TMEM106B* degradation due to impaired lysosomal acidification and thus impaired lysosomal enzyme maturation.

Together, my data indicate that the lysosomal but not the proteasomal pathway are important for *TMEM106B* degradation [155], a finding that now has been verified by others [25, 39, 200, 26].

#### 4.4 The relationship between *TMEM106B* and *GRN*

In 2010, van Deerlin *et al.* published that the risk allele of rs1990622 of *TMEM106B* was associated with higher *TMEM106B* mRNA levels in FTLT-TDP patients carrying a *GRN* mutation [301] thereby being the first ones to suggest a direct relationship between *TMEM106B* and *GRN*. In subsequent studies, conflicting results have been published concerning the matter of *TMEM106B* and *GRN*, as Finch *et al.* claimed that homozygosity for the protective minor allele of *TMEM106B* was associated with an increase in *GRN* protein levels and a significantly delayed disease onset [72]. In accordance with Finch *et al.*, Cruchaga *et al.* observed a decrease in the age-at-onset for the risk allele of *TMEM106B* as well as lower plasma *GRN* levels, but were not able to show any correlation between *TMEM106B* and *GRN* mRNA levels [51]. However, van der Zee *et al.* were not able to confirm these results [306] (as a summary, see also table 4.1).

**Table 4.1:** Relationship between FTLT-TDP, *TMEM106B* and *GRN*

allele type	observations
T (risk; major)	<ul style="list-style-type: none"> <li>• increased <i>TMEM106B</i> mRNA levels in <i>GRN</i> mutation carriers [301]</li> <li>• decreased <i>GRN</i> plasma levels [51]</li> <li>• earlier disease onset [51]</li> </ul> <hr/> <ul style="list-style-type: none"> <li>• no correlation between <i>TMEM106B</i> and <i>GRN</i> mRNA levels [51]</li> <li>• no increase in <i>TMEM106B</i> protein levels [305]</li> <li>• no association with age-at-onset [306]</li> <li>• no correlation of <i>TMEM106B</i> levels and FTLT-TDP [306]</li> </ul>
C (protective; minor)	<ul style="list-style-type: none"> <li>• 30 % to 50 % reduced risk of developing FTLT [306]</li> <li>• increased <i>GRN</i> protein levels [72]</li> <li>• delayed disease onset [72]</li> </ul>

Therefore, in the present study, I used cell lines to analyse whether TMEM106B overexpression or TMEM106B knockdown had an impact on GRN expression. However, I could not detect any influence of TMEM106B on GRN on either transcriptional or translational level [155] indicating that GRN and TMEM106B levels do not influence each other directly. These findings were confirmed by Satoh *et al.*, who overexpressed either GRN or TMEM106B in SK-N-SH neuroblastoma cells, but did not observe any immediate effect on endogenous levels of either TMEM106B or GRN mRNA suggesting that TMEM106B is not involved in transcriptional regulation of *GRN* and *vice versa* [257]. Also, Schwenk *et al.* did not detect any differences in GRN protein levels in cell lysates of primary rat cortical neurons transduced with lentiviruses expressing TMEM106B short hairpin (sh) RNA to knockdown TMEM106B [263]. Furthermore, in *C9orf72* expansion carriers homozygous for either the risk or protective alleles of rs1990622, plasma GRN levels were not found to be significantly different from each other [77] even though TMEM106B was identified as genetic modifier for FTL-DPR [299].

In contrast, Brady *et al.* reported that TMEM106B overexpression in N2a cells resulted in an increase in intra- and extracellular GRN levels along with an accumulation of GRN in lysosomes and an enlarged lysosomal phenotype [25]. They therefore concluded that TMEM106B might regulate GRN levels through its function in the endolysosomal degradation pathway [25]. However, notably, they were not able to detect any changes in GRN expression upon TMEM106B knockdown [25]. Nicholson *et al.* also reported an increase in intra- and extracellular GRN levels, however, like Brady *et al.*, the differences between TMEM106B overexpressing cells and controls were quite small (a less than 1.2- to 1.4-fold increase). Chen-Plotkin *et al.* also observed abnormalities in the endolysosomal pathway upon TMEM106B overexpression represented by enlarged LAMP1-positive organelles which they showed in several different cell lines [39]. Importantly, they were able to demonstrate that this phenotype resulted from a block in endosomal-lysosomal fusion and speculated that retrograde transport from the late endosome to the TGN was affected [39]. Furthermore, they confirmed that intracellular GRN levels increased upon TMEM106B overexpression (about 1.3-fold), but were not able to detect any differences in secreted GRN [39]. These observations might be explained by GRN being internalized and transported to the lysosome, probably by sortilin [114]. Thereby, GRN binds with high affinity to sortilin and thus mediates rapid endocytosis [114]. Subsequently, GRN is transported to lysosomes whereas sortilin is recycled from endosomes and re-transported to the plasma membrane [114]. Therefore, under normal conditions, GRN would subsequently be degraded in the lysosomal lumen. However, if TMEM106B overexpression inhibits endosomal-lysosomal fusion, the transport of GRN to the lysosome would be abolished. Thus, intracellular GRN levels would increase, but secretion of GRN would probably remain unaffected.

The discrepancies between the data of Brady *et al.*, Chen-Plotkin *et al.* and my data lie within the experimental set-up. In opposition to my data, Brady *et al.* and Chen-Plotkin *et al.* did not use stable cell lines for TMEM106B overexpression experiments, but transiently transfected tagged TMEM106B wt constructs (either flag-tagged or GFP-tagged) into various cell lines [25,

39, 155]. Thus, expression levels of TMEM106B might have been different to my experiments, as I chose a low TMEM106B overexpression clone to analyse the relationship between GRN and TMEM106B. However, when I transiently transfected HeLa cells with a HA-tagged TMEM106B wt construct, I also observed enlarged LAMP1-positive vesicles, similar to Brady *et al.* and Chen-Plotkin *et al.* (data not shown). Therefore, the differences in exogenous TMEM106B levels might account for the different results concerning GRN. Supporting this assumption, Brady *et al.* reported that endogenous TMEM106B co-localized much better with LAMP1 than overexpressed TMEM106B which appeared frequently within the lumen of LAMP1-positive vesicles or was mislocalized to the plasma membrane [25], a finding that I could confirm (data not shown). Thus, they concluded that TMEM106B overexpression might cause its mislocalization or the disturbance of lysosomal compartments and therefore that expression levels of TMEM106B critically affect TMEM106B localization [25].

Until now, it has not been finally clarified whether the increase in lysosomal size is indeed a true effect or an artefact due to heavy TMEM106B overexpression. It is possible that increasing the amount of a lysosomal membrane protein might result in expanding lysosomal size. Accordingly, this increase in lysosomal size might result in decreased acidification as the number of H<sup>+</sup>-ATPases probably remains unchanged, but the lysosomal lumen is expanded many-fold thereby diluting the proton concentration. Impaired lysosomal acidification might in turn result in a decreased degradation capacity of the lysosome and thereby also affect the degradation of GRN which is internalized and transported to the lysosome, probably by sortilin [114]. Therefore, it is conceivable that TMEM106B overexpression might increase GRN protein levels, however, it cannot be ruled out that this is due to an overexpression artefact.

Moreover, the observed changes in GRN levels were rather small (about 15 %) [11]. In contrast, TMEM106B levels were up to 250 % increased upon T185 compared to S185 TMEM106B isoform expression even though the increase in GRN levels remained the same [11, 200]. Thus, the differential abundance of TMEM106B might contribute to a greater extent to disease progression than the changes in GRN expression [11]. Notably, in FTLT-TDP patients with a *GRN* mutation (i.e. GRN levels were up to 50 % reduced), TMEM106B mRNA [39, 301] as well as protein levels [87] were increased. This finding was further supported by Götzl *et al.* who demonstrated that in *Grn* knockout mice, TMEM106B protein levels were increased [87]. However, these findings are in contrast to the data of Brady *et al.*, Chen-Plotkin *et al.* and Nicholson *et al.* who all demonstrated an increase in GRN levels when TMEM106B was overexpressed [200, 39, 25]. Therefore, a functional relationship rather than a direct influence on each other on a transcriptional level is more likely.

Furthermore, as in cortex samples of FTLT-TDP patients lysosomes did not seem to present with a vacuolation phenotype [34, 39], the *in vitro* TMEM106B overexpression models might not represent the disease phenotype. Interestingly, complete loss of GRN had recently been described to cause NCL, a lysosomal storage disorder, which thus links GRN to lysosomal function [273]. Moreover, increased TMEM106B levels have been observed in a mouse model

for NCL [87]. Thus, the observed increased TMEM106B levels in FTLT-DTP patients might also be explained as a consequence of lysosomal dysfunction.

In summary, it is still under debate whether and, if so, how TMEM106B might affect GRN levels. As there is accumulating evidence that TMEM106B levels are increased in FTLT-DTP patients carrying a *GRN* mutation [39, 301, 87], a relationship between both proteins is quite certain. However, whether they influence each other directly or whether they act in a common pathway still remains to be elucidated.

### 4.5 TMEM106B influences lysosomal positioning

As increased TMEM106B levels were reported to be associated with FTLT-DTP by several independent groups [301, 39, 200], scientists used overexpression models to elucidate TMEM106B function [25, 39, 155, 200]. Nevertheless, proteins can have misleading actions when they are overexpressed [11]. This is especially important for TMEM106B as expression levels of TMEM106B critically affect its localization [25]. Thus, I mainly concentrated on knockdown experiments to elucidate the endogenous function of TMEM106B.

Upon TMEM106B knockdown, lysosomes changed their intracellular positioning and clustered at the MTOC (see figure 3.15, page 67) suggesting that TMEM106B might affect lysosomal trafficking [263]. Transfection of single siRNAs against TMEM106B demonstrated that clustering increased with the knockdown efficiency of the used siRNAs (see figures 3.14 and 3.15, pages 67 and 66). The quantification of the clustering phenotype confirmed that in TMEM106B #3 siRNA-treated HeLa cells, lysosomes presented with a more compact subcellular distribution and were significantly more shifted towards the nucleus than controls (see figure 3.19, page 72). Moreover, lysosomal clustering upon TMEM106B knockdown could be rescued by careful titration of TMEM106B wt levels back to endogenous levels (see figure 3.17, page 70) thereby proving the specificity of the TMEM106B knockdown phenotype. As expected, neither expression of the empty vector nor of the N4 glycosylation mutant of TMEM106B, which was shown to be retained in the ER, rescued the clustering phenotype (see figure 3.17, page 70).

However, Brady *et al.* were not able to detect any differences in lysosomal size or morphology upon TMEM106B knockdown [25] and did not comment on lysosomal positioning. Yet, by looking at their immunofluorescence pictures, clustering was not discernible upon TMEM106B knockdown. Compared to my studies, Brady *et al.* only achieved a knockdown efficiency of an estimated 50 % to 70 % [25] which is probably not enough to see the clustering effect upon TMEM106B knockdown as I demonstrated that the clustering phenotype correlates with knockdown efficiency (see figure 3.16, page 68). Moreover, they used N2a cells, a murine neuroblastoma cell line, instead of HeLa cells for their experiments. Since the clustering effect also seemed less prominent in human SH-SY5Y cells (see figure 3.15 b, page 67), it might also be possible that this phenotype is generally not as evident in neuroblastoma cell lines as in HeLa cells.

Stagi *et al.* reported that *TMEM106B* knockdown reduced lysosomal size and number [277]. Moreover, in contrast to my findings, they claim that in neurons transduced with *TMEM106B* shRNA, lysosomes were distributed more distally throughout the neurites [277]. One possible explanation are the different experimental conditions as well as the different models used. Whereas I worked with HeLa cells, an epithelial cell line, Stagi *et al.* utilized mouse cortical neurons [277]. It is known that vesicular transport in neurons differs from the transport in other cells of the body as microtubules in dendrites present with mixed polarity [132] in contrast to cells like HeLa cells where microtubules only possess one polarity. Thus, in dendrites, dynein can move bidirectionally whereas in HeLa cells, it only mediates the retrograde transport. These differences might account for the different results, however, further investigations are needed. Conversely, Schwenk *et al.* demonstrated that *TMEM106B* knockdown by shRNA in rat cortical neurons mediates a significant increase in dendritic retrograde lysosomal trafficking [263] which would argue against a more distal distribution of lysosomes, as claimed by Stagi *et al.* [277], and for the clustering phenotype I observed.

Indirectly supporting my data, Busch *et al.* and Chen-Plotkin *et al.* demonstrated that neurons of FTLT-DTP patients exhibited a more disorganized *TMEM106B* expression pattern [34] in which *TMEM106B* appeared diffusely expressed and more widely distributed in the cytoplasm compared to controls [34, 39]. This would, at least in part, reflect my observations in HeLa cells where lysosomes, upon moderate *TMEM106B* overexpression, appeared more diffuse and more distributed towards the cellular tips (see figure 3.17, page 70). Interestingly, Busch *et al.* reported that disorganization was especially prominent in *GRN* mutation carriers where *TMEM106B* expression even extended beyond the cell body into neuronal processes [34, 39]. As *TMEM106B* is localized on lysosomes and, in FTLT-DTP patients, its expression was found to be increased (with the highest *TMEM106B* levels detected in *GRN* mutation carriers) [39, 301], these data implicate that high levels of *TMEM106B* result in the distribution of lysosomes, which represents the opposite phenotype of the one I observed upon *TMEM106B* knockdown, namely lysosomal clustering.

To summarize, these data together with the data of Schwenk *et al.* [263], Busch *et al.* [34] and Chen-Plotkin *et al.* [39] therefore suggest that *TMEM106B* might play a crucial role in lysosomal transport.

However, *TMEM106B* might not only influence lysosomal positioning but might also generally affect trafficking of other cellular organelles either by influencing the cytoskeleton or motor proteins. A general disruption of the cellular transport system might impair trafficking [112] due to the loss of transit routes along which motor proteins transport their cargo. Furthermore, it is known that after the deletion of dynein, the motor protein that regulates retrograde transport, not only lysosomes but also endosomes and the Golgi are distributed throughout the cytosol

[100]. Moreover, mitochondria are known to cluster upon impaired kinesin-mediated anterograde transportation [96], which can be reversed upon knockdown of dynein [180].

Yet, investigation of the morphology of the actin and microtubule cytoskeleton did not reveal any obvious changes upon TMEM106B knockdown thereby excluding a general disruption of the cellular transport system. Concomitantly, the Golgi and mitochondria remained unaffected by the knockdown of TMEM106B. Interestingly, however, EEA1-positive vesicles, which are presumably early endosomes, but might also represent amphisomes [69], clustered near the MTOC indicating that TMEM106B might specifically affect the endocytic pathway.

### 4.6 TMEM106B and microtubule-dependent transport

Microtubules support intracellular transport and are nucleated at the MTOC [88, 177]. As all types of endosomes as well as lysosomes move actively along microtubules and, upon TMEM106B knockdown, lysosomes clustered at the MTOC, I examined whether a functional microtubule network was in fact one of the prerequisites for lysosomal clustering. Therefore, I treated control and TMEM106B siRNA-transfected cells with nocodazole, a drug that interferes with the polymerization of microtubules and thus would abolish vesicular transport. Indeed, as expected, the inhibition of microtubule network formation by nocodazole treatment compromised lysosomal clustering upon TMEM106B knockdown.

Lysosomes move bidirectionally along microtubules [88] with a spectrum of different kinesins promoting their anterograde transport while dynein mediates their retrograde transport [29, 88]. These movements are controlled by the intracellular pH as acidification disperses lysosomes into the cytosol whereas alkalization causes clustering at the MTOC [213, 107].

To determine whether retrograde transport was necessary to cause lysosomal clustering observed upon TMEM106B knockdown, the dynein-dynactin complex formation was impaired by dynamitin overexpression, a known tool to inhibit dynein-dynactin assembly and thus retrograde transport [121, 33, 181] (see also 3.9, page 77).

Interestingly, dynamitin overexpression reversed the TMEM106B knockdown phenotype irrespective of whether lysosomes had already been clustered at the time of transfection or not. Hence, on the one hand, a functional retrograde transport is indeed the second prerequisite for lysosomal clustering upon TMEM106B knockdown. On the other hand, anterograde transport was most likely not impaired by the knockdown of TMEM106B. This is because, in case of TMEM106B knockdown combined with dynamitin transfection on day 2, lysosomes, which at that point are normally already clustered at the MTOC, were redistributed from the cluster at the MTOC to the cellular tips.

Together, these data indicate that perinuclear lysosomal clustering upon TMEM106B knockdown is dependent on an intact microtubule network as well as on functional dynein-dynactin-mediated retrograde transport, the essential components of retrograde microtubular transport

[298]. Moreover, TMEM106B knockdown does not seem to influence the anterograde transport of lysosomes, however, more experiments are needed for confirmation.

One possible explanation for lysosomal clustering upon TMEM106B knockdown is that either TMEM106B promotes the anterograde transport or inhibits the retrograde transport of lysosomes. Conversely, in case of reduced TMEM106B expression, the anterograde transport would not be promoted any more or the retrograde transport would be restored resulting in overall increased retrograde transportation of lysosomes towards the MTOC (figure 4.1).

If the hypothesis that TMEM106B promotes the anterograde transport holds true, I would have expected that upon TMEM106B knockdown and dynamitin expression, lysosomes are clustered at the cellular tips as retrograde transport is abolished, but not so tightly as anterograde transport is also not promoted any longer. However, if the hypothesis that TMEM106B inhibits the retrograde transport holds true, lysosomes should tightly cluster at the cellular tips upon the inhibition of the retrograde transport by dynamitin as the anterograde transport is still intact. Since in TMEM106B siRNA-transfected cells expressing dynamitin, lysosomes seemed to be as tightly clustered at the cellular tips as lysosomes of control siRNA-transfected cells expressing dynamitin (see figure 3.23 b, page 78), TMEM106B probably inhibits the retrograde transport of lysosomes rather than promotes the anterograde transport (figure 4.1).

This assumption was supported by the data of Schwenk *et al.* who reported that under normal conditions, the binding of TMEM106B to MAP6 inhibited active retrograde transport of lysosomes along dendrites [263]. Importantly, they showed that knocking down TMEM106B increased the number and speed of retrogradely moving lysosomes in dendrites resulting in impaired dendritic branching [263]. Moreover, promoting anterograde lysosomal transport rescued this phenotype in TMEM106B knockdown cells [263]. Additionally, Stagi *et al.* claimed that TMEM106B suppression in neurons increased the fraction of moving lysosomes by 30 % further indicating that TMEM106B is involved in lysosomal transport [277].

Together with my data, this suggests that TMEM106B might indeed affect lysosomal transport probably by limiting retrograde trafficking of lysosomes.

Functional trafficking is especially important for neurons as it ensures neuronal survival and differentiation [60]. Neurons need to transport their cellular waste over long distances towards the cell body, where the majority of lysosomes is located [205] (see also 1.4, page 35). Moreover, vesicular trafficking allows for a rapid cellular adaptation to the changing extracellular environment [144, 73].

Accordingly, impaired axonal transport is implicated in neurodegeneration as evidenced by the identification of mutations in motor protein genes like *KIF1B*, which causes Charcot-Marie-Tooth Disease Type 2A, or *DCTN1*, encoding for a dynactin subunit, which is associated with

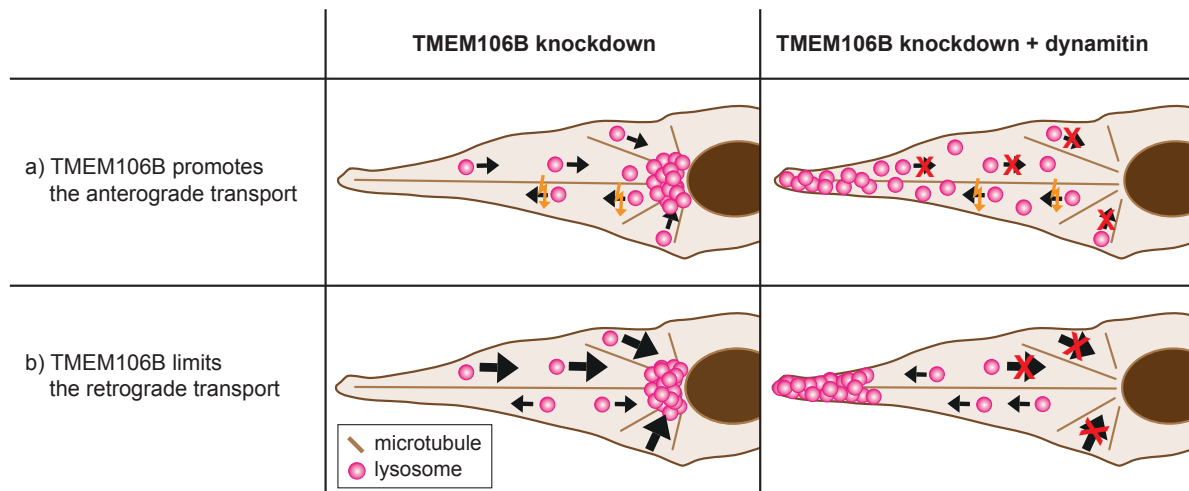


**Figure 4.1: Hypotheses of how TMEM106B might influence microtubule-dependent transport**

The hypotheses for the influence of TMEM106B on microtubule-dependent transport are depicted for TMEM106B knockdown and TMEM106B knockdown combined with concomitant dynamin expression. The crosses represent an abolishment of transport, the lightnings an impairment.

motor neuron degeneration in an Alabama kindred as well as with ALS and FTLN [40, 190, 279, 112, 154, 119]. Interestingly, key components of the retrograde transport routes, which are responsible for targeting neurotrophins and their survival signals to the soma, have been especially associated with motor neuron disease [94, 60, 119, 154].

However, not only motor proteins but also lysosomal membrane proteins which may influence lysosomal positioning have been described to be implicated in neurodegeneration. One example is ceroid-lipofuscinosis, neuronal 3 (CLN3), an endosomal/lysosomal transmembrane protein which had been reported to interact with several motor components, but especially with Rab7 and RILP. Mutations in *CLN3* that are causative for juvenile NCL (Batten disease) were associated with an imbalanced Rab7 GTP/GDP cycle and a loss of Rab7 and CLN3 interaction. This subsequently resulted in defects in neuronal endocytic trafficking and autophagic processes ultimately leading to neurodegeneration [298]. Other examples are the lysosomal membrane proteins LAMP1 and LAMP2 (see also section 1.3.1, page 25), the latter of which is implicated in Danon disease, another lysosomal storage disorder. Cells lacking both proteins showed a more diffuse distribution of lysosomes in the cytosol which is caused by a defective dynein-mediated transport. In a cell culture model for phagocytosis, this resulted in impaired lysosome-phagosome fusion probably due to the reduced ability of phagosomes and lysosomes to move towards the MTOC precluding their interaction [117]. Similarly, autophagosome maturation and their fusion with lysosomes might be impaired by the delayed migration towards the MTOC [248].

Interestingly, neurons of FTLN-TDP patients have been reported to present with a diffuse distribution of TMEM106B-positive vesicles which are probably lysosomes [34, 39]. Thus, the lysosomal phenotype might be comparable to *LAMP1/LAMP2* knockout cells. Since increased TMEM106B levels might, like in *LAMP1/2* double-knockout, impair the retrograde transport of

lysosomes, it is tempting to speculate that as a result, phagocytosis and autophagy are likewise inhibited thereby promoting neurodegeneration. Moreover, it is probable that both too high and too low TMEM106B levels are detrimental to neurons, as both might lead to an imbalance in lysosomal trafficking which would result in axonal transport deficits and in impaired dendrite and synapse stability [263, 40, 190, 279, 112, 154, 119].

## 4.7 The autophagic pathway is influenced by TMEM106B knockdown

Clustering of lysosomes might not only be caused by defective lysosomal transportation but also be the result of a cellular stress response caused by impaired lysosomal function [150]. Therefore, I analysed whether lysosomal acidification and the processing and activity of lysosomal enzymes were affected by TMEM106B knockdown. However, no changes between control and TMEM106B siRNA-treated cells were detected arguing for fully functional lysosomes. Thus, if, upon TMEM106B knockdown, lysosomal clustering was indeed a lysosomal stress response and the stress did not result from lysosomal dysfunction, it might instead have been caused by inhibited fusion of lysosomes and autophagosomes or endosomes, i.e. from impaired autophagy. It has been demonstrated that lysosomal clustering can influence the autophagic pathway in two different ways, namely by enhancing the autophagic flux and by increasing the expression of autophagosomal and lysosomal genes [150] (see section 1.3.4, page 33). I therefore investigated whether upon TMEM106B knockdown, autophagosomal or lysosomal markers were altered.

Indeed, p62 protein levels were increased upon TMEM106B knockdown, however, only to a mild extent. Interestingly though, Korolchuk *et al.* also showed an only 1.2- to 1.3-fold increase in p62 levels upon *Atg7* knockdown which abolishes autophagy and is known to be sufficient to cause neurodegeneration (see also section 1.4, page 35). Thus, even though the autophagic pathway is compromised, p62 levels might not be heavily elevated as a consequence [149].

Yet, upon TMEM106B knockdown, the number of p62 particles increased significantly. Moreover, these particles co-localized with both LC3, a marker for autophagosomes, and Apu2, a marker for lysine 48-linked polyubiquitin suggesting that autophagic turnover and maybe also proteasomal degradation might be impaired. Interestingly, it has been shown that excess p62 inhibits the clearance of ubiquitinated proteins destined for proteasomal degradation due to a delay in their delivery to proteasomal proteases mediated by reduced autophagic activity [149]. Hence, inhibition of autophagy might also inhibit the ubiquitin-proteasome system [149] thereby explaining the increase in both LC3 and lysine 48-linked polyubiquitin under the paradigm that, upon TMEM106B knockdown, autophagy is impaired. Moreover, Filimonenko *et al.* speculated that polyubiquitinated proteins might also be autophagic substrates which could be directed to the autophagic pathway by p62 [71]. However, the increase in p62 levels still has to be re-evaluated with different siRNAs against TMEM106B to exclude siRNA-specific side effects.

Moreover, whether autophagy is the only degradation pathway to be affected or whether the ubiquitin-proteasome system is also influenced by TMEM106B remains to be determined.

Another protein that was found to be increased upon TMEM106B knockdown was LC3, an autophagic marker protein. Interestingly, both soluble LC3I and membrane-bound, PE-conjugated LC3II protein levels were elevated indicating an increase in LC3 expression rather than just a conversion of LC3I into LC3II. These results were also obtained upon starvation and thus activation of autophagy, where the quantification of protein levels revealed a 2.0- (LC3I) to 2.3-fold (LC3II) increase in LC3 protein levels upon TMEM106B knockdown.

Strikingly, upon starvation, not only differences in LC3 levels but also in lysosomal protein levels were revealed that had not been apparent under normal growth conditions. Accordingly, protein levels of LAMP2, a lysosomal membrane protein, and of cathepsin D, a lysosomal enzyme, were significantly elevated upon TMEM106B knockdown. The increase in immature as well as mature cathepsin D levels suggests that in TMEM106B #3 siRNA-treated cells, lysosomal biogenesis might have been activated faster or earlier than in control siRNA-transfected cells. Moreover, a reduced turnover might also explain the increased cathepsin D and LAMP2 protein levels. Therefore, determining the mRNA levels of both proteins might elucidate which of these two scenarios reflects the truth.

Together, these data implicate that TMEM106B affects, even though probably mildly, the lysosomal and autophagic pathway. Furthermore, applying additional stress, like starvation, in an experimental set-up might be crucial to reveal the consequences of TMEM106B loss as, by challenge, differences between protein levels might become more apparent.

Inhibition of the autophagic pathway is sufficient to cause neurodegeneration as functional autophagy is crucial for neuronal survival [99] (see also sections 1.3.3, page 29 and 1.4, page 35).

As *TMEM106B* is not a disease-causing gene but a risk factor, it might only have a minor impact on cellular function under normal conditions. However, a second hit like stress in addition to TMEM106B dysfunction might accelerate neurodegeneration in FTLD-TDP.

Supporting this assumption, the risk allele of *TMEM106B* had been found to be especially associated with *GRN* mutation carriers. Interestingly, a homozygous *GRN* mutation has recently been identified to cause NCL, a lysosomal storage disorder, thereby strongly arguing for GRN playing a crucial role in lysosomal function [273]. Moreover, lysosomal proteins were demonstrated to be increased in *Grn* knockout mice [87, 286] as well as in brain lysates of FTLD-TDP patients carrying a *GRN* mutation [87] possibly due to decreased mTORC1 activity and thus increased lysosomal biogenesis [286]. Tanaka *et al.* claim that this increase in lysosomal proteins subsequently resulted in exacerbated neuronal damage [286] (see also section 1.1.3.1.2, page 12). Thus, it is tempting to speculate that even though GRN probably affects lysosomal function independently of TMEM106B, however, both proteins might have an impact on the same pathway,

namely lysosomal biogenesis and autophagy, which would thereby accelerate disease progression if both a *GRN* mutation and the risk allele of *TMEM106B* were present.

#### 4.8 Hypotheses of how *TMEM106B* might influence the pathogenesis of *F<sup>T</sup>LD-TDP*

Both transport and autophagy have been inextricably linked with neurodegeneration. As already mentioned, neurons are highly dependent on functional transportation due to the fact that axons can represent more than 99 % of the cellular volume whereas protein and lipid synthesis occur almost exclusively in the cell body [112]. Thus, active transport is required for supplying the neuron with newly synthesized material [112]. Moreover, the large expanses of dendritic and axonal cytosol result in long transport routes of cellular waste towards the cell body, where the majority of lysosomes is located [205, 234] (see also 1.4, page 35). Together with the fact that neurons cannot dilute their toxic burden by cell division [235, 319, 158], this is why neurons are especially vulnerable to any defects in cellular transport.

As microtubule motors function interdependently of each other [112], both the anterograde and the retrograde transport machinery have to work properly to ensure neuronal survival [60].

Interestingly, the data of this study indicate, that *TMEM106B* might play a role in one or both of these pathways as *TMEM106B* seems to influence lysosomal transport and to affect the lysosomal degradation pathway. However, there are several options to explain the observed phenotypes after *TMEM106B* knockdown. In a first hypothesis, *TMEM106B* directly affects lysosomal transport by either promoting the anterograde transport or by inhibiting the retrograde transport machinery (figure 4.2, upper panel), the latter of which is more likely due to evidence from Schwenk *et al.* [263] (see also section 4.6, page 101). The second hypothesis is that *TMEM106B* might promote the fusion process between autophagosomes and lysosomes, i.e. autophagy (figure 4.2, lower panel). Supporting the latter hypothesis, Stagi *et al.* reported that *TMEM106B* might interact with *Vps11*, a class C protein of the HOPS complex. Interestingly, in 2014, *Vps11* has been reported to mediate autophagosome-lysosome fusion [122]. However, whether *TMEM106B* indeed interacts with *Vps11* and whether this interaction might influence autophagosome-lysosome fusion remains to be elucidated.

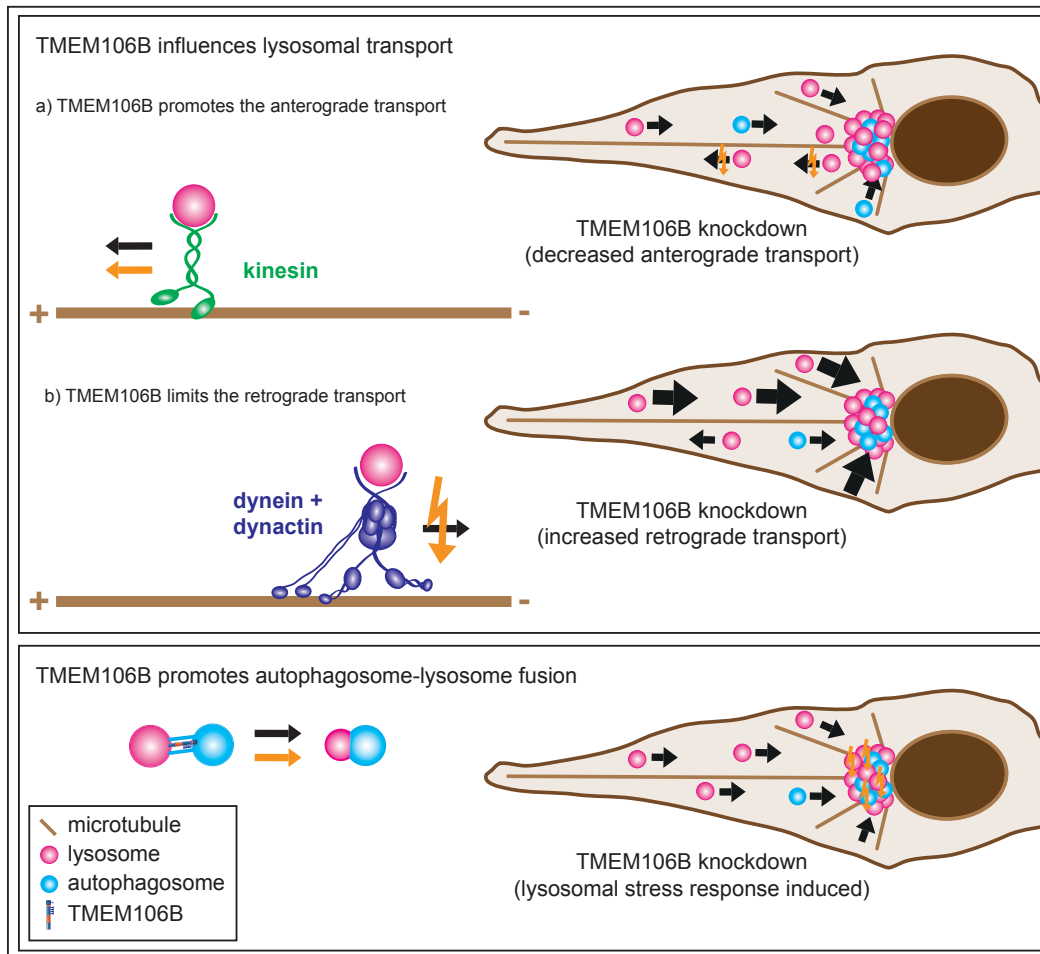


**Figure 4.2: Hypotheses why lysosomes cluster upon TMEM106B knockdown**

Upon TMEM106B knockdown, lysosomes cluster at the MTOC. One possible explanation for this phenotype is that TMEM106B affects lysosomal transport (see upper panel). Thereby, it could either promote the anterograde transport (see upper panel, a) or limit the retrograde transport (see upper panel, b). Another possibility is that TMEM106B influences the lysosomal stress response pathway (see lower panel). As lysosomes are still acidic and lysosomal enzymes still functional upon TMEM106B knockdown, lysosomal dysfunction is very unlikely. However, the fusion between autophagosomes and lysosomes might be impaired thus inducing the lysosomal stress response pathway which, as a consequence, results in clustering of lysosomes (see lower panel).

Derived from these hypotheses, there are two different scenarios of how TMEM106B might affect neurodegeneration (figure 4.3), namely by impaired lysosomal transportation or an impaired fusion of lysosomes and autophagosomes. Concomitantly, following the fusion hypothesis, impaired TMEM106B function might result in a loss-of-TMEM106B-function which may cause a decrease in the fusion capacity of autophagosomes and lysosomes (see also figure 4.2, lower panel, page 107). This is supported by the fact that p62 accumulates upon TMEM106B knockdown. Consequently, autophagosomes and thus dysfunctional proteins or organelles would accumulate, further compromising the autophagic degradation system. Moreover, impaired autophagy would subsequently also inhibit the proteasomal degradation machinery [149] resulting in accelerated neurodegeneration as both degradation machineries would be impaired. In addition, the accumulation of autophagosomes would probably activate the lysosomal stress response pathway to compensate for the decreased autophagic flux explaining the increase in LC3, cathepsin D and LAMP2 protein levels as well as lysosomal clustering upon TMEM106B knockdown. Interestingly, in some LSDs like Niemann-Pick type C, late endosomes and lysosomes were also found to cluster at the MTOC [298, 242].

Together, over a long period of time, this would mean a constantly activated lysosomal stress response pathway combined with impaired autophagy which likely would result in neurodegeneration [99, 286] (figure 4.3, left panel).

In the second scenario, the transport hypothesis, impaired TMEM106B function might result in increased TMEM106B levels and/or a gain-of-function mechanism which may subsequently decrease the retrograde transport within the cell. This is supported by the fact that in FTL D-TDP patients, TMEM106B levels were indeed found to be increased [301, 87] accompanied by a more diffuse distribution of TMEM106B-positive vesicles (i.e. probably lysosomes) in the cell periphery [34, 39]. Moreover, the latter presents the opposite phenotype of which could be observed upon TMEM106B knockdown. A decrease in retrograde transport would subsequently lead to an imbalanced axonal transport combined with decreased dendritic branching [277] and synaptic plasticity [40, 112], the latter of which has been reported in FTL D patients [43]. Moreover, the fusion of autophagosomes and lysosomes would be impaired [234] resulting in an accumulation of misfolded or dysfunctional proteins over time. In addition, due to higher TMEM106B expression, lysosomes would not as efficiently be transported to the MTOC as in healthy individuals, the lysosomal stress response pathway would probably be impaired. mTORC1 would remain active due to the predominant positioning of lysosomes in the cell periphery [150] mediating TFEB phosphorylation which concomitantly would inhibit autophagic and lysosomal biogenesis [40]. Upon TMEM106B knockdown, the opposite phenotype, namely an increase in LC3, p62, cathepsin D and LAMP2 was detected supporting this hypothesis.

In summary, both a direct influence of TMEM106B on autophagy as well as an impact of TMEM106B on the retrograde transport machinery would, in case of TMEM106B malfunctioning, lead to an inhibition of the autophagic flux resulting in an accumulation of dysfunctional proteins, and a compromised stress response pathway, which might render neurons more suscep-

tible to cellular stress [215, 40]. All these mechanisms would ultimately promote neurodegeneration (figure 4.3, right panel). Notably, a similar mechanism was described in neurons where snapin, a protein implicated in linking late endosomes to the dynein motor, was knocked out [36]. Thereby, retrograde transport was impaired, late endosomes clustered and autophagy was inhibited leading to neurodegeneration, thus providing a mechanistic link between retrograde transport, lysosomal maturation and autophagy [36]. Hence, it is tempting to speculate that a similar disease mechanism might apply for FTLN-TDP where the *TMEM106B* risk allele is present.

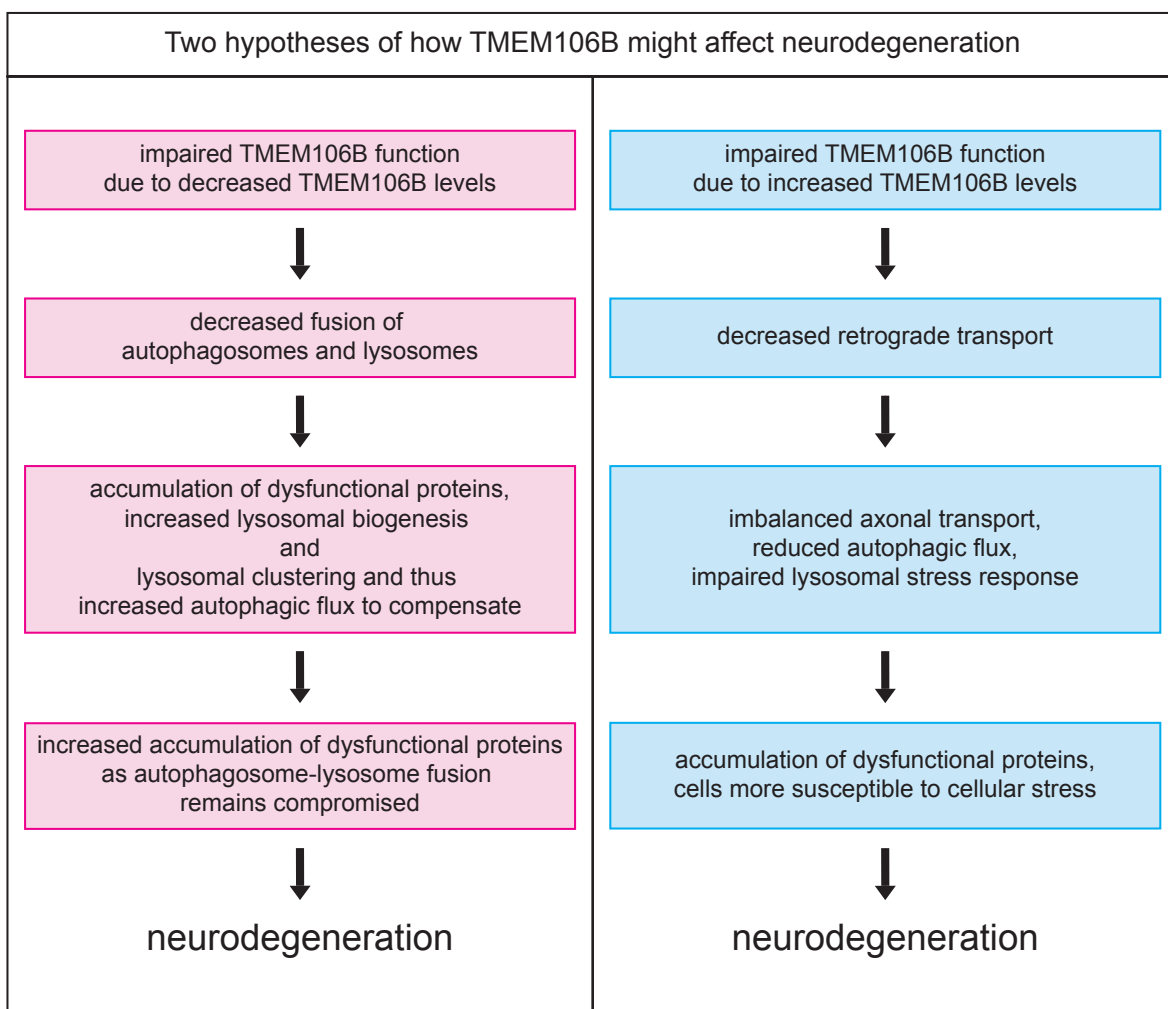


**Figure 4.3: Scheme of how TMEM106B might affect neurodegeneration**

On the left (in pink), disease progression under the paradigm that TMEM106B affects autophagosome-lysosome fusion is depicted. On the right (in blue), disease progression under the paradigm that TMEM106B inhibits the retrograde transport is depicted.

At present, it has not yet been conclusively determined which of both hypotheses might hold true. Thus, further investigation is crucial to elucidate TMEM106B function, i.e. to delineate whether TMEM106B might indeed affect cellular trafficking directly or influence autophagosome-lysosome fusion. However, TMEM106B might also be involved in both pathways as, interestingly, van der Kant *et al.* recently published that lysosomal tethering and transport are combined processes [302]. Moreover, to resolve whether a TMEM106B gain- or a loss-of-function mechanism promotes FTLN-TDP disease progression will be intriguing.

#### 4.9 Is an increase in TMEM106B levels detrimental or beneficial for FTLN-TDP disease progression?

Until now, the question of whether the observed increase in TMEM106B levels in FTLN-TDP patients is a cause or a consequence, i.e. detrimental or beneficial, could not be sufficiently clarified. On the one hand, Stagi *et al.* stated that elevated TMEM106B levels would constantly activate TFEB resulting in a greater lysosomal and autophagic function, which might be protective for TDP-43 pathology [277, 12]. Yet, if elevated TMEM106B levels activate the lysosomal stress response pathway that strongly, this would more likely suggest that TMEM106B overexpression would cause lysosomal dysfunction rather than exert a positive effect on cells. This is in line with the findings of Brady *et al.* and Chen-Plotkin *et al.* who reported that TMEM106B overexpression caused an increase in lysosomal size accompanied by poor lysosomal acidification and a subsequent impairment of endolysosomal degradation [39, 25]. Moreover, Nicholson *et al.* claimed that the disease-associated TMEM106B variant (T185) was more stable than the protective variant (S185) [200], again arguing for increased TMEM106B levels to be detrimental. Schwenk *et al.* observed that dendritic branching was inhibited upon TMEM106B knockdown, suggesting that overexpression of TMEM106B might positively affect dendrite morphology [263]. However, they claimed that TMEM106B might limit retrograde trafficking and thus that the dendritic phenotype was caused by lysosomal misrouting [263]. Thus, both too much and too little TMEM106B expression would result in imbalanced cellular transportation and therefore be detrimental to neurons.

On the other hand, the observed increase in TMEM106B levels in FTLN-TDP could represent a rescue attempt of the cells to compensate for impaired lysosomal function due to GRN reduction. GRN was implicated to play a role in lysosomal function [273, 15] and *GRN* haploinsufficiency might therefore result in dysfunctional lysosomes. Accordingly, Tanaka *et al.* demonstrated that GRN deficiency in a mouse model resulted in an increased activity of the lysosomal stress response pathway accompanied by an elevation in lysosome-related gene expression [286]. Götzel *et al.* also observed an increase in lysosomal proteins in *Grn* knockout mice, one of which was TMEM106B [87]. As TMEM106B levels also increased in *Ctsd* knockout mice, an NCL mouse model, they argued that TMEM106B along with other lysosomal membrane proteins was

increased due to the enlargement of lysosomes which were unable to cope with the accumulation of cellular debris [87].

In summary, it is still under debate whether the increase in TMEM106B levels observed in FTLD-TDP patients is a cause or a consequence of disease progression which stresses the need for further investigations to elucidate TMEM106B function. One attempt might be the use of better models like TMEM106B knock-in mice instead of using transient TMEM106B overexpression in cell lines. Moreover, as additional stressors might be necessary to reveal the probably mild effects of TMEM106B on lysosomal function, TMEM106B mice might be crossed with *Grn* knockout mice and/or additionally treated with autophagy inducers or inhibitors.

### 4.10 Impaired trafficking and autophagy as common disease mechanisms in FTLD?

Multiple FTLD-causative or -associated genes are linked to vesicle transport and autophagy. For instance, *tau* mutations, the cause for FTLD-tau, destabilize microtubules along which vesicles are transported. This results in impaired axonal transport in addition to tau filament aggregation [239, 270]. Moreover, mutations in *CHMP2B* identified in FTLD-UPS patients have been reported to disrupt endocytic trafficking by a gain-of-function mechanism [295]. Thereby, mutant CHMP2B constitutively binds to MVBs concomitantly preventing Rab7 recruitment [295]. Rab7, however, is crucial for anterograde and retrograde transportation of late endosomes [242, 314], autophagosome maturation and endosome-lysosome fusion [118]. Accordingly, CHMP2B mutants displayed a decrease in axonal trafficking along with an altered dendritic spine morphology [83], increased neuroinflammation [83] and an accumulation of autophagosomes and p62-positive aggregates [71] due to impaired autophagy [295, 71].

Another protein known to be causative for FTLD is VCP. This protein had been demonstrated to impair autophagy at different stages like autophagosome formation [152] and fusion with lysosomes [131]. Recently, also *C9orf72* was added to the list of FTLD-causing genes [61, 238]. Interestingly, it was reported to be structurally associated with the DENN protein family [49, 77] which regulates Rab GTPase function and thus membrane trafficking [49, 77]. Accordingly, Farg *et al.* were able to show that C9orf72 interacted with several different Rabs, actin and ubiquilin-2 [70]. Furthermore, C9orf72 knockdown was demonstrated to inhibit endocytosis and autophagy further indicating that C9orf72, like tau, CHMP2B and VCP, is involved in intracellular trafficking pathways linked to protein degradation [70]. Interestingly, my data suggest that TMEM106B either alters lysosomal trafficking probably by slowing down the retrograde transport or that it affects autophagy presumably by promoting autophagosome-lysosome fusion. Hence, the FTLD risk factor *TMEM106B* would fit in well into the general picture of impaired transport and autophagy being common disease mechanisms in FTLD. However, which functions exactly are performed by TMEM106B and which other proteins are involved remains to be elucidated.

## 4.11 Concluding remarks

Together, in this study, TMEM106B has been demonstrated to be a lysosomal type II transmembrane protein with three non-complex and two complex N-glycosylation sites, the latter of which are important for correct TMEM106B localisation within the cell. Moreover, even though no direct association with GRN could be detected, an indirect relationship between those proteins was suggested as both proteins seem to affect the lysosomal degradation pathway. Strikingly, TMEM106B knockdown presented with tight lysosomal clustering and an increase in autophagosomal and lysosomal proteins. Thus, two possible disease mechanisms were proposed in which either impaired trafficking or autophagy was suggested to be the origin of disease progression. Hence, this study provides the first thorough biochemical characterization of TMEM106B along with strong indications of how TMEM106B might influence FTLD pathology. Moreover, it stresses the importance of the role of lysosomes in the development and progression of neurodegenerative diseases. Interestingly, lysosomes are the proteolytic system probably most affected by ageing [103] as during ageing, they become more and more susceptible to free radical oxidative stress [8]. However, also the activity of the proteasomal system is known to decrease during ageing adding to the accumulation of misfolded proteins and, as a consequence, promoting neurodegeneration [164, 134, 41]. Thus, during ageing, both proteolytic machineries, the proteasome and the lysosome, are increasingly impaired [41].

Bahr *et al.* speculated that the gradual alterations in the lysosomal system during ageing might be the cause for ageing being the primary risk factor for many neurodegenerative diseases [8]. This might explain why mutations in *GRN*, even though they probably affect lysosomes only mildly, cause neurodegeneration and also why TMEM106B might accelerate this process. Possibly, during ageing, lysosomes at some point cannot compensate any longer for the ever-growing decrease in lysosomal degradation that is further aggravated by mutations in *GRN* which consequently would result in neurodegeneration. *TMEM106B* mutations might accelerate this process as they might very mildly affect the same pathway.

However, TMEM106B was not only implicated in FTLD-TDP with *GRN* mutations and FTLD-DPR with *C9orf72* hexanucleotide expansions, but also in other neurodegenerative diseases like ALS and AD as well as in a general risk for cognitive decline (see section 1.2, page 21). Hence, TMEM106B might influence neurodegeneration on a broader level. Interestingly, not only FTLD, but also AD, PD, ALS and HD show a strong autophagic/lysosomal component along with trafficking defects (see also 1.4, page 35). For instance, in AD, autophagic vesicles accumulate and, as a consequence, intracellular trafficking is impaired [176], linking vesicular transport and autophagy. Moreover, in PD, *LRRK2* mutations were associated with endosomal-lysosomal trafficking and lysosomal pH, again linking transport and autophagy [220, 176, 175]. Familial ALS can be caused by mutations in *DCTN1*, a subunit of dynactin which is part of the dynein-dynactin complex responsible for retrograde transport [189, 190]. Transgenic mice which express the mutant protein have been reported to have increased LC3II levels and accumulated

ubiquitin-positive aggregates along with autophagic vacuoles in affected neurons [153]. Interestingly, it was also shown that mutant but not normal superoxide dismutase 1 (SOD1), causative for ALS and degraded by autophagy, co-localizes with the dynein-dynactin complex. This seems to inhibit retrograde vesicular transport and to promote neurodegeneration [325, 283]. In HD, huntingtin, which normally helps to link cargo to actin and coordinates the switch between actin and microtubules in preparation for dynein-dependent movement [88], is mutated and thus not functional. Furthermore, after inhibiting the UPS [62], mutant huntingtin aggregates can recruit beclin-1 which in turn would impair autophagosome formation and thus autophagy [269]. These examples demonstrate, that trafficking and autophagy are cellular mechanisms that are often linked with each other and are implicated in various neurodegenerative diseases. Therefore, if TMEM106B influences one or even both mechanisms, it would be conceivable that TMEM106B does not only play an important role for FTLD, but might constitute a general risk for neurodegeneration.

Elucidating TMEM106B's biochemical characteristics along with understanding the mechanisms of how TMEM106B affects cellular pathways might therefore aid the development of strategies to slow down disease progression of various neurodegenerative diseases.

# 5 Material and Methods

## 5.1 Material

### 5.1.1 Laboratory equipment and chemicals

All experiments were performed using standard laboratory equipment. Chemicals were purchased from the companies Merck Millipore, Roth and Sigma-Aldrich with analytical grade *pro analysi (p.a.)* unless otherwise stated. The compositions of solutions and buffers are listed in the respective methods part.

### 5.1.2 Primers

Primers were synthesized by Thermo Fisher Scientific, purified by high performance liquid chromatography and lyophilized. Stock solutions of 100  $\mu\text{M}$  (100 pmol/ $\mu\text{l}$ ) were prepared in double distilled water (ddH<sub>2</sub>O) and stored at  $-20^\circ\text{C}$ . The list of primers with name, construct used for and sequence from 5' to 3' end is given in table 5.1 (Fwd indicates forward primer, Rev indicates reverse primer and mut means mutated).

**Table 5.1:** Primer list

primer name	construct	sequence
TMEM106B_Glyc_NIT1(S) Fwd	TM_NIT1 <sub>mut</sub>	GTT ATG ATG TTC AGA AGC GTA CAA TTT ATT TAA GTA TCA CAA ACA CAC T
TMEM106B_Glyc_NIT1(S) Rev		AGT GTG TTT GTG ATA CTT AAA TAA ATT GTA CGC TTC TGA ACA TCA TAA C
TMEM106B_Glyc_NIT2(S) Fwd	TM_NIT1-2 <sub>mut</sub>	CAC AAA CAC ACT AAG TAT AAC AAA CAA TAA CTA TTA CTC TGT CGA AGT TG
TMEM106B_Glyc_NIT2(S) Rev		CAA CTT CGA CAG AGT AAT AGT TAT TGT TTG TTA TAC TTA GTG TGT TTG TG
TMEM106B_Glyc_NIT3(S) Fwd	TM_NIT1-3 <sub>mut</sub>	CTA TTA CTC TGT CGA AGT TGA AAG CAT CAC TGC CCA AGT TCA ATT TTC
TMEM106B_Glyc_NIT3(S) Rev		GAA AAT TGA ACT TGG GCA GTG ATG CTT TCA ACT TCG ACA GAG TAA TAG
TMEM106B_Glyc_NIT4(S) Fwd	TM_NIT1-4 <sub>mut</sub> / siRNA TM3- resistant N4	GGA AAG GCA CGC TTA AAC AGC ATA ACC ATT ATT GGT CCA CTT G
TMEM106B_Glyc_NIT4(S) Rev		CAA GTG GAC CAA TAA TGG TTA TGC TGT TTA AGC GTG CCT TTC C

**Table 5.1:** Primer list

primer name	construct	sequence
TMEM106B_Glyc_NTT5(S) Fwd	TM_NIT1-5mut	GTA TGT CGA CTG TGG AAG AAG CAC AAC TTA TCA GTT GG
TMEM106B_Glyc_NTT5(S) Rev		CCA ACT GAT AAG TTG TGC TTC TTC CAC AGT CGA CAT AC
TMEMsiRNA3 Fwd	TM3 siRNA-resistant HA-TMEM106B	CCA TAT AGT GAC CAA CGA TTA CGG CCG AGA AG
TMEMsiRNA3 Rev		CTT CTC GGC CGT AAT CGT TGG TCA CTA TAT GG
HA-TMEM106B (BamHI) Fwd	HA-TM/ HA-TM pcDNA6	CGC GGA TCC GCC ACC ATG TAC CCA TAC GAC GTC CCA GAC TAC GCT GGA AAG TCT CTT TCT CAT TTG
TMEM106B STOP (XhoI) Rev		CCG CTC GAG TTA CTG TTG TGG CTG AAG TAC ATT TAA ATA
TMEM106B (BamHI) Fwd	TM-HA	CGC GGA TCC TCA GAC ATG GGA AAG TCT CTT TCT CAT TTG
TMEM106B-HA-Stop (XhoI) Rev		CCG CTC GAG TTA AGC GTA GTC TGG GAC GTC GTA TGG GTA CTG TTG TGG CTG AAG TAC ATT TAA ATA TTC

In table 5.2, the TaqMan primers used for real-time PCR are depicted.

**Table 5.2:** TaqMan primer list

target	name	provider
human GAPDH	4326317E	Applied Biosystems
human TMEM106B	Hs00998849 (exon boundary 7-8)	Applied Biosystems
human GRN	Hs00173570 (exon boundary 1-2)	Applied Biosystems

### 5.1.3 Constructs

Vectors and plasmids used in this study are depicted in table 5.3. Furthermore, it is stated how the plasmids were cloned. Notably, in this study, when TMEM106B is mentioned, the T185 isoform of TMEM106B is meant (the protective S185 isoform was termed T185S, but data are not shown in this study).

\*Affiliations: Serge Bénichou, Institut Cochin, Paris; Marino Zerial, Max Planck Institute of Molecular Cell Biology and Genetics, Dresden; Nicole Exner, Ludwig-Maximilians-University Munich, Adolf Butenandt Institute, Munich.

**Table 5.3:** Constructs

construct abbreviation	construct name	vector backbone	cloning	provider
IMAGE full length clone IRATp970G1031D	human TMEM106B cDNA	pBluescriptR	SalI + XhoI	imaGenes GmbH
HA-TM pcDNA6	pcDNA6/V5-His STOP HA-TMEM106B	pcDNA6/V5-HisA (Life Technologies)	BamHI + XhoI	lab

Table 5.3: Constructs

construct abbreviation	construct name	vector backbone	cloning	provider
HA-TM	pcDNA 4 /TO/myc HA-TMEM106B	pcDNA4/TO/myc (Life Technologies)	BamHI + XhoI	Christina Lang
TM-HA	pcDNA3.1 TMEM106B-HA	pcDNA 3.1 Hygro (Life Technologies)	BamHI + XhoI	Christina Lang
TM_NIT1 <sub>mut</sub>	TM_NIT1	pcDNA6/V5-HisA (Life Technologies)	site-directed mutagenesis on HA-TM pcDNA6	Christina Lang
TM_NIT1-2 <sub>mut</sub>	TM_NIT1-2 (NIT2)	pcDNA6/V5-HisA (Life Technologies)	site-directed mutagenesis on TM_NIT1 <sub>mut</sub>	Christina Lang
TM_NIT1-3 <sub>mut</sub>	TM_NIT1-3 (NIT3)	pcDNA6/V5-HisA (Life Technologies)	site-directed mutagenesis on TM_NIT1-2 <sub>mut</sub>	Christina Lang
TM_NIT1-4 <sub>mut</sub>	TM_NIT1-4 (NIT4)	pcDNA6/V5-HisA (Life Technologies)	site-directed mutagenesis on TM_NIT1-3 <sub>mut</sub>	Christina Lang
TM_NIT1-5 <sub>mut</sub>	TM_NIT1-5 (NIT5)	pcDNA6/V5-HisA (Life Technologies)	site-directed mutagenesis on TM_NIT1-4 <sub>mut</sub>	Christina Lang
N3 (HA-TMEM)	N3 only (HA-TMEM)	HA-TM in pcDNA4/TO/myc (Life Technologies)	site-directed mutagenesis on HA-TM	lab
N4 (HA-TMEM)	N4 only (HA-TMEM)	HA-TM in pcDNA4/TO/myc (Life Technologies)	site-directed mutagenesis on HA-TM	lab
N5 (HA-TMEM)	N5 only (HA-TMEM)	HA-TM in pcDNA4/TO/myc (Life Technologies)	site-directed mutagenesis on HA-TM	lab
N3 TMEM-HA	N3 only TMEM-HA	pcDNA 3.1 Hygro (Life Technologies)	site-directed mutagenesis on TM-HA	Christina Lang
N4 TMEM-HA	N4 only TMEM-HA	pcDNA 3.1 Hygro (Life Technologies)	site-directed mutagenesis on TM-HA	Christina Lang
N5 TMEM-HA	N5 only TMEM-HA	pcDNA 3.1 Hygro (Life Technologies)	site-directed mutagenesis on TM-HA	Christina Lang
NIT4+5	NIT4+5only	HA-TM in pcDNA4/TO/myc	site-directed mutagenesis on HA-TM	Christina Lang
LAMP1-mGFP	addgene plasmid 34831	pEGFP-N	EcoRI + SalI	addgene
TM3 siRNA-resistant HA-TMEM106B	TM3 siRNA-resistant HA-TMEM106B	pcDNA4/TO/myc (Life Technologies)	site-directed mutagenesis on HA-TMEM	Christina Lang
siRNA TM3-resistant N4	siRNA TM3-resistant N4 only HA-TMEM106B	pcDNA4/TO/myc (Life Technologies)	site-directed mutagenesis on N4 (HA-TMEM)	Christina Lang
chk-dyn	0347-pEGFPC2-DynChk (GFP-chicken dynamitin)	pEGFP-C2 (Clontech)	EcoR1	Serge Benichou* [121]
Rab4-GFP	Rab4-GFP	pEGFP-Vektor (Clontech)	HindIII+XhoI	Marino Zerial* [287]
Rab5a-GFP	Rab5a-GFP	pEGFP-Vektor (Clontech)	HindIII+Pst	Marino Zerial* [240]
Rab7-GFP	Rab7-GFP	pEGFP-Vektor (Clontech)	BamHI	Marino Zerial* [240]

**Table 5.3:** Constructs

construct abbreviation	construct name	vector backbone	cloning	provider
Rab11-GFP	Rab11-GFP	pEGFP-Vektor (Clontech)	HindIII+XhoI	Marino Zerial* [318]
Mfn2	Mitofusin2	pcDNA 3.1 (Life Technologies)	BamHI + HindIII	Nicole Exner* [198]
Mito-GFP	CellLight <sup>®</sup> Mitochondria-GFP, BacMam 2.0			Life Technologies

### 5.1.4 Small interfering RNAs

For RNA interference, the siRNAs depicted in table 5.4 were used. Moreover, the abbreviations that I have given them in this study, their sequence (if known) and their provider are listed.

**Table 5.4:** siRNA sequences

abbreviation	name	sequence	provider
TMEM106B pool	SMART pool siGENOME TMEM106B siRNA D-020307-01	TM2, TM3, TM4 + TM17	GE Healthcare Dharmacon RNAi & Gene Expression
TMEM106B #2 (#2)	individual siGENOME TMEM106B siRNA D-020307-02	GGA AUG GAC UGG UUA AUA G	GE Healthcare Dharmacon RNAi & Gene Expression
TMEM106B #3 (#3)	individual siGENOME TMEM106B siRNA D-020307-03	GAU CAG AGA UUA AGG CCA A	GE Healthcare Dharmacon RNAi & Gene Expression
TMEM106B #4 (#4)	individual siGENOME TMEM106B siRNA D-020307-04	GCU CUA UCG ACG UGA AAU A	GE Healthcare Dharmacon RNAi & Gene Expression
TMEM106B #17 (#17)	individual siGENOME TMEM106B siRNA D-020307-17	GUA GCU GGG UUG AGA UUA A	GE Healthcare Dharmacon RNAi & Gene Expression
Neg1 (control for pool)	siGENOME Non-Targeting siRNA Pool #1 D-001206-13-05	not given	GE Healthcare Dharmacon RNAi & Gene Expression

**Table 5.4:** siRNA sequences

abbreviation	name	sequence	provider
Neg4 (control for single siRNAs)	siGENOME Non-Targeting siRNA #4 D-001210-04	not given	GE Healthcare Dharmacon RNAi & Gene Expression

### 5.1.5 Drugs and fluorescent dyes

In table 5.5, all drugs used in this study are listed giving the used concentration, treatment duration, provider and a brief description of the target or function.

**Table 5.5:** Drug treatment

drug	concentration	time	provider	description
actinomycin D	20 µg/ml	16 h	Sigma-Aldrich	transcription inhibitor
cycloheximide	20 µg/ml	16 h	Sigma-Aldrich	translation inhibitor
leupeptin hemisulfate	10 µM	16 h	Merck Millipore	serine/cystein protease inhibitor
E-64	10 µM	16 h	Biomol	cystein protease inhibitor
antipain hydrochloride	5 µM	16 h	Calbiochem	serine/cystein protease inhibitor
epoxomicin	1 µM	16 h	Sigma-Aldrich	proteasome inhibitor
bafilomycin A1 (BafA1)	30 nM	6 h to 16 h	Merck Millipore	H <sup>+</sup> -ATPase inhibitor
tunicamycin	10 µg/ml	16 h	Sigma-Aldrich	N-glycosylation inhibitor
nocodazole	0.33 µM, 3.3 µM	16 h	Sigma-Aldrich	microtubule polymerization inhibitor
rapamycin	1 mM	6 h	Life Technologies	autophagy inducer

In table 5.6, all fluorescent dyes used in this study are listed giving the used concentration, treatment duration, provider and a brief description of the target or function.

**Table 5.6:** Dyes

dye	concentration	time	provider	description
LysoTracker Red DND-99	75 nM	30 min	Life Technologies	stains acidic organelles
DQ <sup>TM</sup> Red BSA (DQ-BSA)	100 ng/ml	5 h	Molecular Probes	fluorogenic substrate for proteases
Alexa Fluor® 555 Phalloidin	1:200	30 min	Life Technologies	stains F-actin
4',6-diamidino-2-phenylindole (DAPI)	1:5,000	15 min	Vector Laboratories	stains DNA

### 5.1.6 Cell lines

In this study, the cell lines depicted in table 5.7 were used and cultured as described in section 5.2.2.1.

**Table 5.7:** Cell lines

name	description	resistance	culture medium
HEK293T	human embryonic kidney (HEK) cells (DSMZ # ACC 305)	non	DMEM high glucose + GlutaMAX (Life Technologies), penicillin/streptomycin (P/S) (50 U/ml / 50 µg/ml; PAA laboratories), 10 % fetal calf serum (FCS; Life Technologies)
SH-SY5Y	human neuroblastoma cell line (DSMZ # ACC 209)	non	DMEM F12 (Life Technologies), P/S (50 U/ml / 50 µg/ml), 1 % non-essential amino acids (NEAA), 15 % FCS
T-REx <sup>TM</sup> HEK293	human embryonic kidney cells stably expressing the tetracycline repressor protein (ATCC CRL-1573)	blasticidine	DMEM high glucose + GlutaMAX, P/S (50 U/ml / 50 µg/ml), 10 % FCS, 5 µg/ml blasticidine
HeLa	human cervical carcinoma cells (DSMZ # ACC 57)	non	DMEM high glucose + GlutaMAX, P/S (50 U/ml / 50 µg/ml), 10 % FCS
HeLa Kyoto	human cervical carcinoma cells	non	DMEM high glucose + GlutaMAX, P/S (50 U/ml / 50 µg/ml), 10 % FCS

### 5.1.7 The T-REx<sup>TM</sup> system

The T-REx<sup>TM</sup> system (Life Technologies) is a mammalian expression system regulated by tetracycline. Importantly, it consists of an inducible expression plasmid (for example pcDNA4/TO/myc, figure 5.1) containing two copies of the *tet* operator 2 (TetO<sub>2</sub>) sequence, which is a regulatory element from the *E. coli* TN10-encoded tetracycline (Tet) resistance operon [108, 109].

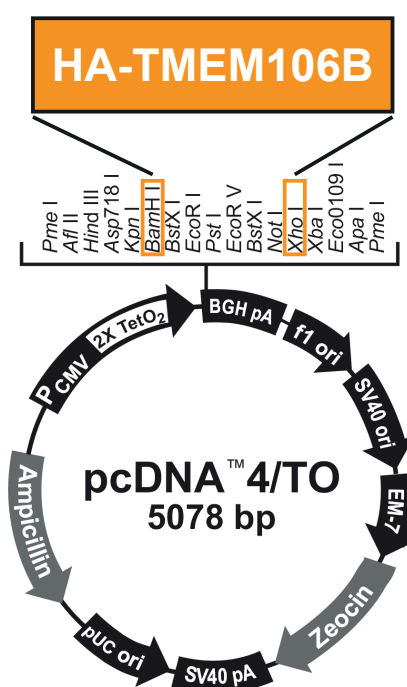


**Figure 5.1: Cloning of pcDNA4-HA-TMEM106B**

The purified HA-TM PCR product as well as the pcDNA4/TO/myc vector were digested with BamHI and XhoI and ligated to create the HA-TM construct that was used for the generation of T-REx<sup>TM</sup> 293 cells stably expressing wt HA-TMEM106B.

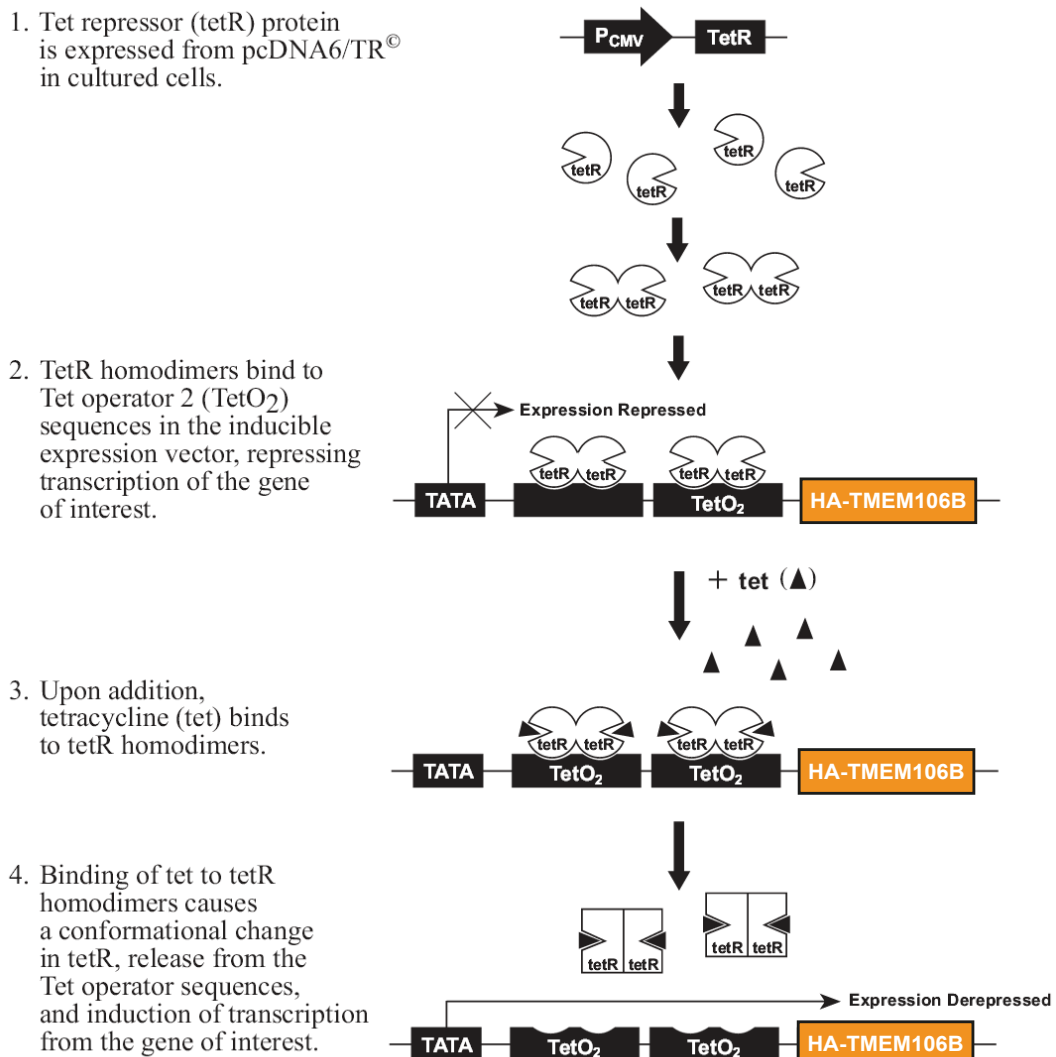


**Figure 5.2: Mechanism of repression in the T-REx™ system**

This scheme was taken and modified from the T-REx™ System User Guide (Revision date: 8th November 2011, Publication Part number 25-0271, Life Technologies). It depicts the mechanism of repression of the T-REx™ system.

Moreover, a second plasmid is needed that contains the pcDNA6/TR regulatory vector which is responsible for the expression of the Tet repressor.

In this study, T-REx<sup>TM</sup> 293 cells were used which stably express the pcDNA6/TR regulatory vector resulting in high expression levels of the *TetR* gene, encoding for the Tet repressor [222]. In the absence of tetracycline, the Tet repressor dimerizes and binds to the TetO<sub>2</sub> sequence in the promoter region of the inducible expression plasmid (pcDNA4/TO/myc HA-TMEM) [108] thereby repressing the transcription of the gene of interest, in this case HA-TMEM106B. However, when tetracycline is added to the cell culture medium, it binds to the Tet repressor dimer leading to a conformational change of the repressor which makes it unable to bind to the Tet operator. Thus, the repressor-tetracycline complex dissociates from the Tet operator allowing for HA-TMEM106B transcription (figure 5.2).

### 5.1.8 Antibodies

All antibodies used for immunofluorescence (IF), western blotting (WB) or immunoprecipitation (IP) are listed in table 5.8 along with their host, provider and dilution used in this study. Furthermore, in table 5.9, the secondary antibodies used in this study are depicted along with the provider and the used dilution.

\*Affiliations: Prof. Dr. Dieter Edbauer, German Center for Neurodegenerative Diseases (DZNE), Ludwig-Maximilians-University Munich, Munich, Germany; Dr. Dorothee Dormann, Institute of Cell Biology, Ludwig-Maximilians-University Munich, Munich, Germany; Dr. Anja Capell, Ludwig-Maximilians-University Munich, Adolf Butenandt Institute, Munich, Germany; Dr. Elisabeth Kremmer, Institute of Molecular Immunology, Helmholtz Center, Munich, Germany.

**Table 5.8:** Antibody list

antibodies	host	provider	dilution
Anti-HA High Affinity (clone 3F10)	rat	Roche Applied Sciences	IF: 1:200
Anti-Grp78/Bip (KDEL)	mouse	StressGen	IF: 1:200
Giantin, mAb (G1/133)	mouse	Enzo Life Sciences, Inc.	IF: 1:600
LAMP1 (clone H4A3)	mouse	Developmental Studies Hybridoma Bank	IF: 1:400
LAMP2 (clone H4B4)	mouse	Developmental Studies Hybridoma Bank	IF: 1:400
LAMP1 (D2D11) XP <sup>®</sup> Rabbit mAb #9091	rabbit	Cell Signaling	IF: 1:400
Anti- $\beta$ -catenin	rabbit	Sigma-Aldrich	IF: 1:400
Anti- $\gamma$ -tubulin Clone GTU-88	rabbit	Sigma-Aldrich	IF: 1:200
Purified Mouse Anti-Tom20	mouse	Santa Cruz	IF: 1:1,000

**Table 5.8:** Antibody list

<b>antibodies</b>	<b>host</b>	<b>provider</b>	<b>dilution</b>
Anti- $\alpha$ -tubulin	mouse	Sigma-Aldrich	IF: 1:500
Calnexin Polyclonal Antibody	rabbit	StressGen	IF: 1:2,000
Golgin-97 (D8P2K) Rabbit mAb	rabbit	Cell Signaling	IF: 1:100
EEA1 (C45B10) Rabbit mAb	rabbit	Cell Signaling	IF: 1:250
Purified Mouse Anti-EEA1 Clone 14/EEA1 (RUO)	mouse	BD Transduction Laboratories <sup>TM</sup>	IF: 1:100
Anti-p62 (SQSTM1) pAb	rabbit	MBL	IF: 1:1,000
Purified Mouse Anti-p62 Ick ligand	mouse	BD Biosciences	IF: 1:100
Monoclonal antibody to LC3 (microtubule-associated protein 1 light chain 3B)	mouse	Nanotools	IF: 1:200
Anti-Ubiquitin, Lys48-Specific, clone Apu2	mouse	Millipore	IF: 1:100
anti-TMEM 344	rabbit	Dieter Edbauer*, Eurogentic [155]	IF: 1:43
Anti-HA-Peroxidase, High Affinity (3F10)	rat	Roche Applied Sciences	WB: 1:1000
PCDGF Polyclonal Antibody, Rabbit (anti-GRN)	rabbit	Life Technologies	WB: 1:700
Monoclonal Anti- $\beta$ -Actin antibody produced in mouse clone AC-74	mouse	Sigma-Aldrich	WB: 1:2,000
cathepsin D (C-20): sc-6486	mouse	Santa Cruz	WB: 1:400
cathepsin B (FL-339): sc-13985	rabbit	Santa Cruz	WB: 1:1,000
LC3	rabbit	Dorothee Dormann* [261]	WB: 1:4,000
14-3-3 $\beta$ (C-20): sc-628	mouse	Santa Cruz	WB: 1:200
6F2 anti-TMEM106B	rat	Anja Capell*, Elisabeth Kremmer* [155]	WB: 1:10 - 1:50
anti-TMEM 345	rabbit	Dieter Edbauer*, Eurogentic [263]	WB: 1 $\mu$ g/ml
LAMP2 (clone H4B4)	mouse	Developmental Studies Hybridoma Bank	WB: 1:2,000
Anti-p62 (SQSTM1) pAb	rabbit	MBL	WB: 1:1,000
Anti-HA antibody	rabbit	Sigma-Aldrich	IP: 1:250

**Table 5.9:** Secondary antibodies

Secondary antibodies	provider	dilution
Alexa 555/488/647-conjugated anti-mouse IgG	Life Technologies	IF: 1:500
Alexa 555/488/647-conjugated anti-rabbit IgG	Life Technologies	IF: 1:500
Alexa 555/488/647-conjugated anti-rat IgG	Life Technologies	IF: 1:500
horse-radish peroxidase (HRP)-conjugated anti-mouse IgG	Promega	WB: 1:10,000
HRP-conjugated anti-rabbit IgG	Promega	WB: 1:10,000
HRP-conjugated anti-rat IgG	Promega	WB: 1:10,000
HRP-conjugated anti-goat IgG	Promega	WB: 1:5,000
HRP-conjugated anti-rat 2c IgG	Elisabeth Kremmer*	WB: 1:1,000

### 5.1.9 Validation of the anti-TMEM106B antibody 6F2

The monoclonal antibody against TMEM106B 6F2 was validated by immunoblot (figure 5.3). Therefore, SH-SY5Y cells were either transfected with the siRNA pool against *TMEM106B* for *TMEM106B* knockdown (KD), control siRNA for endogenous TMEM106B expression (/) or with a HA-tagged wt TMEM106B cDNA construct for TMEM106B overexpression (OE). As the overexpression construct was tagged, the proteins ran a little bit higher than endogenous TMEM106B (figure 5.3). The protein bands marked with an asterisk probably represent aggregated or dimerized TMEM106B (figure 5.3). As these bands do not appear in the knockdown lane, they are TMEM106B-specific.

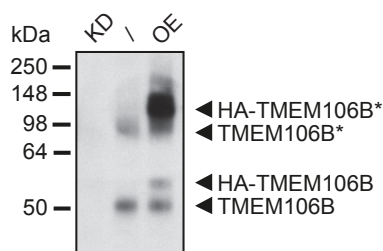


**Figure 5.3: Validation of the anti-TMEM106B antibody 6F2 in SH-SY5Y cells**

SH-SY5Y cells were either not transfected or transfected with a non-targeting control siRNA or with an siRNA pool against TMEM106B on day 0. On day 2 after siRNA transfection, the untransfected cells were transfected with a HA-tagged wt TMEM106B cDNA construct. On day 3, cells were harvested and analysed by SDS-PAGE and subsequent immunoblotting with the anti-TMEM106B antibody 6F2. Probably aggregated or dimerized TMEM106B is marked with an asterisk (\*).

## 5.2 Methods

### 5.2.1 Molecular biology and nucleic acid techniques

#### 5.2.1.1 Polymerase chain reaction (PCR)

PCRs were performed with the aforementioned primers and appropriate cDNA plasmids as templates (see sections 5.1.2, page 115 and 5.1.3, page 116). Thereby, *Pwo* polymerase from *Pyrococcus woesei* was used owing to its proofreading activity. A typical experimental set-up is presented below.

10x reaction buffer for Pwo complete (PeqLab)	5 $\mu$ l
template DNA (10 ng/ $\mu$ l)	1 $\mu$ l
forward primer (10 pmol/ $\mu$ l)	1 $\mu$ l
reverse primer (10 pmol/ $\mu$ l)	1 $\mu$ l
dNTP-Mix (10 mM, Roche Applied Science)	2 $\mu$ l
ddH <sub>2</sub> O	39 $\mu$ l
Pwo polymerase (1 U/ $\mu$ l, peqLab)	1 $\mu$ l
<hr/>	
	50 $\mu$ l

All PCR reactions were prepared on ice and performed in a pre-heated thermocycler using the PCR programme depicted below. Of note, the annealing temperature was adjusted to the melting temperature of the primers starting usually with 5°C below the respective melting temperature.

<b>step</b>	<b>temperature</b>	<b>time</b>	
initial denaturation	95 °C	5 min	
denaturation	95 °C	30 s	] 30 x
annealing	52 °C to 72 °C	30 s	
elongation	72 °C	250 bp/min	
final extension	72 °C	7 min	
storage	4 °C	hold	

---

#### 5.2.1.2 Site-directed mutagenesis

To introduce point mutations into a plasmid, the QuikChange<sup>®</sup> Site-Directed Mutagenesis Kit (Stratagene) was used according to the manufacturer's instructions. Briefly, primers were de-

signed that contained the desired mutation according to the guidelines listed in the kit's manual. Then, a PCR was performed using the following set-up:

10x reaction buffer for <i>Pfu Turbo</i>	5 $\mu$ l
template DNA (10 ng/ $\mu$ l)	1.3 $\mu$ l
forward primer (125 ng)	1.3 $\mu$ l
reverse primer (125 ng)	1.3 $\mu$ l
dNTP-Mix (10 mM, Roche Applied Science)	2 $\mu$ l
ddH <sub>2</sub> O	38.1 $\mu$ l
<i>Pfu Turbo</i> polymerase (1 U/ $\mu$ l)	1 $\mu$ l
	50 $\mu$ l

All PCR reactions were prepared on ice and performed in a pre-heated thermocycler using the cycling parameters depicted below.

step	temperature	time	
initial denaturation	95 °C	30 s	
denaturation	95 °C	30 s	} 16 x
annealing	55 °C	1 min	
elongation	68 °C	1 min/kb of plasmid length	
final extension	68 °C	7 min	
storage	4 °C	hold	

Subsequently, 1  $\mu$ l of *DpnI* restriction enzyme was added to the amplification reaction and incubated at 37 °C for 3 h to digest the non-mutated, methylated template DNA. Following digestion, the remaining mutated DNA was transformed into chemically competent DH5 $\alpha$  *E. coli* as described in section 5.2.1.7.

### 5.2.1.3 Restriction digest

Restriction enzymes, the appropriate buffers and additives were purchased from Fermentas, Roche Applied Science or New England Biolabs (NEB) and used according to the manufacturers' instructions. Usually, 1  $\mu$ g of plasmid DNA or 10  $\mu$ l of purified PCR product were used and mixed with 5 U of restriction enzyme(s) together with the appropriate buffer in a final volume of 20  $\mu$ l. For an analytical digest, 5  $\mu$ l of "Miniprep"-DNA were utilized (see section 5.2.1.8.1, page 129). Subsequently, the reaction mix was incubated for 1 h to 3 h at 37 °C. Digested PCR

products were purified by using the NucleoSpin<sup>®</sup> Extract II kit (Macherey-Nagel) according to the manufacturer's instructions whereas digested plasmids were separated on an agarose gel, first (see section 5.2.1.4). Subsequently, digested DNA was subjected to ligation (see section 5.2.1.5).

### 5.2.1.4 Agarose gel electrophoresis and gel extraction of DNA

---

TBE buffer (10x)	0.9 M Tris (pH 8.3), 0.9 M boric acid, 20 mM ethylenediaminetetraacetic acid (EDTA; pH 8.0) in ddH <sub>2</sub> O
DNA loading buffer (10x)	100 mM Tris (pH 9.0), 10 mM EDTA, 50 % (volume/volume; v/v) glycerol, 0.5 % (mass/volume; w/v) Orange G in ddH <sub>2</sub> O (pH 9.0)

---

Agarose gel electrophoresis was used to separate DNA. Thereby, ultrapure agarose (Life Technologies) was dissolved in 1x TBE buffer and 0.3 µg/ml of ethidium bromide were added prior to casting the 1 % to 2 % agarose gel (depending on the DNA size analysed) in order to visualize DNA under UV light. DNA samples were mixed with 6x DNA loading buffer and electrophoresis was performed in 1x TBE buffer at 120 V. A 1 kb-DNA ladder (Life Technologies) served as standard. Subsequently, DNA was visualized under UV light and, if required, cut and extracted from the gel by using the NucleoSpin<sup>®</sup> Extract II kit (Macherey-Nagel) which was done according to the manufacturer's instructions. However, DNA was eluted in ddH<sub>2</sub>O instead of NE buffer.

### 5.2.1.5 Ligation

After purifying the digested DNA, PCR products or DNA fragments were ligated into linearized vectors using the T4 DNA ligase (Thermo Scientific). Typically, a 1:5 ratio between vector and insert DNA was used in a total volume of 30 µl together with 5 U of T4 DNA ligase. As controls, a reaction mix was either prepared without the insert or without both the insert and the ligase. After incubating at room temperature for 2 h or at 4 °C over night (o/n), 20 µl of the ligation mix were used to transform competent *E.coli* (see section 5.2.1.7).

### 5.2.1.6 Preparation of competent bacteria

---

Transformation buffer	50 mM CaCl <sub>2</sub> , 10 mM PIPES (pH 6.6), 15 % (v/v) glycerol in ddH <sub>2</sub> O (sterile-filtered)
LB <sub>0</sub> medium	1 % (w/v) Bacto Tryptone (Becton Dickinson), 0.5 % (w/v) yeast extract (Becton Dickinson), 17.25 mM NaCl in ddH <sub>2</sub> O (pH 7.0), autoclaved at 1.2 bar, 120 °C for 20 min

---

To prepare chemically competent *Escherichia coli* (*E.coli*) DH5α, bacteria of a glycerol stock were plated on agar plates without antibiotics and incubated at 37 °C o/n. The next day, 2 ml of LB<sub>0</sub> medium were inoculated with a fresh *E.coli* clone and incubated o/n at 37 °C. Subsequently,

200 ml of LB<sub>0</sub> medium were inoculated with the pre-culture and grown to an optical density of OD<sub>600</sub> = 0.2. Then, bacteria were put on ice for 10 min before being centrifuged at 800 g and 4 °C for 10 min. The cell pellet was resuspended in ice-cold transformation buffer and incubated on ice for 20 min. Again, cells were centrifuged at 800 g and 4 °C for 10 min before being resuspended in 10 ml ice-cold transformation buffer. Subsequently, aliquots of 100 µl and 300 µl were frozen in liquid nitrogen before being stored at −80 °C.

### 5.2.1.7 Transformation of bacteria

LB <sub>0</sub> medium	1 % (w/v) Bacto Tryptone (Becton Dickinson), 0.5 % (w/v) yeast extract (Becton Dickinson), 17.25 mM NaCl in ddH <sub>2</sub> O (pH 7.0), autoclaved at 1.2 bar, 120 °C for 20 min
LB agar plates	LB medium supplemented with 15 % agar (15 g/l, Becton Dickinson), autoclaved at 1.2 bar, 120 °C for 20 min. If needed, either kanamycin or ampicillin were added after cooling.
kanamycin	A stock solution of 50 mg/ml was prepared in ddH <sub>2</sub> O (sterile-filtered; 0.2 µm). For the working concentration, the stock was diluted 1:1,000.
ampicillin	A stock solution of 100 mg/ml was prepared in ddH <sub>2</sub> O (sterile-filtered; 0.2 µm). For the working concentration, the stock was diluted 1:1,000.

To transform bacteria, a 100 µl-aliquot of competent *E.coli* (see section 5.2.1.6) was thawed on ice before adding 20 µl of ligation mix or 0.5 µg of plasmid DNA (re-trafo). The suspension was incubated on ice for 30 min. Then, heat-shock was applied for 2 min at 42 °C followed by a 2 min-incubation step on ice. Afterwards, 1 ml of room temperature-LB<sub>0</sub> medium was added to the bacteria. The suspension was subsequently incubated for 1 h at 37 °C with agitation. The bacteria were pelleted by very short centrifugation (15 s) and resuspended in 50 µl of LB<sub>0</sub> medium before being plated on agar plates containing the appropriate selection antibiotic (typically ampicillin (Roth) or kanamycin (Roth)). The plates were incubated at 37 °C until single colonies appeared, usually o/n.

Clones were selected and amplified by inoculating 6 ml of LB medium containing the appropriate selection antibiotic with single colonies picked from the agar plate. Positive clones were identified by analytical digest (see section 5.2.1.3) and sequencing (see section 5.2.1.9).

### 5.2.1.8 Plasmid DNA preparation

#### 5.2.1.8.1 Small scale, analytical plasmid preparation ("*Miniprep*")

To analyse whether cloning had been successful, small amounts of plasmid DNA were purified out of 5 ml of 6 ml of pre-culture (LB medium that was inoculated with the respective bacterial colony (see section 5.2.1.7)). The remaining 1 ml of pre-culture was used for large scale plasmid preparation after the clone proved to be correct (see below). For small scale plasmid preparation, the NucleoSpin<sup>®</sup> Plasmid kit (Macherey-Nagel) was used according to the manufacturer's

instructions. Plasmid DNA was eluted in ddH<sub>2</sub>O instead of AE buffer to allow sequencing (see section 5.2.1.9).

### **5.2.1.8.2 Large scale, preparative plasmid preparation ("Midiprep" or "Maxiprep")**

For subsequent cloning or transfection into cell lines, sufficient amounts of plasmid DNA were needed and obtained by large scale, preparative plasmid preparation. Thereby, 200 ml of LB medium containing the appropriate selection antibiotic were inoculated with 1 ml of pre-culture left from small scale plasmid preparation (see above). Alternatively, 200 ml of LB medium containing the appropriate selection antibiotic were directly inoculated with a clone picked from a selection plate (usually done when a plasmid was re-transformed). After incubating the inoculated LB medium at 37 °C o/n (with agitation), bacteria were harvested by centrifugation and plasmid DNA extracted by using the NucleoBond<sup>®</sup> Xtra Midi/Maxi plasmid DNA purification kit (Macherey-Nagel) according to the manufacturer's instructions. DNA was eluted in ddH<sub>2</sub>O and diluted to a final concentration of about 1 µg/µl. Thereby, DNA concentration and purity were determined by photometric measurement using a NanoDrop photospectrometer (PeqLab). Thereby, the absorption at 260 nm (DNA concentration) and the adsorption at 280 nm (contamination with protein) of the DNA solution were determined. The ratio of A<sub>260</sub>/A<sub>280</sub> should at least be 1.8.

### **5.2.1.9 Sequencing of DNA**

DNA sequencing was performed by the GATC Biotech AG using Sanger sequencing on a Sanger ABI 3730xl DNA analyzer (Applied Biosystems). Sequencing data was analysed and processed with the CLC Main Workbench 6.6 software (CLC bio).

### **5.2.1.10 Isolation of cellular RNA**

Isolation of cellular RNA was performed with the RNeasy Mini Kit (Qiagen) according to the manufacturer's instructions. Briefly, cells were harvested and pelleted as described in section 5.2.3.1. Subsequently, the cells were resuspended in RTL lysis buffer (provided by the kit) before being homogenized by using the QIAshredder kit (Qiagen) according to the manufacturer's instructions. To avoid DNA contamination, samples were treated with the enzyme DNase I (RNase-Free DNase Set, Qiagen) according to the manufacturer's instructions. RNA was eluted in RNase-free water (provided by the kit) and either put on ice until further processing or stored at -80 °C. RNA concentration and purity were determined by photometric measurement using a NanoDrop photospectrometer (PeqLab). Thereby, the absorption at 260 nm (RNA concentration) and the adsorption at 280 nm (contamination with protein) of the RNA solution were determined. A ratio of A<sub>260</sub>/A<sub>280</sub> ~ 2.0 was usually accepted for pure RNA.

### 5.2.1.11 Reverse transcription of RNA

Transcription of RNA into cDNA was performed using M-MLV reverse transcriptase (Promega) together with the appropriate buffers according to the manufacturer's instructions. Thereby, 2 µg of RNA were transcribed into cDNA by the use of oligo dTs, dNTPs and M-MLV reverse transcriptase. The resulting cDNA was analysed by real-time PCR.

### 5.2.1.12 Real-time PCR

To determine mRNA expression levels, real-time PCR was performed using TaqMan technology. Thereby, 1 µl of TaqMan primers (see TaqMan primer list, table 5.2) was mixed with 10 µl of TaqMan Universal PCR Master mix (2x, ROX, Applied Biosystems) and pipetted into fast optical 96-well reaction plates (Applied Biosystems). Subsequently, 0.1 µg/µl of sample cDNA were mixed with 8 µl of ddH<sub>2</sub>O and added to the TaqMan primer mix. For analysis, the 96-well plate was sealed with adhesive foil, briefly centrifuged and put into the 7500 Fast Real-Time PCR system (Applied Biosystems) for measuring. Usually, samples were measured in triplicates and normalized to GAPDH cDNA levels according to the  $\Delta\Delta C_t$  method using the following equation:  $2^{-(Ct_{TMEM106B}-Ct_{GAPDH})_{treatment} - (Ct_{TMEM106B}-Ct_{GAPDH})_{control}}$ .

## 5.2.2 Cell culture methods

### 5.2.2.1 Cultivation of continuous cell lines

Phosphate-buffered saline (PBS)	140 mM NaCl, 10 mM Na <sub>2</sub> HPO <sub>4</sub> , 1.75 mM KH <sub>2</sub> PO <sub>4</sub> , 2.7 mM KCl in ddH <sub>2</sub> O (pH 7.4), autoclaved at 1.2 bar, 120 °C for 20 min
Trypsin-EDTA solution (Life Technologies)	0.05 % (w/v) trypsin, 0.53 mM EDTA-4NA, 0.025 mM phenol-red
Penicillin/streptomycin (PAA laboratories)	5000 units/ml penicillin, 5 mg/ml streptomycin
Zeocin <sup>TM</sup> selection reagent (Life Technologies)	200 ng/µl to 400 ng/µl working concentration
Geneticin <sup>TM</sup> selective antibiotic (G418 sulfate, Life Technologies)	200 ng/µl to 500 ng/µl working concentration
Blasticidine	5 µg/ml working concentration

Human cervical carcinoma (HeLa and HeLa Kyoto) cells and human embryonic kidney (HEK 293T) cells were cultured in Dulbecco's Modified Eagle Medium (DMEM) with Glutamax I (Life Technologies) supplemented with 10 % (v/v) fetal calf serum (FCS, Life Technologies) and 1% (v/v) P/S (PAA laboratories). Human neuroblastoma SH-SY5Y cells were cultured in Dulbecco's Modified Eagle Medium: Nutrient Mixture F-12 (DMEM/F12) (Life Technologies) supplemented with 15 % (v/v) FCS (Life Technologies), 1 % (v/v) non-essential amino acids (NEAA; Life Technologies) and 1% (v/v) P/S (PAA laboratories). All cell lines were cultured in a standard incubator which was set to 37 °C, 5 % CO<sub>2</sub> and 95 % relative humidity. For

passaging, cells were washed with autoclaved PBS once and were incubated in trypsin solution until the cell layer detached from the culture dish. Subsequently, cells were suspended in culture medium and transferred in a dilution of 1:3 to 1:20 to new cell culture dishes containing the appropriate culture medium.

### 5.2.2.2 Preparation of stable cell lines

A stable cell line for TMEM106B overexpression was obtained through transfection of the pcDNA4/TO-HA-TMEM106B wt construct (N-terminally tagged) into a T-REx<sup>TM</sup>-293 cell line (Life Technologies). A stable cell line was obtained by selection in DMEM with Glutamax I supplemented with 10 % (v/v) FCS, 1% (v/v) P/S and 400 ng/ $\mu$ l of Zeocin<sup>TM</sup> (Life Technologies) and single cell clones were picked. After selection, the Zeocin concentration was reduced to 200 ng/ $\mu$ l. To induce TMEM106B expression, stable cell clones were treated with 0.2 ng/ $\mu$ l tetracycline (Sigma-Aldrich) for 12 h to 24 h (see also supplement 5.1.7).

Stable cell lines for LAMP1 overexpression were gained by transient transfection of the plasmid 34831: LAMP1-mGFP (Addgene) into a HeLa Kyoto cell line. Cells were selected as described above, but with 300 ng/ $\mu$ l to 500 ng/ $\mu$ l G418 as selection antibiotic, and single cell clones picked.

### 5.2.2.3 Cryopreservation of cell lines

---

Freezing medium	Fetal calf serum (Life Technologies) supplemented with 10 % (v/v) DMSO
-----------------	--

---

For cryopreservation, cells grown to a confluency of about 80 % to 90 % in a 10 cm dish were trypsinised (trypsin-EDTA; Life Technologies) and pelleted by centrifugation (5 min, 1000 g at RT). Subsequently, cells were resuspended in 0.5 ml freezing medium and transferred into a micro cryotube (Sarstedt). Cells were frozen at  $-80^{\circ}\text{C}$  using an isopropanol cryo  $1^{\circ}\text{C}$  freezing container (Nalgene).

For thawing, cells in a micro cryotube were shortly placed into a  $37^{\circ}\text{C}$  water bath and immediately afterwards diluted in 10 ml of culture medium. After six to eight hours, the medium was replaced.

### 5.2.2.4 Transfection of cells via lipofection

Transient transfection of cells was carried out using either Lipofectamine<sup>TM</sup> 2000 (Life Technologies), Fugene<sup>®</sup>HD (Roche Applied Science) transfection reagent or X-tremeGENE 9 DNA (Roche Applied Science) transfection reagent according to the manufacturers' protocols. Briefly, cells were plated and transfected at 60 % to 80 % confluency. Thereby, DNA and transfection reagent were prepared in OptiMEM (Life Technologies), incubated for 20 min and added to the cells. After six to 16 h, medium was replaced by fresh medium and cells were incubated for at

least 24 h in total before being harvested. Usually, Fugene<sup>®</sup>HD or X-tremeGENE 9 DNA transfection reagent were used for HeLa cells whereas Lipofectamine<sup>™</sup> 2000 was used for SH-SY5Y cells and HEK293T cells.

For RNA interference experiments, 10 nM siRNA were mixed with Lipofectamin<sup>®</sup> RNAiMAX reagent (Life Technologies) in OptiMEM (Life Technologies) according to the manufacturer's instructions. After 15 min, cells were reversely transfected and subsequently incubated for 72 h before analysis (if not stated differently in the text). After 24 h of siRNA treatment, new medium was added to the cell culture dishes to dilute the transfection reagent and after 48 h, the medium was replaced by new culture medium, respectively.

To rescue the TMEM106B knockdown phenotype, a TM3 siRNA-resistant HA-TMEM106B construct or the empty vector were additionally transfected after 48 h of siRNA transfection, using X-tremeGENE 9 DNA reagent (Roche Applied Science).

### 5.2.2.5 Drug treatment

The drugs used in this study are listed in section 5.1.5, table 5.5. To inhibit transcription, cells were treated with 1  $\mu$ M actinomycin D whereas translation was inhibited by 20  $\mu$ g/ml cycloheximide. Lysosomal degradation was inhibited by 10  $\mu$ M leupeptin or a mixture of 10  $\mu$ M leupeptin, 10  $\mu$ M E-64 and 5  $\mu$ M antipain. Proteasomal degradation was blocked by 1  $\mu$ M epoxomicin (Sigma-Aldrich). All treatments mentioned above were carried out for 16 h at 37 °C. H<sup>+</sup>-ATPase and thus lysosomal acidification was inhibited by treating the cells for 6 h to 16 h with 30 nM bafilomycin A1 (BafA1) (Merck Millipore) at 37 °C. For inhibiting microtubule polymerization, cell were treated with 0.33  $\mu$ M and 3.3  $\mu$ M for 16 h, respectively.

## 5.2.3 Protein biochemistry

### 5.2.3.1 Collection of media and cell harvest

---

PBS	140 mM NaCl, 10 mM Na <sub>2</sub> HPO <sub>4</sub> , 1.75 mM KH <sub>2</sub> PO <sub>4</sub> , 2.7 mM KCl in ddH <sub>2</sub> O (pH 7.4)
-----	---

---

For analysing the cell media, cells were incubated in OptiMEM (Life Technologies) 16 h prior to cell harvest. Then, cells were put on ice and the supernatant was collected in an Eppendorf tube. Cellular debris was removed by centrifugation at 10,000 g for 10 min at 4 °C. If not analysed directly, the supernatant was stored at -20 °C. To harvest the cells, the cell monolayer was washed three times with PBS and scraped in 1 ml PBS. The cell suspension was transferred to an Eppendorf tube and cells were pelleted by centrifugation (5 min, 1.000 g, 4 °C), respectively. The cells were either stored at -80 °C or lysed directly afterwards.

### 5.2.3.2 Preparation of total cell lysates

---

**Phosphatase and protease inhibitors**

Na <sub>3</sub> VO <sub>4</sub>	A stock solution of 100 mM Na <sub>3</sub> VO <sub>4</sub> was prepared in ddH <sub>2</sub> O. For the working concentration, the stock solution was diluted 1:50.
NaF	A stock solution of 1 M NaF was prepared in ddH <sub>2</sub> O. For the working concentration, the stock solution was diluted 1:1,000.
protease inhibitor cocktail (Roche Applied Sciences)	The stock solution was diluted 1:500.

**Lysis buffers**

RIPA	150 mM NaCl, 10 mM Tris (pH 7.2), 0.1 % (w/v) SDS, 1 % (v/v) TritonX 100, 1 % (w/v) deoxycholate, 5 mM EDTA in dH <sub>2</sub> O
STEN	50 mM Tris (pH 7.6), 150 mM NaCl, 2 mM EDTA (pH 8.0), 1 % (v/v) NP-40 in dH <sub>2</sub> O

---

Depending on the size of the cell pellet, cells were lysed in 50 µl to 500 µl of lysis buffer supplemented with phosphatase and protease inhibitors. After incubating on ice for 30 min, the cell lysate was centrifuged at 10,000 g for 30 min at 4 °C to remove undissolved cell debris and, in the case of STEN lysis, the nuclei. If cells were lysed with RIPA lysis buffer, the cell lysate was additionally sonicated before centrifugation to shear the DNA. Subsequently, cell lysates were analysed on immunoblot or stored at −20 °C.

### 5.2.3.3 Measurement of the protein concentration

The protein concentration of cell lysates was determined by applying the colorimetric bicinchoninic acid (BCA) method (Thermo Scientific, Pierce) according to the manufacturer's instructions. Briefly, the assay was performed in a 96-well plate in a total volume of 200 µl. Usually, 198 µl of the BCA solution were added to 2 µl of the cell lysate. As standard served serial dilutions of bovine serum albumin (BSA, included in the kit). After incubating for 30 min at 37 °C, the samples were analysed by measuring the absorbance at 562 nm using an ELISA reader (PowerWave XS, BioTek).

### 5.2.3.4 Membrane preparation

---

RSB buffer	10 mM Tris (pH 7.6), 1 mM EDTA, 1 mM ethylene glycol tetraacetic acid (EGTA) in dH <sub>2</sub> O
Carbonate buffer	0.1 M Na <sub>2</sub> CO <sub>3</sub> (pH 11.5) in dH <sub>2</sub> O, 10 mM dithiothreitol (DTT) added freshly
Laemmli buffer (4x)	4 g sodium dodecyl sulfate (SDS) ultra pure, 7.5 ml dH <sub>2</sub> O, 12.5 ml Tris (1 M, pH 6.8), 20 ml glycerol, 1 spatula of bromophenol blue
Laemmli buffer (2x)	800 µl Laemmli buffer, 200 µl β-mercaptoethanol (freshly added), 1 ml dH <sub>2</sub> O
Urea Laemmli buffer (2x)	1 ml Laemmli buffer, 1 ml urea solution (8 M)

---

Cells were scraped and pelleted as described above. Then, they were lysed for 30 min on ice in RSB buffer supplemented with protease and phosphatase inhibitors. Subsequently, lysates were

needed (20 times; needle size 0.6 x 30 mm) and centrifuged for 10 min at 4 °C and 1,500 g to separate the cell debris from the nuclear fraction. The resulting supernatant was ultra-centrifuged for 1 h at 4 °C and 100,000 g. The pellet contained all membrane proteins whereas the supernatant comprised all cytosolic proteins. To distinguish between integral membrane proteins and membrane-associated proteins, a carbonate extraction was subsequently performed by incubating the pellet in carbonate buffer supplemented with protease and phosphatase inhibitors on ice for 30 min. Then, the sample was ultra-centrifuged as described above. The resulting pellet contained the integral membrane proteins whereas the supernatant comprised the membrane-associated ones. For immunoblot analysis of TMEM106B, pellets were directly resuspended in 2x urea Laemmli sample buffer and incubated at 65 °C for 15 min before being loaded on a urea gel containing 12 % of acrylamide (see section 5.2.3.7).

### 5.2.3.5 Direct deglycosylation with N-glycosidase F

---

N-glycosidase F buffer	100 mM sodium phosphate (pH 8.0), 25 mM EDTA, 0.1 % (v/v) TritonX 100, 2.5 mM phenylmethylsulfonylfluoride (PMSF)
------------------------	---

---

STEN-lysates were mixed in a ratio of 1:5 with N-glycosidase F buffer. N-glycosidase F (Roche Applied Sciences) was added and the samples incubated o/n at 37 °C on a shaker. The next day, the samples were mixed with urea loading buffer and loaded on urea gels containing 12 % of acrylamide (see section 5.2.3.7).

### 5.2.3.6 Immunoprecipitation and Deglycosylation

---

STEN-NaCl buffer	50 mM Tris (pH 7.6), 500 mM NaCl, 2 mM EDTA (pH 8.0), 0.2 % (v/v) NP-40
STEN-SDS buffer	50 mM Tris (pH 7.6), 150 mM NaCl, 2 mM EDTA (pH 8.0), 0.2 % (v/v) NP-40, 0.1 % (w/v) SDS
STEN wash buffer	50 mM Tris (pH 7.6), 150 mM NaCl, 2 mM EDTA (pH 8.0), 0.2 % (v/v) NP-40
beads elution buffer	100 mM Tris pH (7.4), 1 % (w/v) SDS, 1 % (v/v) $\beta$ -mercaptoethanol
N-glycosidase F buffer	100 mM sodium phosphate (pH 8.0), 25 mM EDTA, 0.1 % (v/v) TritonX 100, 2.5 mM PMSF, 1 % (v/v) $\beta$ -mercaptoethanol, 1 % (w/v) SDS
endoglycosidase H buffer	200 mM sodium citrate (pH 5.8), 2.5 mM PMSF

---

STEN-lysates were pre-cleared for 30 min at 4 °C. Then, Protein A Sepharose 4 Fast Flow beads (GE Healthcare) and 1  $\mu$ l of rabbit polyclonal anti-HA antibody (Sigma-Aldrich) were added to pull down HA-tagged TMEM106B. After 2 h of incubation at 4 °C on a shaker, samples were centrifuged for 5 min at 4 °C and 3,500 g. The supernatant was discarded and the beads were subsequently washed with STEN-NaCl buffer, STEN-SDS buffer and STEN wash buffer. The proteins were separated from the beads by adding the beads elution buffer and incubating the mixture at 65 °C for 5 min. After 2 min of centrifugation at 17,000 g, the supernatant was taken off and mixed with either N-glycosidase F or endoglycosidase H buffer to dilute the SDS concentration to 0.1 %. Then, the enzymes N-glycosidase F (Roche Applied Sciences) or

endoglycosidase H (Roche Applied Sciences) were added and the samples incubated at 37 °C o/n on a shaker. Subsequently, proteins were precipitated with trichloroacetic acid (100 %, w/v). The protein pellet was re-suspended in STEN lysis buffer supplemented with phosphatase and protease inhibitors. Subsequently, samples were subjected to urea SDS-PAGE (see section 5.2.3.7).

### 5.2.3.7 Sodium dodecyl sulfate polyacrylamid gel electrophoresis (SDS-PAGE)

Lower Tris (4x)	1.5 M Tris (pH 8.8), 0.4 % (w/v) SDS in dH <sub>2</sub> O
Upper Tris (4x)	0.5 M Tris (pH 6.8), 0.4 % (w/v) SDS in dH <sub>2</sub> O
Acrylamide	40 % (w/v) acrylamide-BIS-acrylamide 37, 5:1 in dH <sub>2</sub> O
10 % ammoniumpersulfate (APS)	10 % APS (w/v) in dH <sub>2</sub> O
Laemmli buffer (4x)	8 % SDS ultra pure, 0.25 M Tris (pH 6.8), 40 % glycerol, 1 spatula of bromophenol blue in dH <sub>2</sub> O
Laemmli buffer (2x)	800 µl Laemmli buffer (4x), 200 µl β-mercaptoethanol (freshly added), 1 ml dH <sub>2</sub> O
Urea Laemmli buffer (2x)	1 ml Laemmli buffer (4x), 1 ml urea solution (8 M)
Tris-glycine buffer	25 mM Tris, 190 mM glycine, 0.1 % (v/v) SDS in ddH <sub>2</sub> O

Proteins were analysed under denaturing conditions by utilizing SDS-PAGE. Therefore, polyacrylamide gels containing a separating and a stacking gel were cast according to table 5.21.

**Table 5.21:** Protocol for one thick (1.5 mm) SDS gel

step	8 % gel	10 % gel	12 % gel	15 % gel	stacking gel
H <sub>2</sub> O [ml]	4.4	4.0	3.6	3.0	3.3
40 % Acrylamid [ml]	1.6	2.0	2.4	3.0	0.5
Lower Tris [ml]	2.0	2.0	2.0	2.0	1.25 (Upper Tris!)
TEMED [µl]	15	15	15	15	15
10 % APS [µl]	15	15	15	15	15

To analyse TMEM106B, in the stacking and separation gel, water was substituted by an 8 M urea solution to reach a final urea concentration of at least 4 M in the gels. To prepare the samples for loading on SDS gels, cell lysates were mixed with 2x Laemmli buffer and boiled at 95 °C for 5 min. Samples (not frozen before) for TMEM106B analysis were mixed with 2x urea Laemmli buffer and either heated to 65 °C for 15 min or incubated at room temperature for 30 min. To analyse LC3, (fresh) cell lysates were put into the 65 °C-heating block before directly adding 2x Laemmli buffer without β-mercaptoethanol and incubating the samples for 10 min. After short centrifugation, equal amounts of protein were loaded on the gel together with 6 µl of the SeeBlue Plus2 Prestained Molecular Weight Standard (Life Technologies) which served as molecular weight standard. Electrophoresis was performed in a Tris-glycine buffer system using the Mini-PROTEAN system (BIORAD). Gels were run at 120 V for 90 min to 120 min depending on the acrylamid concentration of the gel.

### 5.2.3.8 Western blotting and immunodetection

---

Transfer buffer (1x)	25 mM Tris, 0.2 M glycine in dH <sub>2</sub> O
TBS-T buffer	0.3 M NaCl, 10 mM Tris-HCl (pH 7.6), 0.3 % (v/v) TritonX 100 in dH <sub>2</sub> O
I-Block solution	0.2 % (w/v) Tropix I-Block (Applied Biosystems), 0.1 % (v/v) Tween 20 in PBS

---

After SDS-PAGE, proteins were transferred onto polyvinylidene fluoride (PVDF) membranes (0.45 µm; Immobilon-P Transfer Membrane, Merck Millipore) using the Mini Trans-Blot cell system (BIORAD). Thereby, membranes were activated in isopropanol followed by three washes in dH<sub>2</sub>O and a 10 min-incubation step in transfer buffer to equilibrate the membrane. WB was performed in transfer buffer for 1 h at a constant current of 400 mA. Subsequently, membranes were incubated in I-Block solution for 1 h at room temperature. After blocking, membranes were incubated in primary antibodies diluted in I-Block solution at 4 °C o/n or alternatively, at room temperature for 2 h (with agitation). Then, membranes were washed with TBS-T several times in a time frame of 1 h before they were incubated in HRP-coupled secondary antibodies diluted in I-Block solution for 1 h (with agitation). Again, membranes were washed with TBS-T for 1 h before proteins were detected using enhanced chemiluminescence (ECL). Thereby, membranes were incubated in 2 ml of HRP substrate (ECL, GE Healthchare or ECL Plus, Thermo Scientific) at room temperature for 1 min to 5 min before being developed by using X-ray films (Super RX Medical X-Ray, Fujifilm Life Science) and an automated film developer (CAWOMAT 2000 IR, CAWO).

To quantify protein levels, WB signals were detected by the Luminescent Image Analyzer LAS-4000 (Fujifilm Life Science) and subsequently analysed by using the Multi Gauge software version 3.0 (Fujifilm Life Science).

### 5.2.3.9 Cathepsin D activity assay

To measure the cathepsin D activity, the Cathepsin D Activity Assay Kit (Abnova) was used according to the manufacturer's instructions. Briefly, HeLa cells grown in 6-well plates were lysed in 200 µl of cathepsin D lysis buffer, incubated on ice for 20 min and centrifuged at 16,000 g for 15 min at 4 °C. The supernatant was adjusted to 1 µg of protein in 50 µl of lysis buffer. Subsequently, 50 µl of reaction buffer together with 2 µl of substrate were added. Immediately afterwards, the samples were measured every ten minutes over a period of 110 min while at 37 °C in a fluorometer. As controls of specificity served a sample that only contained the cathepsin D substrate in the appropriate buffer and a sample that had been treated with 5 µM cathepsin D inhibitor pepstatin (Calbiochem).

### 5.2.3.10 Enzyme-linked immunosorbent assay (ELISA) for human GRN

Secreted GRN in conditioned media was quantified in a sandwich ELISA as described in Capell *et al.* [37].

## 5.2.4 Microscopy

### 5.2.4.1 Immunofluorescence

---

Poly-L-lysine	1% (v/v) poly-L-lysine hydrobromide (Sigma-Aldrich) in dH <sub>2</sub> O
Paraformaldehyde (PFA)	4 % PFA (w/v) and 4 % (w/v) sucrose in PBS
NH <sub>4</sub> Cl solution	0.2 % (v/v) Triton X 100, 50 mM NH <sub>4</sub> Cl in PBS
blocking buffer	5 % (w/v) bovine serum albumin (BSA) in PBS
10 % (w/v) saponin	2 g saponin in 20 ml sterile dH <sub>2</sub> O
PBS-S	0.01 % (w/v) saponin in PBS

---

Transfected HeLa, transfected SH-SY5Y or transfected HEK293T cells, T-REx<sup>TM</sup>-293 cells stably expressing HA-TMEM106B or HeLa Kyoto cells stably expressing LAMP1-GFP were grown on glass cover slips. In the case of HEK cells, the cover slips were additionally coated with poly-L-lysine for better attachment. Usually, 24 h after transient plasmid transfection or induction of HA-TMEM106B expression or 72 h after siRNA transfection, cells were washed in PBS and either fixed with ice-cold methanol for 5 min at  $-20^{\circ}\text{C}$  or with PFA for 20 min with subsequent permeabilization with 0.2 % (v/v) Triton X 100 for 10 min at  $25^{\circ}\text{C}$ . Then, cells were blocked in blocking buffer for 30 min followed by an incubation with the indicated first antibodies for 60 min at  $25^{\circ}\text{C}$ . After washing with PBS-S for six times, cells were incubated in Alexa-488- and Alexa-555-coupled secondary anti-mouse, anti-rat or anti-rabbit antibodies (Life Technologies) diluted in blocking buffer for 30 min at room temperature. For F-actin staining, cells were incubated in phalloidin conjugated with a fluorophore diluted in blocking buffer before being washed and nuclei stained with DAPI for 15 min at  $25^{\circ}\text{C}$ . Subsequently, cells were washed in PBS-S six times and in dH<sub>2</sub>O once before the cover slips were mounted on glass slides using ProLong<sup>®</sup>Gold Antifade Reagent (Life Technologies). Images were taken on a Zeiss LSM 510 or 710 laser scanning microscope using the 63x oil objective (Plan Apochromat) with a numerical aperture of 1.4 (differential interference contrast (DIC)). Images were processed with the LSM software v3.5 (Carl Zeiss MicroImaging) or the ZEN software (Carl Zeiss MicroImaging).

### 5.2.4.2 DQ-BSA and lysotracker staining

To analyse whether lysosomal enzymes were proteolytically active, cells were stained with DQ-BSA, a quenched fluorogenic substrate for proteases which only fluoresce when it is hydrolysed [310] (see section 5.1.5, table 5.6). Thereby, HeLa cells seeded on coverslips were incubated in DMEM high glucose and GlutaMAX and 1 % (v/v) P/S, but only 1 % (v/v) FCS for 30 min. Subsequently, 100 ng/ml DQ-BSA were added for 2 h to 6 h according to the manufacturer's instructions. Then, life-cell imaging was performed with the Zeiss LSM 710 laser scanning microscope as described before.

To determine whether lysosomes were acidic upon TMEM106B knockdown, cells were stained with lysotracker (see section 5.1.5, table 5.6) and life-cell imaging was performed. Thereby, HeLa cells stably expressing LAMP1-GFP were used for this experiment and seeded on coverslips.

75 nM lysotracker were added to the cells 30 min prior to life-cell imaging according to the manufacturer's instructions.

### 5.2.5 Quantification of lysosomal clustering

For the quantification of the lysosomal clustering phenotype observed upon TMEM106B knock-down, immunofluorescence experiments were performed in HeLa cells. Thereby, TMEM106B #3 siRNA-treated HeLa cells and mock controls were stained with antibodies against LAMP2 and  $\beta$ -catenin. Nuclei were stained with DAPI. Images were taken on a Zeiss LSM 710 laser scanning confocal microscope by using z-stacks. Subsequently, lysosomal positioning was determined by automated quantitative image analysis measuring the mean distance of the lysosomes to the nucleus, done by Christoph Moehl (Image and Data Analysis Facility, DZNE Bonn). Moreover, lysosomal distribution was illustrated by using the Clark aggregation index (CAI) [44] (see equations 5.1, 5.2 and 5.3):

$$\text{CAI} = \frac{\text{observed mean distance}}{\text{expected mean distance}} \quad (5.1)$$

whereas

$$\text{observed mean distance} = \frac{\sum D(x)}{N(x)} \quad (5.2)$$

and

$$\text{expected mean distance} = \frac{1}{\sqrt{\frac{N(x)}{A}}} \quad (5.3)$$

$D(x)$  is the spatial distance to the next neighbour of pixels belonging to the lysosome region,  $N(x)$  is the number of pixels belonging to the lysosome region and  $A$  is the number of pixels of the cell object (area). In total, 510 control cells and 422 TMEM106B siRNA-treated cells were analysed.

### 5.2.6 Statistics

Statistical analysis was performed using GraphPad Prism 5 (GraphPad Software) or ImageJ [231]. All statistical data are represented as mean  $\pm$  standard deviation (S.D.). If more than two groups were compared, one-way analysis of variance (ANOVA) followed by the Dunnett's test or the Tukey's test was applied. If only two groups were compared, an unpaired student's t-test was used with a significance level  $\alpha$  of 0.05 (p-values: \*:  $p < 0.05$ , \*\*:  $p < 0.01$ , \*\*\*:  $p < 0.001$ , \*\*\*\*:  $p < 0.0001$ ). Usually, data was normalized and set to 1.0 as indicated in the figures. Calculations were performed with Excel 2010 (Microsoft).



## List of abbreviations

A $\beta$	amyloid- $\beta$ peptide
AA	amino acid
AD	Alzheimer's disease
ALS	amyotrophic lateral sclerosis
AMC	arthrogryposis multiplex congenita
ANOVA	analysis of variance
AP-2	adaptor protein 2
APOE	apolipoprotein E
APP	$\beta$ -amyloid precursor protein
APS	ammoniumpersulfate
ATP	adenosine triphosphosphate
AV	autophagic vacuole
BACE	$\beta$ -secretase
BafA1	bafilomycin A1
BCA	bicinchoninic acid
BiP	binding immunoglobulin protein
BSA	bovine serum albumin
bvFTD	behavioural variant frontotemporal dementia
CAI	Clark aggregation index
CBD	corticobasal degeneration
cDNA	complementary DNA
chk-dyn	chicken-dynamitin
CHMP2B	charged multivesicular body protein 2B
CLN3	ceroid-lipofuscinosis, neuronal 3
CMA	chaperone-mediated autophagy
COVERT	class C core vacuole/endosome tethering factor
CQ	chloroquine
DAPI	4',6-diamidino-2-phenylindole
DCTN1	dynactin subunit 1
ddH <sub>2</sub> O	double-distilled water
DENN	differentially expressed in normal and neoplastic cells
dH <sub>2</sub> O	distilled water

DMEM	Dulbecco's Modified Eagle Medium
DNA	deoxyribonucleic acid
dNTPs	deoxynucleotide solution containing dATP, dCTP, dGTP and dTTP
DPR	dipeptide-repeat protein
E.coli	Escherichia coli
ECL	enhanced chemiluminescence
EDTA	ethylenediaminetetraacetic acid
EEA1	early endosome antigen 1
EGTA	ethylene glycol tetraacetic acid
ELISA	enzyme-linked immunosorbent assay
ER	endoplasmic reticulum
ERAD	ER-associated degradation
ESCRT	endosomal sorting complex required for transport
et al.	<i>et alii</i> , latin for "and others"
EWS	Ewing sarcoma breakpoint region 1
FCS	fetal calf serum
FET family	FUS, EWS and TAF15 family
FTD	frontotemporal dementia, the clinical presentation of FTLD
FTLD	frontotemporal lobar degeneration
FUS	Fused in Sarcoma
GBA	glucocerebrosidase
GEF	guanine nucleotide exchange factor
GFP	green fluorescent protein
GRN	progranulin
GTP	guanosine triphosphate
GWAS	genome-wide association study
HA	human influenza haemagglutinin
HD	Huntington's disease
HEK cells	human embryonic kidney cells
HeLa cells	human cervical carcinoma cells
HOPS	homotypic fusion and protein sorting
HRP	horse-radish peroxidase
Hsc70	heat shock cognate protein of 70 kDa
i.e.	<i>id est</i> , latin for "that is"
IBM	inclusion body myopathy
IBMPFD	inclusion body myopathy associated with Paget's disease of the bone
ICD	intracellular domain
IF	immunofluorescence
IP	immunoprecipitation

---

Ist1	increased sodium tolerance protein 1
kDa	kilo dalton
LAMP1	lysosome-associated membrane protein 1
LAMP2	lysosome-associated membrane protein 2
LC3	microtubule-associated protein 1 light chain 3
LIR	LC3-interaction region
LOAD	late-onset AD
LRRK2	leucine-rich repeat kinase 2
LSD	lysosomal storage disorder
lvPPA	logopenic variant PPA
MAPT	microtubule-associated protein tau
miR	microRNA
MPR	mannose 6-phosphate receptor
mRNA	messenger RNA
MTOC	microtubule-organizing center
mTOR	mammalian target of rapamycin
mTORC1	mammalian target of rapamycin complex 1
MVBs	multivesicular bodies
n.s.	not significant
NBR1	neighbour of Brca1 gene
NCL	neuronal ceroid lipofuscinosis
NEAA	non-essential amino acids
NES	nuclear export signal
NFTs	intraneuronal fibrillary tangles
nfvPPA	nonfluent variant PPA
NIH	National Institutes of Health
NII	neuronal intranuclear inclusions
NLS	nuclear localization signal
NTF	N-terminal fragment
o/n	over night
OD <sub>600</sub>	optical density of a sample measured at a wavelength of 600 nm
ORD	Office of Rare Diseases
P/S	penicillin/streptomycin
p62/SQSTM1	sequestosome-1
PAGE	polyacrylamid gel electrophoresis
PB1 domain	Phox and Bem 1p domain
PBS	phosphate-buffered saline
PCR	polymerase chain reaction
PD	Parkinson's disease

---

PDB	.....	Paget's disease of the bone
PE	.....	phospholipid phosphatidylethanolamine
PFA	.....	paraformaldehyde
PI3P	.....	phosphatidylinositol 3-phosphate
PMSF	.....	phenylmethylsulfonylfluoride
PPA	.....	primary progressive aphasia
PVDF	.....	polyvinylidene fluoride
Rab	.....	Ras-related protein
RILP	.....	RAB7-interaction lysosomal protein
RIP	.....	regulated intramembrane proteolysis
RNA	.....	ribonucleic acid
RRM	.....	RNA recognition motif
S.D.	.....	standard deviation
SDS	.....	sodium dodecyl sulfate
SDS-PAGE	.....	sodium dodecyl sulfate polyacrylamid gel electrophoresis
siRNA	.....	small interfering RNA
SLPI	.....	secretory leukocyte protease inhibitor
SNCA	.....	$\alpha$ -synuclein
SNP	.....	single-nucleotide polymorphism
SOD1	.....	superoxide dismutase 1
svPPA	.....	semantic variant PPA
TAF15	.....	TATA-binding protein-associated factor 2N
TARDBP	.....	TAR-DNA binding protein
TBI	.....	traumatic brain injury
TDP-43	.....	TAR-DNA binding protein 43
TEMED	.....	tetramethylethylenediamine
TFEB	.....	transcription factor EB
TMEM106B	.....	transmembrane protein 106B
TNF $\alpha$	.....	tumor necrosis factor $\alpha$
TREM2	.....	triggering receptor expressed on myeloid cells 2
Ub	.....	ubiquitin
UBA domain	.....	Ub-associated domain
UK	.....	United Kingdom
UPS	.....	ubiquitin-proteasome system
UTR	.....	untranslated region
UV	.....	ultraviolet
v/v	.....	volume concentration: volume/volume
VCP	.....	valosin containing protein
VPS	.....	vacuolar protein sorting-associated protein

w/v	.....	mass concentration: mass/volume
WB	.....	western blotting
wt	.....	wild-type
ZnF	.....	zinc finger

**Amino acids**

A	...	Ala	.....	alanine
C	...	Cys	.....	cysteine
D	...	Asp	.....	aspartic acid
E	...	Glu	.....	glutamic acid
F	...	Phe	.....	phenylalanine
G	...	Gly	.....	glycine
H	...	His	.....	histidine
I	....	Ile	.....	isoleucine
K	...	Lys	.....	lysine
L	...	Leu	.....	leucine
M	...	Met	.....	methionine
N	...	Asn	.....	asparagine
P	...	Pro	.....	proline
Q	...	Gln	.....	glutamine
R	...	Arg	.....	arginine
S	...	Ser	.....	serine
T	...	Thr	.....	threonine
V	...	Val	.....	valine
W	..	Trp	.....	tryptophan
Y	...	Tyr	.....	tyrosine

**Nucleobases**

A	...	.....	adenine
G	...	.....	guanine
T	...	.....	thymine
C	...	.....	cytosine
U	...	.....	uracil



# Bibliography

- [1] Adams, H. H., Verhaaren, B. F., Vrooman, H. A., Uitterlinden, A. G., Hofman, A., van Duijn, C. M., van der Lugt, A., Niessen, W. J., Vernooij, M. W., and Ikram, M. A. “TMEM106B Influences Volume of Left-Sided Temporal Lobe and Interhemispheric Structures in the General Population”. *Biological Psychiatry* (2014).
- [2] Alzforum. *MAPT Mutations in Frontotemporal Dementia. Search results of Mutation Database*. URL: [http://www.alzforum.org/mutations/search?genes\[\]=492&diseases\[\]=150&keywords-entry=&keywords=#results](http://www.alzforum.org/mutations/search?genes[]=492&diseases[]=150&keywords-entry=&keywords=#results) (visited on 04/19/2014).
- [3] Armstrong, R. A. and Cairns, N. J. “A morphometric study of the spatial patterns of TDP-43 immunoreactive neuronal inclusions in frontotemporal lobar degeneration (FTLD) with progranulin (GRN) mutation”. *Histology and Histopathology* 26 (2011), pp. 185–190.
- [4] Arrasate, M., Mitra, S., Schweitzer, E. S., Segal, M. R., and Finkbeiner, S. “Inclusion body formation reduces levels of mutant huntingtin and the risk of neuronal death”. *Nature* 431 (2004), pp. 805–810.
- [5] Ash, Peter E A, Bieniek, K. F., Gendron, T. F., Caulfield, T., Lin, W.-L., DeJesus-Hernandez, M., van Blitterswijk, Marka M, Jansen-West, K., Paul, Joseph W 3rd, Rademakers, R., Boylan, K. B., Dickson, D. W., and Petrucelli, L. “Unconventional translation of C9ORF72 GGGGCC expansion generates insoluble polypeptides specific to c9FTD/ALS”. *Neuron* 77 (2013), pp. 639–646.
- [6] Babst, M. and Odorizzi, G. “The balance of protein expression and degradation: an ESCRTs point of view”. *Current Opinion in Cell Biology* 25 (2013), pp. 489–494.
- [7] Bagshaw, R. D., Callahan, J. W., and Mahuran, D. J. “The Arf-family protein, Arl8b, is involved in the spatial distribution of lysosomes”. *Biochemical and Biophysical Research Communications* 344 (2006), pp. 1186–1191.
- [8] Bahr, B. A. and Bendiske, J. “The neuropathogenic contributions of lysosomal dysfunction”. *Journal of Neurochemistry* 83 (2002), pp. 481–489.
- [9] Baker, M., Mackenzie, I. R., Pickering-Brown, S. M., Gass, J., Rademakers, R., Lindholm, C., Snowden, J., Adamson, J., Sadovnick, A. D., Rollinson, S., Cannon, A., Dwosh, E., Neary, D., Melquist, S., Richardson, A., Dickson, D., Berger, Z., Eriksen, J., Robinson, T., Zehr, C., Dickey, C. A., Crook, R., McGowan, E., Mann, D., Boeve, B., Feldman, H., and Hutton, M. “Mutations in progranulin cause tau-negative frontotemporal dementia linked to chromosome 17”. *Nature* 442 (2006), pp. 916–919.
- [10] Ballabio, A. and Gieselmann, V. “Lysosomal disorders: from storage to cellular damage”. *Biochimica et Biophysica Acta* 1793 (2009), pp. 684–696.
- [11] Barger, S. W. “TMEM106B and frontotemporal lobar degeneration: can over-expression tell us how reductions are beneficial?” *Journal of Neurochemistry* 126 (2013), pp. 696–698.
- [12] Barmada, S. J., Serio, A., Arjun, A., Bilican, B., Daub, A., Ando, D. M., Tsvetkov, A., Pleiss, M., Li, X., Peisach, D., Shaw, C., Chandran, S., and Finkbeiner, S. “Autophagy induction enhances TDP43 turnover and survival in neuronal ALS models”. *Nature Chemical Biology* 10 (2014), pp. 677–685.

- [13] Bathgate, D., Snowden, J. S., Varma, A., Blackshaw, A., and Neary, D. "Behaviour in frontotemporal dementia, Alzheimer's disease and vascular dementia". *Acta Neurologica Scandinavica* 103 (2001), pp. 367–378.
- [14] Bause, E. and Legler, G. "The role of the hydroxy amino acid in the triplet sequence Asn-Xaa-Thr(Ser) for the N-glycosylation step during glycoprotein biosynthesis". *The Biochemical Journal* 195 (1981), pp. 639–644.
- [15] Belcastro, V., Siciliano, V., Gregoretto, F., Mithbaokar, P., Dharmalingam, G., Berlingieri, S., Iorio, F., Oliva, G., Polishchuck, R., Brunetti-Pierri, N., and Di Bernardo, D. "Transcriptional gene network inference from a massive dataset elucidates transcriptome organization and gene function". *Nucleic Acids Research* 39 (2011), pp. 8677–8688.
- [16] Bellettato, C. M. and Scarpa, M. "Pathophysiology of neuropathic lysosomal storage disorders". *Journal of Inherited Metabolic Disease* 33 (2010), pp. 347–362.
- [17] Belly, A., Bodon, G., Blot, B., Bouron, A., Sadoul, R., and Goldberg, Y. "CHMP2B mutants linked to frontotemporal dementia impair maturation of dendritic spines". *Journal of Cell Science* 123 (2010), pp. 2943–2954.
- [18] Benes, P., Vetvicka, V., and Fusek, M. "Cathepsin D—many functions of one aspartic protease". *Critical Reviews in Oncology/Hematology* 68 (2008), pp. 12–28.
- [19] Bentmann, E., Haass, C., and Dormann, D. "Stress granules in neurodegeneration—lessons learnt from TAR DNA binding protein of 43 kDa and fused in sarcoma". *FEBS Journal* 280 (2013), pp. 4348–4370.
- [20] Bigio, E. H. "Making the diagnosis of frontotemporal lobar degeneration". *Archives of Pathology & Laboratory Medicine* 137 (2013), pp. 314–325.
- [21] Bit-Ivan, E. N., Suh, E., Shim, H.-S., Weintraub, S., Hyman, B. T., Arnold, S. E., McCarty-Wood, E., Van Deerlin, Viviana M, Schneider, J. A., Trojanowski, J. Q., Frosch, M. P., Baker, M. C., Rademakers, R., Mesulam, M., and Bigio, E. H. "A Novel GRN Mutation (GRN c.708+6\_+9delTGAG) in Frontotemporal Lobar Degeneration With TDP-43-Positive Inclusions: Clinicopathologic Report of 6 Cases". *Journal of Neuropathology and Experimental Neurology* (2014).
- [22] Bjorkoy, G., Lamark, T., Brech, A., Outzen, H., Perander, M., Overvatn, A., Stenmark, H., and Johansen, T. "p62/SQSTM1 forms protein aggregates degraded by autophagy and has a protective effect on huntingtin-induced cell death". *Journal of Cell Biology* 171 (2005), pp. 603–614.
- [23] Bonner, M. F., Ash, S., and Grossman, M. "The new classification of primary progressive aphasia into semantic, logopenic, or nonfluent/agrammatic variants". *Current Neurology and Neuroscience Reports* 10 (2010), pp. 484–490.
- [24] Borroni, B., Ferrari, F., Galimberti, D., Nacmias, B., Barone, C., Bagnoli, S., Fenoglio, C., Piaceri, I., Archetti, S., Bonvicini, C., Gennarelli, M., Turla, M., Scarpini, E., Sorbi, S., and Padovani, A. "Heterozygous TREM2 mutations in frontotemporal dementia". *Neurobiology of Aging* 35 (2014), 934.e7–10.
- [25] Brady, O. A., Zheng, Y., Murphy, K., Huang, M., and Hu, F. "The frontotemporal lobar degeneration risk factor, TMEM106B, regulates lysosomal morphology and function". *Human Molecular Genetics* 22 (2013), pp. 685–695.
- [26] Brady, O. A., Zhou, X., and Hu, F. "Regulated intramembrane proteolysis of the frontotemporal lobar degeneration (FTLD) risk factor, TMEM106B, by Signal Peptide Peptidase-like 2a (SPPL2a)". *Journal of Biological Chemistry* (2014).
- [27] Braulke, T. and Bonifacino, J. S. "Sorting of lysosomal proteins". *Biochimica et Biophysica Acta* 1793 (2009), pp. 605–614.

- 
- [28] Bright, N. A., Gratian, M. J., and Luzio, J. P. “Endocytic delivery to lysosomes mediated by concurrent fusion and kissing events in living cells”. *Current Biology* 15 (2005), pp. 360–365.
- [29] Brown, C. L., Maier, K. C., Stauber, T., Ginkel, L. M., Wordeman, L., Vernos, I., and Schroer, T. A. “Kinesin-2 is a motor for late endosomes and lysosomes”. *Traffic* 6 (2005), pp. 1114–1124.
- [30] Browning, D. *FTD: 'The most common disease no one has ever heard of'*. Ed. by Star Tribune. 2014. URL: <http://www.startribune.com/lifestyle/health/246704241.html> (visited on 04/18/2014).
- [31] Bucci, C., Thomsen, P., Nicoziani, P., McCarthy, J., and van Deurs, B. “Rab7: a key to lysosome biogenesis”. *Molecular Biology of the Cell* 11 (2000), pp. 467–480.
- [32] Bug, M. and Meyer, H. “Expanding into new markets—VCP/p97 in endocytosis and autophagy”. *Journal of Structural Biology* 179 (2012), pp. 78–82.
- [33] Burkhardt, J. K., Echeverri, C. J., Nilsson, T., and Vallee, R. B. “Overexpression of the dynamitin (p50) subunit of the dynactin complex disrupts dynein-dependent maintenance of membrane organelle distribution”. *Journal of Cell Biology* 139 (1997), pp. 469–484.
- [34] Busch, J. I., Martinez-Lage, M., Ashbridge, E., Grossman, M., Van Deerlin, Viviana M, Hu, F., Lee, V. M., Trojanowski, J. Q., and Chen-Plotkin, A. S. “Expression of TMEM106B, the frontotemporal lobar degeneration-associated protein, in normal and diseased human brain”. *Acta Neuropathologica Communications* 1 (2013), p. 36.
- [35] Cady, J., Koval, E. D., Benitez, B. A., Zaidman, C., Jockel-Balsarotti, J., Allred, P., Baloh, R. H., Ravits, J., Simpson, E., Appel, S. H., Pestronk, A., Goate, A. M., Miller, T. M., Cruchaga, C., and Harms, M. B. “TREM2 variant p.R47H as a risk factor for sporadic amyotrophic lateral sclerosis”. *JAMA Neurology* 71 (2014), pp. 449–453.
- [36] Cai, Q., Lu, L., Tian, J.-H., Zhu, Y.-B., Qiao, H., and Sheng, Z.-H. “Snapin-regulated late endosomal transport is critical for efficient autophagy-lysosomal function in neurons”. *Neuron* 68 (2010), pp. 73–86.
- [37] Capell, A., Liebscher, S., Fellerer, K., Brouwers, N., Willem, M., Lammich, S., Gijssels, I., Bittner, T., Carlson, A. M., Sasse, F., Kunze, B., Steinmetz, H., Jansen, R., Dormann, D., Sleegers, K., Cruts, M., Herms, J., van Broeckhoven, C., and Haass, C. “Rescue of progranulin deficiency associated with frontotemporal lobar degeneration by alkalizing reagents and inhibition of vacuolar ATPase”. *Journal of Neuroscience* 31 (2011), pp. 1885–1894.
- [38] Caviston, J. P., Zajac, A. L., Tokito, M., and Holzbaur, Erika L F. “Huntingtin coordinates the dynein-mediated dynamic positioning of endosomes and lysosomes”. *Molecular Biology of the Cell* 22 (2011), pp. 478–492.
- [39] Chen-Plotkin, A. S., Unger, T. L., Gallagher, M. D., Bill, E., Kwong, L. K., Volpicelli-Daley, L., Busch, J. I., Ake, S., Grossman, M., van Deerlin, V., Trojanowski, J. Q., and Lee, V. M.-Y. “TMEM106B, the risk gene for frontotemporal dementia, is regulated by the microRNA-132/212 cluster and affects progranulin pathways”. *Journal of Neuroscience* 32 (2012), pp. 11213–11227.
- [40] Chevalier-Larsen, E. and Holzbaur, Erika L F. “Axonal transport and neurodegenerative disease”. *Biochimica et Biophysica Acta* 1762 (2006), pp. 1094–1108.
- [41] Chondrogianni, N., Voutetakis, K., Kapetanou, M., Delitsikou, V., Papaevgeniou, N., Sakellari, M., Lefaki, M., Filippopoulou, K., and Gonos, E. S. “Proteasome activation: An innovative promising approach for delaying aging and retarding age-related diseases”. *Ageing Research Reviews* (2014).
- [42] Chouery, E., Delague, V., Bergougnoux, A., Koussa, S., Serre, J.-L., and Megarbane, A. “Mutations in TREM2 lead to pure early-onset dementia without bone cysts”. *Human Mutation* 29 (2008), E194–204.
- [43] Clare, R., King, V. G., Wirenfeldt, M., and Vinters, H. V. “Synapse loss in dementias”. *Journal of Neuroscience Research* 88 (2010), pp. 2083–2090.
-

- [44] Clark, P. J. and Evans, F. C. "Distance to nearest neighbor as a measure of spatial relationships in populations." *Ecology* (1954), pp. 445–453.
- [45] Coen, K., Flannagan, R. S., Baron, S., Carraro-Lacroix, L. R., Wang, D., Vermeire, W., Michiels, C., Munck, S., Baert, V., Sugita, S., Wuytack, F., Hiesinger, P. R., Grinstein, S., and Annaert, W. "Lysosomal calcium homeostasis defects, not proton pump defects, cause endo-lysosomal dysfunction in PSEN-deficient cells". *Journal of Cell Biology* 198 (2012), pp. 23–35.
- [46] Colonna, M. "TREM2s in the immune system and beyond". *Nature Reviews Immunology* 3 (2003), pp. 445–453.
- [47] Conus, S., Perozzo, R., Reinheckel, T., Peters, C., Scapozza, L., Yousefi, S., and Simon, H.-U. "Caspase-8 is activated by cathepsin D initiating neutrophil apoptosis during the resolution of inflammation". *Journal of Experimental Medicine* 205 (2008), pp. 685–698.
- [48] Conus, S. and Simon, H.-U. "Cathepsins and their involvement in immune responses". *Swiss Medical Weekly* 140 (2010), w13042.
- [49] Cooper-Knock, J., Shaw, P. J., and Kirby, J. "The widening spectrum of C9ORF72-related disease; genotype/phenotype correlations and potential modifiers of clinical phenotype". *Acta Neuropathologica* 127 (2014), pp. 333–345.
- [50] Corder, E. H., Saunders, A. M., Strittmatter, W. J., Schmechel, D. E., Gaskell, P. C., Small, G. W., Roses, A. D., Haines, J. L., and Pericak-Vance, M. A. "Gene dose of apolipoprotein E type 4 allele and the risk of Alzheimer's disease in late onset families". *Science* 261 (1993), pp. 921–923.
- [51] Cruchaga, C., Graff, C., Chiang, H.-H., Wang, J., Hinrichs, A. L., Spiegel, N., Bertelsen, S., Mayo, K., Norton, J. B., Morris, J. C., and Goate, A. "Association of TMEM106B gene polymorphism with age at onset in granulin mutation carriers and plasma granulin protein levels". *Archives of Neurology* 68 (2011), pp. 581–586.
- [52] Cruts, M., Gijselinck, I., van der Zee, J., Engelborghs, S., Wils, H., Pirici, D., Rademakers, R., Vandenberghe, R., Dermaut, B., Martin, J.-J., van Duijn, C., Peeters, K., Sciot, R., Santens, P., Pooter, T. d., Mattheijssens, M., Van den Broeck, M., Cuijt, I., Vennekens, K., De Deyn, P. P., Kumar-Singh, S., and van Broeckhoven, C. "Null mutations in progranulin cause ubiquitin-positive frontotemporal dementia linked to chromosome 17q21". *Nature* 442 (2006), pp. 920–924.
- [53] Cuervo, A. M., Stefanis, L., Fredenburg, R., Lansbury, P. T., and Sulzer, D. "Impaired degradation of mutant alpha-synuclein by chaperone-mediated autophagy". *Science* 305 (2004), pp. 1292–1295.
- [54] CurePSP-Foundation for PSP, CBD and Related Brain Diseases. *CurePSP*. URL: <http://www.psp.org/> (visited on 04/18/2014).
- [55] Cuyvers, E., Bettens, K., Philtjens, S., van Langenhove, T., Gijselinck, I., van der Zee, J., Engelborghs, S., Vandenbulcke, M., van Dongen, J., Geerts, N., Maes, G., Mattheijssens, M., Peeters, K., Cras, P., Vandenberghe, R., De Deyn, P. P., van Broeckhoven, C., Cruts, M., and Sleegers, K. "Investigating the role of rare heterozygous TREM2 variants in Alzheimer's disease and frontotemporal dementia". *Neurobiology of Aging* 35 (2014), 726.e11–9.
- [56] Daniel, R., He, Z., Carmichael, K. P., Halper, J., and Bateman, A. "Cellular localization of gene expression for progranulin". *Journal of Histochemistry and Cytochemistry* 48 (2000), pp. 999–1009.
- [57] de Duve, C. "Lysosomes revisited". *European Journal of Biochemistry / FEBS* 137 (1983), pp. 391–397.
- [58] Dehay, B., Martinez-Vicente, M., Caldwell, G. A., Caldwell, K. A., Yue, Z., Cookson, M. R., Klein, C., Vila, M., and Bezaud, E. "Lysosomal impairment in Parkinson's disease". *Movement Disorders* 28 (2013), pp. 725–732.

- 
- [59] Dehay, B., Ramirez, A., Martinez-Vicente, M., Perier, C., Canron, M.-H., Doudnikoff, E., Vital, A., Vila, M., Klein, C., and Bezdard, E. "Loss of P-type ATPase ATP13A2/PARK9 function induces general lysosomal deficiency and leads to Parkinson disease neurodegeneration". *Proceedings of the National Academy of Sciences of the United States of America* 109 (2012), pp. 9611–9616.
- [60] Deinhardt, K., Salinas, S., Verastegui, C., Watson, R., Worth, D., Hanrahan, S., Bucci, C., and Schiavo, G. "Rab5 and Rab7 control endocytic sorting along the axonal retrograde transport pathway". *Neuron* 52 (2006), pp. 293–305.
- [61] DeJesus-Hernandez, M., Mackenzie, I. R., Boeve, B. F., Boxer, A. L., Baker, M., Rutherford, N. J., Nicholson, A. M., Finch, N. A., Flynn, H., Adamson, J., Kouri, N., Wojtas, A., Sengdy, P., Hsiung, G.-Y. R., Karydas, A., Seeley, W. W., Josephs, K. A., Coppola, G., Geschwind, D. H., Wszolek, Z. K., Feldman, H., Knopman, D. S., Petersen, R. C., Miller, B. L., Dickson, D. W., Boylan, K. B., Graff-Radford, N. R., and Rademakers, R. "Expanded GGGGCC hexanucleotide repeat in noncoding region of C9ORF72 causes chromosome 9p-linked FTD and ALS". *Neuron* 72 (2011), pp. 245–256.
- [62] Diaz-Hernandez, M., Valera, A. G., Moran, M. A., Gomez-Ramos, P., Alvarez-Castelao, B., Castano, J. G., Hernandez, F., and Lucas, J. J. "Inhibition of 26S proteasome activity by huntingtin filaments but not inclusion bodies isolated from mouse and human brain". *Journal of Neurochemistry* 98 (2006), pp. 1585–1596.
- [63] Dixit, R., Ross, J. L., Goldman, Y. E., and Holzbaur, Erika L F. "Differential regulation of dynein and kinesin motor proteins by tau". *Science* 319 (2008), pp. 1086–1089.
- [64] Dormann, D. and Haass, C. "Fused in sarcoma (FUS): an oncogene goes awry in neurodegeneration". *Molecular and Cellular Neurosciences* 56 (2013), pp. 475–486.
- [65] Ebner, A., Godemann, R., Stamer, K., Illenberger, S., Trinczek, B., and Mandelkow, E. "Overexpression of tau protein inhibits kinesin-dependent trafficking of vesicles, mitochondria, and endoplasmic reticulum: implications for Alzheimer's disease". *Journal of Cell Biology* 143 (1998), pp. 777–794.
- [66] *Ensembl genome browser 75: Homo sapiens - Marked-up sequence - Gene: TMEM106B (ENSG00000106460)*. 15.05.2014. URL: [http://www.ensembl.org/Homo\\_sapiens/Gene/Sequence?db=core;g=ENSG00000106460;r=7:12250867-12282993](http://www.ensembl.org/Homo_sapiens/Gene/Sequence?db=core;g=ENSG00000106460;r=7:12250867-12282993) (visited on 05/15/2014).
- [67] Eskelinen, E.-L. "Roles of LAMP-1 and LAMP-2 in lysosome biogenesis and autophagy". *Molecular Aspects of Medicine* 27 (2006), pp. 495–502.
- [68] Eskelinen, E.-L., Schmidt, C. K., Neu, S., Willenborg, M., Fuentes, G., Salvador, N., Tanaka, Y., Lullmann-Rauch, R., Hartmann, D., Heeren, J., Figura, K. v., Knecht, E., and Saftig, P. "Disturbed cholesterol traffic but normal proteolytic function in LAMP-1/LAMP-2 double-deficient fibroblasts". *Molecular Biology of the Cell* 15 (2004), pp. 3132–3145.
- [69] Fader, C. M. and Colombo, M. I. "Autophagy and multivesicular bodies: two closely related partners". *Cell Death and Differentiation* 16 (2009), pp. 70–78.
- [70] Farg, M. A., Sundaramoorthy, V., Sultana, J. M., Yang, S., Atkinson, Rachel A K, Levina, V., Halloran, M. A., Gleeson, P. A., Blair, I. P., Soo, K. Y., King, A. E., and Atkin, J. D. "C9ORF72, implicated in amyotrophic lateral sclerosis and frontotemporal dementia, regulates endosomal trafficking". *Human Molecular Genetics* 23 (2014), pp. 3579–3595.
- [71] Filimonenko, M., Stuffers, S., Raiborg, C., Yamamoto, A., Malerod, L., Fisher, Elizabeth M C, Isaacs, A., Brech, A., Stenmark, H., and Simonsen, A. "Functional multivesicular bodies are required for autophagic clearance of protein aggregates associated with neurodegenerative disease". *Journal of Cell Biology* 179 (2007), pp. 485–500.
-

- [72] Finch, N., Carrasquillo, M. M., Baker, M., Rutherford, N. J., Coppola, G., DeJesus-Hernandez, M., Crook, R., Hunter, T., Ghidoni, R., Benussi, L., Crook, J., Finger, E., Hantanpaa, K. J., Karydas, A. M., Sengdy, P., Gonzalez, J., Seeley, W. W., Johnson, N., Beach, T. G., Mesulam, M., Forloni, G., Kertesz, A., Knopman, D. S., Uitti, R., White, C L 3rd, Caselli, R., Lippa, C., Bigio, E. H., Wszolek, Z. K., Binetti, G., Mackenzie, I. R., Miller, B. L., Boeve, B. F., Younkin, S. G., Dickson, D. W., Petersen, R. C., Graff-Radford, N. R., Geschwind, D. H., and Rademakers, R. "TMEM106B regulates progranulin levels and the penetrance of FTLD in GRN mutation carriers". *Neurology* 76 (2011), pp. 467–474.
- [73] Fujiwara, T., Morimoto, K., Kakita, A., and Takahashi, H. "Dynein and dynactin components modulate neurodegeneration induced by excitotoxicity". *Journal of Neurochemistry* 122 (2012), pp. 162–174.
- [74] Futerman, A. H. and van Meer, G. "The cell biology of lysosomal storage disorders". *Nature Reviews Molecular Cell Biology* 5 (2004), pp. 554–565.
- [75] Futter, C. E., Pearse, A., Hewlett, L. J., and Hopkins, C. R. "Multivesicular endosomes containing internalized EGF-EGF receptor complexes mature and then fuse directly with lysosomes". *Journal of Cell Biology* 132 (1996), pp. 1011–1023.
- [76] Galimberti, D. and Scarpini, E. "Genetics and biology of Alzheimer's disease and frontotemporal lobar degeneration". *International Journal of Clinical and Experimental Medicine* 3 (2010), pp. 129–143.
- [77] Gallagher, M. D., Suh, E., Grossman, M., Elman, L., McCluskey, L., van Swieten, J. C., Al-Sarraj, S., Neumann, M., Gelpi, E., Ghetti, B., Rohrer, J. D., Halliday, G., van Broeckhoven, C., Seilhean, D., Shaw, P. J., Frosch, M. P., Alafuzoff, I., Antonell, A., Bogdanovic, N., Brooks, W., Cairns, N. J., Cooper-Knock, J., Cotman, C., Cras, P., Cruets, M., De Deyn, P. P., DeCarli, C., Dobson-Stone, C., Engelborghs, S., Fox, N., Galasko, D., Gearing, M., Gijssels, I., Grafman, J., Hartikainen, P., Hatanpaa, K. J., Highley, J. R., Hodges, J., Hulette, C., Ince, P. G., Jin, L.-W., Kirby, J., Kofler, J., Kril, J., Kwok, J. B., Levey, A., Lieberman, A., Llado, A., Martin, J.-J., Masliah, E., McDermott, C. J., McKee, A., McLean, C., Mead, S., Miller, C. A., Miller, J., Munoz, D. G., Murrell, J., Paulson, H., Piguet, O., Rossor, M., Sanchez-Valle, R., Sano, M., Schneider, J., Silbert, L. C., Spina, S., van der Zee, J., van Langenhove, T., Warren, J., Wharton, S. B., White, C. L. 3., Woltjer, R. L., Trojanowski, J. Q., Lee, V. M., van Deerlin, V., and Chen-Plotkin, A. S. "TMEM106B is a genetic modifier of frontotemporal lobar degeneration with C9orf72 hexanucleotide repeat expansions". *Acta Neuropathologica* 127 (2014), pp. 407–418.
- [78] Gao, X., Joselin, A. P., Wang, L., Kar, A., Ray, P., Bateman, A., Goate, A. M., and Wu, J. Y. "Progranulin promotes neurite outgrowth and neuronal differentiation by regulating GSK-3beta". *Protein & Cell* 1 (2010), pp. 552–562.
- [79] Garcia-Arencia, M., Hochfeld, W. E., Toh, Pearl P C, and Rubinsztein, D. C. "Autophagy, a guardian against neurodegeneration". *Seminars in Cell & Developmental Biology* 21 (2010), pp. 691–698.
- [80] Gass, J., Cannon, A., Mackenzie, I. R., Boeve, B., Baker, M., Adamson, J., Crook, R., Melquist, S., Kuntz, K., Petersen, R., Josephs, K., Pickering-Brown, S. M., Graff-Radford, N., Uitti, R., Dickson, D., Wszolek, Z., Gonzalez, J., Beach, T. G., Bigio, E., Johnson, N., Weintraub, S., Mesulam, M., White, C. L. 3., Woodruff, B., Caselli, R., Hsiung, G.-Y., Feldman, H., Knopman, D., Hutton, M., and Rademakers, R. "Mutations in progranulin are a major cause of ubiquitin-positive frontotemporal lobar degeneration". *Human Molecular Genetics* 15 (2006), pp. 2988–3001.
- [81] GeneCards Human Gene Database. *TMEM106A Gene - GeneCards | T106A Protein | T106A Antibody*. 15.05.2014. URL: <http://www.genecards.org/cgi-bin/carddisp.pl?gene=TMEM106A> (visited on 05/15/2014).
- [82] Genini, S., Nguyen, T. T., Malek, M., Talbot, R., Gebert, S., Rohrer, G., Nonneman, D., Stranzinger, G., and Vögeli, P. "Radiation hybrid mapping of 18 positional and physiological candidate genes for arthrogryposis multiplex congenita on porcine chromosome 5". *Animal Genetics* 37 (2006), pp. 239–244.

- 
- [83] Ghazi-Noori, S., Froud, K. E., Mizielinska, S., Powell, C., Smidak, M., Fernandez de Marco, Mar, O'Malley, C., Farmer, M., Parkinson, N., Fisher, Elizabeth M C, Asante, E. A., Brandner, S., Collinge, J., and Isaacs, A. M. "Progressive neuronal inclusion formation and axonal degeneration in CHMP2B mutant transgenic mice". *Brain* 135 (2012), pp. 819–832.
- [84] Gijssels, I., van Langenhove, T., van der Zee, J., Slegers, K., Philtjens, S., Kleinberger, G., Janssens, J., Bettens, K., van Cauwenberghe, C., Pereson, S., Engelborghs, S., Sieben, A., Jonghe, P. d., Vandenberghe, R., Santens, P., Bleecker, J. d., Maes, G., Baumer, V., Dillen, L., Joris, G., Cuijt, I., Corsmit, E., Elinck, E., van Dongen, J., Vermeulen, S., Van den Broeck, M., Vaerenberg, C., Mattheijssens, M., Peeters, K., Robberecht, W., Cras, P., Martin, J.-J., De Deyn, P. P., Cruts, M., and van Broeckhoven, C. "A C9orf72 promoter repeat expansion in a Flanders-Belgian cohort with disorders of the frontotemporal lobar degeneration-amyotrophic lateral sclerosis spectrum: a gene identification study". *Lancet Neurology* 11 (2012), pp. 54–65.
- [85] Giraldo, M., Lopera, F., Siniard, A. L., Corneveaux, J. J., Schrauwen, I., Carvajal, J., Munoz, C., Ramirez-Restrepo, M., Gaiteri, C., Myers, A. J., Caselli, R. J., Kosik, K. S., Reiman, E. M., and Huentelman, M. J. "Variants in triggering receptor expressed on myeloid cells 2 are associated with both behavioral variant frontotemporal lobar degeneration and Alzheimer's disease". *Neurobiology of Aging* 34 (2013), 2077.e11–8.
- [86] Glenner, G. G. and Wong, C. W. "Alzheimer's disease: initial report of the purification and characterization of a novel cerebrovascular amyloid protein. 1984". *Biochemical and Biophysical Research Communications* 425 (2012), pp. 534–539.
- [87] Goetzl, J. K., Mori, K., Damme, M., Fellerer, K., Tahirovic, S., Kleinberger, G., Janssens, J., van der Zee, J., Lang, C. M., Kremmer, E., Martin, J.-J., Engelborghs, S., Kretschmar, H. A., Arzberger, T., van Broeckhoven, C., Haass, C., and Capell, A. "Common pathobiochemical hallmarks of progranulin-associated frontotemporal lobar degeneration and neuronal ceroid lipofuscinosis". *Acta Neuropathologica* (2014).
- [88] Granger, E., McNee, G., Allan, V., and Woodman, P. "The role of the cytoskeleton and molecular motors in endosomal dynamics". *Seminars in Cell & Developmental Biology* 31 (2014), pp. 20–29.
- [89] Gruenberg, J. and Maxfield, F. R. "Membrane transport in the endocytic pathway". *Current Opinion in Cell Biology* 7 (1995), pp. 552–563.
- [90] Grundke-Iqbal, I., Iqbal, K., Tung, Y. C., Quinlan, M., Wisniewski, H. M., and Binder, L. I. "Abnormal phosphorylation of the microtubule-associated protein tau (tau) in Alzheimer cytoskeletal pathology". *Proceedings of the National Academy of Sciences of the United States of America* 83 (1986), pp. 4913–4917.
- [91] Guerreiro, R. J., Lohmann, E., Bras, J. M., Gibbs, J. R., Rohrer, J. D., Guranlian, N., Dursun, B., Bilgic, B., Hanagasi, H., Gurvit, H., Emre, M., Singleton, A., and Hardy, J. "Using exome sequencing to reveal mutations in TREM2 presenting as a frontotemporal dementia-like syndrome without bone involvement". *JAMA Neurology* 70 (2013), pp. 78–84.
- [92] Haass, C., Koo, E. H., Mellon, A., Hung, A. Y., and Selkoe, D. J. "Targeting of cell-surface beta-amyloid precursor protein to lysosomes: alternative processing into amyloid-bearing fragments". *Nature* 357 (1992), pp. 500–503.
- [93] Haass, C. and Selkoe, D. J. "Soluble protein oligomers in neurodegeneration: lessons from the Alzheimer's amyloid beta-peptide". *Nature Reviews Molecular Cell Biology* 8 (2007), pp. 101–112.
-

- [94] Hafezparast, M., Klocke, R., Ruhrberg, C., Marquardt, A., Ahmad-Annur, A., Bowen, S., Lalli, G., Witherden, A. S., Hummerich, H., Nicholson, S., Morgan, P. J., Oozageer, R., Priestley, J. V., Averill, S., King, V. R., Ball, S., Peters, J., Toda, T., Yamamoto, A., Hiraoka, Y., Augustin, M., Korthaus, D., Wattler, S., Wabnitz, P., Dickneite, C., Lampel, S., Boehme, F., Peraus, G., Popp, A., Rudelius, M., Schlegel, J., Fuchs, H., Hrabe de Angelis, M., Schiavo, G., Shima, D. T., Russ, A. P., Stumm, G., Martin, J. E., and Fisher, E. M. "Mutations in dynein link motor neuron degeneration to defects in retrograde transport". *Science* 300 (2003), pp. 808–812.
- [95] Haliloglu, G. and Topaloglu, H. "Arthrogryposis and fetal hypomobility syndrome". *Handbook of Clinical Neurology* 113 (2013), pp. 1311–1319.
- [96] Hallmann, A., Milczarek, R., Lipinski, M., Kossowska, E., Spodnik, J. H., Wozniak, M., Wakabayashi, T., and Klimek, J. "Fast perinuclear clustering of mitochondria in oxidatively stressed human choriocarcinoma cells". *Folia Morphologica* 63 (2004), pp. 407–412.
- [97] Hamasaki, M., Shibutani, S. T., and Yoshimori, T. "Up-to-date membrane biogenesis in the autophagosome formation". *Current Opinion in Cell Biology* 25 (2013), pp. 455–460.
- [98] Hansen, T. E. and Johansen, T. "Following autophagy step by step". *BMC Biology* 9 (2011), p. 39.
- [99] Hara, T., Nakamura, K., Matsui, M., Yamamoto, A., Nakahara, Y., Suzuki-Migishima, R., Yokoyama, M., Mishima, K., Saito, I., Okano, H., and Mizushima, N. "Suppression of basal autophagy in neural cells causes neurodegenerative disease in mice". *Nature* 441 (2006), pp. 885–889.
- [100] Harada, A., Takei, Y., Kanai, Y., Tanaka, Y., Nonaka, S., and Hirokawa, N. "Golgi vesiculation and lysosome dispersion in cells lacking cytoplasmic dynein". *Journal of Cell Biology* 141 (1998), pp. 51–59.
- [101] Hardy, J. "ApoE, amyloid, and Alzheimer's disease". *Science* 263 (1994), pp. 454–455.
- [102] Harris, H. and Rubinsztein, D. C. "Control of autophagy as a therapy for neurodegenerative disease". *Nature Reviews Neurology* 8 (2012), pp. 108–117.
- [103] He, L.-q., Lu, J.-h., and Yue, Z.-y. "Autophagy in ageing and ageing-associated diseases". *Acta Pharmacologica Sinica* 34 (2013), pp. 605–611.
- [104] He, Z. and Bateman, A. "Progranulin gene expression regulates epithelial cell growth and promotes tumor growth in vivo". *Cancer Research* 59 (1999), pp. 3222–3229.
- [105] He, Z. and Bateman, A. "Progranulin (granulin-epithelin precursor, PC-cell-derived growth factor, acrogranin) mediates tissue repair and tumorigenesis". *Journal of Molecular Medicine* 81 (2003), pp. 600–612.
- [106] healthgrades. *Prevalence and Incidence of Frontotemporal dementia*. 2014-03-21. URL: [http://www.rightdiagnosis.com/f/frontotemporal\\_dementia/prevalence.htm](http://www.rightdiagnosis.com/f/frontotemporal_dementia/prevalence.htm) (visited on 04/18/2014).
- [107] Heuser, J. "Changes in lysosome shape and distribution correlated with changes in cytoplasmic pH". *Journal of Cell Biology* 108 (1989), pp. 855–864.
- [108] Hillen, W. and Berens, C. "Mechanisms underlying expression of Tn10 encoded tetracycline resistance". *Annual Review of Microbiology* 48 (1994), pp. 345–369.
- [109] Hillen, W. and Schollmeier, K. "Nucleotide sequence of the Tn10 encoded tetracycline resistance gene". *Nucleic Acids Research* 11 (1983), pp. 525–539.
- [110] Hirokawa, N. "Microtubule organization and dynamics dependent on microtubule-associated proteins". *Current Opinion in Cell Biology* 6 (1994), pp. 74–81.
- [111] Hirokawa, N., Niwa, S., and Tanaka, Y. "Molecular motors in neurons: transport mechanisms and roles in brain function, development, and disease". *Neuron* 68 (2010), pp. 610–638.

- 
- [112] Holzbaur, E. L. “Motor neurons rely on motor proteins”. *Trends in Cell Biology* 14 (2004), pp. 233–240.
- [113] Hsieh, C. L., Koike, M., Spusta, S. C., Niemi, E. C., Yenari, M., Nakamura, M. C., and Seaman, W. E. “A role for TREM2 ligands in the phagocytosis of apoptotic neuronal cells by microglia”. *Journal of Neurochemistry* 109 (2009), pp. 1144–1156.
- [114] Hu, F., Padukkavidana, T., Vaegter, C. B., Brady, O. A., Zheng, Y., Mackenzie, I. R., Feldman, H. H., Nykjaer, A., and Strittmatter, S. M. “Sortilin-mediated endocytosis determines levels of the frontotemporal dementia protein, progranulin”. *Neuron* 68 (2010), pp. 654–667.
- [115] Huotari, J. and Helenius, A. “Endosome maturation”. *The EMBO Journal* 30 (2011), pp. 3481–3500.
- [116] Hutton, M., Lendon, C. L., Rizzu, P., Baker, M., Froelich, S., Houlden, H., Pickering-Brown, S., Chakraverty, S., Isaacs, A., Grover, A., Hackett, J., Adamson, J., Lincoln, S., Dickson, D., Davies, P., Petersen, R. C., Stevens, M., Graaff, E. d., Wauters, E., van Baren, J., Hillebrand, M., Joosse, M., Kwon, J. M., Nowotny, P., Che, L. K., Norton, J., Morris, J. C., Reed, L. A., Trojanowski, J., Basun, H., Lannfelt, L., Neystat, M., Fahn, S., Dark, F., Tannenberg, T., Dodd, P. R., Hayward, N., Kwok, J. B., Schofield, P. R., Andreadis, A., Snowden, J., Craufurd, D., Neary, D., Owen, F., Oostra, B. A., Hardy, J., Goate, A., van Swieten, J., Mann, D., Lynch, T., and Heutink, P. “Association of missense and 5'-splice-site mutations in tau with the inherited dementia FTDP-17”. *Nature* 393 (1998), pp. 702–705.
- [117] Huynh, K. K., Eskelinen, E.-L., Scott, C. C., Malevanets, A., Saftig, P., and Grinstein, S. “LAMP proteins are required for fusion of lysosomes with phagosomes”. *The EMBO Journal* 26 (2007), pp. 313–324.
- [118] Hyttinen, J. M., Niittykoski, M., Salminen, A., and Kaarniranta, K. “Maturation of autophagosomes and endosomes: a key role for Rab7”. *Biochimica et Biophysica Acta* 1833 (2013), pp. 503–510.
- [119] Ikenaka, K., Kawai, K., Katsuno, M., Huang, Z., Jiang, Y.-M., Iguchi, Y., Kobayashi, K., Kimata, T., Waza, M., Tanaka, F., Mori, I., and Sobue, G. “dnc-1/dynactin 1 knockdown disrupts transport of autophagosomes and induces motor neuron degeneration”. *PLoS One* 8 (2013), e54511.
- [120] Isaacs, A. M., Johannsen, P., Holm, I., and Nielsen, J. E. “Frontotemporal dementia caused by CHMP2B mutations”. *Current Alzheimer Research* 8 (2011), pp. 246–251.
- [121] Jacquot, G., Maidou-Peindara, P., and Benichou, S. “Molecular and functional basis for the scaffolding role of the p50/dynamin subunit of the microtubule-associated dynactin complex”. *Journal of Biological Chemistry* 285 (2010), pp. 23019–23031.
- [122] Jiang, P., Nishimura, T., Sakamaki, Y., Itakura, E., Hatta, T., Natsume, T., and Mizushima, N. “The HOPS complex mediates autophagosome-lysosome fusion through interaction with syntaxin 17”. *Molecular Biology of the Cell* 25 (2014), pp. 1327–1337.
- [123] Johansen, T. and Lamark, T. “Selective autophagy mediated by autophagic adapter proteins”. *Autophagy* 7 (2011), pp. 279–296.
- [124] Johansson, A.-C., Appelqvist, H., Nilsson, C., Kagedal, K., Roberg, K., and Ollinger, K. “Regulation of apoptosis-associated lysosomal membrane permeabilization”. *Apoptosis* 15 (2010), pp. 527–540.
- [125] Johnson, J. O., Mandrioli, J., Benatar, M., Abramzon, Y., Van Deerlin, Viviana M, Trojanowski, J. Q., Gibbs, J. R., Brunetti, M., Gronka, S., Wu, J., Ding, J., McCluskey, L., Martinez-Lage, M., Falcone, D., Hernandez, D. G., Arepalli, S., Chong, S., Schymick, J. C., Rothstein, J., Landi, F., Wang, Y.-D., Calvo, A., Mora, G., Sabatelli, M., Monsurro, M. R., Battistini, S., Salvi, F., Spataro, R., Sola, P., Borghero, G., Galassi, G., Scholz, S. W., Taylor, J. P., Restagno, G., Chio, A., and Traynor, B. J. “Exome sequencing reveals VCP mutations as a cause of familial ALS”. *Neuron* 68 (2010), pp. 857–864.
-

- [126] Johnson, J. K., Diehl, J., Mendez, M. F., Neuhaus, J., Shapira, J. S., Forman, M., Chute, D. J., Roberson, E. D., Pace-Savitsky, C., Neumann, M., Chow, T. W., Rosen, H. J., Forstl, H., Kurz, A., and Miller, B. L. “Frontotemporal lobar degeneration: demographic characteristics of 353 patients”. *Archives of Neurology* 62 (2005), pp. 925–930.
- [127] Jones, C. B., Ott, E. M., Keener, J. M., Curtiss, M., Sandrin, V., and Babst, M. “Regulation of membrane protein degradation by starvation-response pathways”. *Traffic* 13 (2012), pp. 468–482.
- [128] Jonsson, T., Stefansson, H., Steinberg, S., Jonsdottir, I., Jonsson, P. V., Snaedal, J., Bjornsson, S., Huttenlocher, J., Levey, A. I., Lah, J. J., Rujescu, D., Hampel, H., Giegling, I., Andreassen, O. A., Engedal, K., Ulstein, I., Djurovic, S., Ibrahim-Verbaas, C., Hofman, A., Ikram, M. A., van Duijn, Cornelia M., Thorsteinsdottir, U., Kong, A., and Stefansson, K. “Variant of TREM2 associated with the risk of Alzheimer’s disease”. *New England Journal of Medicine* 368 (2013), pp. 107–116.
- [129] Jordens, I., Fernandez-Borja, M., Marsman, M., Dusseljee, S., Janssen, L., Calafat, J., Janssen, H., Wubolts, R., and Neefjes, J. “The Rab7 effector protein RILP controls lysosomal transport by inducing the recruitment of dynein-dynactin motors”. *Current Biology* 11 (2001), pp. 1680–1685.
- [130] Josephs, K. A., Hodges, J. R., Snowden, J. S., Mackenzie, I. R., Neumann, M., Mann, D. M., and Dickson, D. W. “Neuropathological background of phenotypical variability in frontotemporal dementia”. *Acta Neuropathologica* 122 (2011), pp. 137–153.
- [131] Ju, J.-S., Fuentealba, R. A., Miller, S. E., Jackson, E., Piwnica-Worms, D., Baloh, R. H., and Weihl, C. C. “Valosin-containing protein (VCP) is required for autophagy and is disrupted in VCP disease”. *Journal of Cell Biology* 187 (2009), pp. 875–888.
- [132] Kapitein, L. C., Schlager, M. A., Kuijpers, M., Wulf, P. S., van Spronsen, M., MacKintosh, F. C., and Hoogenraad, C. C. “Mixed microtubules steer dynein-driven cargo transport into dendrites”. *Current Biology* 20 (2010), pp. 290–299.
- [133] Kegel, K. B., Kim, M., Sapp, E., McIntyre, C., Castano, J. G., Aronin, N., and DiFiglia, M. “Huntingtin expression stimulates endosomal-lysosomal activity, endosome tubulation, and autophagy”. *Journal of Neuroscience* 20 (2000), pp. 7268–7278.
- [134] Keller, J. N., Gee, J., and Ding, Q. “The proteasome in brain aging”. *Ageing Research Reviews* 1 (2002), pp. 279–293.
- [135] Kessenbrock, K., Frohlich, L., Sixt, M., Lammermann, T., Pfister, H., Bateman, A., Belaouaj, A., Ring, J., Ollert, M., Fassler, R., and Jenne, D. E. “Proteinase 3 and neutrophil elastase enhance inflammation in mice by inactivating antiinflammatory progranulin”. *Journal of Clinical Investigation* 118 (2008), pp. 2438–2447.
- [136] Kins, S., Lauther, N., Szodorai, A., and Beyreuther, K. “Subcellular trafficking of the amyloid precursor protein gene family and its pathogenic role in Alzheimer’s disease”. *Neurodegenerative Diseases* 3 (2006), pp. 218–226.
- [137] Kirkin, V., McEwan, D. G., Novak, I., and Dikic, I. “A role for ubiquitin in selective autophagy”. *Molecular Cell* 34 (2009), pp. 259–269.
- [138] Kleinberger, G., Capell, A., Haass, C., and van Broeckhoven, C. “Mechanisms of granulin deficiency: lessons from cellular and animal models”. *Molecular Neurobiology* 47 (2013), pp. 337–360.

- 
- [139] Kleinberger, G., Yamanishi, Y., Suarez-Calvet, M., Czirr, E., Lohmann, E., Cuyvers, E., Struyfs, H., Pettkus, N., Wenninger-Weinzierl, A., Mazaheri, F., Tahirovic, S., Lleo, A., Alcolea, D., Fortea, J., Willem, M., Lammich, S., Molinuevo, J. L., Sanchez-Valle, R., Antonell, A., Ramirez, A., Heneka, M. T., Slegers, K., van der Zee, J., Martin, J.-J., Engelborghs, S., Demirtas-Tatlidede, A., Zetterberg, H., van Broeckhoven, C., Gurvit, H., Wyss-Coray, T., Hardy, J., Colonna, M., and Haass, C. "TREM2 mutations implicated in neurodegeneration impair cell surface transport and phagocytosis". *Science Translational Medicine* 6 (2014).
- [140] kleine Balderhaar, H. J. and Ungermann, C. "CORVET and HOPS tethering complexes - coordinators of endosome and lysosome fusion". *Journal of Cell Science* 126 (2013), pp. 1307–1316.
- [141] Klionsky, D. J. "Autophagy: from phenomenology to molecular understanding in less than a decade". *Nature Reviews Molecular Cell Biology* 8 (2007), pp. 931–937.
- [142] Klionsky, D. J. and Codogno, P. "The mechanism and physiological function of macroautophagy". *Journal of Innate Immunity* 5 (2013), pp. 427–433.
- [143] Knopman, D. S. and Roberts, R. O. "Estimating the number of persons with frontotemporal lobar degeneration in the US population". *Journal of Molecular Neuroscience* 45 (2011), pp. 330–335.
- [144] Koga, H. and Cuervo, A. M. "Chaperone-mediated autophagy dysfunction in the pathogenesis of neurodegeneration". *Neurobiology of Disease* 43 (2011), pp. 29–37.
- [145] Komatsu, M., Waguri, S., Ueno, T., Iwata, J., Murata, S., Tanida, I., Ezaki, J., Mizushima, N., Ohsumi, Y., Uchiyama, Y., Kominami, E., Tanaka, K., and Chiba, T. "Impairment of starvation-induced and constitutive autophagy in Atg7-deficient mice". *Journal of Cell Biology* 169 (2005), pp. 425–434.
- [146] Komatsu, M., Wang, Q. J., Holstein, G. R., Friedrich, Victor L Jr, Iwata, J.-i., Kominami, E., Chait, B. T., Tanaka, K., and Yue, Z. "Essential role for autophagy protein Atg7 in the maintenance of axonal homeostasis and the prevention of axonal degeneration". *Proceedings of the National Academy of Sciences of the United States of America* 104 (2007), pp. 14489–14494.
- [147] Koo, E. H. and Squazzo, S. L. "Evidence that production and release of amyloid beta-protein involves the endocytic pathway". *Journal of Biological Chemistry* 269 (1994), pp. 17386–17389.
- [148] Kornfeld, S. and Mellman, I. "The biogenesis of lysosomes". *Annual Review of Cell Biology* 5 (1989), pp. 483–525.
- [149] Korolchuk, V. I., Mansilla, A., Menzies, F. M., and Rubinsztein, D. C. "Autophagy inhibition compromises degradation of ubiquitin-proteasome pathway substrates". *Molecular Cell* 33 (2009), pp. 517–527.
- [150] Korolchuk, V. I., Saiki, S., Lichtenberg, M., Siddiqi, F. H., Roberts, E. A., Imarisio, S., Jahreiss, L., Sarkar, S., Futter, M., Menzies, F. M., O’Kane, C. J., Deretic, V., and Rubinsztein, D. C. "Lysosomal positioning coordinates cellular nutrient responses". *Nature Cell Biology* 13 (2011), pp. 453–460.
- [151] Kosik, K. S., Joachim, C. L., and Selkoe, D. J. "Microtubule-associated protein tau (tau) is a major antigenic component of paired helical filaments in Alzheimer disease". *Proceedings of the National Academy of Sciences of the United States of America* 83 (1986), pp. 4044–4048.
- [152] Krick, R., Bremer, S., Welter, E., Schlotterhose, P., Muehe, Y., Eskelinen, E.-L., and Thumm, M. "Cdc48/p97 and Shp1/p47 regulate autophagosome biogenesis in concert with ubiquitin-like Atg8". *Journal of Cell Biology* 190 (2010), pp. 965–973.
- [153] Laird, F. M., Farah, M. H., Ackerley, S., Hoke, A., Maragakis, N., Rothstein, J. D., Griffin, J., Price, D. L., Martin, L. J., and Wong, P. C. "Motor neuron disease occurring in a mutant dynactin mouse model is characterized by defects in vesicular trafficking". *Journal of Neuroscience* 28 (2008), pp. 1997–2005.

- [154] LaMonte, B. H., Wallace, K. E., Holloway, B. A., Shelly, S. S., Ascano, J., Tokito, M., van Winkle, T., Howland, D. S., and Holzbaur, Erika L F. “Disruption of dynein/dynactin inhibits axonal transport in motor neurons causing late-onset progressive degeneration”. *Neuron* 34 (2002), pp. 715–727.
- [155] Lang, C. M., Fellerer, K., Schwenk, B. M., Kuhn, P.-H., Kremmer, E., Edbauer, D., Capell, A., and Haass, C. “Membrane orientation and subcellular localization of transmembrane protein 106B (TMEM106B), a major risk factor for frontotemporal lobar degeneration”. *Journal of Biological Chemistry* 287 (2012), pp. 19355–19365.
- [156] Lattante, S., Le Ber, I., Galimberti, D., Serpente, M., Rivaud-Pechoux, S., Camuzat, A., Clot, F., Fenoglio, C., Scarpini, E., Brice, A., and Kabashi, E. “Defining the association of TMEM106B variants among frontotemporal lobar degeneration patients with GRN mutations and C9orf72 repeat expansions”. *Neurobiology of Aging* (2014).
- [157] Lee, J.-H., Yu, W. H., Kumar, A., Lee, S., Mohan, P. S., Peterhoff, C. M., Wolfe, D. M., Martinez-Vicente, M., Massey, A. C., Sovak, G., Uchiyama, Y., Westaway, D., Cuervo, A. M., and Nixon, R. A. “Lysosomal proteolysis and autophagy require presenilin 1 and are disrupted by Alzheimer-related PS1 mutations”. *Cell* 141 (2010), pp. 1146–1158.
- [158] Lee, J.-A. “Autophagy in neurodegeneration: two sides of the same coin”. *BMB Reports* 42 (2009), pp. 324–330.
- [159] Li, J., Kanekiyo, T., Shinohara, M., Zhang, Y., LaDu, M. J., Xu, H., and Bu, G. “Differential regulation of amyloid-beta endocytic trafficking and lysosomal degradation by apolipoprotein E isoforms”. *Journal of Biological Chemistry* 287 (2012), pp. 44593–44601.
- [160] Li, W., Yang, Q., and Mao, Z. “Chaperone-mediated autophagy: machinery, regulation and biological consequences”. *Cellular and Molecular Life Sciences* 68 (2011), pp. 749–763.
- [161] Lichtenthaler, S. F., Haass, C., and Steiner, H. “Regulated intramembrane proteolysis—lessons from amyloid precursor protein processing”. *Journal of Neurochemistry* 117 (2011), pp. 779–796.
- [162] Ling, S.-C., Polymenidou, M., and Cleveland, D. W. “Converging mechanisms in ALS and FTD: disrupted RNA and protein homeostasis”. *Neuron* 79 (2013), pp. 416–438.
- [163] LoPresti, P., Szuchet, S., Papasozomenos, S. C., Zinkowski, R. P., and Binder, L. I. “Functional implications for the microtubule-associated protein tau: localization in oligodendrocytes”. *Proceedings of the National Academy of Sciences of the United States of America* 92 (1995), pp. 10369–10373.
- [164] Low, P. “The role of ubiquitin-proteasome system in ageing”. *General and Comparative Endocrinology* 172 (2011), pp. 39–43.
- [165] Lu, R.-C., Wang, H., Tan, M.-S., Yu, J.-T., and Tan, L. “TMEM106B and APOE polymorphisms interact to confer risk for late-onset Alzheimer’s disease in Han Chinese”. *Journal of Neural Transmission* 121 (2014), pp. 283–287.
- [166] Luzio, J. P., Rous, B. A., Bright, N. A., Pryor, P. R., Mullock, B. M., and Piper, R. C. “Lysosome-endosome fusion and lysosome biogenesis”. *Journal of Cell Science* 113 ( Pt 9) (2000), pp. 1515–1524.
- [167] Luzio, J. P., Poupon, V., Lindsay, M. R., Mullock, B. M., Piper, R. C., and Pryor, P. R. “Membrane dynamics and the biogenesis of lysosomes”. *Molecular Membrane Biology* 20 (2003), pp. 141–154.
- [168] Luzio, J. P., Pryor, P. R., and Bright, N. A. “Lysosomes: fusion and function”. *Nature Reviews Molecular Cell Biology* 8 (2007), pp. 622–632.
- [169] Lwin, A., Orvisky, E., Goker-Alpan, O., LaMarca, M. E., and Sidransky, E. “Glucocerebrosidase mutations in subjects with parkinsonism”. *Molecular Genetics and Metabolism* 81 (2004), pp. 70–73.

- 
- [170] Mackenzie, I. R. A., Baker, M., Pickering-Brown, S., Hsiung, G.-Y. R., Lindholm, C., Dwosh, E., Gass, J., Cannon, A., Rademakers, R., Hutton, M., and Feldman, H. H. "The neuropathology of frontotemporal lobar degeneration caused by mutations in the progranulin gene". *Brain* 129 (2006), pp. 3081–3090.
- [171] Mackenzie, I. R. A., Neumann, M., Bigio, E. H., Cairns, N. J., Alafuzoff, I., Kril, J., Kovacs, G. G., Ghetti, B., Halliday, G., Holm, I. E., Ince, P. G., Kamphorst, W., Revesz, T., Rozemuller, Annemieke J M, Kumar-Singh, S., Akiyama, H., Baborie, A., Spina, S., Dickson, D. W., Trojanowski, J. Q., and Mann, David M A. "Nomenclature and nosology for neuropathologic subtypes of frontotemporal lobar degeneration: an update". *Acta Neuropathologica* 119 (2010), pp. 1–4.
- [172] Mackenzie, I. R. A., Rademakers, R., and Neumann, M. "TDP-43 and FUS in amyotrophic lateral sclerosis and frontotemporal dementia". *Lancet Neurology* 9 (2010), pp. 995–1007.
- [173] Mackenzie, I. R. A., Shi, J., Shaw, C. L., Duplessis, D., Neary, D., Snowden, J. S., and Mann, D. M. A. "Dementia lacking distinctive histology (DLDH) revisited". *Acta Neuropathologica* 112 (2006), pp. 551–559.
- [174] Maday, S., Wallace, K. E., and Holzbaur, E. L. "Autophagosomes initiate distally and mature during transport toward the cell soma in primary neurons". *Journal of Cell Biology* 196 (2012), pp. 407–417.
- [175] Manzoni, C. and Lewis, P. A. "Dysfunction of the autophagy/lysosomal degradation pathway is a shared feature of the genetic synucleinopathies". *FASEB Journal* 27 (2013), pp. 3424–3429.
- [176] Martinez-Vicente, M. and Cuervo, A. M. "Autophagy and neurodegeneration: when the cleaning crew goes on strike". *Lancet Neurology* 6 (2007), pp. 352–361.
- [177] Matteoni, R. and Kreis, T. E. "Translocation and clustering of endosomes and lysosomes depends on microtubules". *Journal of Cell Biology* 105 (1987), pp. 1253–1265.
- [178] Mazzulli, J. R., Xu, Y.-H., Sun, Y., Knight, A. L., McLean, P. J., Caldwell, G. A., Sidransky, E., Grabowski, G. A., and Krainc, D. "Gaucher disease glucocerebrosidase and alpha-synuclein form a bidirectional pathogenic loop in synucleinopathies". *Cell* 146 (2011), pp. 37–52.
- [179] McNeil, P. L. and Kirchhausen, T. "An emergency response team for membrane repair". *Nature Reviews Molecular Cell Biology* 6 (2005), pp. 499–505.
- [180] Al-Mehdi, A.-B., Pastukh, V. M., Swiger, B. M., Reed, D. J., Patel, M. R., Bardwell, G. C., Pastukh, V. V., Alexeyev, M. F., and Gillespie, M. N. "Perinuclear mitochondrial clustering creates an oxidant-rich nuclear domain required for hypoxia-induced transcription". *Science Signaling* 5 (2012), ra47.
- [181] Melkonian, K. A., Maier, K. C., Godfrey, J. E., Rodgers, M., and Schroer, T. A. "Mechanism of dynamitin-mediated disruption of dynactin". *Journal of Biological Chemistry* 282 (2007), pp. 19355–19364.
- [182] Mercy, L., Hodges, J. R., Dawson, K., Barker, R. A., and Brayne, C. "Incidence of early-onset dementias in Cambridgeshire, United Kingdom". *Neurology* 71 (2008), pp. 1496–1499.
- [183] Meyer, H., Bug, M., and Bremer, S. "Emerging functions of the VCP/p97 AAA-ATPase in the ubiquitin system". *Nature Cell Biology* 14 (2012), pp. 117–123.
- [184] Minthon, L., Hesse, C., Sjogren, M., Englund, E., Gustafson, L., and Blennow, K. "The apolipoprotein E epsilon4 allele frequency is normal in fronto-temporal dementia, but correlates with age at onset of disease". *Neuroscience Letters* 226 (1997), pp. 65–67.
- [185] Mori, K., Arzberger, T., Grasser, F. A., Gijselinck, I., May, S., Rentzsch, K., Weng, S.-M., Schludi, M. H., van der Zee, J., Cruts, M., van Broeckhoven, C., Kremmer, E., Kretzschmar, H. A., Haass, C., and Edbauer, D. "Bidirectional transcripts of the expanded C9orf72 hexanucleotide repeat are translated into aggregating dipeptide repeat proteins". *Acta Neuropathologica* 126 (2013), pp. 881–893.
-

- [186] Mori, K., Lammich, S., Mackenzie, Ian R A, Forne, I., Zilow, S., Kretzschmar, H., Edbauer, D., Janssens, J., Kleinberger, G., Cruts, M., Herms, J., Neumann, M., van Broeckhoven, C., Arzberger, T., and Haass, C. "hnRNP A3 binds to GGGGCC repeats and is a constituent of p62-positive/TDP43-negative inclusions in the hippocampus of patients with C9orf72 mutations". *Acta Neuropathologica* 125 (2013), pp. 413–423.
- [187] Mori, K., Weng, S.-M., Arzberger, T., May, S., Rentzsch, K., Kremmer, E., Schmid, B., Kretzschmar, H. A., Cruts, M., van Broeckhoven, C., Haass, C., and Edbauer, D. "The C9orf72 GGGGCC repeat is translated into aggregating dipeptide-repeat proteins in FTL/ALS". *Science* 339 (2013), pp. 1335–1338.
- [188] Mullins, C. and Bonifacino, J. S. "The molecular machinery for lysosome biogenesis". *BioEssays* 23 (2001), pp. 333–343.
- [189] Munch, C., Sedlmeier, R., Meyer, T., Homberg, V., Sperfeld, A. D., Kurt, A., Prudlo, J., Peraus, G., Hanemann, C. O., Stumm, G., and Ludolph, A. C. "Point mutations of the p150 subunit of dynactin (DCTN1) gene in ALS". *Neurology* 63 (2004), pp. 724–726.
- [190] Munch, C., Rosenbohm, A., Sperfeld, A.-D., Uttner, I., Reske, S., Krause, B. J., Sedlmeier, R., Meyer, T., Hanemann, C. O., Stumm, G., and Ludolph, A. C. "Heterozygous R1101K mutation of the DCTN1 gene in a family with ALS and FTD". *Annals of Neurology* 58 (2005), pp. 777–780.
- [191] Nagaoka, U., Kim, K., Jana, N. R., Doi, H., Maruyama, M., Mitsui, K., Oyama, F., and Nukina, N. "Increased expression of p62 in expanded polyglutamine-expressing cells and its association with polyglutamine inclusions". *Journal of Neurochemistry* 91 (2004), pp. 57–68.
- [192] Neary, D., Snowden, J. S., and Mann, D. M. "Classification and description of frontotemporal dementias". *Annals of the New York Academy of Sciences* 920 (2000), pp. 46–51.
- [193] Neary, D., Snowden, J., Gustafson, L., Passant, U., Stuss, D., and Black, S. "Frontotemporal lobar degeneration: a consensus on clinical diagnostic criteria". *Neurology* (1998), pp. 1546–1554.
- [194] Neely, K. M., Green, K. N., and LaFerla, F. M. "Presenilin is necessary for efficient proteolysis through the autophagy-lysosome system in a gamma-secretase-independent manner". *Journal of Neuroscience* 31 (2011), pp. 2781–2791.
- [195] Neumann, M., Sampathu, D., Kwong, L., Truax, A., Micsenyi, M., Chou, T., Bruce, J., Schuck, T., Grossman, M., Clark, C., McCluskey, L., Miller, B., Masliah, E., Mackenzie, I. R., Feldman, H., Feiden, W., Kretzschmar, H., Trojanowski, J., and Lee, V. "Ubiquitinated TDP-43 in frontotemporal lobar degeneration and amyotrophic lateral sclerosis". *Science* (2006), pp. 130–133.
- [196] Neumann, M., Rademakers, R., Roeber, S., Baker, M., Kretzschmar, H. A., and Mackenzie, Ian R A. "A new subtype of frontotemporal lobar degeneration with FUS pathology". *Brain* 132 (2009), pp. 2922–2931.
- [197] Neumann, M., Tolnay, M., and Mackenzie, Ian R A. "The molecular basis of frontotemporal dementia". *Expert Reviews in Molecular Medicine* 11 (2009), e23.
- [198] Neuspiel, M., Zunino, R., Gangaraju, S., Rippstein, P., and McBride, H. "Activated mitofusin 2 signals mitochondrial fusion, interferes with Bax activation, and reduces susceptibility to radical induced depolarization". *Journal of Biological Chemistry* 280 (2005), pp. 25060–25070.
- [199] Ng, A. S. L., Rademakers, R., and Miller, B. L. "Frontotemporal dementia: a bridge between dementia and neuromuscular disease". *Annals of the New York Academy of Sciences* 1338 (2015), pp. 71–93.
- [200] Nicholson, A. M., Finch, N. A., Wojtas, A., Baker, M. C., Perkerson, Ralph B 3rd, Castanedes-Casey, M., Rousseau, L., Benussi, L., Binetti, G., Ghidoni, R., Hsiung, G.-Y. R., Mackenzie, I. R., Finger, E., Boeve, B. F., Ertekin-Taner, N., Graff-Radford, N. R., Dickson, D. W., and Rademakers, R. "TMEM106B p.T185S regulates TMEM106B protein levels: implications for frontotemporal dementia". *Journal of Neurochemistry* 126 (2013), pp. 781–791.

- 
- [201] Nielsen, T. T., Mizielińska, S., Hasholt, L., Isaacs, A. M., and Nielsen, J. E. “Reversal of pathology in CHMP2B-mediated frontotemporal dementia patient cells using RNA interference”. *Journal of Gene Medicine* 14 (2012), pp. 521–529.
- [202] Nishino, I., Fu, J., Tanji, K., Yamada, T., Shimojo, S., Koori, T., Mora, M., Riggs, J. E., Oh, S. J., Koga, Y., Sue, C. M., Yamamoto, A., Murakami, N., Shanske, S., Byrne, E., Bonilla, E., Nonaka, I., DiMauro, S., and Hirano, M. “Primary LAMP-2 deficiency causes X-linked vacuolar cardiomyopathy and myopathy (Danon disease)”. *Nature* 406 (2000), pp. 906–910.
- [203] Nixon, R. A., Cataldo, A. M., and Mathews, P. M. “The endosomal-lysosomal system of neurons in Alzheimer’s disease pathogenesis: a review”. *Neurochemical Research* 25 (2000), pp. 1161–1172.
- [204] Nixon, R. A. “Autophagy, amyloidogenesis and Alzheimer disease”. *Journal of Cell Science* 120 (2007), pp. 4081–4091.
- [205] Nixon, R. A. “The role of autophagy in neurodegenerative disease”. *Nature Medicine* 19 (2013), pp. 983–997.
- [206] Nixon, R. A., Wegiel, J., Kumar, A., Yu, W. H., Peterhoff, C., Cataldo, A., and Cuervo, A. M. “Extensive involvement of autophagy in Alzheimer disease: an immuno-electron microscopy study”. *Journal of Neuropathology and Experimental Neurology* 64 (2005), pp. 113–122.
- [207] Nukina, N. and Ihara, Y. “One of the antigenic determinants of paired helical filaments is related to tau protein”. *Journal of Biochemistry* 99 (1986), pp. 1541–1544.
- [208] Otero, K., Shinohara, M., Zhao, H., Cella, M., Gilfillan, S., Colucci, A., Faccio, R., Ross, F. P., Teitelbaum, S. L., Takayanagi, H., and Colonna, M. “TREM2 and beta-catenin regulate bone homeostasis by controlling the rate of osteoclastogenesis”. *Journal of Immunology* 188 (2012), pp. 2612–2621.
- [209] Palmieri, M., Impey, S., Kang, H., Di Ronza, A., Pelz, C., Sardiello, M., and Ballabio, A. “Characterization of the CLEAR network reveals an integrated control of cellular clearance pathways”. *Human Molecular Genetics* 20 (2011), pp. 3852–3866.
- [210] Paloneva, J., Autti, T., Raininko, R., Partanen, J., Salonen, O., Puranen, M., Hakola, P., and Haltia, M. “CNS manifestations of Nasu-Hakola disease: a frontal dementia with bone cysts”. *Neurology* 56 (2001), pp. 1552–1558.
- [211] Paloneva, J., Manninen, T., Christman, G., Hovanes, K., Mandelin, J., Adolfsson, R., Bianchin, M., Bird, T., Miranda, R., Salmaggi, A., Tranebjaerg, L., Konttinen, Y., and Peltonen, L. “Mutations in two genes encoding different subunits of a receptor signaling complex result in an identical disease phenotype”. *American Journal of Human Genetics* 71 (2002), pp. 656–662.
- [212] Park, J.-S. and Neiman, A. M. “VPS13 regulates membrane morphogenesis during sporulation in *Saccharomyces cerevisiae*”. *Journal of Cell Science* 125 (2012), pp. 3004–3011.
- [213] Parton, R. G., Dotti, C. G., Bacallao, R., Kurtz, I., Simons, K., and Prydz, K. “pH-induced microtubule-dependent redistribution of late endosomes in neuronal and epithelial cells”. *Journal of Cell Biology* 113 (1991), pp. 261–274.
- [214] Pawlikowska, P., Gajkowska, B., and Orzechowski, A. “Mitofusin 2 (Mfn2): a key player in insulin-dependent myogenesis in vitro”. *Cell and Tissue Research* 327 (2007), pp. 571–581.
- [215] Perlson, E., Hanz, S., Ben-Yaakov, K., Segal-Ruder, Y., Seger, R., and Fainzilber, M. “Vimentin-dependent spatial translocation of an activated MAP kinase in injured nerve”. *Neuron* 45 (2005), pp. 715–726.
- [216] Petkau, T. L., Neal, S. J., Orban, P. C., MacDonald, J. L., Hill, A. M., Lu, G., Feldman, H. H., Mackenzie, I. R. A., and Leavitt, B. R. “Progranulin expression in the developing and adult murine brain”. *Journal of Comparative Neurology* 518 (2010), pp. 3931–3947.
-

- [217] Pick, A. “Über die Beziehungen der senilen Hirnatrophie zur Aphasie.” *Prager Medicinische Wochenschrift* (1892), pp. 165–167.
- [218] Pickford, F., Masliah, E., Britschgi, M., Lucin, K., Narasimhan, R., Jaeger, P. A., Small, S., Spencer, B., Rockenstein, E., Levine, B., and Wyss-Coray, T. “The autophagy-related protein beclin 1 shows reduced expression in early Alzheimer disease and regulates amyloid beta accumulation in mice”. *Journal of Clinical Investigation* 118 (2008), pp. 2190–2199.
- [219] Pierzynska-Mach, A., Janowski, P. A., and Dobrucki, J. W. “Evaluation of acridine orange, LysoTracker Red, and quinacrine as fluorescent probes for long-term tracking of acidic vesicles”. *Cytometry Part A* (2014).
- [220] Pils, A. and Winklhofer, K. F. “Parkin, PINK1 and mitochondrial integrity: emerging concepts of mitochondrial dysfunction in Parkinson’s disease”. *Acta Neuropathologica* 123 (2012), pp. 173–188.
- [221] Platt, F. M., Boland, B., and van der Spoel, Aarnoud C. “The cell biology of disease: lysosomal storage disorders: the cellular impact of lysosomal dysfunction”. *Journal of Cell Biology* 199 (2012), pp. 723–734.
- [222] Postle, K., Nguyen, T. T., and Bertrand, K. P. “Nucleotide sequence of the repressor gene of the TN10 tetracycline resistance determinant”. *Nucleic Acids Research* 12 (1984), pp. 4849–4863.
- [223] Pous, C. and Codogno, P. “Lysosome positioning coordinates mTORC1 activity and autophagy”. *Nature Cell Biology* 13 (2011), pp. 342–344.
- [224] Premi, E., Formenti, A., Gazzina, S., Archetti, S., Gasparotti, R., Padovani, A., and Borroni, B. “Effect of TMEM106B polymorphism on functional network connectivity in asymptomatic GRN mutation carriers”. *JAMA Neurology* 71 (2014), pp. 216–221.
- [225] Rabinovici, G. D. and Miller, B. L. “Frontotemporal lobar degeneration: epidemiology, pathophysiology, diagnosis and management”. *CNS Drugs* 24 (2010), pp. 375–398.
- [226] Rademakers, R., Cruts, M., and Van Broeckhoven, C. “The role of tau (MAPT) in frontotemporal dementia and related tauopathies”. *Human Mutation* 24 (2004), pp. 277–295.
- [227] Rademakers, R., Neumann, M., and Mackenzie, I. R. “Advances in understanding the molecular basis of frontotemporal dementia”. *Nature Reviews Neurology* 8 (2012), pp. 423–434.
- [228] Rademakers, R. and Rovelet-Lecrux, A. “Recent insights into the molecular genetics of dementia”. *Trends in Neuroscience* (2009), pp. 451–461.
- [229] Rami, A. “Review: autophagy in neurodegeneration: firefighter and/or incendiary?” *Neuropathology and Applied Neurobiology* 35 (2009), pp. 449–461.
- [230] Ramirez, A., Heimbach, A., Grundemann, J., Stiller, B., Hampshire, D., Cid, L. P., Goebel, I., Mubaidin, A. F., Wriekat, A.-L., Roeper, J., Al-Din, A., Hillmer, A. M., Karsak, M., Liss, B., Woods, C. G., Behrens, M. I., and Kubisch, C. “Hereditary parkinsonism with dementia is caused by mutations in ATP13A2, encoding a lysosomal type 5 P-type ATPase”. *Nature Genetics* 38 (2006), pp. 1184–1191.
- [231] Rasband, W. S. *ImageJ*. National Institutes of Health. 1997-2014. URL: <http://imagej.nih.gov/ij/>.
- [232] Rascovsky, K., Hodges, J. R., Knopman, D., Mendez, M. F., Kramer, J. H., Neuhaus, J., van Swieten, Seelaar, H., Dopper, Elise G P, Onyike, C. U., Hillis, A. E., Josephs, K. A., Boeve, B. F., Kertesz, A., Seeley, W. W., Rankin, K. P., Johnson, J. K., Gorno-Tempini, M.-L., Rosen, H., Prioleau-Latham, C. E., Lee, A., Kipps, C. M., Lillo, P., Piguet, O., Rohrer, J. D., Rossor, M. N., Warren, J. D., Fox, N. C., Galasko, D., Salmon, D. P., Black, S. E., Mesulam, M., Weintraub, S., Dickerson, B. C., Diehl-Schmid, J., Pasquier, F., Deramecourt, V., Lebert, F., Pijnenburg, Y., Chow, T. W., Manes, F., Grafman, J., Cappa, S. F., Freedman, M., Grossman, M., and Miller, B. L. “Sensitivity of revised diagnostic criteria for the behavioural variant of frontotemporal dementia”. *Brain* 134 (2011), pp. 2456–2477.

- 
- [233] Ratnavalli, E., Brayne, C., Dawson, K., and Hodges, J. R. “The prevalence of frontotemporal dementia”. *Neurology* 58 (2002), pp. 1615–1621.
- [234] Ravikumar, B., Acevedo-Arozena, A., Imarisio, S., Berger, Z., Vacher, C., O’Kane, C. J., Brown, Steve D M, and Rubinsztein, D. C. “Dynein mutations impair autophagic clearance of aggregate-prone proteins”. *Nature Genetics* 37 (2005), pp. 771–776.
- [235] Ravikumar, B. and Rubinsztein, D. C. “Can autophagy protect against neurodegeneration caused by aggregate-prone proteins?” *Neuroreport* 15 (2004), pp. 2443–2445.
- [236] Ravikumar, B., Vacher, C., Berger, Z., Davies, J. E., Luo, S., Oroz, L. G., Scaravilli, F., Easton, D. F., Duden, R., O’Kane, C. J., and Rubinsztein, D. C. “Inhibition of mTOR induces autophagy and reduces toxicity of polyglutamine expansions in fly and mouse models of Huntington disease”. *Nature Genetics* 36 (2004), pp. 585–595.
- [237] Rayaprolu, S., Mullen, B., Baker, M., Lynch, T., Finger, E., Seeley, W. W., Hatanpaa, K. J., Lomen-Hoerth, C., Kertesz, A., Bigio, E. H., Lippa, C., Josephs, K. A., Knopman, D. S., White, C. L. 3., Caselli, R., Mackenzie, I. R., Miller, B. L., Boczarska-Jedynak, M., Opala, G., Krygowska-Wajs, A., Barcikowska, M., Younkin, S. G., Petersen, R. C., Ertekin-Taner, N., Uitti, R. J., Meschia, J. F., Boylan, K. B., Boeve, B. F., Graff-Radford, N. R., Wszolek, Z. K., Dickson, D. W., Rademakers, R., and Ross, O. A. “TREM2 in neurodegeneration: evidence for association of the p.R47H variant with frontotemporal dementia and Parkinson’s disease”. *Molecular Neurodegeneration* 8 (2013), p. 19.
- [238] Renton, A. E., Majounie, E., Waite, A., Simon-Sanchez, J., Rollinson, S., Gibbs, J. R., Schymick, J. C., Laaksovirta, H., van Swieten, Myllykangas, L., Kalimo, H., Paetau, A., Abramzon, Y., Remes, A. M., Kaganovich, A., Scholz, S. W., Duckworth, J., Ding, J., Harmer, D. W., Hernandez, D. G., Johnson, J. O., Mok, K., Ryten, M., Trabzuni, D., Guerreiro, R. J., Orrell, R. W., Neal, J., Murray, A., Pearson, J., Jansen, I. E., Sondervan, D., Seelaar, H., Blake, D., Young, K., Halliwell, N., Callister, J. B., Toulson, G., Richardson, A., Gerhard, A., Snowden, J., Mann, D., Neary, D., Nalls, M. A., Peuralinna, T., Jansson, L., Isoviita, V.-M., Kaivorinne, A.-L., Holtta-Vuori, M., Ikonen, E., Sulkava, R., Benatar, M., Wu, J., Chio, A., Restagno, G., Borghero, G., Sabatelli, M., Heckerman, D., Rogaeva, E., Zinman, L., Rothstein, J. D., Sendtner, M., Drepper, C., Eichler, E. E., Alkan, C., Abdullaev, Z., Pack, S. D., Dutra, A., Pak, E., Hardy, J., Singleton, A., Williams, N. M., Heutink, P., Pickering-Brown, S., Morris, H. R., Tienari, P. J., and Traynor, B. J. “A hexanucleotide repeat expansion in C9ORF72 is the cause of chromosome 9p21-linked ALS-FTD”. *Neuron* 72 (2011), pp. 257–268.
- [239] Riedl, L., Mackenzie, I. R., Forstl, H., Kurz, A., and Diehl-Schmid, J. “Frontotemporal lobar degeneration: current perspectives”. *Neuropsychiatric Disease and Treatment* 10 (2014), pp. 297–310.
- [240] Rink, J., Ghigo, E., Kalaidzidis, Y., and Zerial, M. “Rab conversion as a mechanism of progression from early to late endosomes”. *Cell* 122 (2005), pp. 735–749.
- [241] Ritz, D., Vuk, M., Kirchner, P., Bug, M., Schutz, S., Hayer, A., Bremer, S., Lusk, C., Baloh, R. H., Lee, H., Glatzer, T., Gstaiger, M., Aebbersold, R., Wehl, C. C., and Meyer, H. “Endolysosomal sorting of ubiquitylated caveolin-1 is regulated by VCP and UBXD1 and impaired by VCP disease mutations”. *Nature Cell Biology* 13 (2011), pp. 1116–1123.
- [242] Rocha, N., Kuijl, C., van der Kant, R., Janssen, L., Houben, D., Janssen, H., Zwart, W., and Neefjes, J. “Cholesterol sensor ORP1L contacts the ER protein VAP to control Rab7-RILP-p150 Glued and late endosome positioning”. *Journal of Cell Biology* 185 (2009), pp. 1209–1225.
- [243] Roczniak-Ferguson, A., Petit, C. S., Froehlich, F., Qian, S., Ky, J., Angarola, B., Walther, T. C., and Ferguson, S. M. “The transcription factor TFEB links mTORC1 signaling to transcriptional control of lysosome homeostasis”. *Science Signaling* 5 (2012), ra42.
-

- [244] Rogov, V., Dotsch, V., Johansen, T., and Kirkin, V. "Interactions between autophagy receptors and ubiquitin-like proteins form the molecular basis for selective autophagy". *Molecular Cell* 53 (2014), pp. 167–178.
- [245] Rossi, G., Bastone, A., Piccoli, E., Mazzoleni, G., Morbin, M., Uggetti, A., Giaccone, G., Sperber, S., Beeg, M., Salmona, M., and Tagliavini, F. "New mutations in MAPT gene causing frontotemporal lobar degeneration: biochemical and structural characterization". *Neurobiology of Aging* 33 (2012), 834.e1–6.
- [246] Rosso, S. M., Donker Kaat, L., Baks, T., Joosse, M., Koning, I. d., Pijnenburg, Y., Jong, D. d., Dooijes, D., Kamphorst, W., Ravid, R., Niermeijer, M. F., Verheij, F., Kremer, H. P., Scheltens, P., van Duijn, Cornelia M, Heutink, P., and van Swieten. "Frontotemporal dementia in The Netherlands: patient characteristics and prevalence estimates from a population-based study". *Brain* 126 (2003), pp. 2016–2022.
- [247] Rubinsztein, D. C., Shpilka, T., and Elazar, Z. "Mechanisms of autophagosome biogenesis". *Current Biology* 22 (2012), R29–34.
- [248] Ruivo, R., Anne, C., Sagne, C., and Gasnier, B. "Molecular and cellular basis of lysosomal transmembrane protein dysfunction". *Biochimica et Biophysica Acta* 1793 (2009), pp. 636–649.
- [249] Rumpf, S., Bagley, J. A., Thompson-Peer, K. L., Zhu, S., Gorczyca, D., Beckstead, R. B., Jan, L. Y., and Jan, Y. N. "Drosophila Valosin-Containing Protein is required for dendrite pruning through a regulatory role in mRNA metabolism". *Proceedings of the National Academy of Sciences of the United States of America* 111 (2014), pp. 7331–7336.
- [250] Rutherford, N. J., Carrasquillo, M. M., Li, M., Bisceglia, G., Menke, J., Josephs, K. A., Parisi, J. E., Petersen, R. C., Graff-Radford, N. R., Younkin, S. G., Dickson, D. W., and Rademakers, R. "TMEM106B risk variant is implicated in the pathologic presentation of Alzheimer disease". *Neurology* 79 (2012), pp. 717–718.
- [251] Saftig, P. *Lysosomes*. Medical intelligence unit. New York, N.Y: Springer Science & Business Media, 2005.
- [252] Saftig, P. and Klumperman, J. "Lysosome biogenesis and lysosomal membrane proteins: trafficking meets function". *Nature Reviews Molecular Cell Biology* 10 (2009), pp. 623–635.
- [253] Samson, F., Donoso, J. A., Heller-Bettinger, I., Watson, D., and Himes, R. H. "Nocodazole action on tubulin assembly, axonal ultrastructure and fast axoplasmic transport". *Journal of Pharmacology and Experimental Therapeutics* 208 (1979), pp. 411–417.
- [254] Sardiello, M., Palmieri, M., Di Ronza, A., Medina, D. L., Valenza, M., Gennarino, V. A., Di Malta, C., Donaudy, F., Embrione, V., Polishchuk, R. S., Banfi, S., Parenti, G., Cattaneo, E., and Ballabio, A. "A gene network regulating lysosomal biogenesis and function". *Science* 325 (2009), pp. 473–477.
- [255] Sarkar, S., Ravikumar, B., and Rubinsztein, D. C. "Autophagic clearance of aggregate-prone proteins associated with neurodegeneration". *Methods in Enzymology* 453 (2009), pp. 83–110.
- [256] Sato, C., Morgan, A., Lang, A. E., Salehi-Rad, S., Kawarai, T., Meng, Y., Ray, P. N., Farrer, L. A., St George-Hyslop, P., and Rogaeva, E. "Analysis of the glucocerebrosidase gene in Parkinson's disease". *Movement Disorders* 20 (2005), pp. 367–370.
- [257] Satoh, J.-I., Kino, Y., Kawana, N., Yamamoto, Y., Ishida, T., Saito, Y., and Arima, K. "TMEM106B expression is reduced in Alzheimer's disease brains". *Alzheimer's Research & Therapy* 6 (2014), p. 17.
- [258] Sato-Harada, R., Okabe, S., Umeyama, T., Kanai, Y., and Hirokawa, N. "Microtubule-associated proteins regulate microtubule function as the track for intracellular membrane organelle transports". *Cell Structure and Function* 21 (1996), pp. 283–295.

- 
- [259] Saunders, A. M., Strittmatter, W. J., Schmechel, D., George-Hyslop, P. H., Pericak-Vance, M. A., Joo, S. H., Rosi, B. L., Gusella, J. F., Crapper-MacLachlan, D. R., and Alberts, M. J. "Association of apolipoprotein E allele epsilon 4 with late-onset familial and sporadic Alzheimer's disease". *Neurology* 43 (1993), pp. 1467–1472.
- [260] Schliwa, M. and Woehlke, G. "Molecular motors". *Nature* 422 (2003), pp. 759–765.
- [261] Schmid, D., Pypaert, M., and Munz, C. "Antigen-loading compartments for major histocompatibility complex class II molecules continuously receive input from autophagosomes". *Immunity* 26 (2007), pp. 79–92.
- [262] Schwake, M., Schroder, B., and Saftig, P. "Lysosomal membrane proteins and their central role in physiology". *Traffic* 14 (2013), pp. 739–748.
- [263] Schwenk, B. M., Lang, C. M., Hogg, S., Tahirovic, S., Orozco, D., Rentzsch, K., Lichtenthaler, S. F., Hoogenraad, C. C., Capell, A., Haass, C., and Edbauer, D. "The FTL risk factor TMEM106B and MAP6 control dendritic trafficking of lysosomes". *The EMBO Journal* 33 (2014), pp. 450–467.
- [264] Seelaar, H., Rohrer, J. D., Pijnenburg, Yolande A L, Fox, N. C., and van Swieten. "Clinical, genetic and pathological heterogeneity of frontotemporal dementia: a review". *Journal of Neurology, Neurosurgery, and Psychiatry* 82 (2011), pp. 476–486.
- [265] Settembre, C., Cegli, R. d., Mansueto, G., Saha, P. K., Vetrini, F., Visvikis, O., Huynh, T., Carissimo, A., Palmer, D., Jürgen Klisch, T., Wollenberg, A. C., Di Bernardo, D., Chan, L., Irazoqui, J. E., and Ballabio, A. "TFEB controls cellular lipid metabolism through a starvation-induced autoregulatory loop". *Nature Cell Biology* 15 (2013), pp. 647–658. URL: <http://dx.doi.org/10.1038/ncb2718>.
- [266] Settembre, C., Di Malta, C., Polito, V. A., Garcia Arencibia, M., Vetrini, F., Erdin, S., Erdin, S. U., Huynh, T., Medina, D., Colella, P., Sardiello, M., Rubinsztein, D. C., and Ballabio, A. "TFEB links autophagy to lysosomal biogenesis". *Science* 332 (2011), pp. 1429–1433.
- [267] Settembre, C., Zoncu, R., Medina, D. L., Vetrini, F., Erdin, S., Erdin, S., Huynh, T., Ferron, M., Karsenty, G., Vellard, M. C., Facchinetti, V., Sabatini, D. M., and Ballabio, A. "A lysosome-to-nucleus signalling mechanism senses and regulates the lysosome via mTOR and TFEB". *The EMBO Journal* 31 (2012), pp. 1095–1108.
- [268] Shankaran, S. S., Capell, A., Hruscha, A. T., Fellerer, K., Neumann, M., Schmid, B., and Haass, C. "Missense mutations in the progranulin gene linked to frontotemporal lobar degeneration with ubiquitin-immunoreactive inclusions reduce progranulin production and secretion". *Journal of Biological Chemistry* 283 (2008), pp. 1744–1753.
- [269] Shibata, M., Lu, T., Furuya, T., Degtarev, A., Mizushima, N., Yoshimori, T., MacDonald, M., Yankner, B., and Yuan, J. "Regulation of intracellular accumulation of mutant Huntingtin by Beclin 1". *Journal of Biological Chemistry* 281 (2006), pp. 14474–14485.
- [270] Sieben, A., van Langenhove, T., Engelborghs, S., Martin, J.-J., Boon, P., Cras, P., Deyn, P.-P. d., Santens, P., van Broeckhoven, C., and Cruts, M. "The genetics and neuropathology of frontotemporal lobar degeneration". *Acta Neuropathologica* 124 (2012), pp. 353–372.
- [271] Skibinski, G., Parkinson, N. J., Brown, J. M., Chakrabarti, L., Lloyd, S. L., Hummerich, H., Nielsen, J. E., Hodges, J. R., Spillantini, M. G., Thusgaard, T., Brandner, S., Brun, A., Rossor, M. N., Gade, A., Johannsen, P., Sorensen, S. A., Gydesen, S., Fisher, Elizabeth M C, and Collinge, J. "Mutations in the endosomal ESCRTIII-complex subunit CHMP2B in frontotemporal dementia". *Nature Genetics* 37 (2005), pp. 806–808.
- [272] Sleegers, K., Cruts, M., and van Broeckhoven, C. "Molecular Pathways of Frontotemporal Lobar Degeneration". *Annual Review of Neuroscience* (2010), pp. 71–88.
-

- [273] Smith, K. R., Damiano, J., Franceschetti, S., Carpenter, S., Canafoglia, L., Morbin, M., Rossi, G., Pareyson, D., Mole, S. E., Staropoli, J. F., Sims, K. B., Lewis, J., Lin, W.-L., Dickson, D. W., Dahl, H.-H., Bahlo, M., and Berkovic, S. F. “Strikingly different clinicopathological phenotypes determined by progranulin-mutation dosage”. *American Journal of Human Genetics* 90 (2012), pp. 1102–1107.
- [274] Snowden, J. S., Thompson, J. C., Stopford, C. L., Richardson, Anna M T, Gerhard, A., Neary, D., and Mann, David M A. “The clinical diagnosis of early-onset dementias: diagnostic accuracy and clinicopathological relationships”. *Brain* 134 (2011), pp. 2478–2492.
- [275] Spillantini, M. G., Goedert, M., Crowther, R. A., Murrell, J. R., Farlow, M. R., and Ghetti, B. “Familial multiple system tauopathy with presenile dementia: a disease with abundant neuronal and glial tau filaments”. *Proceedings of the National Academy of Sciences of the United States of America* 94 (1997), pp. 4113–4118.
- [276] Spillantini, M. G., Murrell, J. R., Goedert, M., Farlow, M. R., Klug, A., and Ghetti, B. “Mutation in the tau gene in familial multiple system tauopathy with presenile dementia”. *Proceedings of the National Academy of Sciences of the United States of America* 95 (1998), pp. 7737–7741.
- [277] Stagi, M., Klein, Z. A., Gould, T. J., Bewersdorf, J., and Strittmatter, S. M. “Lysosome size, motility and stress response regulated by fronto-temporal dementia modifier TMEM106B”. *Molecular and Cellular Neurosciences* (2014).
- [278] Stefanis, L., Larsen, K. E., Rideout, H. J., Sulzer, D., and Greene, L. A. “Expression of A53T mutant but not wild-type alpha-synuclein in PC12 cells induces alterations of the ubiquitin-dependent degradation system, loss of dopamine release, and autophagic cell death”. *Journal of Neuroscience* 21 (2001), pp. 9549–9560.
- [279] Stockmann, M., Meyer-Ohlendorf, M., Achberger, K., Putz, S., Demestre, M., Yin, H., Hendrich, C., Linta, L., Heinrich, J., Brunner, C., Proepper, C., Kuh, G. F., Baumann, B., Langer, T., Schwalenstocker, B., Braunstein, K. E., Arnim, C. v., Schneuwly, S., Meyer, T., Wong, P. C., Boeckers, T. M., Ludolph, A. C., and Liebau, S. “The dynactin p150 subunit: cell biology studies of sequence changes found in ALS/MND and Parkinsonian syndromes”. *Journal of Neural Transmission* 120 (2013), pp. 785–798.
- [280] Stoorvogel, W., Strous, G. J., Geuze, H. J., Oorschot, V., and Schwartz, A. L. “Late endosomes derive from early endosomes by maturation”. *Cell* 65 (1991), pp. 417–427.
- [281] Storrie, B. and Desjardins, M. “The biogenesis of lysosomes: is it a kiss and run, continuous fusion and fission process?” *BioEssays* 18 (1996), pp. 895–903.
- [282] Strittmatter, W. J., Saunders, A. M., Schmechel, D., Pericak-Vance, M., Enghild, J., Salvesen, G. S., and Roses, A. D. “Apolipoprotein E: high-avidity binding to beta-amyloid and increased frequency of type 4 allele in late-onset familial Alzheimer disease”. *Proceedings of the National Academy of Sciences of the United States of America* 90 (1993), pp. 1977–1981.
- [283] Strom, A.-L., Shi, P., Zhang, F., Gal, J., Kilty, R., Hayward, L. J., and Zhu, H. “Interaction of amyotrophic lateral sclerosis (ALS)-related mutant copper-zinc superoxide dismutase with the dynein-dynactin complex contributes to inclusion formation”. *Journal of Biological Chemistry* 283 (2008), pp. 22795–22805.
- [284] Suzuki, K., Kirisako, T., Kamada, Y., Mizushima, N., Noda, T., and Ohsumi, Y. “The pre-autophagosomal structure organized by concerted functions of APG genes is essential for autophagosome formation”. *The EMBO Journal* 20 (2001), pp. 5971–5981.
- [285] Takahashi, K., Rochford, C. D., and Neumann, H. “Clearance of apoptotic neurons without inflammation by microglial triggering receptor expressed on myeloid cells-2”. *Journal of Experimental Medicine* 201 (2005), pp. 647–657.

- 
- [286] Tanaka, Y., Matsuwaki, T., Yamanouchi, K., and Nishihara, M. "Increased lysosomal biogenesis in activated microglia and exacerbated neuronal damage after traumatic brain injury in progranulin-deficient mice". *Neuroscience* 250 (2013), pp. 8–19.
- [287] Tang, D., Xiang, Y., Renzis, S. d., Rink, J., Zheng, G., Zerial, M., and Wang, Y. "The ubiquitin ligase HACE1 regulates Golgi membrane dynamics during the cell cycle". *Nature Communications* 2 (2011), p. 501.
- [288] Tanida, I. "Autophagosome formation and molecular mechanism of autophagy". *Antioxidants & Redox Signaling* 14 (2011), pp. 2201–2214.
- [289] Taylor, J. P., Tanaka, F., Robitschek, J., Sandoval, C. M., Taye, A., Markovic-Plese, S., and Fischbeck, K. H. "Aggresomes protect cells by enhancing the degradation of toxic polyglutamine-containing protein". *Human Molecular Genetics* 12 (2003), pp. 749–757.
- [290] The Association for Frontotemporal Degeneration. *FTD Fast Facts*. Ed. by The Association for Frontotemporal Degeneration. URL: <http://www.theaftd.org/frontotemporal-degeneration/ftd-fast-facts> (visited on 04/18/2014).
- [291] The Huntington's Disease Collaborative Research Group. "A novel gene containing a trinucleotide repeat that is expanded and unstable on Huntington's disease chromosomes". *Cell* 72 (1993), pp. 971–983.
- [292] Tresse, E., Salomons, F. A., Vesa, J., Bott, L. C., Kimonis, V., Yao, T.-P., Dantuma, N. P., and Taylor, J. P. "VCP/p97 is essential for maturation of ubiquitin-containing autophagosomes and this function is impaired by mutations that cause IBMPFD". *Autophagy* 6 (2010), pp. 217–227.
- [293] Trojanowski, J. Q., Schuck, T., Schmidt, M. L., and Lee, V. M. "Distribution of tau proteins in the normal human central and peripheral nervous system". *Journal of Histochemistry and Cytochemistry* 37 (1989), pp. 209–215.
- [294] Urwin, H., Authier, A., Nielsen, J. E., Metcalf, D., Powell, C., Froud, K., Malcolm, D. S., Holm, I., Johannsen, P., Brown, J., Fisher, Elizabeth M C, van der Zee, J., Bruyland, M., van Broeckhoven, C., Collinge, J., Brandner, S., Futter, C., and Isaacs, A. M. "Disruption of endocytic trafficking in frontotemporal dementia with CHMP2B mutations". *Human Molecular Genetics* 19 (2010), pp. 2228–2238.
- [295] Urwin, H., Authier, A., Nielsen, J. E., Metcalf, D., Powell, C., Froud, K., Malcolm, D. S., Holm, I., Johannsen, P., Brown, J., Fisher, Elizabeth M C, van der Zee, J., Bruyland, M., van Broeckhoven, C., Collinge, J., Brandner, S., Futter, C., and Isaacs, A. M. "Disruption of endocytic trafficking in frontotemporal dementia with CHMP2B mutations". *Human Molecular Genetics* 19 (2010), pp. 2228–2238.
- [296] Urwin, H., Ghazi-Noori, S., Collinge, J., and Isaacs, A. "The role of CHMP2B in frontotemporal dementia". *Biochemical Society Transactions* 37 (2009), pp. 208–212.
- [297] Usenovic, M., Tresse, E., Mazzulli, J. R., Taylor, J. P., and Krainc, D. "Deficiency of ATP13A2 leads to lysosomal dysfunction, alpha-synuclein accumulation, and neurotoxicity". *Journal of Neuroscience* 32 (2012), pp. 4240–4246.
- [298] Uusi-Rauva, K., Kyttila, A., van der Kant, R., Vesa, J., Tanhuanpaa, K., Neefjes, J., Olkkonen, V. M., and Jalanko, A. "Neuronal ceroid lipofuscinosis protein CLN3 interacts with motor proteins and modifies location of late endosomal compartments". *Cellular and Molecular Life Sciences* 69 (2012), pp. 2075–2089.
- [299] van Blitterswijk, M., Mullen, B., Nicholson, A. M., Bieniek, K. F., Heckman, M. G., Baker, M. C., DeJesus-Hernandez, M., Finch, N. A., Brown, P. H., Murray, M. E., Hsiung, G.-Y. R., Stewart, H., Karydas, A. M., Finger, E., Kertesz, A., Bigio, E. H., Weintraub, S., Mesulam, M., Hatanpaa, K. J., White, C. L. 3., Strong, M. J., Beach, T. G., Wszolek, Z. K., Lippa, C., Caselli, R., Petrucelli, L., Josephs, K. A., Parisi, J. E., Knopman, D. S., Petersen, R. C., Mackenzie, I. R., Seeley, W. W., Grinberg, L. T., Miller, B. L., Boylan, K. B., Graff-Radford, N. R., Boeve, B. F., Dickson, D. W., and Rademakers, R. "TMEM106B protects C9ORF72 expansion carriers against frontotemporal dementia". *Acta Neuropathologica* 127 (2014), pp. 397–406.
-

- [300] van Damme, P., van Hoecke, A., Lambrechts, D., Vanacker, P., Bogaert, E., van Swieten, J., Carmeliet, P., Van Den Bosch, Ludo, and Robberecht, W. "Progranulin functions as a neurotrophic factor to regulate neurite outgrowth and enhance neuronal survival". *Journal of Cell Biology* 181 (2008), pp. 37–41.
- [301] Van Deerlin, V. M., Sleiman, P. M. A., Martinez-Lage, M., Chen-Plotkin, A., Wang, L.-S., Graff-Radford, N. R., Dickson, D. W., Rademakers, R., Boeve, B. F., Grossman, M., Arnold, S. E., Mann, David M A, Pickering-Brown, S. M., Seelaar, H., Heutink, P., van Swieten, Murrell, J. R., Ghetti, B., Spina, S., Grafman, J., Hodges, J., Spillantini, M. G., Gilman, S., Lieberman, A. P., Kaye, J. A., Woltjer, R. L., Bigio, E. H., Mesulam, M., Al-Sarraj, S., Troakes, C., Rosenberg, R. N., White, C. L. 3., Ferrer, I., Llado, A., Neumann, M., Kretschmar, H. A., Hulette, C. M., Welsh-Bohmer, K. A., Miller, B. L., Alzualde, A., Lopez de Munain, Adolfo, McKee, A. C., Gearing, M., Levey, A. I., Lah, J. J., Hardy, J., Rohrer, J. D., Lashley, T., Mackenzie, Ian R A, Feldman, H. H., Hamilton, R. L., Dekosky, S. T., van der Zee, J., Kumar-Singh, S., van Broeckhoven, C., Mayeux, R., Vonsattel, Jean Paul G, Troncoso, J. C., Kril, J. J., Kwok, John B J, Halliday, G. M., Bird, T. D., Ince, P. G., Shaw, P. J., Cairns, N. J., Morris, J. C., McLean, C. A., DeCarli, C., Ellis, W. G., Freeman, S. H., Frosch, M. P., Growdon, J. H., Perl, D. P., Sano, M., Bennett, D. A., Schneider, J. A., Beach, T. G., Reiman, E. M., Woodruff, B. K., Cummings, J., Vinters, H. V., Miller, C. A., Chui, H. C., Alafuzoff, I., Hartikainen, P., Seilhean, D., Galasko, D., Masliah, E., Cotman, C. W., Tunon, M. T., Martinez, M Cristina Caballero, Munoz, D. G., Carroll, S. L., Marson, D., Riederer, P. F., Bogdanovic, N., Schellenberg, G. D., Hakonarson, H., Trojanowski, J. Q., and Lee, V. M.-Y. "Common variants at 7p21 are associated with frontotemporal lobar degeneration with TDP-43 inclusions". *Nature Genetics* 42 (2010), pp. 234–239.
- [302] van der Kant, R., Fish, A., Janssen, L., Janssen, H., Krom, S., Ho, N., Brummelkamp, T., Carette, J., Rocha, N., and Neefjes, J. "Late endosomal transport and tethering are coupled processes controlled by RILP and the cholesterol sensor ORP1L". *Journal of Cell Science* 126 (2013), pp. 3462–3474.
- [303] van der Zee, J., Gijssels, I., Dillen, L., van Langenhove, T., Theuns, J., Engelborghs, S., Philtjens, S., Vandenbulcke, M., Sleegers, K., Sieben, A., Baumer, V., Maes, G., Corsmit, E., Borroni, B., Padovani, A., Archetti, S., Pernecky, R., Diehl-Schmid, J., Mendonca, A. d., Miltenberger-Miltenyi, G., Pereira, S., Pimentel, J., Nacmias, B., Bagnoli, S., Sorbi, S., Graff, C., Chiang, H.-H., Westerlund, M., Sanchez-Valle, R., Llado, A., Gelpi, E., Santana, I., Almeida, M. R., Santiago, B., Frisoni, G., Zanetti, O., Bonvicini, C., Synofzik, M., Maetzler, W., Vom Hagen, Jennifer Muller, Schols, L., Heneka, M. T., Jessen, F., Matej, R., Parobkova, E., Kovacs, G. G., Strobel, T., Sarafov, S., Tournev, I., Jordanova, A., Danek, A., Arzberger, T., Fabrizi, G. M., Testi, S., Salmon, E., Santens, P., Martin, J.-J., Cras, P., Vandenberghe, R., De Deyn, Peter Paul, Cruys, M., van Broeckhoven, C., De Deyn, P. P., Muller Vom Hagen, Jennifer, Ramirez, A., Kurzweil, D., Sachtleben, C., Mairer, W., Firmo, C., Antonell, A., Molinuevo, J., Kinhult Stahlbom, A., Thonberg, H., Nennesmo, I., Borjesson-Hanson, A., Bessi, V., Piaceri, I., Helena Ribeiro, M., Rosario Almeida, M., Oliveira, C., Massano, J., Garret, C., Pires, P., Danel, A., Maria Fabrizi, G., Ferrari, S., and Cavallaro, T. "A pan-European study of the C9orf72 repeat associated with FTL: geographic prevalence, genomic instability, and intermediate repeats". *Human Mutation* 34 (2013), pp. 363–373.
- [304] van der Zee, J., Urwin, H., Engelborghs, S., Bruyland, M., Vandenberghe, R., Dermaut, B., Pooter, T. d., Peeters, K., Santens, P., De Deyn, P. P., Fisher, E. M., Collinge, J., Isaacs, A. M., and van Broeckhoven, C. "CHMP2B C-truncating mutations in frontotemporal lobar degeneration are associated with an aberrant endosomal phenotype in vitro". *Human Molecular Genetics* 17 (2008), pp. 313–322.
- [305] van der Zee, J. and van Broeckhoven, C. "TMEM106B a novel risk factor for frontotemporal lobar degeneration". *Journal of Molecular Neuroscience* 45 (2011), pp. 516–521.
- [306] van der Zee, J., van Langenhove, T., Kleinberger, G., Sleegers, K., Engelborghs, S., Vandenberghe, R., Santens, P., Van den Broeck, M., Joris, G., Brys, J., Mattheijssens, M., Peeters, K., Cras, P., De Deyn, P. P.,

- Cruts, M., and van Broeckhoven, C. "TMEM106B is associated with frontotemporal lobar degeneration in a clinically diagnosed patient cohort". *Brain* 134 (2011), pp. 808–815.
- [307] van Langenhove, T., van der Zee, J., and van Broeckhoven, C. "The molecular basis of the frontotemporal lobar degeneration-amyotrophic lateral sclerosis spectrum". *Annals of Medicine* 44 (2012), pp. 817–828.
- [308] van Swieten and Heutink, P. "Mutations in progranulin (GRN) within the spectrum of clinical and pathological phenotypes of frontotemporal dementia". *Lancet Neurology* 7 (2008), pp. 965–974.
- [309] Vass, R., Ashbridge, E., Geser, F., Hu, W. T., Grossman, M., Clay-Falcone, D., Elman, L., McCluskey, L., Lee, Virginia M Y, Van Deerlin, Vivianna M, Trojanowski, J. Q., and Chen-Plotkin, A. S. "Risk genotypes at TMEM106B are associated with cognitive impairment in amyotrophic lateral sclerosis". *Acta Neuropathologica* 121 (2011), pp. 373–380.
- [310] Vazquez, C. L. and Colombo, M. I. "Assays to assess autophagy induction and fusion of autophagic vacuoles with a degradative compartment, using monodansylcadaverine (MDC) and DQ-BSA". *Methods in Enzymology* 452 (2009), pp. 85–95.
- [311] Vershinin, M., Carter, B. C., Razafsky, D. S., King, S. J., and Gross, S. P. "Multiple-motor based transport and its regulation by Tau". *Proceedings of the National Academy of Sciences of the United States of America* 104 (2007), pp. 87–92.
- [312] Wang, J., VanDamme, P., Cruchaga, C., Gitcho, M. A., Vidal, J. M., Seijo-Martinez, M., Wang, L., Robberecht, W., and Goate, A. "Pathogenic cysteine mutations affect progranulin function and production of mature granulins". *Journal of Neurochemistry* (2010), pp. 1305–1315.
- [313] Wang, Q., Song, C., and Li, C.-C. H. "Molecular perspectives on p97-VCP: progress in understanding its structure and diverse biological functions". *Journal of Structural Biology* 146 (2004), pp. 44–57.
- [314] Wang, T., Ming, Z., Xiaochun, W., and Hong, W. "Rab7: role of its protein interaction cascades in endolysosomal traffic". *Cellular Signalling* 23 (2011), pp. 516–521.
- [315] Warren, J. D., Rohrer, J. D., and Rossor, M. N. "Clinical review. Frontotemporal dementia". *British Medical Journal (Clinical Research Edition)* 347 (2013), f4827.
- [316] Watts, Giles D J, Wymer, J., Kovach, M. J., Mehta, S. G., Mumm, S., Darvish, D., Pestronk, A., Whyte, M. P., and Kimonis, V. E. "Inclusion body myopathy associated with Paget disease of bone and frontotemporal dementia is caused by mutant valosin-containing protein". *Nature Genetics* 36 (2004), pp. 377–381.
- [317] Weihl, C. C., Pestronk, A., and Kimonis, V. E. "Valosin-containing protein disease: inclusion body myopathy with Paget's disease of the bone and fronto-temporal dementia". *Neuromuscular Disorders* 19 (2009), pp. 308–315.
- [318] Winter, J. F., Hopfner, S., Korn, K., Farnung, B. O., Bradshaw, C. R., Marsico, G., Volkmer, M., Habermann, B., and Zerial, M. "Caenorhabditis elegans screen reveals role of PAR-5 in RAB-11-recycling endosome positioning and apicobasal cell polarity". *Nature Cell Biology* 14 (2012), pp. 666–676.
- [319] Wong, E. and Cuervo, A. M. "Autophagy gone awry in neurodegenerative diseases". *Nature Neuroscience* 13 (2010), pp. 805–811.
- [320] Yu, C.-E., Bird, T. D., Bekris, L. M., Montine, T. J., Leverenz, J. B., Steinbart, E., Galloway, N. M., Feldman, H., Woltjer, R., Miller, C. A., Wood, E. M., Grossman, M., McCluskey, L., Clark, C. M., Neumann, M., Danek, A., Galasko, D. R., Arnold, S. E., Chen-Plotkin, A., Karydas, A., Miller, B. L., Trojanowski, J. Q., Lee, V. M.-Y., Schellenberg, G. D., and Van Deerlin, Vivianna M. "The spectrum of mutations in progranulin: a collaborative study screening 545 cases of neurodegeneration". *Archives of Neurology* 67 (2010), pp. 161–170.

- [321] Yu, W. H., Cuervo, A. M., Kumar, A., Peterhoff, C. M., Schmidt, S. D., Lee, J.-H., Mohan, P. S., Mercken, M., Farmery, M. R., Tjernberg, L. O., Jiang, Y., Duff, K., Uchiyama, Y., Naslund, J., Mathews, P. M., Cataldo, A. M., and Nixon, R. A. “Macroautophagy—a novel Beta-amyloid peptide-generating pathway activated in Alzheimer’s disease”. *Journal of Cell Biology* 171 (2005), pp. 87–98.
- [322] Zerial, M. and McBride, H. “Rab proteins as membrane organizers”. *Nature Reviews Molecular Cell Biology* 2 (2001), pp. 107–117.
- [323] Zerial, M. and McBride, H. “Rab proteins as membrane organizers”. *Nature Reviews Molecular Cell Biology* 2 (2001), pp. 107–117.
- [324] Zhang, D., Iyer, L. M., He, F., and Aravind, L. “Discovery of Novel DENN Proteins: Implications for the Evolution of Eukaryotic Intracellular Membrane Structures and Human Disease”. *Frontiers in Genetics* 3 (2012), p. 283.
- [325] Zhang, F., Strom, A.-L., Fukada, K., Lee, S., Hayward, L. J., and Zhu, H. “Interaction between familial amyotrophic lateral sclerosis (ALS)-linked SOD1 mutants and the dynein complex”. *Journal of Biological Chemistry* 282 (2007), pp. 16691–16699.
- [326] Zhang, L., Sheng, R., and Qin, Z. “The lysosome and neurodegenerative diseases”. *Acta Biochimica et Biophysica Sinica* 41 (2009), pp. 437–445.
- [327] Zhang, X. and Song, W. “The role of APP and BACE1 trafficking in APP processing and amyloid-beta generation”. *Alzheimer’s Research & Therapy* 5 (2013), p. 46.
- [328] Zhang, X., Garbett, K., Veeraraghavalu, K., Wilburn, B., Gilmore, R., Mirnics, K., and Sisodia, S. S. “A role for presenilins in autophagy revisited: normal acidification of lysosomes in cells lacking PSEN1 and PSEN2”. *Journal of Neuroscience* 32 (2012), pp. 8633–8648.
- [329] Zhu, J., Nathan, C., Jin, W., Sim, D., Ashcroft, G. S., Wahl, S. M., Lacomis, L., Erdjument-Bromage, H., Tempst, P., Wright, C. D., and Ding, A. “Conversion of proepithelin to epithelins: roles of SLPI and elastase in host defense and wound repair”. *Cell* 111 (2002), pp. 867–878.

# Acknowledgements

First and foremost, I would like to thank my mentor, **Prof. Dr. Dr. h.c. Christian Haass**, for giving me the opportunity to work in his group and for his constant support and helpful and competent advice. However, most importantly, I thank him for his contagious passion for science and his ability to motivate and inspire everybody in the lab including me.

Then, I would like to thank my supervisor, **Dr. Anja Capell**, for her constant supervision and for passing her extensive expertise in biochemical and cell biological methods as well as her comprehensive knowledge in writing scientific publications on to me. Moreover, I really appreciated our lively discussions about scientific theories, which helped me to look at things from a different angle.

I am also very grateful to the members of **the examination committee**.

Moreover, I would like to thank **Prof. Dr. Dieter Edbauer** and **Dr. Benjamin Schwenk** for our great collaboration on TMEM106B. In addition, I thank **Dr. Nicole Exner** for her mitofusin2 construct and the protocol for staining mitochondria, **Dr. Dorothee Dormann** for the anti-LC3 antibody and her support concerning autophagy and immunofluorescence issues and **Dr. Eva Bentmann** for her help in the lab and showing me how to produce stress granules and beautiful immunofluorescence pictures. I also thank **Prof. Dr. Serge Bénichou** for the chicken-dynamitin constructs and **Prof. Dr. Marino Zerial** for the Rab-GFP constructs.

Special thanks also to my Thesis Advisory Committee, **Prof. Dr. Michael Kiebler** and **Prof. Dr. Günter Höglinger**, for taking the time to discuss the further directions of my PhD thesis with me.

Furthermore, I would like to thank **my group members**, particularly **Katrin Fellerer** for her patience, good mood and mental balance and her great and competent support in the lab especially during the preparation of our papers. Also many thanks to **Julia Götzl** for reading my thesis and for the discussions about GRN, TMEM106B and other matters.

Moreover, I am very grateful to the **members of the FTLD group**, whose advice was very valuable to me and from whom I learnt a lot.

In addition, I would like to thank **all my colleagues** for their constant support and helpfulness. In particular, I thank **Alice Sülzen** for supporting me with the TMEM106B antibody purification and her great readiness to help in any matter. Moreover, I especially thank her, **the members of my group** as well as **Ann-Katrin Bergmann, Claudia Abou-Ajram, Andrea Wenninger-Weinzierl** and **Dr. Carolin Schweimer** for the wonderful atmosphere, all scientific and non-scientific discussions and for the fun we had during my time at the lab.

Many thanks also to **Sabine Odoy, Barbara Kassner, Andrea Dankwardt, Annette Schell, Benno Fredmüller** and **Brigitte Nuscher**, who were doing a great job in keeping everything going.

Moreover, I thank the **Hans & Ilse Breuer Foundation** for their financial support and giving me the opportunity to attend many top-level conferences, where I gained a lot of new ideas for my project and got to know scientists from all over the world.

Last but not least, I would especially like to thank my boyfriend **Christoph Nophut**, who not only helped me with every computer issue that arose while I was writing my thesis, but who was always there listening, supporting and motivating me to go on and to never give up.

However, above all, I would like to thank **my family**, especially my parents **Ursula** and **Hermann Lang**. Thank you so much for having been there for me all my life and supporting me in everything I do.

# Eidesstattliche Versicherung

Ich, Christina Maria Lang, erkläre hiermit an Eides statt, dass ich die vorliegende Dissertation mit dem Thema “Transmembrane protein 106B, a risk factor in frontotemporal lobar degeneration, is a lysosomal type II transmembrane protein and affects autophagy” selbstständig verfasst, mich außer der angegebenen keiner weiteren Hilfsmittel bedient und alle Erkenntnisse, die aus dem Schrifttum ganz oder annähernd übernommen sind, als solche kenntlich gemacht und nach ihrer Herkunft unter Bezeichnung der Fundstelle einzeln nachgewiesen habe.

Ich erkläre des Weiteren, dass die hier vorgelegte Dissertation nicht in gleicher oder in ähnlicher Form bei einer anderen Stelle zur Erlangung eines akademischen Grades eingereicht wurde.

Freising, den 08.05.2015

---

Christina Lang

